1 April 2005

Science

Vol. 308 No. 5718
Pages 1 –148 $10

125 YEARS OF GLOBAL Science

AAAS

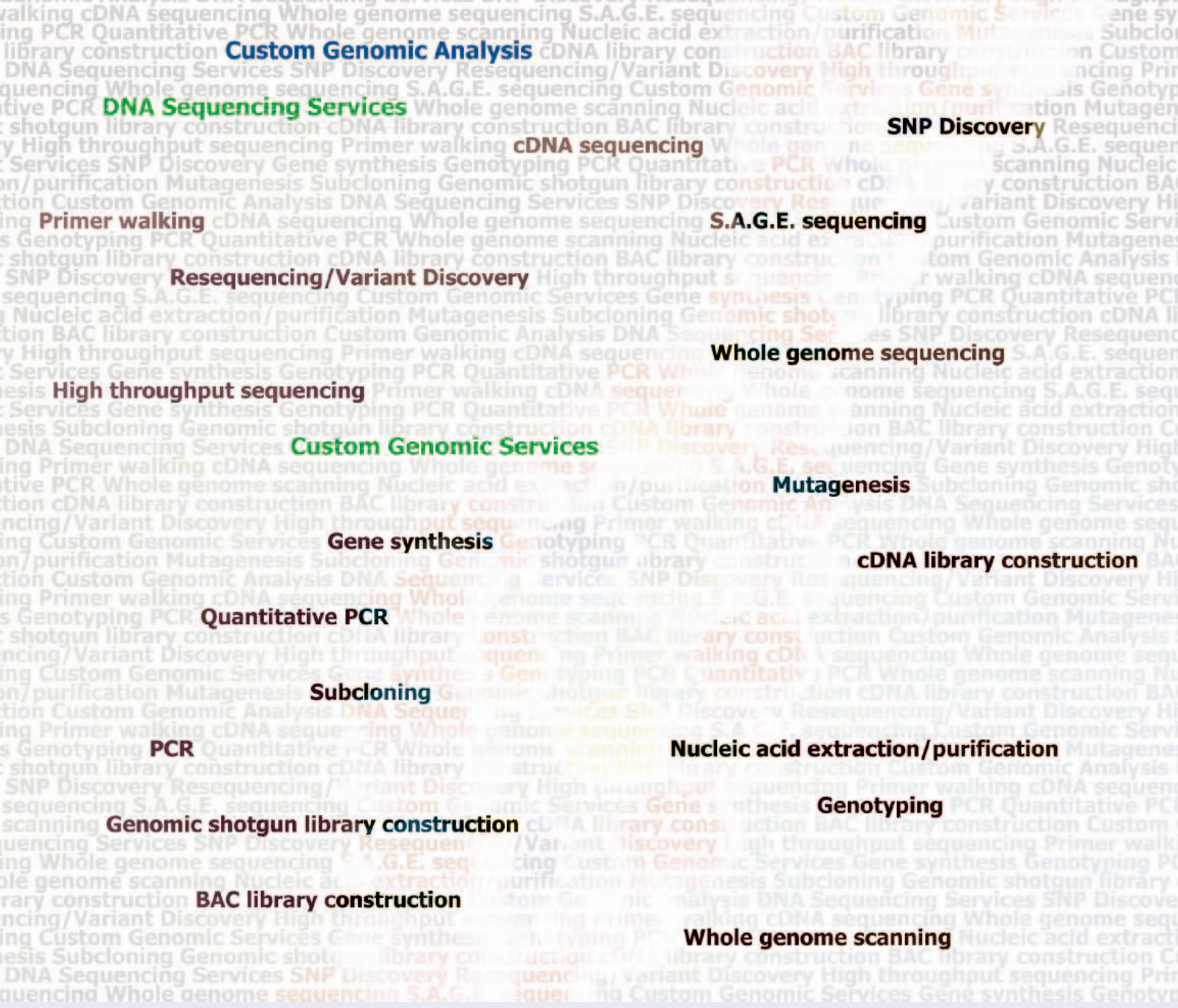

DNA Sequencing Services

SNP Discovery/Resequencing/ Variant Discovery	**$0.01 per base, per direction**
High throughput sequencing	**$5 per reaction**
cDNA sequencing	**$5 per reaction**
S.A.G.E. sequencing	**$5 per reaction**

Custom Genomic Services

Custom Gene synthesis	**$1 per base pair**
PCR	**$1 per amplicon**
Real Time PCR	**$500 per assay**
Whole genome scanning	**$5 per locus, per sample**
Nucleic acid extraction/ purification	**$2.50 per mini-prep**
Mutagenesis	**$400 any mutation within 5 bp frame**
Subcloning	**$400 per clone**
Library construction: Genomic, cDNA, BAC	**Please inquire for pricing**

POLYMORPHIC
Polymorphic DNA Technologies, Inc.℠

www.polymorphicdna.com
info@polymorphicdna.com

1125 Atlantic Ave., Ste. 102
Alameda, CA 94501

888.362.0888

For more information please visit www.polymorphicdna.com

The perfect assortment.

With GeneMorph® mutagenesis kits, a balanced spectrum of mutations is right at your fingertips.

GeneMorph® random mutagenesis kits* feature our patented Mutazyme® II DNA polymerase, which delivers a balanced mutational spectrum with more robust yields than *Taq* polymerase under error-prone PCR conditions. This allows you to discover more key residues responsible for protein function easier and faster than before, thus enhancing the evolution of your protein.

- **Simple protocol to control mutation frequency**
- **Efficient mutagenesis rates of 1 to 16 bases per kb**
- **Overcome poor PCR yield and mutational bias of *Taq* polymerase**

Our GeneMorph® II Kits include Mutazyme® II Polymerase, which delivers a balanced mutational spectrum.

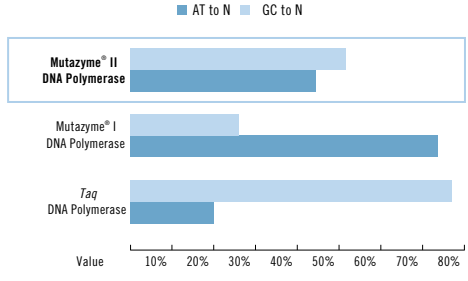

Need More Information? Give Us A Call:

Stratagene USA and Canada
Order: (800) 424-5444 x3
Technical Services: (800) 894-1304

Stratagene Europe
Order: 00800-7000-7000
Technical Services: 00800-7400-7400

Stratagene Japan K.K.
Order: 03-5159-2060
Technical Services: 03-5159-2070

* U.S. Patent No. 6,803,216 and patent pending

www.stratagene.com

Ask us about these great products:

GeneMorph® II Random Mutagenesis kit	30 rxns	200550
GeneMorph® II EZClone Domain Mutagenesis kit	10 rxns	200552

Purchase of these products is accompanied by a license to use them in the Polymerase Chain Reaction (PCR) process in conjunction with a thermal cycler whose use in the automated performance of the PCR process is covered by the up-front license fee, either by payment to Applied Biosystems or as purchased, i.e., an authorized thermal cycler.

STRATAGENE

GE Healthcare

Ni Sepharose™

4x greater binding capacity in histidine-tagged protein purification

Ni Sepharose™ products from GE Healthcare give you the highest binding capacity available for histidine-tagged protein purification. With up to four times the binding capacity, it's no longer pure imagination to dramatically increase your yield, while saving time and costs. Maximum target protein activity is assured, thanks to tolerance of a wide range of additives and negligible nickel ion leakage. The flexibility to use a variety of protocols ensures the highest possible purity. Ni Sepharose 6 FF is excellent for manual procedures such as gravity/batch and easy scale-up, while the HP version is designed for high-performance in automated purification systems – both are available in different formats, including prepacked columns. Outstanding performance has never been easier to achieve.

www.amershambiosciences.com/his

imagination at work

GE10-05

Science

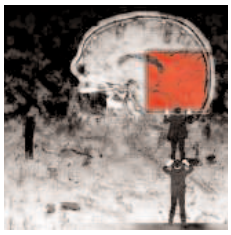

COVER The ability to trust another human is a crucial component of normal social interaction. Hyperscanning, a brain imaging approach for multibrain recording, reveals the related activity in two brains as trust is built during a monetary exchange game. See page 78. [Image: Min Kim/Human Neuroimaging Laboratory/BCM]

Volume 308
1 April 2005
Number 5718

DEPARTMENTS

NEWS OF THE WEEK

NEWS FOCUS

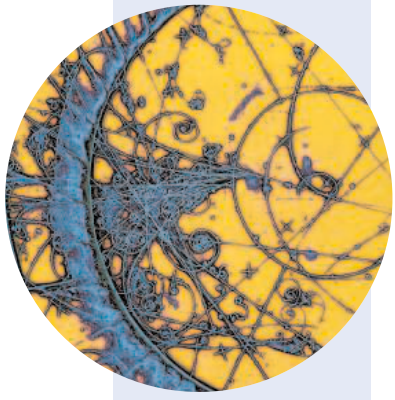

38

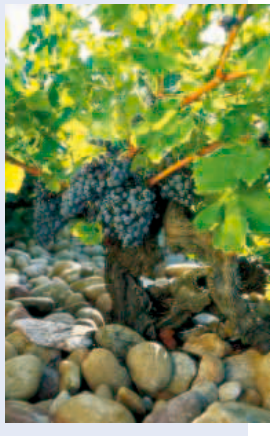

53

55

LETTERS

BOOKS *ET AL.*

ESSAY

PERSPECTIVES

REVIEW

Contents continued

Integrated Solutions — Automated Sample Preparation

Free up your time — leave your sample preparation to the affordable BioSprint 15!

New

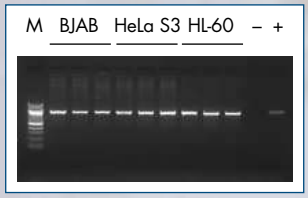

Efficient amplification of the single-copy gene MECL-1 from a range of cultured-cell samples

Save time and effort by automating your sample preparation!

The new BioSprint 15 workstation and kits provide rapid and cost-efficient sample preparation for a wide range of applications. Kits enabling purification of high-quality genomic DNA from cells, tissue, and blood are available now, with more applications to follow. Look for the new protein purification kits, available in early 2005!

The BioSprint 15 workstation and expanding range of kits give you:

- **A convenient automated procedure** — saving you time and effort
- **A cost-effective solution** — economically priced automation for 1–15 samples per run
- **Fast startup and immediate results** — with easy-to-use, preinstalled BioSprint protocols
- **Flexibility and versatility** — use the protocols supplied or easily design your own

Visit www.qiagen.com/goto/BioSprint15 to see how the BioSprint 15 can free up your time!

QIAGEN

SCIENCE EXPRESS www.sciencexpress.org

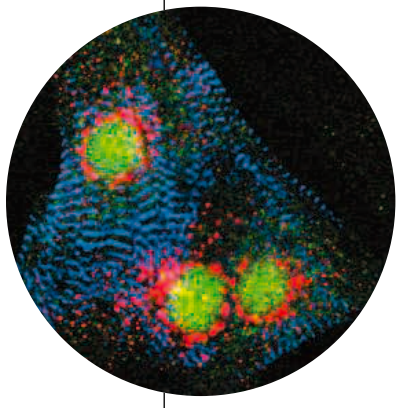

TECHNICAL COMMENT ABSTRACTS

98

BREVIA

RESEARCH ARTICLES

REPORTS

Contents continued

PIERCE

Grasp the Proteome™

Protein Purification/Detection

Still using Streptavidin?

NeutrAvidin™ Protein offers ultra-low nonspecific binding at an *unbelievably* low price

NeutrAvidin™ Protein offers the highest possible specificity for biotin, yielding the lowest nonspecific binding. NeutrAvidin™ Protein provides exceptional performance for both purification and detection of biotin-labeled proteins. If you're still using Streptavidin, it's time to discover the advantages of NeutrAvidin™ Tools.

Advantages over streptavidin:

- Highest specificity for biotin binding
- No nonspecific binding to cell-surface proteins
- High signal-to-noise ratio in detection systems
- Saves money without sacrificing quality

Properties of biotin-binding proteins

	Avidin	Streptavidin	NeutrAvidin™ Protein
Molecular Weight	67K	53K	60K
Biotin-binding Sites	4	4	4
Isoelectric Point (pI)	10	6.8-7.5	6.3
Specificity	Low	High	Highest
Affinity for Biotin (K_d)	10^{-15} M	10^{-15} M	10^{-15} M
Nonspecific Binding	High	Low	Lowest

Available in bulk quantities and in the following convenient formats:

- Immobilized NeutrAvidin™ Protein on Agarose
- UltraLink® Immobilized NeutrAvidin™ Protein
- Soluble NeutrAvidin™ Protein
- HRP- and Alkaline Phosphatase-labeled NeutrAvidin™ Protein
- Fluorescein-labeled NeutrAvidin™ Protein
- Maleimide-activated NeutrAvidin™ Protein
- 96- and 384-well NeutrAvidin™ Plates

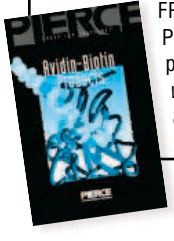

FREE Avidin-Biotin Handbook from Pierce, the leader in avidin-biotin products! Visit the Pierce web site at *www.piercenet.com/ab95d* or call 800-874-3723 to request your copy today.

www.piercenet.com/neu22d

PIERCE

Tel: 815-968-0747 or 800-874-3723 • Fax: 815-968-7316
Technical Assistance E-mail: TA@piercenet.com • Customer Assistance E-mail: CS@piercenet.com

Outside the United States, visit our web site or call 815-968-0747 to locate your local Perbio Science branch office (below) or distributor

Belgium & Dist.:	China:	France:	Germany:	Hong Kong:	The Netherlands:	United Kingdom:	Switzerland:
Tel +32 53 85 71 84	Tel +86 10 8049 9033	Tel 0800 50 82 15	Tel 0228 9125650	Tel 852 2753 0686	Tel 076 50 31 880	Tel 0800 252185	Tel 0800 56 31 40
euromarketing@perbio.com	support@perbio.com.cn	euromarketing@perbio.com	de.info@perbio.com	SalesHK@perbio.com	euromarketing@perbio.com	uk.info@perbio.com	euromarketing@perbio.com

Reports continued

103

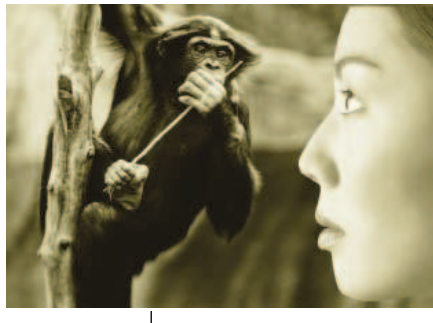

60 & 107

AAAS
ADVANCING SCIENCE, SERVING SOCIETY

SCIENCE (ISSN 0036-8075) is published weekly on Friday, except the last week in December, by the American Association for the Advancement of Science, 1200 New York Avenue, NW, Washington, DC 20005. Periodicals Mail postage (publication No. 484460) paid at Washington, DC, and additional mailing offices. Domestic individual membership and subscription (51 issues): $135 ($74 allocated to subscription). Domestic institutional subscription (51 issues): $550; Foreign postage extra: Mexico, Caribbean (surface mail) $55; other countries (air assist delivery) $85. First class, airmail, student, and emeritus rates on request. Canadian rates with GST available upon request, GST #1254 88122. Publications Mail Agreement Number 1069624. **Printed in the U.S.A.**

Change of address: allow 4 weeks, giving old and new addresses and 8-digit account number. **Postmaster:** Send change of address to *Science*, P.O. Box 1811, Danbury, CT 06813–1811. **Single copy sales:** $10.00 per issue prepaid includes surface postage; bulk rates on request. **Authorization to photocopy** material for internal or personal use under circumstances not falling within the fair use provisions of the Copyright Act is granted by AAAS to libraries and other users registered with the Copyright Clearance Center (CCC) Transactional Reporting Service, provided that $15.00 per article is paid directly to CCC, 222 Rosewood Drive, Danvers, MA 01923. The identification code for *Science* is 0036-8075/83 $15.00. *Science* is indexed in the *Reader's Guide to Periodical Literature* and in several specialized indexes.

Contents continued ▶

The MJ Line of Amplification Products

A giant among its peers.

Introducing the MJ Mini™ thermal cycler and MiniOpticon™ real-time PCR system: Small on size, big on performance.

The 48-well MJ Mini cycler delivers the high-performance features found in higher-capacity instruments. When fitted with a two-color real-time detector, it's transformed into the MiniOpticon real-time system — one of the smallest and most portable real-time PCR systems available.

- A thermal gradient optimizes reactions for maximum efficiency and accurate quantification
- Fast achievement of thermal uniformity ensures reliable results and shortened run times
- The MiniOpticon system incorporates an array of 48 LEDs for excitation and a pair of sensitive photodiodes for detection in a robust design with no moving parts
- Light weight and compact size allow these systems to fit just about anywhere

MJ Mini cycler — 18 x 32 x 20 cm; 4 kg
MiniOpticon system — 18 x 32 x 33 cm; 8 kg

For more information, visit us on the Web at **www.bio-rad.com/ad/mini/**

Practice of the patented polymerase chain reaction (PCR) process requires a license. The MJ Mini thermal cycler and the MiniOpticon system include an Authorized Thermal Cycler, and may be used with PCR licenses available from Applied Biosystems. Their use with Authorized Reagents also provides a limited PCR license in accordance with the label rights accompanying such reagents. Some applications may also require licenses from other third parties.

Visit us on the Web at **discover.bio-rad.com**
Call toll free at 1-800-4BIORAD (1-800-424-6723);
outside the US, contact your local sales office.

BIO-RAD

sciencenow www.sciencenow.org Daily News Coverage

More Than One Way to Skin a Cat Allergy
Researchers tackle condition by creating a cat-human hybrid.

Save a Lizard, Save a Plant
New findings illustrate delicate interdependence between flora and fauna.

What Color Are Your 2's?
Study provides new insights into why letters and numbers look different to synesthetes.

Success with GEM.

science's next wave www.nextwave.org Career Resources for Young Scientists

US: Bridges to Nowhere? *J. Austin*
A new National Research Council report contains some intriguing proposals for postdocs.

Canada: Visualizing Science at University of Toronto *A. Fazekas*
The Biomedical Communications program prepares students for careers in scientific visualization.

Netherlands: Young Scientists Take to the Streets *T. Vrijenhoek*
Does taking time to communicate science to the public help or hinder a young scientist's career?

MiSciNet: A GEM of a Program *C. Parks*
The Graduate Degrees for Minorities for Engineering and Science Consortium provides funding and support to underrepresented minority graduate students.

Postdoc Network: A Taxing Question on Postdoc Pay *B. Benderly*
New IRS regulation demands deductions from all postdocs.

GrantsNet: April 2005 Funding News *Next Wave Staff*
Get the latest index of research funding opportunities, scholarships, fellowships, and internships.

science's sage ke www.sageke.org Science of Aging Knowledge Environment

News Focus: Feeling Spunky with JNK *R. J. Davenport*
Protein funnels stress signals into insulin pathway and extends life.

News Focus: Mopping Up Nuclear Waste *M. Leslie*
Molecule helps dispose of damaged proteins in the cell's command center.

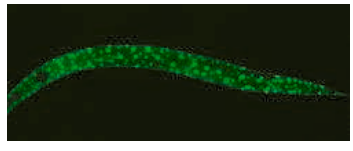

JNK nudges Foxo to center stage.

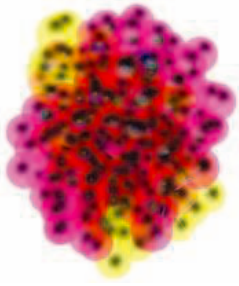

Multicellular signaling systems.

science's stke www.stke.org Signal Transduction Knowledge Environment

Perspective: Meeting Report—The Future and Limits of Systems Biology *E. Werner*
Who will prove more important as engineers and biologists tackle the new frontiers of systems biology?

Events
Check out the updates to this list of meetings and conferences relevant to cell signaling.

Separate individual or institutional subscriptions to these products may be required for full-text access.

Our global network is your advantage – Everywhere under the sun!

Greiner Bio-One is a leading designer, manufacturer, and supplier of leading edge consumables to biotechnology, diagnostic and pharmaceutical partners worldwide.

Offering an unsurpassed scope of products and services across a variety of disciplines, we focus on the evolving needs of our customers in the development of innovative products, to refine existing technologies, and redefine the state of the art.

Our fast and flexible response for customer specific programs, combined with multiple strategic manufacturing sites, ensures an uninterrupted supply of critical components to meet your product needs.

With worldwide locations and effective global distribution, you will always be within reach of the service, product and support you need, everywhere under the sun.

To find the Greiner Bio-One location most convenient for you visit us at www.gbo.com/bioscience/distribution.

www.gbo.com/bioscience/distribution

greiner bio-one

For further information please contact Greiner Bio-One: **Germany (Main office):** (+49) 7022 948-0 · info@de.gbo.com
Belgium: (+32) 2-4 61 09 10 · info@be.gbo.com, **France:** (+33) 1 69-86 25 50 · infos@fr.gbo.com, **Japan:** (+81) 3-35 05-88 75 · info@jp.gbo.com
Netherlands: (+31) 172-42 09 00 · info@nl.gbo.com, **UK:** (+44) 14 53-82 52 55 · info@uk.gbo.com, **USA:** (+1) 8 00-8 84-47 03 · info@us.gbo.com

edited by Stella Hurtley and Phil Szuromi

Probing Luttinger Liquids

Strongly interacting electron systems in low dimensions provide a theoretically tractable system for studying such complex electronic interactions. However, experimental realization and probing of such systems has lagged behind the theoretical efforts. **Auslaender *et al.*** (p. 88) now play catch-up with their study of the fractionalization of electrons in a well-controlled one-dimensional system. Using a pair of coupled semiconducting wires with variable electron density, they directly measured the spin and charge excitations of the system and followed the dispersive behavior of the electronic transport as a function of the strength of the Coulomb interaction. They found clear evidence for the theoretically predicted separation of the spin and charge degrees of freedom.

Sneaking a Peak at Creep

Creep is the slow deformation of a material that occurs when it is held under constant load, such as the gradual stretching of a piano or violin string. During creep in a metal or metallic alloy, voids form and grow with time, in addition to changes in the texture and orientation of the crystal grains. **Pyzalla *et al.*** (p. 92) have developed a technique to monitor all of these changes at once, and they use it to track creep in a brass alloy. They confirm that the transition from homogeneous creep to localized deformation occurs late in the creep process and suggest ways of how other simultaneous diffraction and tomography measurements may be used to track crack growth or load partitioning within a composite.

Translational Repression at 5.5 Angstroms

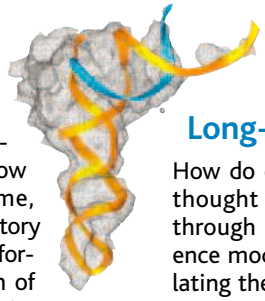

Gene expression must be tightly regulated at both the level of transcription and translation. X-ray crystallography studies have helped to elucidate the mechanism by which threonyl-tRNA synthetase regulates its own expression. **Jenner *et al.*** (p. 120) now examine the complex that includes the ribosome, structured messenger RNA (mRNA) carrying a regulatory domain, and initiator transfer RNA, with structural information shown at 5.5 angstrom resolution. The path of the mRNA on the 70*S* ribosome in the presence of initiator tRNA and the localization of the regulatory element of mRNA on the ribosome suggest the molecular mechanisms by which translational repressors can work.

CREDITS (TOP TO BOTTOM): KOHFELD *ET AL.*; JENNER *ET AL.*

Marine Biology and Climate

The CO_2 content of the anthropogenically unperturbed atmosphere has varied consistently between a minimum of around 180 parts per million (ppm) at glacial maxima and a maximum of around 280 ppm during interglacials. Why peak glacial intervals and warm periods have such apparently well-constrained atmospheric CO_2 concentrations is still unexplained. Climate models uniformly fail to account for the observed difference through physical mechanisms alone, so marine biological processes often have been invoked as a probable cause. **Kohfeld *et al.*** (p. 74) combined multiple records of biological activity from more than 150 marine sediment records extending back into the penultimate glacial period. They show that ocean biology could have been responsible for no more than half of that difference during that time, which implies that physical processes must somehow be responsible for the rest.

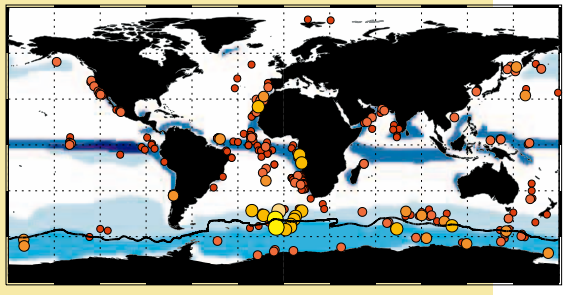

Rafts and Regulation

Regulation of the transcription factor NF-κB is central to the activation of T cells in the immune system. Activation of the T cell receptor leads to accumulation of a group of signaling proteins within lipid rafts in the plasma membrane. Somehow this process results in activation of the IKK (IκB kinase) complex, which leads to activation of NF-κB. **Lee *et al.*** (p. 114; see the Perspective by **van Oers and Chen**) provide a mechanism that helps link these processes. The 3-phosphoinositide-dependent kinase 1 (PDK-1) interacts with and activates another protein kinase, PKCθ, which in turn interacts with components of the IKK complex and is required for their recruitment to the lipid rafts. PDK1 also interacts with a scaffold protein CARD11, which in turn recruits the Bcl10 and MALT1 proteins. The latter proteins mediate ubiquitination of a component of the IKK complex—the signal that eventually activates NF-κB.

A Trusting Trustee

For most of us, games are merely a source of enjoyment, but mathematicians and economists have analyzed their theoretical and experimental aspects, and now neuroscientists are taking their turn. The trust game involves exchanges of money between two players, where the amounts transferred reflect an inclination to trust (or mistrust) the generosity of the other player. **King-Casas *et al.*** (p. 78; see the cover and the news story by **Miller**) examined the neural correlates of these inclinations during the course of repeated interactions within pairs of subjects separated by thousands of miles. The cut-and-thrust character of the game establishes the investor's reputation in the mind of the trustee, and the trustee's intention to increase the repayment equates to the well-known reinforcement learning signal that predicts reward.

Long-Distance Synchrony

How do distant brain areas communicate with each other? It is thought that neurons increase their impact on target groups through precise oscillatory synchronization. Long-range coherence modulation might represent a general mechanism for regulating the flow of information within the nervous system. To test this idea in human volunteers, **Schoffelen *et al.*** (p. 111) combined magneto-encephalography and electromyographic recordings during the performance of a basic reaction time task, where

CONTINUED ON PAGE 15

STRUGGLE TOGETHER FOR A CLEAN FUTURE

2005 INTERNATIONAL (IHEC' 2005)

www.ihec2005.org

HYDROGEN ENERGY CONGRESS

13 - 15 JULY 2005
Lütfi Kırdar Exhibition Center
İstanbul - Turkey

Committee

Honorary Chairman
Prof. Dr. T.Nejat VEZİROĞLU
International Hydrogen Energy Society Chairman
ICHET- International Centre for Hydrogen Energy Technologies

Chairman
Prof.Dr. İ.Engin TÜRE
Haliç University

Vice Chairmen
Prof.Dr. Figen KADIRGAN - İTU
Prof.Dr. İnci EROĞLU - ODTU
Hüseyin AĞACAN - Elimsan

RENEWABLE ENERGY EXHIBITION

Wind Energy - Solar Energy - Hydro Energy- Fuel Cells
Hydrogen Generators - Bio Mass Energy - Natural Gas Generators
Inverters - Electrical Energy Production and Distribution Equipment

13 - 16 JULY 2005
Lütfi Kırdar Exhibition Center

sponsors

UNIDO
UNIDO-ICHET
International Centre for Hydrogen Energy Technologies
ICHET
Municipality of Istanbul
Ministry of Environment and Forestry
International Association for Hydrogen Energy
Clean Energy Research Institute University of Miami
Haliç University
Ministry of Trade and Industry
TUBITAK
Turkish Scientific and Technical Research Council
GarantiBank
elimsan
The Pioneer Of Switchgear Technology
www.elimsangroup.com
FENİS
FORD OTOSAN
Istanbul Technical University
Bogazici University

organizer

HİDRENER
www.hidrener.com
HYDROGEN ENERGY SYSTEMS Com.
CHEF
www.hidrojenforumu.com
HYDROGEN ENERGY FORUMS

www.ihec2005.org

Secretariat Enrollment
DEKON
www.dekon.com.tr

the subjects implicitly learned the increasing or decreasing probability of a signal. The coherence of gamma-band (40 to 70 Hertz) oscillations between the motor cortex and the spinal cord did indeed make motor outputs more effective.

Jurassic Termite Trouble

A few mammals, such as the anteater and some rodents, have evolved special limbs for digging and teeth for a diet feasting on just a few types of abundant social insects. These mammals appeared in the Paleocene, about 30 to 40 million years ago. **Luo and Wible** (p. 103) now describe a fossil of a similarly specialized mammal that appeared about 150 million years ago and appears to represent a new, but now extinct, line of basal mammals. The fossil, *Fruitafossor windscheffelia*, has large forelimbs, specialized for digging, and hollow teeth, probably used for feeding on termites.

Listen, Learn, Freeze

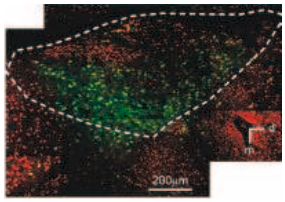

Rats and mice learn to freeze when they hear a tone previously encountered at the same time as an electric shock. This type of learning takes place in the amygdala. **Rumpel *et al.*** (p. 83, published online 3 March 2005) examined the cellular basis of the learning by tagging the glutamate receptors that are recruited into synapses during learning with a subunit that can be detected electrophysiologically. They found that fear conditioning drives these receptors into synapses in about 35% of the cells in the lateral amygdala. Inhibition of this recruitment inhibits the formation of the tone-shock memory. If only 10 to 20% of the synapses are inactivated, learning is blocked. Thus, synaptic modification is required for behavioral learning, which is unexpectedly sensitive to the loss of a small fraction of modified synapses.

Animal Horizons

The Doushantuo Formation, China, preserved perhaps the earliest examples of animals, including many exquisite embryos. Its deposition after a global glacial period has raised questions about the relation between climate stability and major evolution cycles. **Condon *et al.*** (p. 95, published online 24 February 2005; see the Perspective by **Kaufman**) now provide uranium-lead ages from zircons for the Doushantuo Formation that bracket its deposition between 635 and 550 million years ago. This formation, approximately 100 meters thick, was deposited gradually during a very long interval. Most of the fossils in the upper part of this formation may be correlative with other metazoans worldwide.

Dust in the Wind and Sea

Dust contains iron, an essential nutrient for marine phytoplankton and a primary control on marine productivity. Climate, in turn, modulates the sources, amount, and sites of deposition of dust. **Jickells *et al.*** (p. 67) review what is understood about this complicated Earth system, concentrating on the linkages between the various components. Gaps in our current understanding of the cycle are large enough that it would seem premature to embark on ambitious geoengineering schemes that would attempt to reduce atmospheric CO_2 concentrations through iron fertilization of selected areas of the surface ocean.

Not the Same Difference

Much of the recombination in the human genome occurs in "hotspots." The genomic mechanisms and evolutionary forces that direct recombination to specific locations, however, remain unknown. **Winckler *et al.*** (p. 107, published online 10 February 2005; see the Perspective by **Jorde**) studied fine-scale recombination rates over a large span of orthologous DNA in both humans and chimpanzees. Although the species share 99% identity at the level of DNA sequence, in no case did the location of the hotspots coincide, and the rates of recombination across three 500-kilobase regions were significantly different. Thus, recombination hotspots evolve rapidly, and the rate of their evolution is different from that of DNA sequence.

CREDIT: RUMPEL *ET AL.*

Achieve

Optimal Transfection

Plasmid delivery and expression in mammalian cells can be tricky. Relax. The scientists of Mirus Bio have developed ***high-efficiency***, easy-to-use formulations that are compatible with serum while ***minimizing toxicity***. The result? Healthy cells expressing your gene of choice — consistently.

Boost your transfection efficiency with Mirus Bio products. Our family of *Trans*IT® plasmid transfection reagents are designed for optimized delivery — every time. Choose from a range of quality-controlled formulations proven to work in a variety of cell types, such as 293, Hela, CHO and Jurkat cells. What is the best plasmid transfection reagent for your lab? Call **888-530-0801** today and ask our tech support team for advice.

Mirus Bio *Trans*IT® Transfection Reagents

Select *Trans*IT® Cell Line Specific Transfection Reagents	Cell Lines	Transfection Efficiency*
*Trans*IT®-293	HEK 293	75 - 85%
*Trans*IT-HelaMONSTER®	HeLa	50 - 60%
*Trans*IT®-CHO	CHO-K1	50 - 60%
*Trans*IT®-Jurkat	Jurkat	10-25%
*Trans*IT®-Prostate	DU 145, LNCaP, PC-3	50%
*Trans*IT-Neural®	Neuro-2a	75%
*Trans*IT®-Insecta	Sf9	40 - 60%
*Trans*IT®-Keratinocyte	Keratinocytes	20 - 30%

* Using EGFP as a reporter.

Like you, Mirus Bio scientists are hands-on researchers, so you can expect products developed for your specific applications, plus unsurpassed technical support. Ensure expression in your cells. Begin with Mirus Bio — from our bench to yours.

For all your **transfection** needs, rely on ***Trans*IT®** products. From broad spectrum to cell line specific, **Mirus Bio delivers**.

www.mirusbio.com

Mirus®

It All Begins at the Bench

In 1996 Mirus pioneered the development of the TransIT®-LT1 high efficiency/low toxicity transfection formulation for plasmid delivery in mammalian cells — paving the way for the development of the first optimized siRNA delivery reagent in 2001.

All Fools' Day

April 1 coincides with *Science*'s issue date, providing an irresistible invitation for foolishness. Some publications do parodies; others create a fake story just plausible enough to hold the reader's credulity. But why quit at one when there are so many scenarios that might provide some amusement and might even be believable for a line or two? So here is a sampling of stories that even in our wildest moments we don't expect to see in the mainstream press. Each of these April Fool news items is limited to a headline and a lead paragraph; readers are invited to try their own hand at this. And as you read, please recall that our muse is not hampered by such inhibitions as, well, taste.

FRIDAY, APRIL 1, 2005

Bush Administration Announces Ban on Greenhouse Gas Emissions

WASHINGTON, DC, April 1. In a striking reversal, Secretary of Energy Bodman and President Bush in a Rose Garden ceremony today endorsed the McCain-Lieberman bill in the Senate that proposes carbon emissions limitations. The president said, "We will not await passage to undertake immediate mitigation procedures. The science dictates that we must roll back global warming. A carbon tax of $25 per ton will be imposed by Executive Order as soon as possible. The tax will also help restrain the growing deficits, which are needlessly worrying Greenspan."

European Research Council Set to Take Over All Basic Research Funding in Europe

BRUSSELS, April 1. The European Union (EU) has announced that its member nations will phase out their present research programs, recognizing the need for a single strategically positioned funding agency. This surprising move will end the allegedly fragmented character of national and EU-sponsored "framework" research support programs. The relatively new European Research Council (ERC) will supervise all programs from a center in Reggio Calabria, Italy. Asked about the location, the newly appointed ERC head replied: "We like the beach, and we wanted it to be anywhere but Brussels."

Justice Scalia Quits Supreme Court, Accepts Presidency of Harvard

CAMBRIDGE, MA, April 1. In a surprise move, the Harvard Corporation (which last week reluctantly accepted President Larry Summers' resignation to take the job of head of Citibank) announced that Justice Antonin Scalia has accepted the university's presidency after a highly secretive recruitment process. Asked about his unexpected departure from the Court, Scalia explained, "Some of the justices got so annoyed at my dissents that they have made life here difficult. I'm easygoing, and I expect to fit right in at Harvard, where I understand the faculty to be less sensitive and more understanding."

Democrats to Run Michael Crichton for President in '08, Dean Says

WASHINGTON, DC, April 1. In an announcement today, Chairman of the Democratic National Committee Howard Dean revealed that his party plans to run novelist and Hollywood movie figure Michael Crichton in the 2008 presidential race. "After all, this man is a hero to every American boy who grew up loving dinosaurs," Dean said. Crichton's view that environmentalists are terrifying the public is expected to draw some Republican mainstream voters. "Our guy will mount a great campaign against DeLay, or whoever they decide to run. We'll go to Indiana, to Oregon, to California—Yeeaah!!" Dean exclaimed.

Millennium Ecosystem Assessment, Just Out, Says Planet Is in Good Shape

LONDON, April 1. In a surprising turnabout, the Millennium Ecosystem Assessment (MEA), conducted by an international array of distinguished ecologists, gave a positive report on the global state of ecosystem health. Biodiversity, it reports, is actually increasing because many locations have been enriched with invasive species, previously thought to have an adverse impact on native ecosystems. MEA's chair, Stanford biology professor Hal Mooney, explained that the group "just thought it was time to strike a more positive note." Environmental critic Bjorn Lomborg said, "It's a trick. You can't trust these guys."

President's Council on Bioethics Approves Steroid Use in Major League Baseball

WASHINGTON, DC, April 1. In a shocking surprise, the council, which had frequently issued past pronouncements against any kind of intervention into "human nature," has issued a strong statement urging Major League Baseball to accept reality and allow the unlimited use of anabolic steroids by all players. As representatives of the Players' Union expressed satisfaction, Chairman Leon Kass explained, "Everyone says the playing field ought to be level. Well, we just leveled it."

Donald Kennedy
Editor-in-Chief

10.1126/science.1111875

EDITORS' CHOICE

edited by Gilbert Chin

ECOLOGY

Food Preservative

Many solitary predatory wasps have to solve the problem of long-term storage of food items as provisions for developing offpsring. The European beewolf (*Philanthus triangulum*) supplies its larvae with immobilized honeybees as nourishment. The beewolf larva spins a cocoon and overwinters in a brood chamber, snug and warm, which are ideal growth conditions for microbes wishing to share its food cache.

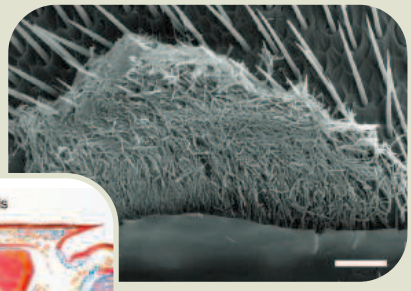

A reservoir of bacteria (red) in the antennal glands (left) and a close-up view of the white exudate (above).

The female beewolf daubs the chamber with a white substance extruded from glands in its antennae, and Kaltenpoth *et al.* have discovered that this exudate is the source of a *Streptomyces* bacterium, which, predictably, produces antibiotics that prevent microbial infestation and deterioration of the food supply. This symbiosis is analogous to that found in leaf-cutting attine ants, and as in that relationship, the *Streptomyces* are transmitted from mother to daughter wasp. If brood cells were not inoculated with the bacterium, larval survival fell from over 80% to less than 7%. Likewise, if a female beewolf fails to acquire the *Streptomyces* preservative, then it appears incapable of breeding successfully. — CA

Curr. Biol. **15**, 475 (2005).

PLANT SCIENCES

Enabling Traffic

KN1 is a transcription factor that moves from cell to cell in order to regulate, among other things, stem cell identity in the shoot apical meristem of maize. Another transcription factor, GL1, prefers to stay in its home cell, where it regulates the formation of tiny hairs (trichomes) in the leaf epidermis of *Arabidopsis*. Whether intercellular transport of KN1 is regulated is addressed by Kim *et al.* By making a chimeric construct of KN1 with GL1, the authors determined which portions of KN1 could drive intercellular transport of misexpressed GL1 and thus rescue trichome formation. A GL1-KN1 fusion using only the C-terminal portion of KN1 supported rescue through intercellular transport, whereas the fusion using the N-terminal portion of KN1 did not. The homeodomain included in that C-terminal portion of KN1 turned out to be critical. Both the mRNA and the KN1 homeodomain protein seem to be required for intercellular trafficking. Thus, the KN1 homeodomain is required to transport both itself and its mRNA through plasmodesmatal channels. — PJH

Genes Dev. 10.1101/gad.332805 (2005).

GEOPHYSICS

What Causes Sprites?

Sprites are transient luminous events in the mesosphere, at heights of about 50 to 90 km. They are associated with positive cloud-to-ground lightning, but may occur up to 50 km from the location of the lightning strike, with a delay of up to 100 ms. The mechanism by which sprites are generated and evolve is not well understood.

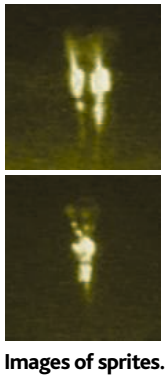

Images of sprites.

Ohkubo *et al.* have analyzed 21 sprites detected on 15 December 2003 during thunderstorms above the coast of the Sea of Japan. By comparing optical measurements with data taken at very low radio frequencies, the authors show that low-frequency discharges occur within the cloud at the same time as the sprite. These intracloud discharges may generate the sprites and help to explain the long time delay between cloud-to-ground lightning and sprite formation. — JFU

Geophys. Res. Lett. **32**, 10.1029/2004GL021943 (2005).

CHEMISTRY

Double Duty

Strategies for homogeneous catalysis of bimolecular reactions tend to focus on activating only one of the two reactants. Recently, several bimetallic systems have been developed for dual activation, but the interactions between the two different catalytic sites are often difficult to predict and control. Takita *et al.* show that a single trivalent indium catalyst can activate both nucleophile and electrophile in the same reaction mixture under relatively mild conditions. The reaction involves the addition of terminal alkynes to aldehydes or to ketones, and it generally requires deprotonation of the alkyne with stoichiometric organometallic base. The catalytic In(III) salt assumes this role in the presence of an amine base, and, at the same time, it acts as a Lewis acid to activate the carbonyl electrophile. Evidence for this dual function comes from infrared and nuclear magnetic resonance spectroscopy. The reaction proceeds under solvent-free conditions and produces high yields from aromatic aldehydes, which have resisted alternative approaches. $InBr_3$ works best for aldehydes, whereas ketones require the triflate salt $In(SO_3CF_3)_3$. — JSY

Org. Lett. 10.1021/ol050069h (2005).

BIOMEDICINE

Tales of Survival

DJ-1 is an intensely studied but mysterious gene with links to two human diseases. Originally identified as a collaborator of the H-*ras* oncogene in conferring tumorigenic properties on normal cells in culture, *DJ-1* was subsequently found to be mutated in a hereditary form of Parkinson's disease. Although this discovery triggered a flurry of research on the mechanistic roles of *DJ-1* in neurodegenerative disease, progress on that front has been slow.

Kim *et al.* revisit the question of how *DJ-1* contributes to tumor formation and show

CONTINUED ON PAGE 21

Break the midiprep speed limit.

New PureYield™ midiprep delivers transfection-ready DNA in only 30 minutes. You choose the format – spin or vacuum. No more post-elution alcohol precipitation. Race through your next plasmid midiprep –

Request a FREE SAMPLE* at www.promega.com/pureyield

PROMEGA CORPORATION • www.promega.com

*Samples to qualified customers where available, while supplies last.

Promega

that the DJ-1 protein is expressed at aberrantly high levels in human breast and lung cancers and that the *DJ-1* gene negatively regulates an important tumor suppressor gene called *PTEN*. In so doing, *DJ-1* appears to activate a key cell survival pathway that is normally inhibited by *PTEN*, thereby preventing the death of tumor cells. Interestingly, another gene recently found to be mutated in hereditary Parkinson's disease, *PINK1* (Valente *et al.*, Reports, 21 May 2004, p. 1158), was originally identified as a gene induced by *PTEN*, raising the possibility that dysregulation of this critical cell survival pathway may underlie both diseases. — PAK

Cancer Cell **7**, 263 (2005).

GEOCHEMISTRY

Night and Day, You Are the One

The hydroxyl (OH) radical is a highly reactive atmospheric component that is involved in many important chemical reactions in the troposphere, particularly the oxidation of organic compounds. One important pathway for OH formation is the photolysis of nitrous acid (HONO), which accumulates in the lower troposphere at night and serves as a significant source of OH radicals in polluted air in the early morning. A daytime source of HONO has been proposed, on the basis of measurements showing higher-than-predicted HONO concentrations during the day.

Kleffmann *et al.* now report direct measurements of nitrous acid and hydroxyl radicals in the atmosphere at a forest site in Jülich, Germany. Their results establish the existence of an efficient daytime formation process for HONO, because they also measured the photolysis frequency of HONO, the other parameter needed to assess the size of the daytime HONO source. They conclude that HONO contributes substantially to the local primary OH production and that it may have an important influence on the oxidation of biogenic volatile organic compounds emitted by the forest. — HJS

Geophys. Res. Lett. **32**, 10.1029/2005GL022524 (2005).

HIGHLIGHTED IN *SCIENCE*'S SIGNAL TRANSDUCTION KNOWLEDGE ENVIRONMENT

Science's stke www.stke.org

Creating Birds of a Feather

Although feather development is known to depend on reciprocal signaling between dermis and epidermis, the mechanisms that program the feather patterns of a pigeon differently than those of a peacock or a parakeet have been unclear. Eames and Schneider exploited the difference in embryonic origin of the dermis and epidermis of the head and neck by exchanging premigratory neural crest cells (destined to form dermis) between quail and duck embryos. The spatiotemporal patterning of feather bud appearance in the two species is distinct—for instance, quail feather placodes start as a medial and two lateral rows along the cranial epidermis, whereas duck feather placodes first appear as rows over each eye—as are the size and spacing of the feather buds. Quail neural crest cells transplanted into duck, creating a "quck," accelerated feather development (consistent with the more rapid maturation of quail) and elicited feather buds with a quail-like pattern. The authors used in situ hybridization to investigate the timing of the expression of components and targets of the bone morphogenetic protein, Sonic Hedgehog, and Delta-Notch signaling pathways in these quail-duck chimeras and observed quail-like timing of gene expression in both quail-derived dermis and duck-derived epidermis. In contrast, duck neural crest delayed feather morphogenesis and the expression of signaling genes when transplanted into quail. The authors conclude that the plasticity with which host epidermis can respond to dermal instructions may promote the evolution of new patterns of feather development. — EMA

Quail-like (brown and black) and duck-like (white) feather development in the quck.

CREDITS: EAMES AND SCHNEIDER, *DEVELOPMENT* **132**, 1499 (2005)

Development **132**, 1499 (2005).

GE Healthcare

What do you call making protein purification easy right from the start?

Pure imagination brought to life.

GE Healthcare is the one name behind all the leading tools in biomolecular research. Our focus is on providing protein purification systems, columns and media that make drug discovery simpler and faster from the outset to help you compete more effectively. Innovations like HiTrap™ and HisTrap™ columns, which offer outstanding convenience and reproducibility. Or the ÄKTAdesign™ platform, combined with the seamless control of UNICORN™ software, which gives you speed, ease and confidence whatever your application or scale.

At GE Healthcare we never stand still. We're constantly working to improve our offering – finding new ways of bringing pure imagination to life, to give you even better performance in tomorrow's race.

Visit www.amershambiosciences.com/pureimagination

imagination at work

GE08-05

www.sciencemag.org

Science

1200 New York Avenue, NW
Washington, DC 20005
Editorial: 202-326-6550, FAX 202-289-7562
News: 202-326-6500, FAX 202-371-9227

Bateman House, 82-88 Hills Road
Cambridge, UK CB2 1LQ
+44 (0) 1223 326500, FAX +44 (0) 1223 326501

SUBSCRIPTION SERVICES For change of address, missing issues, new orders and renewals, and payment questions: 800-731-4939 or 202-326-6417, FAX 202-842-1065. Mailing addresses: AAAS, P.O. Box 1811, Danbury, CT 06813 or AAAS Member Services, 1200 New York Avenue, NW, Washington, DC 20005

INSTITUTIONAL SITE LICENCES please call 202-326-6755 for any questions or information

REPRINTS Ordering/Billing/Status 800-635-7171; Corrections 202-326-6501

PERMISSIONS 202-326-7074, FAX 202-682-0816

MEMBER BENEFITS Bookstore: AAAS/BarnesandNoble.com bookstore www.aaas.org/bn; Car purchase discount: Subaru VIP Program 202-326-6417; Credit Card: MBNA 800-847-7378; Car Rentals: Hertz 800-654-2200 CDP#343457, Dollar 800-800-4000 #AA1115; AAAS Travels: Betchart Expeditions 800-252-4910; Life Insurance: Seabury & Smith 800-424-9883; Other Benefits: AAAS Member Services 202-326-6417 or www.aaasmember.org.

science_editors@aaas.org (for general editorial queries)
science_letters@aaas.org (for queries about letters)
science_reviews@aaas.org (for returning manuscript reviews)
science_bookrevs@aaas.org (for book review queries)

Published by the American Association for the Advancement of Science (AAAS), *Science* serves its readers as a forum for the presentation and discussion of important issues related to the advancement of science, including the presentation of minority or conflicting points of view, rather than by publishing only material on which a consensus has been reached. Accordingly, all articles published in *Science*—including editorials, news and comment, and book reviews—are signed and reflect the individual views of the authors and not official points of view adopted by the AAAS or the institutions with which the authors are affiliated.

AAAS was founded in 1848 and incorporated in 1874. Its mission is to advance science and innovation throughout the world for the benefit of all people. The goals of the association are to: foster communication among scientists, engineers and the public; enhance international cooperation in science and its applications; promote the responsible conduct and use of science and technology; foster education in science and technology for everyone; enhance the science and technology workforce and infrastructure; increase public understanding and appreciation of science and technology; and strengthen support for the science and technology enterprise.

INFORMATION FOR CONTRIBUTORS

See pages 135 and 136 of the 7 January 2005 issue or access www.sciencemag.org/feature/contribinfo/home.shtml

EDITOR-IN-CHIEF **Donald Kennedy**
EXECUTIVE EDITOR **Monica M. Bradford**
DEPUTY EDITORS **R. Brooks Hanson, Katrina L. Kelner**
NEWS EDITOR **Colin Norman**

EDITORIAL SUPERVISORY SENIOR EDITORS Barbara Jasny, Phillip D. Szuromi; **SENIOR EDITOR/PERSPECTIVES** Orla Smith; **SENIOR EDITORS** Gilbert J. Chin, Lisa D. Chong, Pamela J. Hines, Paula A. Kiberstis (Boston), Beverly A. Purnell, L. Bryan Ray, Guy Riddihough (Manila), H. Jesse Smith, Valda Vinson, David Voss; **ASSOCIATE EDITORS** Marc S. Lavine, Jake S. Yeston; **ONLINE EDITOR** Stewart Wills; **CONTRIBUTING EDITOR** Ivan Amato; **ASSOCIATE ONLINE EDITOR** Tara S. Marathe; **BOOK REVIEW EDITOR** Sherman J. Suter; **ASSOCIATE LETTERS EDITOR** Etta Kavanagh; **INFORMATION SPECIALIST** Janet Kegg; **EDITORIAL MANAGER** Cara Tate; **SENIOR COPY EDITORS** Jeffrey E. Cook, Harry Jach, Barbara P. Ordway; **COPY EDITORS** Cynthia Howe, Alexis Wynne Mogul, Sabrah M. n'haRaven, Jennifer Sills, Trista Wagoner; **EDITORIAL COORDINATORS** Carolyn Kyle, Beverly Shields; **PUBLICATION ASSISTANTS** Chris Filiatreau, Joi S. Granger, Jeffrey Hearn, Lisa Johnson, Scott Miller, Jerry Richardson, Brian White, Anita Wynn; **EDITORIAL ASSISTANTS** Ramatoulaye Diop, E. Annie Hall, Patricia M. Moore, Brendan Nardozzi, Jamie M. Wilson; **EXECUTIVE ASSISTANT** Sylvia S. Kihara; **ADMINISTRATIVE SUPPORT** Patricia F. Fisher

NEWS SENIOR CORRESPONDENT Jean Marx; **DEPUTY NEWS EDITORS** Robert Coontz, Jeffrey Mervis, Leslie Roberts, John Travis; **CONTRIBUTING EDITORS** Elizabeth Culotta, Polly Shulman; **NEWS WRITERS** Yudhijit Bhattacharjee, Jennifer Couzin, David Grimm, Constance Holden, Jocelyn Kaiser, Richard A. Kerr, Eli Kintisch, Andrew Lawler (New England), Greg Miller, Elizabeth Pennisi, Charles Seife, Robert F. Service (Pacific NW), Erik Stokstad; Amitabh Avasthi (intern); **CONTRIBUTING CORRESPONDENTS** Marcia Barinaga (Berkeley, CA), Barry A. Cipra, Adrian Cho, Jon Cohen (San Diego, CA), Daniel Ferber, Ann Gibbons, Robert Irion, Mitch Leslie (NetWatch), Charles C. Mann, Evelyn Strauss, Gary Taubes, Ingrid Wickelgren; **COPY EDITORS** Linda B. Felaco, Rachel Curran, Sean Richardson; **ADMINISTRATIVE SUPPORT** Scherraine Mack, Fannie Groom **BUREAUS:** Berkeley, CA: 510-652-0302, FAX 510-652-1867, New England: 207-549-7755, San Diego, CA: 760-942-3252, FAX 760-942-4979, Pacific Northwest: 503-963-1940

PRODUCTION DIRECTOR James Landry; **SENIOR MANAGER** Wendy K. Shank; **ASSISTANT MANAGER** Rebecca Doshi; **SENIOR SPECIALISTS** Vicki J. Jorgensen, Jessica K. Moshell; **SPECIALIST** Jay R. Covert; **PREFLIGHT DIRECTOR** David M. Tompkins; **MANAGER** Marcus Spiegler; **SPECIALIST** Jessie Mudjitaba; **ART DIRECTOR** Joshua Moglia; **ASSOCIATE ART DIRECTOR** Kelly Buckheit; **ILLUSTRATOR** Katharine Sutliff; **SENIOR ART ASSOCIATES** Holly Bishop, Laura Creveling, Preston Huey, Julie White; **ASSOCIATE** Nayomi Kevitiyagala; **PHOTO RESEARCHER** Leslie Blizard

***SCIENCE* INTERNATIONAL**

EUROPE (science@science-int.co.uk) **EDITORIAL: INTERNATIONAL MANAGING EDITOR** Andrew M. Sugden; **SENIOR EDITOR/PERSPECTIVES** Julia Fahrenkamp-Uppenbrink; **SENIOR EDITORS** Caroline Ash (Geneva: +41 (0) 222 346 3106), Stella M. Hurtley, Ian S. Osborne, Peter Stern; **ASSOCIATE EDITOR** Stephen J. Simpson; **EDITORIAL SUPPORT** Emma Westgate; Deborah Dennison **ADMINISTRATIVE SUPPORT** Janet Clements, Phil Marlow, Jill White; **NEWS: INTERNATIONAL NEWS EDITOR** Eliot Marshall **DEPUTY NEWS EDITOR** Daniel Clery; **CORRESPONDENT** Gretchen Vogel (Berlin: +49 (0) 30 2809 3902, FAX +49 (0) 30 2809 8365); **CONTRIBUTING CORRESPONDENTS** Michael Balter (Paris), Martin Enserink (Amsterdam and Paris); **INTERN** Mason Inman

ASIA Japan Office: Asca Corporation, Eiko Ishioka, Fusako Tamura, 1-8-13, Hirano-cho, Chuo-ku, Osaka-shi, Osaka, 541-0046 Japan; +81 (0) 6 6202 6272, FAX +81 (0) 6 6202 6271; asca@os.gulf.or.jp **JAPAN NEWS BUREAU:** Dennis Normile (contributing correspondent, +81 (0) 3 3391 0630, FAX 81 (0) 3 5936 3531; dnormile@gol.com); **CHINA REPRESENTATIVE** Hao Xin, + 86 (0) 10 6307 4439 or 6307 3676, FAX +86 (0) 10 6307 4358; haoxin@earthlink.net; **SOUTH ASIA** Pallava Bagla (contributing correspondent +91 (0) 11 2271 2896; pbagla@vsnl.com); **CENTRAL ASIA** Richard Stone (+7 3272 6413 35, rstone@aaas.org)

EXECUTIVE PUBLISHER **Alan I. Leshner**
PUBLISHER **Beth Rosner**

FULFILLMENT & MEMBERSHIP SERVICES (membership@aaas.org) **DIRECTOR** Marlene Zendell; **MANAGER** Waylon Butler; **SENIOR SPECIALIST** Pat Butler; **SPECIALISTS** Laurie Baker, Tamara Alfson, Karena Smith, Andrew Vargo; **MARKETING ASSOCIATE** Deborah Stromberg

BUSINESS OPERATIONS AND ADMINISTRATION DIRECTOR Deborah Rivera-Wienhold; **BUSINESS MANAGER** Randy Yi; **SENIOR FINANCIAL ANALYSTS** Lisa Donovan, Jason Hendricks; **ANALYST** Jessica Tierney, Farida Yeasmin; **RIGHTS AND PERMISSIONS: ADMINISTRATOR** Emilie David; **ASSOCIATE** Elizabeth Sandler; **MARKETING: DIRECTOR** John Meyers; **MEMBERSHIP MARKETING MANAGER** Darryl Walter; **MARKETING ASSOCIATES** Karen Nedbal, Julianne Wielga; **RECRUITMENT MARKETING MANAGER** Allison Pritchard; **ASSOCIATES** Mary Ellen Crowley, Amanda Donathen, Catherine Featherston; **DIRECTOR OF INTERNATIONAL MARKETING AND RECRUITMENT ADVERTISING** Deborah Harris; **INTERNATIONAL MARKETING MANAGER** Wendy Sturley; **MARKETING/MEMBER SERVICES EXECUTIVE:** Linda Rusk; **JAPAN SALES AND MARKETING MANAGER** Jason Hannaford; **SITE LICENSE SALES: DIRECTOR** Tom Ryan; **SALES AND CUSTOMER SERVICE** Mehan Dossani, Catherine Holland, Adam Banner, Yaniv Snir; **ELECTRONIC MEDIA: INTERNET PRODUCTION MANAGER** Lizabeth Harman; **ASSISTANT PRODUCTION MANAGER** Wendy Stengel; **SENIOR PRODUCTION ASSOCIATES** Sheila Mackall, Amanda K. Skelton, Lisa Stanford; **PRODUCTION ASSOCIATE** Nichele Johnston; **LEAD APPLICATIONS DEVELOPER** Carl Saffell

PRODUCT ADVERTISING (science_advertising@aaas.org); **MIDWEST** Rick Bongiovanni: 330-405-7080, FAX 330-405-7081 • **WEST COAST/W. CANADA** B. Neil Boylan (Associate Director): 650-964-2266, FAX 650-964-2267 • **EAST COAST/E. CANADA** Christopher Breslin: 443-512-0330, FAX 443-512-0331 • **UK/SCANDINAVIA/FRANCE/ITALY/BELGIUM/NETHERLANDS** Andrew Davies (Associate Director): +44 (0)1782 750111, FAX +44 (0) 1782 751999 • **GERMANY/SWITZERLAND/AUSTRIA** Tracey Peers (Associate Director): +44 (0) 1782 752530, FAX +44 (0) 1782 752531 **JAPAN** Mashy Yoshikawa: +81 (0) 33235 5961, FAX +81 (0) 33235 5852 **ISRAEL** Jessica Nachlas +9723 5449123 • **TRAFFIC MANAGER** Carol Maddox; **SALES COORDINATOR** Deiandra Simms

CLASSIFIED ADVERTISING (advertise@sciencecareers.org); **U.S.: SALES DIRECTOR** Gabrielle Boguslawski: 718-491-1607, FAX 202-289-6742; **INTERNET SALES MANAGER** Beth Dwyer: 202-326-6534; **INSIDE SALES MANAGER** Daryl Anderson: 202-326-6543; **WEST COAST/MIDWEST** Kristine von Zedlitz: 415-956-2531; **EAST COAST** Jill Downing: 631-580-2445; **LINE AD SALES** Emnet Tesfaye: 202-326-6740; **SENIOR SALES COORDINATOR** Erika Bryant; **SALES COORDINATORS** Rohan Edmonson, Caroline Gallina, Christopher Normile, Joyce Scott, Shirley Young; **INTERNATIONAL: SALES MANAGER** Tracy Holmes: +44 (0) 1223 326525, FAX +44 (0) 1223 326532; **SALES** Christina Harrison, Gareth Stapp; **SALES ASSISTANT** Helen Moroney; **JAPAN:** Jason Hannaford: +81 (0) 52 789 1860, FAX +81 (0) 52 789 1861; **PRODUCTION: MANAGER** Jennifer Rankin; **ASSISTANT MANAGER** Deborah Tompkins; **ASSOCIATE** Amy Hardcastle; **SENIOR TRAFFICKING ASSOCIATE** Christine Hall; **SENIOR PUBLICATIONS ASSISTANT** Robert Buck; **PUBLICATIONS ASSISTANT** Natasha Pinol

AAAS BOARD OF DIRECTORS RETIRING PRESIDENT, CHAIR Shirley Ann Jackson; **PRESIDENT** Gilbert S. Omenn; **PRESIDENT-ELECT** John P. Holdren; **TREASURER** David E. Shaw; **CHIEF EXECUTIVE OFFICER** Alan I. Leshner; **BOARD** Rosina M. Bierbaum; John E. Burris; John E. Dowling; Lynn W. Enquist; Susan M. Fitzpatrick; Richard A. Meserve; Norine E. Noonan; Peter J. Stang; Kathryn D. Sullivan

AAAS
ADVANCING SCIENCE, SERVING SOCIETY

GetInfo

science.labvelocity.com

Get the lab product info you need — FAST

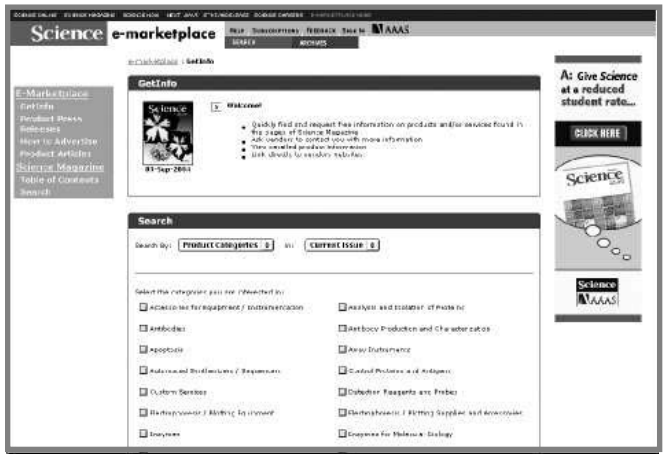

Science announces a new online life science product information system, **GetInfo**, powered by **LabVelocity**

- Quickly find and request free information on products and/or services found in the pages of *Science* magazine
- Ask vendors to contact you with more information
- View detailed product information
- Link directly to vendors' websites

Visit GetInfo today at
science.labvelocity.com

Science
AAAS

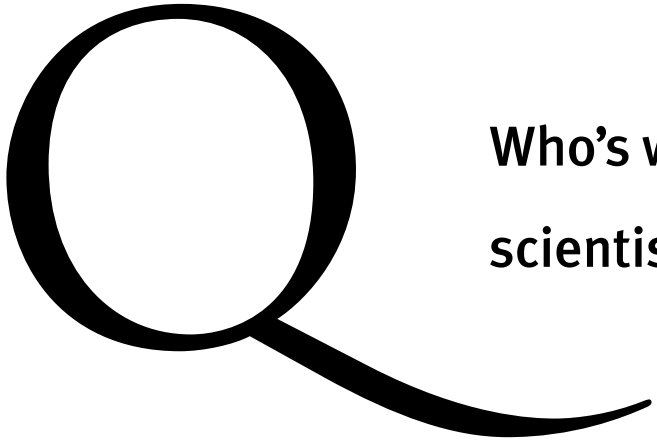

Who's working for tomorrow's scientists today?

"I read my *Science* with my kids. Theodore and Lillian enjoy the pictures of animals, people and planets as I browse through the magazine. It's a fun way for us all to learn more about science."

AAAS member Mark Petersen, post-doctoral researcher for the Climate, Ocean, and Sea Ice Modeling Group, Los Alamos National Laboratory, New Mexico

AAAS

Mark, Theodore and Lillian Petersen

AAAS is committed to advancing science and giving a voice to scientists around the world. We work to improve science education, promote a sound science policy, and support human rights.

Helping our members stay abreast of their field is a key priority for AAAS. One way we do this is through *Science*, which features all the latest breakthroughs and groundbreaking research, and keeps scientists connected wherever they happen to be. Members like Mark find it essential reading.

To join the international family of science, go to www.aaas.org/join

AAAS

ADVANCING SCIENCE, SERVING SOCIETY

www.aaas.org/join

NetWatch

edited by Mitch Leslie

EXHIBITS

Born to Count

Francis Galton (1822–1911) boasted a hefty fortune, wide-ranging curiosity, and the compulsion to measure or count almost everything, from the visual acuity of Londoners to the number of attractive women he passed on the street. The combination helped the English gentleman-scientist make a mark in fields as diverse as statistics, meteorology, and genetics. This virtual library from software engineer Gavan Tredoux of Rochester, New York, who's writing a book on the Victorian polymath, houses all of Galton's major texts and about 300 of his papers, letters, and other writings.

Galton's legacy includes the modern weather chart, which he created by marking locations on a map with the same barometric pressure. He gave fingerprinting a scientific foundation by showing that each person's prints are unique, and he devised the statistical techniques of correlation and regression. You can browse the paper in which he shot down his cousin Charles Darwin's hypothesis for inheritance. Galton, who coined the term "eugenics," was an early apostle of efforts to breed better humans. Readers can page through his 1869 work *Hereditary Genius*, in which he marshaled the pedigrees of English luminaries, including Darwin, to argue that ability was innate.

galton.org

DATABASE

Taking Aim at CREB

By switching on certain genes, the cyclic AMP response element–binding protein (CREB) helps govern processes from cell metabolism to the wiring of the nervous system. Researchers can find out which genes the influential protein activates at the new CREB Target Gene Database from Marc Montminy of the Salk Institute in La Jolla, California, and colleagues. Users can determine whether their favorite gene carries a sequence that CREB recognizes and whether CREB actually latches onto the gene, among other info. The data are for humans, rats, and mice.

natural.salk.edu/CREB

EDUCATION

Animating Possible Worlds

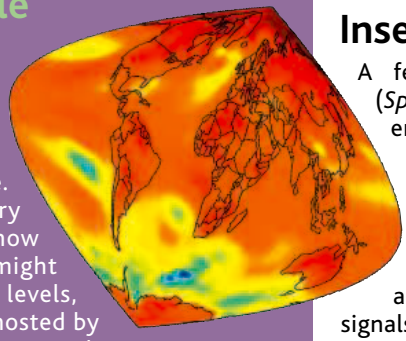

Global warming's future impact depends on factors such as human population growth and fossil fuel use. High school and introductory college classes can learn how these and other variables might influence temperatures, sea levels, and more at a new tutorial hosted by California State University, Los Angeles. The Java applet helps students work through scenarios for the future sketched by the Intergovernmental Panel on Climate Change. For example, animations illustrate flooding in areas such as Florida and Indonesia under different sets of conditions. These diagrams show global temperature increases in 2300 if rapid population growth continues (above), and if population stabilizes faster and countries introduce clean technologies more rapidly.

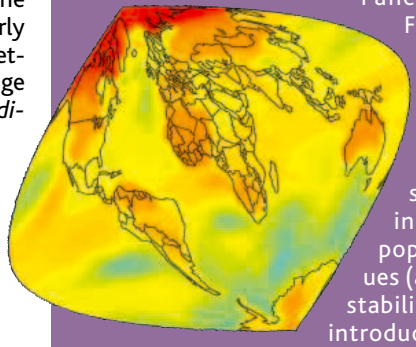

sciencecourseware.com/eec/GlobalWarming

RESOURCES

Scent of an Insect

A female African mantis (*Sphodromantis lineola*) entices males with an irresistible cocktail of the compounds pentadecanal and tetradecanal (below). Her eau de mantis is one of a multitude of chemical signals that insects deploy to announce their receptiveness for mating, mark the route to their nest, repel enemies, or induce other behaviors. Compiled by chemical ecologist Ashraf El-Sayed of the New Zealand–based company HortResearch, Pherobase matches some 3000 of these molecules with the creatures that emit them. For example, the house cricket's alarm signal contains acetic acid, isobutyric acid, and four other molecules. Click on a chemical to see its structure, a 3D model, and for some compounds, a mass spectrum.

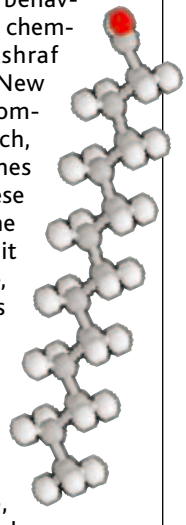

www.pherobase.com

IMAGES

Now Showing at the MicroPlex

A *Paramecium* twirls across the microscope slide, its cilia fluttering. A startled, trumpet-shaped *Stentor* retracts into a hole and then cautiously re-emerges. These microscopic denizens are among the stars of a gallery from the Natural History Museum in London. The site lets you play nearly 1500 short clips of protists oozing, darting, pulsating, and just hanging around. The films don't include descriptions, but they do give students a chance to see the creatures in action.

internt.nhm.ac.uk/jdsml/zoology/protistvideo

Send site suggestions to netwatch@aaas.org. Archive: www.sciencemag.org/netwatch

CREDITS (TOP TO BOTTOM): GALTON.ORG; CALIFORNIA STATE UNIVERSITY, LOS ANGELES; ASHRAF EL-SAYED/PHEROBASE

This Week

PAGE 35
Uproar in Italian universities

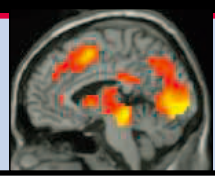

36
The roots of trust

U.K. BIOETHICS

Divided Committee Urges Less Restriction on Embryo Research

CAMBRIDGE, U.K.—The United Kingdom has some of the least restrictive rules in Europe governing research on human embryos. But in a wide-ranging and controversial report* issued last week, the House of Commons Science and Technology Committee argues that they should be relaxed even further: The report says the government should consider lifting the current absolute ban on research involving genetic modification of human embryos and the creation of chimeric human-animal embryos, and that it should even reopen debate on human reproductive cloning.

Some of the recommendations go against mainstream public opinion and venture into territory where many scientists are reluctant to go. And the committee is itself bitterly divided over the report's approach and conclusions: Five of its 11 members signed a statement disavowing the report, saying that the majority adopted "an extreme libertarian approach," producing a report that is "unbalanced, light on ethics, goes too far in the direction of deregulation, and is dismissive of public opinion and much of the evidence."

The report is part of a reevaluation of the country's regulation of medical and scientific use of human embryos. Reproductive research in the United Kingdom is regulated by the 1990 Human Fertilisation and Embryology Act, drawn up before mammals had been cloned or human embryonic stem cell lines created. The U.K. Department of Health requested the report from the parliamentary committee, led by biologist Ian Gibson, now a Labour member of parliament. The report "asks politicians and the public to justify any extra regulation or any legislative prohibitions in arguments of principle with potential harms to be based on evidence rather than myth or prejudice," Gibson said in a statement. Parliament would eventually consider any changes to the law.

Overall, the report argues that "alleged harm to society or to patients need[s] to be demonstrated" before research on reproductive technologies and their clinical use is "unduly impeded" by regulations. The panel offers more than 100 recommendations on specific issues. For example, it says that selection of embryos before implantation should be allowed solely on the basis of their sex. This flies in the face of British public opinion; 85% of the respondents in a 2002 poll said they were against sex selection for nonmedical reasons.

The report says there is no justification "at present" for changing the rule that research on embryos cannot be conducted beyond 14 days after fertilization. But it goes further, arguing that genetic modification of human embryos should be permitted during that 14-day period for research purposes—and perhaps sometime in the future for reproductive uses "under tightly controlled circumstances if and when the technology is further advanced." It also suggests that the government should consider relaxing the ban on the creation of hybrid or chimeric embryos if they are destroyed after 14 days. About such mixtures of human and animal cells or embryos, the report notes, "it could be argued they are less human, and therefore pose fewer ethical problems for research, than fully human embryos."

As for reproductive cloning, the report points out that it is not now safe and that ethics prohibits performing human experiments to work out the bugs. But the government needs to separate issues of feasibility from safety and ethical concerns and come up with principled arguments to maintain a total prohibition on reproductive cloning, the report says: "Without such arguments, an indefinite absolute ban could not be considered rational." One problem the report points to with an absolute ban is a gray area between reproductive and therapeutic cloning, such as the use of cloning techniques to create artificial gametes as an infertility treatment.

"I hope the report will encourage research," says geneticist Robin Lovell-Badge of the U.K.'s National Institute for Medical Research in London. He says the recommendation that research be permitted on human-animal chimeras is logical. "What is the difference between conducting experiments with human embryos up to 14 days and human-animal chimeras up to the same age?"

However, Stephen Minger, a stem cell researcher at King's College London, says "the views that are expressed [in the report] are very much different from those of researchers in stem cell work and reproductive medicine." About the recommendation on reproductive cloning, he says, "I'm a bit surprised that they say that's something we should consider. We already decided reproductive cloning should be banned." He adds: "I don't think it fosters public support to issue a report with so much dissension in it."

—MASON INMAN

Division of opinion. Ian Gibson says rules should be based on "evidence rather than myth or prejudice." (*Inset*) 4-day-old blastocyst.

* www.publications.parliament.uk/pa/cm200405/cmselect/cmsctech/7/7i.pdf

CREDITS (TOP TO BOTTOM): PHOTO BY DAVID GRAEME-BAKER; YORGOS NIKAS/PHOTO RESEARCHERS INC.

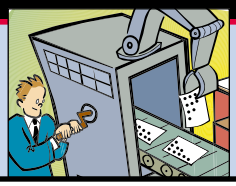

SELECT AGENTS

Researchers Relieved by Final Biosecurity Rules

In a move that many university researchers welcome, the government has slightly relaxed new regulations aimed at beefing up security at biodefense research labs. The final rules on "possession, use, and transfer of select agents and toxins" do not dictate exactly what procedures labs should use but instead allow for flexibility—an approach scientific groups had recommended. At least one critic says the rules are a step backward, however.

The new rules on handling select agents—viruses, bacteria, and toxins that could be used to harm people, crops, or livestock—were required by a bioterror law passed in response to the 2001 anthrax letter attacks. Interim rules issued in December 2002 by the U.S. Centers for Disease Control and Prevention (CDC) in Atlanta, Georgia, and the U.S. Department of Agriculture (USDA) require registration with the government and background checks for anyone handling select agents, and they call for security procedures such as keeping agents in locked containers. The rules also require prior approval from the Department of Health and Human Services (HHS) for genetic engineering experiments that can make an agent more toxic or resistant to drugs. Violations can result in fines and criminal penalties.

When the interim regulations were first issued, scientists and universities protested that they were confusing, expensive—up to $730,000 in start-up costs per lab—and could delay or impede research (*Science*, 21 February 2003, p. 1175).

The final rules, published in the 18 March *Federal Register*, should be more workable, says Emmett Barkley, who heads lab safety for the Howard Hughes Medical Institute in Chevy Chase, Maryland. One key change is that institutions will be allowed to tailor biosecurity plans to their own situations. The rules also now emphasize limiting "access" to select agents rather than securing a physical "area" or lab. This means biodefense researchers can share lab space with other researchers, and only those working with select agents have to undergo background checks. CDC now estimates that the total annual cost per lab will be $15,300 to $170,000.

Although the flexibility is good news, says Janet Shoemaker, public affairs director for the American Society for Microbiology (ASM) in Washington, D.C., universities will need more guidance. Depending on the agent, she says, "do you need guards 24 hours a day? Or are access cards and a locked freezer enough?" But helping institutions get up to speed shouldn't be too arduous, she notes; only 417 labs are now registered to handle select agents, less than half the number predicted when the interim rule came out, and just 105 are academic institutions. Biodefense labs will receive further guidance from CDC and USDA this spring, and more this summer in the latest version of the CDC/National Institutes of Health's biosafety manual.

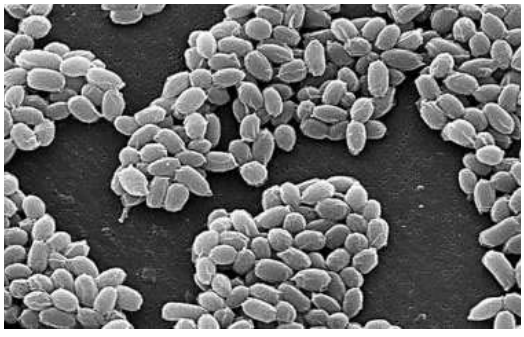

Handle with care. Final rule allows flexibility for labs dealing with agents such as anthrax.

Biodefense critic Richard Ebright, a microbiologist at Rutgers University in Piscataway, New Jersey, asserts that this relaxation of the rules increases the risk of accidents. In particular, he says, the focus on "access" rather than an entire lab "is especially egregious."

Government officials left some issues unresolved—for instance, CDC declined to modify the select agent list, as ASM and others have requested. The government is also "studying" whether other experiments, such as engineering a vaccine-resistant virus or aerosolizing an agent, should require special approval from HHS. **–JOCELYN KAISER**

INFECTIOUS DISEASES

A Puzzling Outbreak of Marburg Disease

As many as 120 people may already have died in northern Angola from what could become the largest recorded outbreak of Marburg virus, a rare cousin of the Ebola virus that also causes hemorrhagic fever. Early this week, experts were rushing to the scene armed with diagnostic equipment, hoping to stanch the epidemic and learn more about the mysterious disease, which has surfaced just six times over the past 4 decades.

To scientists, both the outbreak's location and its manifestation are unusual. Marburg was known to occur only in Eastern and Central Africa, and "based on geography, you'd think this had to be Ebola," says Thomas Geisbert of the U.S. Army Medical Research Institute of Infectious Diseases (USAMRIID) in Fort Detrick, Maryland. According to the World Health Organization (WHO), about 75% of cases occurred in young children, also strange for a hemorrhagic fever virus, says Thomas Ksiazek of the U.S. Centers for Disease Control and Prevention in Atlanta, Georgia, the lab that first identified Marburg almost 2 weeks ago in samples shipped from Angola. Initial sequencing, however, does not suggest it's an unusual strain, Ksiazek adds.

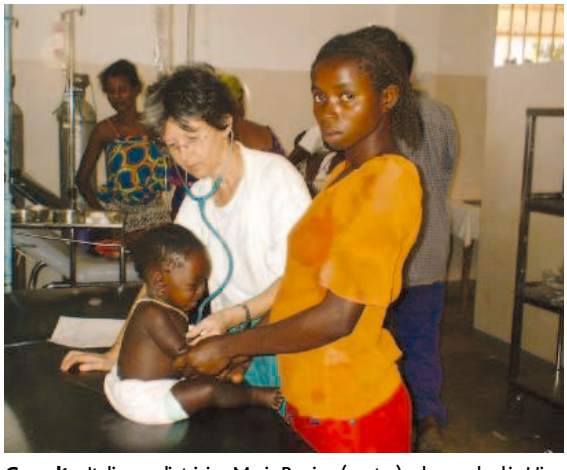

Casualty. Italian pediatrician Maria Bonino (center), who worked in Uige province, has died, presumably from infection with the Marburg virus.

Marburg—which can cause fever, pains, diarrhea, coughing, nausea, and hemorrhaging— ▶

CREDITS (TOP TO BOTTOM): JANICE CARR/CDC; DOCTORS WITH AFRICA CUAMM/HO/AP PHOTO

was first discovered in 1967, when a shipment of monkeys from Uganda caused simultaneous outbreaks in the German towns of Marburg and Frankfurt and in Belgrade, then the capital of Yugoslavia, sickening 31 and killing seven. Three small outbreaks are known to have occurred in Africa in the 1970s and 1980s involving six people, three of whom died. The largest outbreak so far occurred between 1998 and 2000 in the northeastern part of the Democratic Republic of the Congo, with 149 known cases and 123 deaths.

Although a few cases have been identified in the Angolan capital Luanda, the current outbreak is concentrated in the northern province of Uige, according to WHO, which has a team on the ground to help local authorities identify patients and raise awareness of the disease. Overcoming logistical hurdles in a poor, war-ravaged country like Angola can be a challenge, but stopping the outbreak shouldn't be "particularly problematic," Ksiazek says. Marburg is not highly contagious; infection requires close contact with a patient. Tracing and strictly isolating patients will usually bring the virus under control. But contact with patients can be risky: Several health care workers are reported to have died, including Maria Bonino, a pediatrician who worked in the area for CUAMM Medici con l'Africa, an Italian charity.

To help with diagnosis, virologist Heinz Feldmann and lab technician Allen Grolla of Canada's National Microbiology Laboratory left for Angola this weekend, carrying with them a mobile lab—small enough to fit in five or six suitcases—to test samples locally. Although stamping out the disease comes first, the team hopes to do some research as well, says Feldmann's colleague Steven Jones—for instance, by trying to find out which immune response protects some people from the disease.

The presumed animal reservoir for Marburg is still unknown, as is the reservoir for Ebola. Investigating the first cases in the current outbreak, which occurred as early as November, may give researchers clues, says virologist Hans Dieter Klenk of the University of Marburg.

Besides offering supportive care, there's not much health workers can do for patients or those at risk of contracting the virus. There are currently no drugs or vaccines for Marburg. Feldmann and Jones have developed a live vaccine against Ebola that has shown promise in monkeys (*Science*, 14 November 2003, p. 1141), and recently the team reported that a similar vaccine for Marburg protected monkeys as well. USAMRIID researchers are trying several other vaccine and drug strategies, but all are years away from use in the field.

–Martin Enserink

SPACE EXPLORATION

Japan Weighs Moon and Beyond

Tokyo—Japan's space agency has drawn up a new vision for exploration that includes a crewed space program and a scientific base on the moon. But a new report by an outside panel of experts suggests that the agency, which is trying to erase the stain of several costly failures, already is trying to do more than its sagging budget can handle.

Next week, the Japan Aerospace Exploration Agency (JAXA) will lay out a 20-year vision for the agency that would move Japan into the elite circle of nations sending humans to the moon and beyond. The vision is more of a wish list than a plan, however, and would require vast new spending. And although details are sketchy ahead of the 4 April release, space scientists are already concerned that science might take a back seat in such a massive undertaking. "We are not yet confident about whether JAXA top management is really prepared to give proper attention to space science," says Takeo Kosugi, an astrophysicist at the Institute for Space and Astronautical Science (ISAS), a formerly independent body that is now a division within JAXA. "We will need to be continuously battling for a long time."

Hands-on. Dan Goldin presents report on improving mission success rates to JAXA's Keiji Tachikawa.

Hiroshi Matsumoto, a space radio scientist at Kyoto University who served on the committee drafting the vision, says that crewed missions are seen as a way to rekindle public support for space activities. "Otherwise, ordinary people are just not too excited about space," he says. But that blasé public attitude stems in part from "the poor reliability of Japan's spacecraft," says Hiroyuki Yoshikawa, an engineer and former president of the University of Tokyo whose research has focused on manufacturing reliability. ▶

CREDITS (TOP TO BOTTOM): P. BAGLA; COURTESY OF JAXA

ScienceScope

India Rewrites Patent Laws

New Delhi—In a move drawing praise from drug companies and complaints from public health activists, the Indian Parliament last week passed a new patent law. The law paves the way for India's entry into the World Trade Organization.

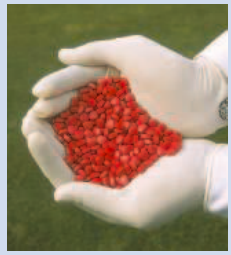

India exports an estimated $4 billion worth of generic drugs each year. Most were initially developed and marketed by Western drug companies under laws that allow a company to patent processes but not products. The new regime "marks India's commitment to move from imitation to innovation," says Raghunath Anant Mashelkar, president of the Indian National Science Academy.

But AIDS activists fear the new law will stifle the flow of cheap generic antiretroviral drugs to poor patients. "New medicines will only be available for the rich, while old treatments will be the only ones available to the poor," says Ellen 't Hoen of the Geneva-based Campaign for Access to Essential Medicines. Besides providing protection for medicines, the statute prohibits the patenting of plants and microorganisms. In an effort to keep drugs affordable, the law also requires firms to provide compulsory licenses to competing companies.

–Pallava Bagla

U.K. to Review Primate Use

Four of the U.K.'s leading medical and scientific organizations have decided to review the scientific and ethical basis for using nonhuman primates in biomedical research.

Last year, activists forced Cambridge University to abandon plans for a primate research center (*Science*, 30 January 2004, p. 605) and halted construction of an animal research facility at Oxford University (*Science*, 23 July 2004, p. 463). But a spokesperson for the Royal Society, one of the groups involved, says the impetus for the review is scientific advances in alternatives to animal testing, not increasing pressure from animal-rights groups. The Academy of Medical Sciences, Medical Research Council, and Wellcome Trust are also participating.

In a statement, the British Union for the Abolition of Vivisection welcomed the effort but worried that it "will be little more than propaganda to alleviate growing scepticism amongst the general public."

–Fiona Proffitt

Space advocates see the successful February launch of a weather satellite aboard the error-plagued H-2A rocket as a shot in the arm for JAXA, which was created in 2003 by combining ISAS with two agencies focused on the commercial development of space and on aeronautics. In February 2000, an ISAS M-V rocket failed to place in orbit the Astro-E satellite, intended to study high-energy x-ray sources such as black holes. In December 2003, ISAS's Nozomi probe to Mars missed its target because of thruster problems.

The agency's other components have suffered similar setbacks. Over the past decade, three of the country's 13 heavy rocket launches have failed, and two Earth observation satellites lost power due to problems with their solar panels. Government spending on space has dropped by 20% since a 1999 peak that included the completion of commitments to the international space station.

Back in business. A successful launch of the H-2A rocket in February has improved morale at JAXA.

The failures led to soul-searching at JAXA, which last summer assembled a seven-member Advisory Commission for Mission Success "to see if there were structural or systemic issues within the organization that were contributing to the problems," says Yasushi Horikawa, a JAXA associate executive director. The commission was headed by Daniel Goldin, former head of NASA, and included the former heads of both France's and Germany's national space agencies.

The group's report, submitted last week, listed 21 steps that, "if properly implemented, could allow JAXA to significantly improve" its performance. The report recommends that the agency "resolve the discrepancy between JAXA's broad mandate of mission activities … and its budget." It also urges better integration of the previously separate parts into "one JAXA" with a unified vision and strategic plan.

Kosugi agrees that closer cooperation among the different arms of JAXA could lead to greater sharing of proven technologies for things such as satellite power systems. But Kosugi adds that the merger is already having a negative effect on basic science. A planned launch this winter of a replacement for the Astro-E satellite lost in 2000 was pushed back to this summer, he notes, to make room for the H-2A launch.

The commission also wondered whether Japan's space activities are too extensive for its $1.7 billion budget, which is dwarfed by the $5.4 billion that Europe collectively spends and NASA's $16 billion pot. Despite that disparity, it notes, JAXA has a portfolio that matches those of its rivals in conducting basic science and earth observation missions, launching communications and weather satellites, developing new rockets, and providing components for the space station. Trying to do so much with limited resources, it suggests, may have contributed to the previous failures.

–DENNIS NORMILE

FRENCH SCIENCE

Politician Sails Into a Storm at Oceans Agency

PARIS—Scientists at the French oceanographic research agency Ifremer are furious that a nonscientist with strong political connections has been parachuted in as their director. The new arrival, Jean-Yves Perrot, began work last week, replacing Jean-François Minster, a respected physicist and former official at the main French research agency, CNRS. Minster had sought a second 5-year term as chief of the semipublic Ifremer but was turned down in order to clear the way for Perrot, research union officials say.

Perrot, an adviser to former Finance Minister Hervé Gaymard, found himself out of a job when the minister resigned in February over a housing scandal. Gaymard had rented a 600-square-meter apartment at taxpayers' expense and was accused of misusing public funds. He denied the allegations, but his contradictory statements led to embarrassing press reports, ending in his resignation after 3 months in office.

Mayor of the smart Paris suburb Marly-le-Roi, Perrot is a member of the right-wing UMP party and sits on the Ile-de-France regional council. He has no intention of giving up politics and "is under no obligation to abandon these posts," says an Ifremer official, who declined to be identified. "It is the first time that a politician with no background in science or technology and with important elected posts has been appointed head of a research institute" in France, according to a written statement from the union CFDT.

Biochemist Anne-Marie Alayse, a leader of the CGT union at Ifremer, complains that Perrot "knows nothing about research but will have to take important scientific decisions." Ifremer's $194 million budget supports studies of ocean ecosystems with the goal of aiding the maritime economy. Although Alayse acknowledges that Minster also encountered resistance when he pushed through an unpopular reform, he was unlike Perrot in that he arrived "with ideas in the pipeline," she says.

A graduate of the elite École Nationale d'Administration, Perrot has taught at leading political science schools and held high-level posts in the transport ministry since the mid-1990s. He was chief aide to Gaymard when Gaymard was agriculture, food, fisheries, and rural affairs minister starting in 2002 and became Gaymard's special adviser when the latter was promoted to finance last November.

Perrot dismisses the scientists' criticisms of his appointment. "I am a civil servant and a man of reflection, not a politician, and am not the first nonscientist to be appointed as head of a research agency in France," he tells *Science*. "I will consult all the experts necessary before I take any scientific decisions and will maintain the Ifremer objectives that have already been endorsed," he adds. He insists that political duties will not make him a part-time director. "My job as chief aide to a minister was at least as time-consuming as this one, and my political posts never prevented me from doing what I had to do."

–BARBARA CASASSUS

Barbara Casassus is a writer in Paris.

CREDIT: COURTESY OF JAXA

ITALIAN RESEARCH

Universities and Institutes Face Industrial Revolution

ROME, ITALY—A revolution is sweeping over Italy's universities and scientific community as Prime Minister Silvio Berlusconi's conservative government tries to align publicly funded research more closely with the needs of industry. While a university reform bill that aims to overhaul the structure and recruitment procedures for academic staff lumbers through Parliament, a stopgap government decree partly addressing some of the urgent measures in the bill passed into law this week. University rectors have declared much of it "totally unacceptable." Scientists are also uneasy about a national research plan for 2005–07, which was unveiled last month. Although it injects an additional $2.3 billion into science, it would require many scientists to build closer ties to industry. Berlusconi has called on companies "to make more effort" to similarly boost their R&D spending.

Italy's Ministry for Education, Universities, and Research, headed by Letizia Moratti, has been pushing this pro-business agenda since Berlusconi took power in June 2001. Her aim is to raise private investment and boost high-tech industry. This ties in with the European Union's goal, set out at a meeting in Lisbon in 2000, for member states to spend 3% of their gross domestic product on research by 2010.

Leading the charge. Letizia Moratti is trying to align publicly funded research with industry's needs.

CREDIT: RICCARDO DE LUCA/AP PHOTO

Italy currently spends about 1.2%—more than half of which now comes from public coffers. Berlusconi argues that attracting more industry investment will require reform of the universities and government research institutes. The decree that became law this week fixes an annual 31 March deadline for universities to submit their rolling 3-year programs and staffing requirements and, more controversially, it approves salary hikes for 22,000 entry-level researchers after just 1 year instead of the current three, although it provides no extra cash to pay for the raises. The decree also diverts 7% of university funding from public to private universities.

These measures, plus others in the bill, angered the College of Rectors. It sent a strongly worded letter to Moratti calling for a 10% increase in funding, as well as scrapping the researcher post in favor of a new position which leads more naturally to grades of associate and full professor. Moratti agreed to reconsider and sent the bill back to Parliament for reworking.

Government research centers are facing similar upheavals: The Institute for the Physics of Matter has been folded into the National Research Council (CNR), which itself has been restructured into strategic programs designed to appeal to industry (*Science*, 11 March, p. 1543). This policy is defended by CNR chief Fabio Pistella, who says "state funding is no longer sufficient."

Last month's national research plan continues this trend. The plan is built around 10 programs and creates 11 new technology "districts," each specializing in a particular field, such as telecommunications in Piemonte and nanotechnology in Veneto. The plan has divided scientists. Many are angered by the creation of new institutes—such as one in Lucca for innovation and marketing—when existing centers remain underfunded. But Umberto Veronesi, science director of the European Institute of Oncology in Milan, argues that a new biomedical center in the city—modeled on the National Institutes of Health's complex in Bethesda, Maryland—will help improve people's access to the latest treatments.

Aldo Schiavone, director of the Italian Institute for Human Sciences and a specialist in higher education policy, says the university reform bill provides a unique opportunity for a once-and-for-all overhaul of the academic career structure. The College of Rectors, he says, should seize the chance to modernize and not use it just to wring more resources from government. Moratti insists that achieving the Lisbon goals means the universities must look beyond their own interests to the needs of the private sector: "We need a vision that relates to the country as a whole."

–SUSAN BIGGIN

Susan Biggin is a writer in Trieste, Italy.

ScienceScope

Basic Microbiology Pushed

Seventy-seven intramural scientists at the National Institutes of Health (NIH) have joined calls for more funding of nonbiodefense microbiology.

In a 17 March letter to Director Elias Zerhouni, they argue that support is declining for basic microbiology. Although the plea echoes an open letter signed by more than 700 academic scientists last month (*Science*, 4 March, p. 1409) and cites similar grants data, the scientists are careful not to blame the purported drop on biodefense spending. The letter, organized by Michael Yarmolinsky of the National Cancer Institute, asks Zerhouni to form a committee to review the situation. NIH officials say support for nonbiodefense grants has held steady (see p. 49). **–JOCELYN KAISER**

Rees to Head Royal Society

Astrophysicist Martin Rees is in line to become president of the U.K.'s Royal Society. Holder of the honorary title Astronomer Royal and a professor at Cambridge University, the 62-year-old Rees has studied compact objects such as neutron stars and black holes and promoted the idea that quasars and active galactic nuclei are powered by supermassive black holes.

Next month the society's fellows will vote on the nominee, who would succeed ecologist Robert May and serve a 5-year term. "It's a great honor," says Rees.

–DANIEL CLERY

Report Finds Pay Imbalance

Women are paid 2% to 4% less than men at five of the six nonweapons laboratories of the Department of Energy (DOE), according to a recent report by the Government Accountability Office (GAO). The investigation also found that minorities at one of the six, Lawrence Berkeley National Laboratory, earn 2% less than whites in similar positions.

Released last week, the report comes a year after employees at weapons lab Los Alamos National Laboratory filed a lawsuit alleging wage discrimination against Hispanics and women. Employee groups that the GAO interviewed for the study complained of lack of support from senior management for efforts aimed at providing equal opportunity to women and minorities.

DOE has questioned the accuracy of GAO's findings, arguing that the study used a flawed statistical analysis. Besides, says Leah Dever, acting chief operating officer in the agency's Office of Science, the responsibility for ensuring fair treatment of employees at the labs rests with individual contractors and not with DOE. **–YUDHIJIT BHATTACHARJEE**

NEUROSCIENCE

Economic Game Shows How the Brain Builds Trust

As any economist will tell you, people don't always behave rationally when it comes to money. For instance, we sometimes trust complete strangers with our hard-earned dough. This suggests to many that a tendency to trust is hard-wired into the human brain.

Until now, little was known about the neural circuitry underlying the capacity to trust. But on page 78, neuroscientists and economists from Texas and California report an intriguing insight: Activity in a brain region called the caudate nucleus reflects one person's intention to trust another with a sum of money. Their results also suggest that trust isn't purely noble—it may stem from a cold calculation of expected rewards.

"I think it's a very important paper. It's going to change the way we think of social interactions," says Paul Zak, who directs the Center for Neuroeconomic Studies at Claremont Graduate University in California. "It's an exceedingly well done and rigorous study," agrees Paul Glimcher, a neuroscientist at New York University.

The research exemplifies the fledgling field of neuroeconomics, which combines the brain imaging tools of neuroscience with the exchange games economists have invented to probe how people behave during financial transactions. It's also one of the first studies in which the brains of two people were scanned simultaneously during a social interaction. Two volunteers played a trust game from inside functional magnetic resonance imaging scanners, one at the California Institute of Technology in Pasadena and the other at Baylor College of Medicine in Houston, Texas.

In each of 10 rounds, one player, the designated "investor," received $20. The investor then had the option of sending some, all, or none of the $20 to the other player, the "trustee." According to the rules of the game, which were known to both sides, any money the trustee received tripled. The trustee then had the option of returning a portion of the new sum to the investor. The players' only knowledge of each other came from numbers flashed on a monitor that indicated the amount of money changing hands in each round, as well as each player's total for the game.

The extent to which a player trusted another with his or her money depended on the recent history of the exchange. If an investor increased the contribution to a trustee immediately following a round in which the trustee had reduced payback, the trustee generally rewarded this benevolent reciprocity with a greater return in the next round. But if an investor demonstrated malevolent reciprocity by repaying generosity with stinginess, the trustee usually returned less the next time around.

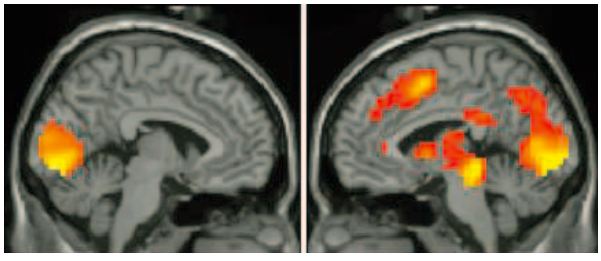

Tête-à-tête. Brain scans of the investor (*left*) and trustee in an economic exchange game shed light on the neural basis of trust.

Examining the trustees' brain scans, the researchers found that activity in the caudate nucleus was greatest when the investor showed benevolent reciprocity and most subdued when the investor showed malevolent reciprocity. Moreover, caudate activity rose and fell with changes in the amount of money trustees returned to their investors on the subsequent round. The team concludes that activity in a trustee's caudate nucleus reflects both the fairness of the investor's decisions and the trustee's intention to repay those decisions with trust (or not).

The caudate nucleus's "intention to trust" signal appeared about 14 seconds sooner in later rounds of the game, an indicator that the trustee is building an opinion of the investor's trustworthiness, says Read Montague, who led the Baylor team.

The caudate nucleus is well connected to the brain's reward pathways, and previous work has shown that it revs up when subjects expect a reward such as juice or money. Montague and colleagues speculate that trust, admirable trait that it is, boils down to predicting rewards—in this case, the "social juice" of the investor's reciprocity. Trust has been an element of human social interactions for many thousands of years, says Ernst Fehr, a neuroeconomist at the University of Zurich in Switzerland, so it makes sense that it would tap into ancient neural systems like the reward pathways.

–GREG MILLER

MATHEMATICS

'Cranky' Proof Reveals Hidden Regularities

Mathematicians crave patterns, and nowhere do they find richer pickings than in the theory of numbers. Five years ago, a breakthrough in a long-standing problem connected with one of the simplest functions of number theory yielded an unexpected bonanza of new patterns. Now, a new proof suggests that that was just the beginning. "It's almost certain that there will be more where this came from," says number theorist George Andrews of Pennsylvania State University, University Park, whose work helped pave the way for the new result.

The proof involves the partition function, which counts the number of ways you can reach any integer by adding other positive integers. For instance, the number 4 can be partitioned in five different ways: 1 + 1 + 1 + 1, 2 + 1 + 1, 2 + 2, 3 + 1, or simply 4 itself. In other words, the fourth "partition number" is 5. Similarly, the fifth partition number is 7. Partitions crop up throughout number theory and have proved handy for balancing energy budgets in particle physics.

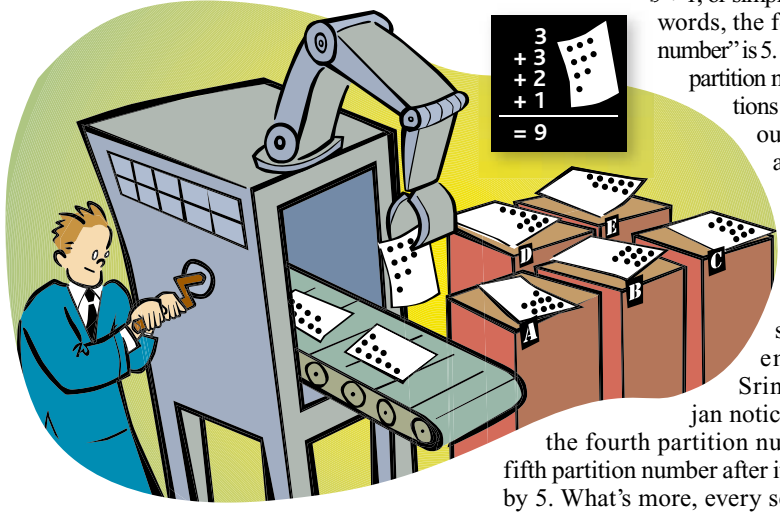

Sorting it out. "Rank" and "crank" functions divide partitions (above, of 9) into classes.

In 1910 or so, Indian mathematical genius Srinivasa Ramanujan noticed that not only the fourth partition number but every fifth partition number after it is also divisible by 5. What's more, every seventh partition number (beginning with 7) is divisible by 7, and every eleventh partition number ▶

CREDITS (TOP TO BOTTOM): R. MONTAGUE; TIM SMITH

(beginning with 11) is divisible by 11. There, mysteriously, the pattern stops.

Freeman Dyson, now a professor emeritus at the Institute for Advanced Study in Princeton, New Jersey, read about the pattern as a schoolboy in the 1940s and discovered an explanation for Ramanujan's first two observations. "It was my first real piece of research," he says.

Dyson defined what he called the "rank" of a partition: the largest number in a partition minus the number of terms in the partition. By noting that the partitions of 4, 9, 14, and so on could be sorted into five equal-sized bins according to rank, Dyson explained why the number of partitions in each case is divisible by five. Similar reasoning showed why the number of partitions of 5, 12, 19, and so on must be divisible by 7. Unfortunately, Dyson's rank formula didn't work for Ramanujan's third pattern, the one dealing with divisibility by 11. He conjectured that some other binning procedure, which he called a "crank," would explain that pattern, but he never found it. Andrews and another number theorist, Frank Garvan of the University of Florida, Gainesville, finally discovered the elusive crank in 1988.

Meanwhile, mathematicians had started turning up a few other patterns like Ramanujan's. In 2000, Scott Ahlgren of the University of Illinois, Urbana-Champaign, and Ken Ono of the University of Wisconsin, Madison, hit the jackpot. Using methods similar to those that Andrew Wiles of Princeton University had used in 1994 to prove Fermat's Last Theorem, they showed that divisibility patterns in the partition function exist not just for 5, 7, and 11, but for *every* prime number greater than 3. For example, every 157,525,693rd partition number, beginning with the 111,247th, is divisible by 13. "Instead of two or three galaxies, they showed that there is a sky full of galaxies," Andrews says.

One of Ono's graduate students, Karl Mahlburg, set out to find a "cranky" proof of the newly discovered patterns, although Ono tried to warn him away from what he considered a hopeless task. "I admit to a certain ignorance," Mahlburg says. "There were a lot of things that could have gone wrong." The effort paid off. In a paper submitted to *Annals of Mathematics*, Mahlburg shows that for prime numbers p bigger than 11, the crank does *not* divide the partitions into equal-sized bins—but it *does* group them in multiples of p. Thus, in a slightly different way, the crank accounts for Ono's congruences after all.

Next, Mahlburg says he plans to use a computer to find new divisibility patterns in the crank function itself. Andrews says he is eager to see what happens when Ono and his students try the Wiles-like technique out on other functions of interest in number theory.

–DANA MACKENZIE

Dana Mackenzie is a freelance writer in Santa Cruz, California.

CREDIT: JAKE FREIMER

ACADEMIC JOBS

Tenured UCLA Professor Under Fire

The University of California, Los Angeles, is taking steps that could lead to the firing of tenured biomathematics professor Sally Blower, accusing her of threatening students and harassing faculty, according to documents supplied to *Science* by Blower and her husband, UCLA geneticist Nelson Freimer. Blower, who left the University of California, San Francisco, 5 years ago with Freimer after accusing the university of gender discrimination (*Science*, 7 April 2000, p. 26), says the charges are false. UCLA administrators declined to comment, citing confidentiality rules.

According to the documents, UCLA Vice Chancellor Donna Vredevoe last week referred five charges against Blower to the school's Committee on Privilege and Tenure, which will help decide Blower's fate. The charges include "failure … to hold examinations as scheduled," "use of the position or powers of a faculty member to coerce the judgment or conscience of a student," and "verbal abuse, false statements, disparagement, and harassment of faculty."

Imminent departure? UCLA's Sally Blower and her husband Nelson Freimer say the school is trying to push her out.

The charges are only the latest storm surrounding Blower. On 12 November 2004, the dean of the UCLA School of Medicine, Gerald Levey, served Blower notice that she was barred from entering the biomathematics administrative offices pending resolution of charges filed in June. The November letter accused Blower of causing hives and increased blood pressure in two department administrators because she allegedly refused to leave their offices until security was summoned. Blower denies intimidating the administrators, noting that the incidents left her "almost in tears."

Several individuals familiar with the case say it appears to have spiraled out of control. "Honestly, I can't figure out why there's such a commotion," says gastroenterologist Peter Anton, who directs UCLA's Center for HIV and Digestive Diseases and has collaborated with Blower on HIV models for several years. "Certain personalities don't click well—but those usually seem to be resolvable without polarization, without … having to isolate and discredit a faculty member." Anton, who filed a letter in support of Blower, adds that he hasn't "seen any evidence of egregious behavior" on her part.

Blower is particularly incensed by the charge that she threatened students. In one case, she says, she is accused of threatening to withdraw as thesis adviser to Emily Kajita, then her only graduate student. Blower says she did e-mail Kajita saying the department was impeding her ability to advise students, but the two chose to proceed. Kajita praises Blower as "the best adviser you could ever have," adding that Blower paid nearly $4000 to cover her living expenses when Kajita was struggling to find graduate school funding.

Blower traces the charge of failing to hold exams to a September 2002 qualifying exam she postponed to attend the funeral of a close family friend in San Francisco.

Blower does admit to sending "rude e-mails" to members of her department but says she wouldn't have done so if they had responded to her inquiries for financial information and for room scheduling, so she could hold classes.

Blower joined the biomathematics department in 2000 after she and her husband struck a deal with UCLA. The university was aggressively recruiting Freimer, who said he would come only if his wife were also offered a tenured position. Blower says she was made to feel "invisible" by a department she had hoped to shake up, for example, by boosting the profile of its graduate program.

"There is a huge other side to this story; unfortunately, I can't divulge any of that," says David Meyer, senior associate dean for graduate studies at UCLA's medical school and one of those who filed a complaint against Blower.

Now, Freimer says that "without a doubt" he will leave UCLA if Blower is terminated. Even if she's found not guilty, he says, "my feelings about the place are so negative" that he might depart anyway.

–JENNIFER COUZIN

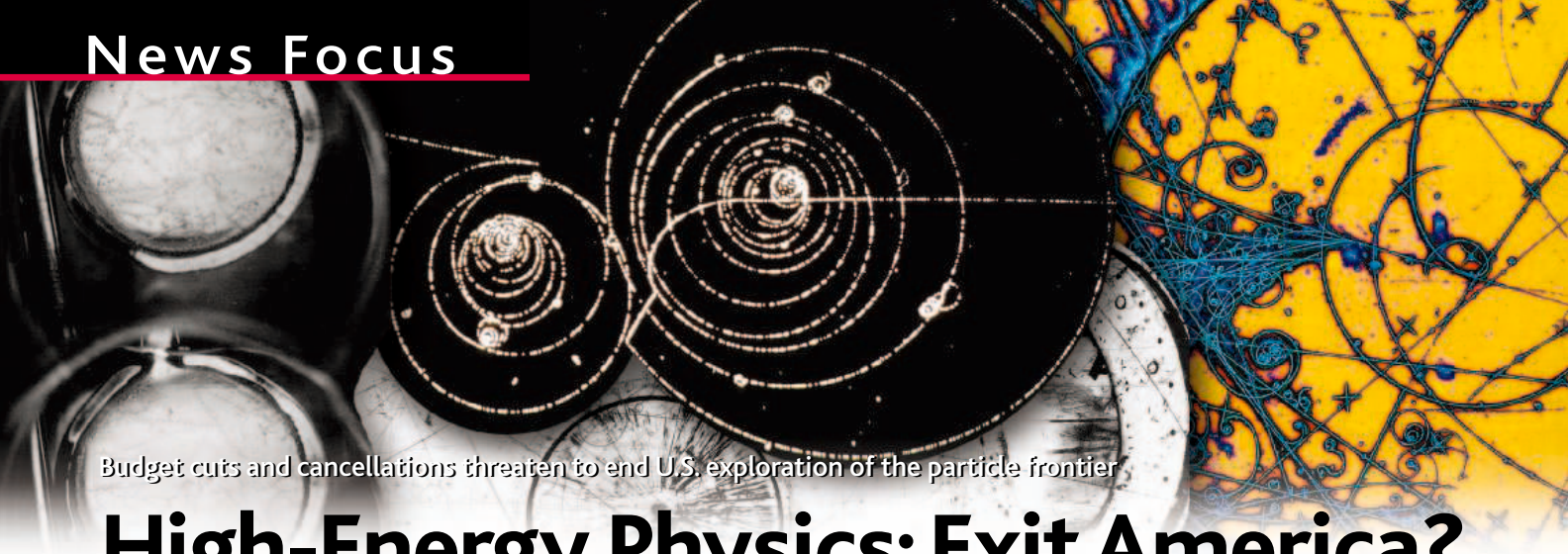

Budget cuts and cancellations threaten to end U.S. exploration of the particle frontier

High-Energy Physics: Exit America?

Monday, 7 February, was a grim day for the Fermi National Accelerator Laboratory (Fermilab). "You wake up, you go to a presentation, and you find out you're dead," says Fermilab physicist Joel Butler. Butler is co-spokesperson of an experiment known as BTeV—a multimillion-dollar project that would allow scientists to study the properties of the bottom quark. But that Monday, when the new Secretary of Energy Samuel Bodman took to the podium to announce the department's budget request for 2006, BTeV scientists were horrified to discover that their project had been canceled.

The decision—which is unlikely to be reversed by a Congress that doesn't have extra money to spend—sent ripples throughout the high-energy physics community. BTeV was the only planned project to study the physics of heavy fundamental particles at Fermilab, which is rapidly becoming the last of what was once a handful of U.S. labs devoted to the study of high-energy physics. Even under the most sanguine projections, the chances are good that no traditional accelerator experiments will be running on U.S. soil after 2010. And if a new linear collider that the Department of Energy (DOE) is gambling heavily on never materializes, the Nobel-filled record of U.S. achievements in high-energy physics could be consigned to history.

"The U.S. program is very weak looking to the future," says Michael Witherell, the outgoing director of Fermilab in Batavia, Illinois. "It's something we have to think very hard about: Is the U.S. getting out of that game?"

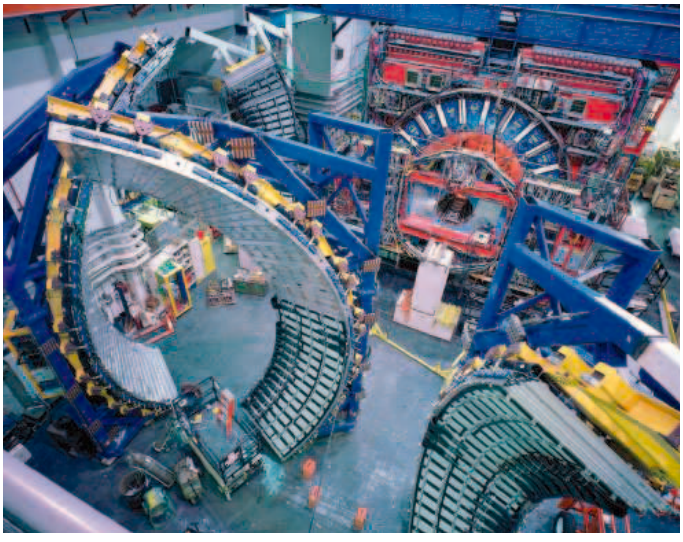

Swan song? Fermilab's Tevatron, due to shut down around 2010, could be the last large particle accelerator in the United States.

Heavy reality

Just as microbiology has its microscopes, high-energy physics has its accelerators. And the bigger the machine, the better physicists can see into the subatomic world.

Particle accelerators are machines that turn energy into matter. Using powerful magnetic fields, they force subatomic particles such as electrons or protons to move faster and faster until they approach the speed of light. When those particles smash into a target, they dump that energy in a sudden flash—and, in that instant, particles leap into existence out of the vacuum, born of the pure energy of the collision. As those particles interact and decay, they leave behind a shower of debris. Physicists root through those debris to figure out what, precisely, took place; the curling and branching trails of particles skittering away from the collision reveal the nature of the exotica that were brought to life for a fraction of a second.

But the exotica you can create are limited by the amount of energy your accelerator can dump into a small space. (In fact, high-energy physicists describe the mass of particles with units of energy: MeV, millions of electron volts.) Broadly speaking, the more powerful your machine, the heavier and more exotic the particles you create and the deeper you look into the laws that govern matter and the forces of nature.

In the mid-1950s, the building-sized Bevatron accelerator at Lawrence Berkeley National Laboratory in California led to the discovery of the antiproton (938 MeV). By the 1970s and 1980s, accelerators no longer fit within a single building. Such an enormous accelerator at CERN, a high-energy physics laboratory created outside Geneva in the 1950s to pool Europe's scientific resources, enabled scientists to spot the W and Z particles, carriers for the weak force that weigh in at about 80,000 MeV and 90,000 MeV respectively. In 1995, Fermilab's Tevatron, roughly 1000 times more powerful than the Bevatron, discovered the top quark (174,000 MeV). And the biggest accelerator of all—the 90-kilometer proton-proton smasher called the Superconducting Super Collider—was killed off in 1993 while still under construction in Texas.

Although these projects were the flagship "discovery" experiments of particle physics, there were others that didn't rely on brute force. By looking at how particles (such as B mesons) interact at slightly lower energies, scientists can infer properties of higher-mass particles—even if they have yet to be discovered. These two types of projects and other high-energy experiments have led to a very effective description of the fundamental components of matter and the forces that affect them: the Standard Model.

But the Standard Model is incomplete, and high-energy physicists believe that they are on the edge of two major discoveries that

CREDITS (BANNER, CLOCKWISE FROM LEFT): ERNEST ORLANDO LAWRENCE BERKELEY NATIONAL LABORATORY; CERN GENEVA; CERN GENEVA; FERMILAB; (BOTTOM): FERMILAB

will bust it wide open. The Large Hadron Collider (LHC) at CERN, the biggest accelerator in history, will come on line in 2007 or so. For a variety of reasons, physicists believe that it may well spot a particle known as the Higgs boson, a particle that will expand the Standard Model to explain why particles have mass. Many scientists also believe that the LHC will spot a "supersymmetric" particle, the first of a whole class of new fundamental particles that lie beyond the Standard Model—and that may be responsible for most of the matter in the universe. When it does, physicists hope to use the next great accelerator under consideration, the International Linear Collider (ILC), to zero in on those fresh discoveries and give theorists the ability to extend the Standard Model to a truly all-inclusive theory of matter (*Science*, 21 February 2003, p. 1171).

Yet even as high-energy physicists anticipate great discoveries in the next decade, the high-energy physics budget in the United States is dropping. This year, DOE, which funds the vast majority of high-energy physics in the United States, requested $716 million for high-energy physics, a decline of about 3% from the previous year. The cut follows years of stagnant budgets that have left labs with barely enough funding to run existing experiments, much less start new projects. "We're running at a lower level than we'd like," says Ray Orbach, head of DOE's Office of Science. "How can we run the current facilities, support current people, and at the same time have a future? That's the central question."

That future looks bleak. "There is no new money," says Robin Staffin, head of DOE's office of high-energy physics, who says that there is insufficient funding to start new projects. "Any new initiatives will have to come from redirection."

A new direction

That redirection caught BTeV scientists off guard. "I was surprised by this," says physicist Sheldon Stone of Syracuse University in New York, co-spokesperson for BTeV. "There was no advance information to either us or to the Fermilab group." Even Fermilab Director Witherell says that he didn't know about BTeV's cancellation until the day of the speech. "The first I found out was when I downloaded the budget from the Web site [that morning]," he says. "It was a shock: There was nothing to replace it, and $20 million was cut from the budget."

"It's looking very difficult in the U.S.," says Roger Forty, deputy spokesperson of LHCb, a similar B-physics experiment that will start up at CERN when the LHC turns on. "From a global perspective, it's a pity."

According to DOE officials, BTeV had to die. "We did not see in our budget how to accommodate this," says Staffin. Orbach agrees that DOE had no alternative but says the decision saddened him: "It's a downer."

The decision to cancel BTeV weakens the program at Fermilab, which will soon be the last remaining high-energy physics laboratory in the United States. Brookhaven National Accelerator Laboratory in Upton, New York, has shifted its focus to nuclear physics, although its plans to host a heavy-particle project known as RSVP recently took a hit after an apparent jump in its projected cost (*Science*, 18 February, p. 1022). The Stanford Linear Accelerator Center (SLAC), which is currently using a collider to produce B mesons, will shut down its B factory in 2008 or so to focus on generating x-ray beams for studies of chemical bonding and other high-speed phenomena on the molecular scale. "Fermilab is the future of high-energy physics in the United States," says Orbach.

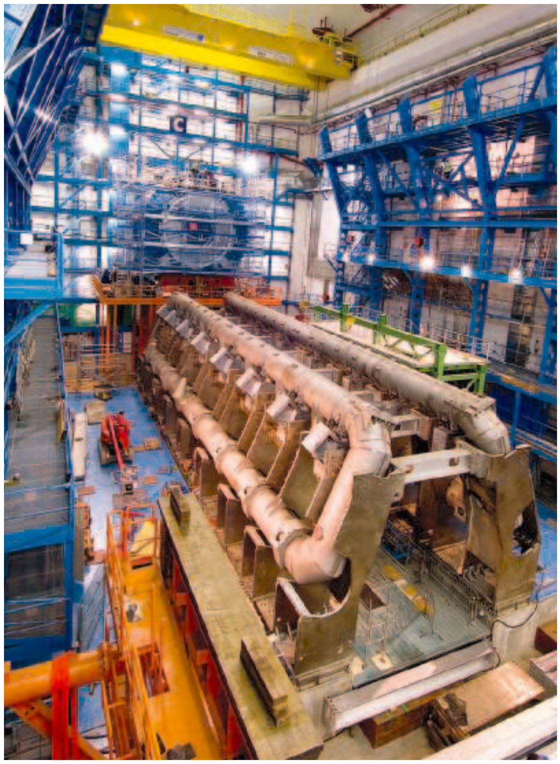

Next big thing. The Large Hadron Collider in Geneva should ensure European dominance of high-energy physics.

CREDIT: CERN GENEVA

Yet Fermilab's future direction is uncertain. The Tevatron will also likely be shutting down in 2010 or so. Unless a new project comes along, after that date the laboratory will not be using its equipment to study quarks at all. And until the ILC turns on—if it ever does—Fermilab and the United States will be out of the traditional high-energy physics game. "This is the first time in my memory that there is nothing in line, no major items of equipment" being requested, says Witherell.

Given those realities, Orbach's pledge that DOE "will continue to support Fermilab" is less than reassuring to high-energy physicists. The support DOE has in mind would require moving away from Fermilab's traditional strengths—the physics of quarks and other heavy fundamental particles—toward areas such as neutrino physics.

In 2002, Fermilab scientists began running MiniBooNE, smashing protons from a Fermilab accelerator ring into a target. The resulting neutrinos are steered to a nearby detector in hopes of learning some of the fundamental properties of those nearly massless particles. Last month Fermilab launched NuMI/MINOS, in which a similar setup sends neutrinos to a detector in Minnesota (*Science*, 11 March, p. 1543).

Although the scientific community is excited about the new experiments—and two or three potential follow-ons to NuMI/MINOS—the shift from studying quark flavors and heavy particles to neutrinos has been an uncomfortable one for many Fermilab physicists. Even the neutrino scientists at Fermilab have their qualms. "This lab used to do so many kinds of physics," says Deborah Harris, a physicist working on the NuMI/MINOS experiment. "It's strange to put all your eggs into one basket. It's a very good basket and an important basket, but it seems strange to focus so narrowly."

Fermilab has not yet abandoned studying quarks and other heavy particles, and the Tevatron will likely run until the end of the decade. "We're going flat out," says Orbach about what he calls a "very vibrant" research program at the Illinois lab. "We're going to leave the Tevatron a burning hulk when we finish with it." Scientists at Fermilab and elsewhere in the United States are also collaborating on planned LHC experiments that will provide fresh opportunities for studying heavy particles. Furthermore, observing cosmic rays and other high-energy phenomena in the heavens might give scientists an indirect way of understanding fundamental particles, as would mineshaft experiments to find exotic dark matter.

Nevertheless, these experiments are not nearly as far-reaching (or expensive) as the accelerator-based experiments in which the United States excelled for so many decades. Combined with the new emphasis on neutrinos, DOE is steering Fermilab—and the high-energy physics community in the United States—away from its traditional strengths in accelerator physics and high-energy experimentation. "The thing I most worry about is that we're allowing an important line of our physics to atrophy because we

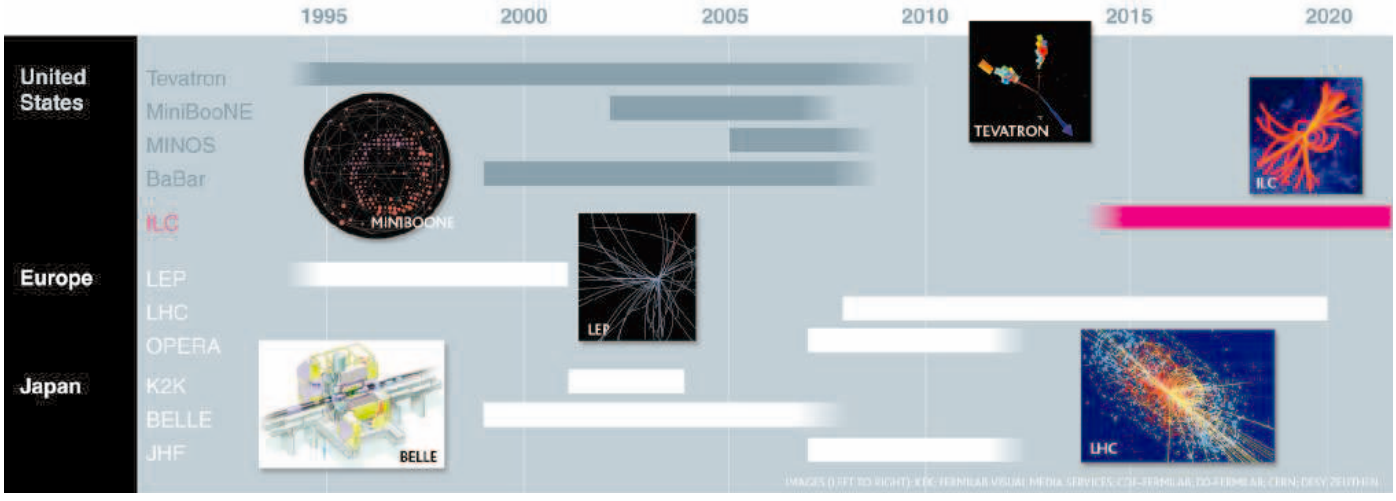

Wild card. An American site for the International Linear Collider would give the U.S. a stake in future experiments—if the ambitious project ever gets built.

can't afford it," says Witherell. "It's an area that the U.S. has always been a leader in. That's a problem."

To remain active, Fermilab's Butler says, "a large number of U.S. physicists at the Tevatron are already planning to work at the LHC; they have exit strategies." But Butler isn't happy about the new venue. "This field is being outsourced," he says.

The one big hope for U.S. accelerator physics is the ILC. "We're going to go for the linear collider," says Orbach. If based in the United States, the collider would not only give high-energy physicists a machine to explore Higgs and supersymmetry physics, it would also prevent a hemorrhage of heavy-particle physicists overseas. That's an appealing prospect to federal politicians. "We want the best minds in the world coming here and not going elsewhere. That's all to our benefit," says Speaker of the House Dennis Hastert (R–IL), who attended the recent start-up of the NuMI/MINOS experiment at Fermilab. But the leader of the majority party in the U.S. House of Representatives isn't ready to make a firm commitment. "If [the ILC] fits within certain parameters, we'd like to keep it in the U.S.," Hastert says.

The biggest of those parameters is the cost, estimated by DOE at $12 billion, of which the host country would presumably pick up half. "Now we have a unified program," says Orbach. "The problem is that it's too expensive." DOE might be able to handle a project of half that size, Orbach says, but the probability of joining a $12 billion project is slim.

The odds are better than that, says physicist Barry Barish of the California Institute of Technology in Pasadena, who heads the ILC design group. He doesn't accept DOE's projected price tag. "There's no way you can get me to talk about cost" until the design group completes some preliminary studies, he says. "But I don't buy $12 billion."

For Butler and other physicists, the projected completion date for the ILC in the middle of the next decade is another huge obstacle. "The schedules put up are frankly incredible and don't do justice to the effort," Butler says. But a timetable that puts the ILC at the end of the next decade or beyond would leave an entire generation of physics students without access to an accelerator in the United States.

Dark forecast. Outgoing Fermilab director Witherell wonders whether the U.S.'s "very weak" future program marks the end of the line.

All or nothing

In an attempt to make the best of a bad situation, high-energy physicists are reprioritizing their projects—again. The High Energy Physics Advisory Panel (HEPAP), which counsels DOE and the National Science Foundation, will apparently be resurrecting its Particle Physics Project Prioritization Panel—a subcommittee that disbanded at the end of 2003 after presenting its recommendations (which included strong support for BTeV). The National Research Council is busy preparing a report, *Elementary Particle Physics in the 21st Century*, that will do a similar job from a broader perspective (as many of the committee members are from outside particle physics). The goal is an attractive, unified program that lawmakers will be able to fund.

But these efforts may be moot if the budget situation doesn't improve. "What use is a 20-year outlook if you can't build anything?" Orbach rhetorically asked HEPAP physicists, who were likely wondering about the same question. Having priorities is not equivalent to having a budget, he adds, although such a list may improve DOE's chances of getting some of its projects funded.

Some high-energy physicists fear that their problems run far deeper, however. Perhaps, they speculate, the United States no longer considers high-energy physics very important, and comments by DOE officials provide little comfort. "Where society goes, the budget also goes," says Staffin. A major discovery—like the Higgs or supersymmetric particles—could win back public support, they say. But will U.S. labs be ready to respond?

Most labs, like SLAC and Brookhaven, will have stopped research in the field. Fermilab will be concentrating on a neutrino physics program and some smaller projects, with all its study of heavy fundamental particles taking place overseas. And if Congress doesn't make room in DOE's budget for the International Linear Collider, then there may be no active U.S. high-energy physics program to take advantage of a breakthrough should it come. "It's a gamble," Orbach admits about the road DOE is taking in high-energy physics. "We're going for broke."

–CHARLES SEIFE

CREDIT (BOTTOM): FERMILAB

Taking the Pulse of Earth's Life-Support Systems

A massive effort to document the state of ecosystems—and their ability to provide food, comfort, and other services—lays out some grand challenges, but no easy answers

The plan was nothing if not ambitious: assess the state of ecosystems across the entire planet, from peat bogs to coral reefs. Rather than solely chart pristine habitats and count species, as many surveys have done, the $20 million Millennium Ecosystem Assessment (MA) put people and their needs front and center. At its core was the question: How well can ecosystems continue to provide the so-called services that people depend on but so often take for granted? These include not just the food and timber already traded on international markets but also assets that are harder to measure in dollar values, such as flood protection and resistance to new infectious diseases.

In another novel approach, the assessment simultaneously examined this issue across a huge range of scales from urban parks to global nutrient cycles. The goal in each case, says director Walter Reid, was to offer policymakers a range of options that might help ecosystems recover or improve their role in providing for human well-being. The participants tried to make clear the tradeoffs involved in managing land; some methods of boosting crop yield, for example, exact a long-term price of degraded soils and incur downstream consequences such as fisheries stunted by fertilizer runoff. What's good for people in one region may cause harm in another place or time.

The project didn't aim to generate new data but to analyze and synthesize published, peer-reviewed research; even that was easier said than done. Some 1360 scientists from 95 countries spent countless hours poring over the literature, hashing out disagreements at meetings, and writing the first volumes of reports that will ultimately number some 3000 pages. In the process, they had to nail down nebulous terms such as biodiversity and cultural services and deal with the headaches of data gaps. "Doing a global assessment of ecosystem services poses huge problems; it really pushes the envelope," says an apparently indefatigable Reid.

There's broad agreement that the envelope has been filled with a valuable status report, the first overview of which was released this week. "It is a magnificent achievement," comments Stuart Pimm, an ecologist at Duke University in Durham, North Carolina, who reviewed parts of the effort. "There will be a 'Wow!' when people see this." But will it actually influence policy? Most say it's much too early to tell. Participants argue that the bottom-line focus boosts the odds for action. "This will make it much more relevant for policymakers," says Peter Bridgewater, secretary general of the Ramsar Convention on Wetlands, who was on the MA's board. "It's not just scientific dancing on the head of the pin."

Fragile. Drylands are some of the most delicate ecosystems in the world and face increasing demands, which could threaten efforts to fight poverty.

CREDIT: WOLFGANG KAEHLER/CORBIS

Ecosystem Services

Provisioning, including food, water, fuel, and fiber.

Regulating, such as the prevention of soil erosion and flooding.

Cultural, including recreation, spiritual values, and a "sense of place."

Basic support, including soil formation, nutrient cycling, and oxygen from photosynthesis.

Widespread degradation

The MA's first report,* a summary of the major technical reports to follow, identifies three main problems with how humans are managing ecosystems. Topping the list is widespread abuse and overexploitation of resources. Although some ecosystems have yielded more and more goods—principally fish, livestock, and crops—their integrity, and the productivity of many more, has been compromised. Of the 24 kinds of services described by the MA, 60% are being degraded, the report found. "We're undermining our ecological capital all around the world," says Robert Watson, chief scientist of the World Bank and a lead author.

Second, and a bit of a surprise to some, the degradation is probably hiking the risk of sudden, drastic changes in ecosystems, such as the collapse of fisheries or the emergence of new diseases from fragmented forests (see box, p. 43). "When we started, that was not something that scientists might have listed as a top conclusion," Reid says.

Finally, the pressure on ecosystems is disproportionately harming the poor. That's particularly true in the drylands of sub-Saharan Africa, central Asia, and Latin America, where a third of the world's population tries to make do with 8% of its fresh water. The report argues that healthy ecosystems are key to alleviating poverty and meeting other objectives in the U.N.'s Millennium Development Goals. "The rationale is that only by protecting and restoring the ecological function will you be able to adequately address hunger and poverty," says Jane Lubchenco of Oregon State University, Corvallis, who co-chaired a report to business and industry.

Another troubling trend is the intense disturbance of global nutrient cycles. Excessive use of nitrogen fertilizers has inadvertently led to the eutrophication of estuaries, algal blooms, massive fish kills, and contamination of groundwater. "The impacts are very large, with direct and sig-

* "Millennium Ecosystem Assessment Synthesis Report," www.maweb.org

Choose Your Own World

What will ecosystems be like in 2050? That depends on decisions made today, so to give policymakers an idea of the consequences, a Millennium Ecosystem Assessment (MA) working group envisioned what life would be like under four types of broad policies. For each of these scenarios, they used standard computer models that predict changes in variables such as gross domestic product, water use, and food production. Where no models were available, they relied on expert opinion to assess the role of technological innovation, human health, and other factors.

Some observers were frustrated at the lack of quantification and reliance on expert opinion. But most say the scenarios are a useful thought exercise. "It's a way of motivating thinking and stimulating the imagination, even at national levels, about the choices involved in ecosystem changes," says Jeffrey Tschirley of the U.N. Food and Agriculture Organization in Rome. "Based on decisions you make, you can create a different world."

"Order from strength." Perhaps not as bad as *Blade Runner*, the world has fragmented into regional markets and alliances. Nations are obsessed with security issues, and the tragedy of the commons deepens. Every category of ecosystem services takes a nosedive, and the developing world bears the brunt of the damage.

"Global orchestration." Free trade and a good heart reign in this scenario. There's no focus on preventing environmental problems, but an emphasis on fighting poverty. The result is a huge boost in food and other provisioning services from developing countries. The costs are borne by regulating services—such as climate change—and a loss in cultural services, such as ecotourism.

"TechnoGarden." Al Gore would love this world—globally connected with green technology abounding and a focus on preventing ecosystem problems. Food and other provisions rise, although they are not maximized. Climate change, floods, and disease are less of a worry. The downside is that biodiversity continues to decline.

"Adapting mosaic." The emphasis here is on low-tech, local solutions. Regional politicians and institutions focus on watershed-scale ecosystems to maximize benefits and prevent problems. If it catches on widely, it pays off: Every type of ecosystem service improves in both developing and industrialized nations. **–E.S.**

nificant consequences for human well-being," Reid says.

The report documents numerous other examples of how humans create problems when they try to wring more out of an ecosystem. Farming shrimp degrades water quality; cutting down forests to make charcoal worsens flooding downstream; rice paddies, cows, and slash-and-burn agriculture all pump carbon into the atmosphere, changing climate in ways that could ultimately hurt farmers. "The key point is that not everything is win-win," Watson says. The harm can stretch down a river or across the ocean, when dust from degraded African soils worsens air quality in North America. And it can pass from generation to generation, when actions today—depleting soil, for instance—compromise the ability of ecosystems to deliver goods and services in the future.

The severity of the problems becomes more tangible when costs are tallied in dollars. The MA cites a litany of examples including $2 billion spent to help communities recover from the crash of the Newfoundland cod fishery in the early 1990s and more than $70 billion worth of damage in 2003 from floods, fires, drought, and other disasters. Valuing the benefits of ecosystems, on the other hand, is still in its infancy. The MA didn't try to make such estimates itself but notes studies such as a 1998 estimate of $346 million in benefits from protecting water quality in the Catawba River, North Carolina.

Nor does the MA recommend particular solutions to broad environmental problems. Instead it lays out four visions of the future (see sidebar, above) that might result from various kinds of policies, such as changing the nature of agricultural subsidies to promote land conservation or investing heavily in green technologies. Effective action will be required, the report urges, and soon: Even though world population is expected to stabilize by 2050, the MA predicts that the challenges will be heightened by climate change and ever-more-voracious demand for resources.

Measuring the intangible

The idea for the global assessment was hatched in 1998 at the World Resources Institute (WRI) in Washington, D.C., where Reid and others were interested in taking a look at the state of the world's ecosystems at the turn of the millennium. Lingering in their minds was the fate of a previous overview, called the Global Biodiversity Assessment (GBA), that had gone essentially unnoticed after its release in 1995 (*Science*, 8 September 2000, p. 1676).

They quickly decided that the way to make a bigger impact would be to focus on goods and services. "You can talk about how ecosystems operate to policymakers, and their eyes glaze over. But if you mention services, they perk up," says Hal Mooney of Stanford University, a lead MA participant.

Watson, a veteran of many assessments—including the GBA—was deeply involved with the much more successful Intergovernmental Panel on Climate Change (IPCC) and decided to take a page from its design, which included winning broad support for the project from the get-go. Watson and Reid approached their target audiences, such as the Convention on Biological Diversity, and involved them on the board and in the design of the project. Various "stakeholders" chimed in on what would be of value to them.

Another key decision was to combine the big picture with many local assessments, ranging in scale from Peruvian villages to all of southern Africa. The reason for including targeted studies, says Reid, is that some ecosystem problems and services such as cultural benefits of green space are local, and decision-makers need specific information. For example, the Southern Africa assessment, the first of 17 such studies to be published, found that the region as a whole has an adequate supply of fuelwood but that there are several areas with severe shortages. At the same time, decisionmakers need to know what's going on globally, as decisions at a larger scale (such as government intervention in the international timber market) affect local communities.

Service. Walter Reid spent 6 years leading a dozen staff and 1300 volunteers.

Over the course of a year, a committee of about 90 scientists hashed out a conceptual framework: a box and arrows

CREDITS (TOP TO BOTTOM): JUPITER IMAGES; JUPITER IMAGES; MILLENNIUM ECOSYSTEM ASSESSMENT

that laid out the components of ecosystems and how to assess the services they provide. Definitions were ironed out for terms such as biodiversity ("the variability among living organisms from all sources … and the ecological complexes of which they are a part") and human well-being ("a combination of physical and social factors including shelter, health, freedom, and the ability to provide for children.")

Unpredictable Changes

Dead zones. Nutrient loading can cause sudden, widespread algal blooms that suffocate animals.

Fisheries collapse. After centuries of fishing, cod stocks in the Atlantic collapsed in 1992.

Alien invaders. Zebra mussels and other invasive species can be a complete surprise.

Forest feedback. Deforestation dries out a region, which can mean even more forest loss.

"Getting everyone to agree on definitions gets rid of the tower of Babel phenomenon," says Shahid Naeem of Columbia University in New York, enabling ecologists to collaborate with anthropologists and economists, for instance.

In an attempt to bring clarity to the nascent field of ecosystem services, the committee divided benefits into four categories: provisioning, regulating, cultural, and basic support (see box, p. 41). Mooney says this methodological framework, laid out in a 2003 book,† has been adopted widely, for example, by an international biodiversity consortium called Diversitas in Paris, France. This standardization should facilitate comparisons of ecosystem services between countries, notes Les Firbank of the Center for Hydrology and Ecology in Lancaster, U.K., who was not involved.

When the actual assessment got under way in April 2001, participants soon found themselves struggling with a critical lack of data. For example, remote-sensing data cover most of the world, but it was possible to extract an accurate description of land cover for only those parts of the world for which scientists had verified the satellite data. The whole exercise "gives us an understanding of how much data we don't have—and the really poor quality of data that we do have," says MA board member Jeffrey Tschirley of the U.N. Food and Agriculture Organization (FAO) in Rome.

Then came the equally tricky task of trying to link the state of ecosystems to human well-being in a rigorous way. "That's a surprising and unfortunate gap," Reid says. Most of the evidence is anecdotal, such as studies of the cost to replace the loss of natural pollinators or pest-eating bats. And although it's well established how to measure the costs and benefits of marketed ecosystem services, such as timber, much less is known about how to do that for other benefits, like the clean water provided by healthy watersheds.

Technical reports from the four working groups will be published this year, as will syntheses aimed for the health and business sectors and four sponsoring conventions. All will be available on the Web site www.maweb.org.

On the agenda

Although the MA reports don't contain any breaking news for ecologists, participants say the MA's main accomplishment is a consensus document that emphasizes that human well-being depends on healthy ecosystems. They hope that, like the IPCC, that consensus will help raise the issue higher on the priority lists of nations.

Beyond the rhetorical value, the collected data will likely be useful for national and local decision-makers, such as those calculating conservation subsidies to farmers or devising certification schemes for sustainable forestry. But that won't happen on its own, so key MA participants are trying to ensure that the report doesn't gather dust. "The outreach task for this is just huge, and we're just at the beginning," says Stephen Carpenter of the University of Wisconsin, Madison, who co-chaired the scenarios report. Robert Scholes of the Council for Scientific and Industrial Research in South Africa says he's been briefing policymakers ever since the southern African assessment was published 6 months ago, targeting key ministers and giving two to three talks a month. He expects to keep up the pace for at least a year more.

The convention leaders say that the MA will help them carry out their own work. In the Ramsar convention, for example, Bridgewater explains that the MA has better defined key terms in the wetlands treaty. Member nations had agreed to foster "wise use" of their wetlands and ensure that "ecological character" does not change; the framework has helped make that more explicit by focusing on long-term delivery of ecosystem services.

Although scientists and policymakers have lauded the MA, some are frustrated at the limits of its conclusions. The MA finds that ecosystems are being degraded, for example, but it couldn't say anything specific about the pace of that degradation or what levels of use are sustainable. That uncertainty can make it tougher to implement policies that cause economic losses in the short-term. The threat of various catastrophic ecosystem failures might make policymakers think twice, but no one knows how close society is to the brink. The report is "pretty anecdotal when it comes to thresholds," says Richard Norgaard, an environmental economist at the University of California, Berkeley. That's not the MA's fault but more a reflection of the immature state of the science, he adds.

What's needed to help design effective policy is more quantification and dollar values of ecosystem services, says FAO's Tschirley. "That's where there is a payoff; that's when it gets value for development and when things can be planned."

The MA was planned to provide a baseline for future assessments but not to organize them. Reid says that the working assumption is that if governments and the private sector find that round one was useful, they'll pony up for more. "If this really succeeds," Reid says, "then people will want to follow the model." Many scientists say that follow-ups will be key, as it took several rounds for the IPCC to work out its kinks. Follow-up assessments would also be a way to confirm trends in ecosystem services.

Regardless, a key legacy is the effect on ecologists and other environmental scientists. "It's been a really big force for shifting mindsets in the science community," says ecologist Gretchen Daily of Stanford University. "There's a whole community of people who are now abuzz with this effort."

—ERIK STOKSTAD

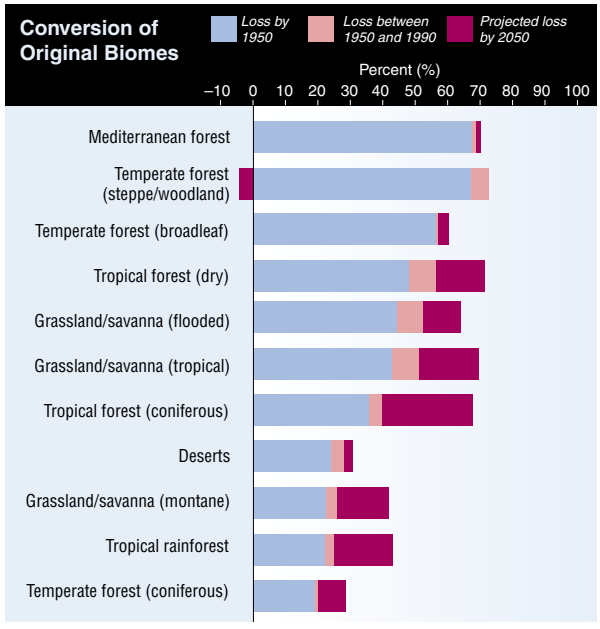

Going, going. Major ecological communities, or biomes, will be turned to farms and other purposes over the next 50 years.

SOURCE (GRAPH): MILLENNIUM ECOSYSTEM ASSESSMENT

† *Ecosystems and Human Well-Being: A Framework for Assessment* (Island Press).

Unnatural Amino Acid Could Prove Boon for Protein Therapeutics

San Diego, California—In this biotech hotbed, biological chemistry was front and center at the 229th national meeting of the American Chemical Society from 12–16 March.

Protein-based therapeutics are a bright spot for drug companies in troubled times. Their annual market is expected to surpass $50 billion by 2010. But proteins can suffer from problems not found with conventional small-molecule drugs. Some trigger immune reactions, and proteases and other compounds inside the body can quickly chop them up and clear them out. Cloaking protein drugs with a polymer called polyethylene glycol (PEG) can help hide them from the immune system. But it also makes some protein drugs less reliable because proteins sporting different numbers of PEGs may behave differently inside the body.

At the meeting, researchers from a California biotech company showed that they could precisely control the number of PEGs on each molecule, and thus the behavior of protein drugs, by inserting unnatural amino acid into proteins. "It's excellent work," says Ryan Mehl, a chemist at Franklin & Marshall College in Lancaster, Pennsylvania, who also specializes in adding unnatural amino acids to proteins. Although such altered proteins are still far from the clinic, Mehl and others say that the new work may eventually enable researchers to tailor the medicinal properties of proteins much as they do with small-drug molecules today.

The new technique builds on more than a decade of work by Peter Schultz, a chemist at the Scripps Research Institute in La Jolla, California, and his colleagues. Schultz's team over the years has created a scheme for altering the basic chemistry of proteins (*Science*, 14 July 2000, p. 232). Virtually all organisms construct their proteins from 20 amino acids, although scores more exist. Those 20 amino acids are encoded by the four nucleic acids that make up DNA. Those nucleic acids form three-letter "codons" that signal which amino acid should be inserted in a growing protein chain. Schultz's team pioneered an approach to hijack one of those codons to have it insert a non-natural amino acid instead. So far Schultz's lab has doctored proteins from *Escherichia coli* and other organisms to include some 50 different amino acids, which provide different chemical handles the researchers can use to alter the chemistry of the proteins.

In 2003, Schultz helped set up a new San Diego biotech company called Ambrx to take advantage of the new technology. At the meeting, Ho Sung Cho, Ambrx's director of molecular technology and process development, reported that he and his colleagues have made rapid strides in making precise modifications to human growth hormone (hGH), a protein used widely to promote growth in undersized children. The current hGH, Cho and others note, is made by linking copies of PEG to some of the 11 lysine amino acids on the protein. Researchers have found that hGH with about four PEGs per molecule strikes the best balance of safety and effectiveness. In practice, however, drugmakers end up with a mishmash of hGH molecules with different numbers of PEGs attached to different sites.

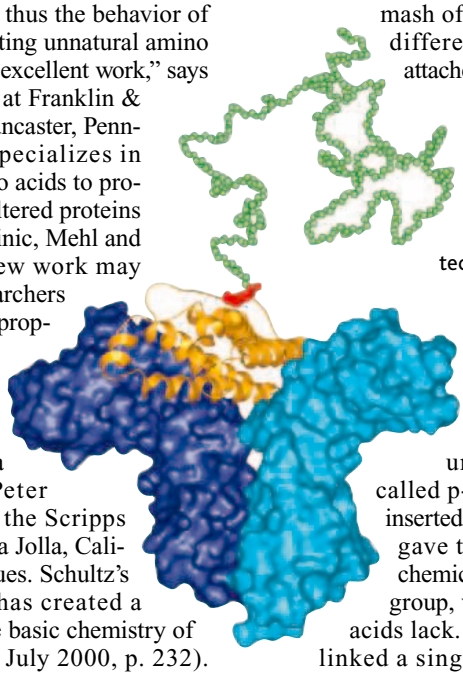

Hookup. Unnatural amino acid (red) added to human growth hormone (gold) helps researchers attach protective polymers (green).

To get around this variability, Cho's team made 20 different versions of hGH, each of which had an unnatural amino acid called p-acetylphenylalanine inserted at a different site. That gave the analogs a unique chemical handle called a keto group, which standard amino acids lack. The researchers then linked a single PEG to each keto group and tested the compounds in cell cultures containing mouse and rat cells. Some of the variations destroyed hGH's effectiveness, but many did not. When the group tested six promising analogs in mice, all worked and lasted longer in the animals than the commercial version of the drug did. A single injection of the best variant, for example, showed the same efficacy after 1 week as daily injections of the commercial hGH. If the result holds up in people, it could not only reduce the number of injections needed for hGH patients but also give drug companies a new way to tailor-make protein-based drugs.

Nanofibers Seed Blood Vessels

Researchers have made heady progress in regenerating tissues such as cartilage and skin, which either don't require an extensive blood supply or are thin enough to tap into nearby blood vessels. They've had far more trouble regenerating thick tissues such as heart muscle that require a blood supply throughout. But nanotechnology may soon provide some help.

At the ACS meeting, chemist Sam Stupp of Northwestern University in Evanston, Illinois, reported that his team has developed a novel variety of self-assembling nanofibers that strongly promote the growth of new blood vessels both in cell cultures and preliminary animal tests. "It's preliminary, but I thought it was the most interesting talk I heard at the meeting," says Harvard University chemist George Whitesides. "It could be the beginning of something genuinely important."

Stupp and his Northwestern colleagues have been perfecting their self-assembling nanofibers for years. A year and a half ago, the group reported making nanofibers that promote the regrowth of nerve cells in rats (*Science*, 3 October 2003, p. 47). Before that, the team had used their nanofibers to promote the growth of hydroxyapatite crystals that form a primary component of bone (*Science*, 23 November 2001, p. 1635).

In each case, the group starts by crafting two-part molecules called peptide amphiphiles (PAs) that contain oily hydrocarbon chains linked to water-friendly peptide groups. In water the hydrocarbons naturally clump together, but negative charges on the peptides repel one another and keep the molecules apart. By sprinkling positive ions into the solution, however, the researchers can counter the peptides' mutual repulsion, allowing the oily hydrocarbon tails to pack together into nanofibers with the peptides facing outward.

In the new study, Stupp—working with graduate student Kanya Rajangam, and John Lomasney, a pathologist at Northwestern University School of Medicine in Chicago—searched for peptides to promote the growth of blood vessels, a process called angiogenesis. Other researchers had discov-

CREDIT: ANNA-MARIA HAYS/AMBRX

ered that the crucial biochemical players in the process include a protein called heparin. Heparin binds to two protein-based growth factors, called fibroblast growth factor (FGF) and vascular endothelial growth factor (VegF), which work together to promote angiogenesis. Several groups had examined peptides that bind heparin, and they had found that each seemed to contain a short sequence of eight critical amino acids. So the Northwestern researchers synthesized PAs containing this octet of amino acid peptides. When they added the PAs to a solution containing heparin and the growth factors, they found that, as expected, the PAs assembled into nanofibers that bound heparin, which in turn bound FGF and VegF.

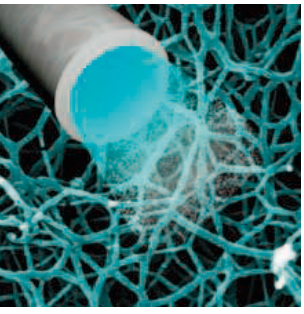

Networking. Nanofibers injected into tissue.

In cell cultures containing endothelial cells from cow lungs, Stupp's team quickly saw the formation of tubular structures resembling capillaries. When they injected PA-containing liquid into a damaged region of rat corneal tissue, they saw a rapid formation of blood vessels. By contrast, few blood vessels formed in control animals injected with a collagen gel containing heparin, FGF, and VegF. Even more enticing, when they injected liquid containing the PAs into the damaged heart tissue of rats, they noticed a "dramatic" improvement in the animals' electrocardiograms after 7 to 10 days, Stupp says.

Stupp suspects that the nanofibers work so well because they possess a very high density of sites that can bind heparin and the other compounds, and they may also slowly release these proteins to stimulate nearby cells as they break down. Whatever the explanation, if the success continues, angiogenesis-promoting nanofibers may one day help restore healthy function in patients who have had heart attacks and even create a new blood supply for a wide range of engineered tissues.

Fast, Sensitive Scan Targets Anthrax

In mid-March, automated anthrax sensors triggered shutdowns at three separate military mail-sorting facilities in the Washington, D.C., area. All reopened within a couple of days, after further tests declared them safe. But confusion between conflicting field and lab tests underscored a common frustration for biowarfare officials: Field tests are fast but typically have either low sensitivity for finding anthrax or a high rate of false alarms, whereas lab tests are more reliable but can take days to yield results. Now, there's new hope for a field test that's both fast and accurate.

At the meeting, chemist Richard Van Duyne of Northwestern University in Evanston, Illinois, reported that he and his students have created a portable laser-based anthrax detector that can turn out highly reliable data within minutes. Van Duyne says the instrument, about the size of a pack of cigarettes, can detect just 2550 anthrax spores, well below the level believed to trigger an infection in humans. And he says its sensitivity could well improve another 10-fold. "They have a phenomenal detector," says Chad Mirkin, a chemist and anthrax-detection expert at Northwestern who is not affiliated with Van Duyne's work.

Spotting tiny amounts of anthrax and other potential biowarfare agents has long been problematic. But in the wake of five anthrax-related deaths in 2001, federal agencies have poured money into research aimed at spotting the pathogen. Nine different technologies are now being tested, but all come with tradeoffs. For example, fluorescence detection—in which a laser shining light on a suspect sample causes different compounds to fluoresce at different wavelengths—is fast, portable, and sensitive, but it has the potential to give false positive readings.

Postal strike. Contaminated mail and false alarms both have spurred demand for better field tests for anthrax.

Van Duyne has long specialized in another laser-based detection technology called surface-enhanced Raman spectroscopy (SERS). Instead of tracking fluorescence, SERS tracks the shift in the light's wavelength that occurs after photons hit the sample and lose some of their energy by exciting the molecules before being re-emitted. Other groups have previously used SERS to detect anthrax, Van Duyne notes, but those tests never approached the ability to detect a mere 4000 or so spores, the number thought to be capable of starting an infection.

SERS works when laser light shines on a specially roughened surface of either silver or gold. The light intensifies the electric field surrounding tiny bumps on the surface. Any molecules sitting atop the surface experience the heightened electric field, which makes them scatter more light. By comparing the intensity and wavelengths of the scattered light to known reference materials, researchers can determine the chemical identity of compounds in a sample.

To detect anthrax, Van Duyne and colleagues look for the spectral signature of calcium dipicolinate, a compound that makes up part of a protective layer around anthrax spores. In tests, they dunk an anthrax sample in nitric acid for 10 minutes and spritz some of the solution onto the metal plate of the detector. In an earlier version of their sensor, the researchers roughened the surface by layering a silver film over plastic spheres of assorted sizes in the several-hundred-nanometer range. Because the wavelength of the laser light is optimal only for spheres of one particular size, however, the SERS enhancement was modest.

For their current study, Van Duyne and his graduate students—Xiaoyu Zhang, Matthew Young, and Olga Lyandres—carefully controlled the size of their spheres. Starting with a copper surface, they topped it with 300-nanometer plastic spheres and laid down a thin silver film on top, leaving behind a surface resembling the corrugations in a human brain. When the researchers sprayed on the anthrax extract and blasted the surface with laser light, the result was a 200-fold increase in detection sensitivity in a test that took less than a minute.

The group's work also appears in the 30 March issue of the *Journal of the American Chemical Society.* The researchers are planning field tests with emergency officials in Evanston and elsewhere.

–ROBERT F. SERVICE

CREDITS (TOP TO BOTTOM): ILLUSTRATION: MARK SENW; AP PHOTO/DANIEL HULSHIZER

Random Samples

Edited by Amitabh Avasthi

$1 Million Reward for Extinct Species

Although it has the hallmarks of an April Fools' Day joke, an Australian magazine says it is offering a $1.25 million (about U.S. $0.97 million) reward for conclusive proof that the Tasmanian tiger, *Thylacinus cynocephalu*, still roams.

The Tasmanian tiger was officially declared extinct in 1986, because there had been no confirmed sightings of a wild thylacine in decades and the last captive tiger had died in Tasmania's Hobart Zoo in 1936. Nevertheless, regular sightings continue to be investigated.

Garry Linnell, editor of *The Bulletin*, says his magazine had already been planning its competition to mark the publication's 125th anniversary when unverified photos of a tiger taken by a German tourist in February sparked a media whirlwind. *The Bulletin* quickly launched its own effort to flush out the elusive animal. One Tasmanian tour operator has since reportedly added another U.S. $1.36 million to the prize pool.

But the money is not just a click away. Entrants will have to submit digital photos of an unharmed tiger and later provide video footage as well as a certificate from a vet who has examined the animal. Finally, a panel of scientists will conduct DNA tests to verify that the animal is indeed a genuine Tasmanian tiger.

Biologists working for the Tasmanian government believe it is almost impossible to claim the reward, because any surviving tiger would still be protected by law and attempts to catch one would require a permit. "We will not issue permits on the basis of public curiosity," says Nick Mooney, a wildlife biologist with the Department of Primary Industries, Water and Environment. "[The reward] is unlikely to be claimed whether Tasmanian tigers are there or not."

Linnell agrees that "the odds are long" but says he is looking for the "scientific story of the century."

Serpentine Robots Inch Ahead

Snakelike robots could one day be slithering around waste disposal sites to check for leaking drums, or inching through building wreckage with a camera and microphone to probe for survivors. This prototype, dubbed OmniTread, was built over the past few years by roboticist Johann Borenstein of the University of Michigan, Ann Arbor, and his colleagues. The 1.2-meter-long machine crawls with treads that cover 80% of its surface and flexes powerfully, thanks to four pneumatic joints. OmniTread can pass through or around obstructions that most other robots cannot, says Borenstein.

In the March issue of *Industrial Robot*, the team describes the results of tests on various terrains. OmniTread "climbs stairs pretty well; it crosses gaps pretty well," says Wendell Sykes of Context Systems in Carlisle, Massachusetts, who consults on robotics for government agencies. Borenstein is "probably about a year ahead of everyone else."

The Michigan researchers are now working on a smaller-diameter version of OmniTread that will hold enough batteries and compressed gas to operate untethered for up to an hour.

Saving the Palm for Future Sundays

Conservationists are hoping that ecofriendly palms recently delivered to Christian churches in three states will prove to be a blessing in disguise. A similar effort in Colombia is meant to give endangered birds a chance for survival.

In a tradition symbolizing Jesus being welcomed to Jerusalem, many churches pass out palm fronds at their Palm Sunday services; the religious holiday accounts for about 10% of the annual U.S. market for the fronds. But fronds come from a rapidly dwindling number of palms, so environmentalists are trying to protect the trees and the rainforest ecosystem in which they thrive.

This year the Canada-based Commission for Environmental Cooperation (CEC) arranged to purchase fronds from Mexico and Guatemala that had been harvested without leaving the tree bare. "You get more out of each plant, and you're not deforesting the rainforest," says CEC spokesperson Spencer Tripp. Twenty-two churches across Minnesota, North Dakota, and Massachusetts used fronds from CEC, which now plans to set up a certification system for ecofriendly palms.

And in Colombia, churches teamed with Washington, D.C.–based Conservation International and other groups to promote the use of alternative palm species. The now commonly used wax palm is one of the last remaining habitats of Colombia's endangered yellow-eared parrots, which currently number fewer than 1000.

Eco-friendly palms, thankful parrots.

CREDITS (TOP TO BOTTOM): *THE BULLETIN*; JOHANN BORENSTEIN; CEC; (INSET): RICHARD MAZALAN/AP

Edited by Yudhijit Bhattacharjee

AWARDS

Abel Prize. The new winner of the $980,000 Abel Prize from the Norwegian Academy of Science and Letters calls himself a hybrid mathematician. Peter Lax, 78, says the "delicate balance between applications of mathematics and pure math" at New York University's Courant Institute, his alma mater, shaped his career.

Born in Budapest, Lax spent a year at Los Alamos National Laboratory during World War II working on equations governing the transport of neutrons and other problems relating to the atomic bomb, and he consulted at the lab throughout his career. His love of pure math was nurtured in part by fellow Hungarian Paul Erdös. "He looked after me, encouraged me, and gave me problems to solve," Lax says. Lax is currently working on an expression known as the Korteweg-de Vries equation. "There are mysteries remaining which I am trying to unravel," he says.

Franklin Institute prizes. French organic chemist Henri Kagan has won the $250,000 Bower Award for Science Achievement from the Franklin Institute in Philadelphia, Pennsylvania. Kagan, a professor emeritus at the University of Paris-Sud in Orsay, France, receives the honor for his work on asymmetric catalysis.

The institute has also announced the winners of its Benjamin Franklin medals: Aravind Joshi for computer and cognitive sciences, Yoichiro Nambu for physics, Peter Vail for earth and environmental sciences, and Andrew Viterbi for electrical engineering.

JOBS

In the vicinity. Dolly the sheep's creator Ian Wilmut will move his labs into town this summer when he joins the faculty of the University of Edinburgh in the U.K. Wilmut says he will continue to collaborate with researchers at the Roslin Institute outside Edinburgh, where he has worked for the past 3 decades.

Call of duty. Physiologist Antonio Scarpa is giving up some of his community service so that he can take a new job at the National Institutes of Health (NIH) that serves the community.

Currently chair of the biophysics and physiology department at Case Western Reserve University in Cleveland, Ohio, Scarpa has been named director of the Center for Scientific Review (CSR), which manages NIH's vast peer review system for extramural awards. "It's a chance to give something back to the community," says the 62-year-old grantee, who has served on several study sections. Ironically, Scarpa has chosen to resign from the board of the Federation of American Societies for Experimental Biology in Bethesda, Maryland, and sever ties to other professional organizations to steer clear of NIH's new—and more stringent—conflict-of-interest rules.

The CSR job, which begins 1 July, will also reunite him and his wife, Meredith Bond, who in 2003 became chair of the physiology department at the University of Maryland School of Medicine in Baltimore.

Got any tips for this page? E-mail people@aaas.org

NONPROFIT WORLD

Moving mainstream. The new president of Science Service in Washington, D.C., wants to get more scientists engaged in public education. "Society is extremely dependent on citizens who may not always have a scientific background, like firefighters and cops," says Elizabeth Marincola, who has been executive director of the American Society for Cell Biology in Bethesda, Maryland, for the past 14 years. "When citizens don't understand science, their instinctive reaction to controversial issues—such as stem cells—is to first fear it and then reject it."

Founded in 1921, Science Service publishes *Science News* and runs the Intel STS prize competition for high school students.

POLITICS

Encore. The new science minister of Portugal has been given a second shot at boosting the country's research profile.

Physicist José Mariano Gago took office on 12 March with orders to carry out the promise of new Socialist Prime Minister José Sócrates to double investment in research. In a previous 7-year term that ended in 2002, Gago received high marks for modernizing a research system that had stagnated under decades of dictatorship (*Science*, 9 March 2001, p. 1889). He also helped draft the Lisbon Strategy, an economic stimulus package for the European Union that calls for countries to boost their research investment to 3% of GDP by 2010.

The appointment is good news for science throughout Europe, says Luc van Dyck of the European Life Sciences Forum in Heidelberg, Germany. He expects Gago to be a strong voice on the E.U.'s Competitiveness Council, which approves E.U. research policies.

CREDITS (TOP TO BOTTOM): SCIENCE SERVICE; SOURCE: NYU; CURENTUL

Q: What is the best way to present my research or showcase new ideas in front of world-renowned scientists and researchers?

A: Propose a symposium for the AAAS Annual Meeting, 16–20 February 2006, St. Louis, MO.

Call for Symposia Proposals:

AAAS Annual Meeting St. Louis, MO

The AAAS Annual Meeting attracts a diverse audience from all scientific disciplines and from the industrial, academic, non-profit and policy communities. The meeting is also attended by more than 1,000 press registrants, including most of the world's major news outlets.

In order to accommodate the tremendous variety of subjects proposed for the Annual Meeting, and due to time and space constraints, 90-minute symposia are strongly encouraged.

The Program Committee is particularly interested in sessions that highlight the interdisciplinary strengths of AAAS, or that address the identified theme for the 2006 Annual Meeting—*Grand Challenges, Great Opportunities*. Successful proposals are characterized by interesting topics that are thoughtfully developed and include capable and articulate presenters who are representative of the diversity of science and society.

All proposals will be peer-reviewed. The deadline for proposal submission is Monday, 2 May 2005. Decisions will be announced in July.

For more information on submitting a proposal, visit:

www.aaasmeeting.org

AAAS

ADVANCING SCIENCE, SERVING SOCIETY

Letters to the Editor

Letters (~300 words) discuss material published in *Science* in the previous 6 months or issues of general interest. They can be submitted through the Web (www.submit2science.org) or by regular mail (1200 New York Ave., NW, Washington, DC 20005, USA). Letters are not acknowledged upon receipt, nor are authors generally consulted before publication. Whether published in full or in part, letters are subject to editing for clarity and space.

NIH Response to Open Letter

ALTHOUGH WE APPRECIATE HEARING THE views of some of our most respected scientists, the open letter from some of our colleagues in the microbiology community ("An open letter to Elias Zerhouni," S. Altman *et al*., Letters, 4 Mar., p. 1409) does not provide a complete picture of funding for the biodefense and nonbiodefense research programs of the National Institutes of Health (NIH), particularly the National Institute of Allergy and Infectious Diseases (NIAID) (*1*).

The letter argues that biodefense research efforts have diverted resources from nonbiodefense research at NIH. This is simply not the case. Funding for biodefense research has been additive to nonbiodefense research efforts supported by NIAID. The letter focuses only on support for research on the agents that cause tularemia, anthrax, plague, glanders, melioidosis, and brucellosis. NIAID biodefense funding is used to support research on a much broader list of more than 50 pathogens, which include "traditional" biodefense pathogens, such as those that cause anthrax and smallpox, as well as newly emerging infectious agents such as the SARS coronavirus and pathogens that cause diseases that affect people around the world on a daily basis (*2*).

The terrorist attacks of September 11, 2001, and the dissemination of anthrax spores through the U.S. mail later that fall prompted the administration, with bipartisan support from Congress, to dramatically increase biodefense spending. Approximately $1.5 billion was added to the NIH budget in 2003 specifically to address concerns raised by bioterrorism, and this level of funding has been maintained with small to modest increases in subsequent years. (see table).

These resources could have been allocated to other agencies that likely would not have embraced the academic microbiology and infectious diseases community, as is the tradition of NIH.

Before the designation of "biodefense funding," many pathogens with bioterror potential (e.g., the agents of anthrax and plague) were funded from a general pool of microbiology funds. With the establishment of the designation of biodefense money, studies of many pathogens previously funded from the general pool of microbiology money were funded by biodefense money, allowing additional grants for nonbiodefense pathogens. Also, in the period from 2000 to 2005, funding for NIAID nonbiodefense research increased by more than 50% and generally kept pace with the overall increases in NIH research funding for other diseases (see table).

The accounting methodology used by the authors of the letter took into account only a fraction of the overall biodefense and nonbiodefense programs at NIH (*1*). In addition, the authors' analyses were based on searches of public databases that were not designed for comparative analyses of relative support for research areas.

The authors' assertion that the peer-review process has been "threatened by unintended consequences of the 2001–2002 decision… to prioritize research of high biodefense, but low public-health significance" is unfounded. Indeed, in 2004, the success rates for NIAID biodefense and nonbiodefense research project grant applications were comparable at 25.9% (316 grants awarded) and 23.5% (845 grants awarded), respectively. More broadly, we disagree with the notion that biodefense concerns are of "low public-health significance." The United States has experienced an anthrax attack, and security experts repeatedly express concern that future attacks with biological weapons are likely, if not inevitable.

We look forward to continuing a dialogue with our colleagues in the microbiology community with regard to the biodefense and nonbiodefense research agenda of the NIH.

ANTHONY S. FAUCI[1]* AND ELIAS A. ZERHOUNI[2]
[1]Director, National Institute of Allergy and Infectious Diseases, [2]Director, National Institutes of Health, 9000 Rockville Pike, Bethesda, MD 20892, USA.
*To whom correspondence should be addressed. E-mail: afauci@niaid.nih.gov

BUDGET COMPARISONS (DOLLARS IN MILLIONS)

	NIH Nonbiodefense*		NIAID Nonbiodefense*		NIAID Biodefense		Total*	
Fiscal year	Amount	Percent change	Amount	Percent change	Amount	Percent change	Amount	Percent change
2000	17,771	—	1,744	—	33	—	1,777	—
2001	20,460	15.1%	1,999	14.6%	42	27.3%	2,041	14.9%
2002	22,802	11.4%	2,153	7.7%	187	345.2%	2,340	14.6%
2003†	25,003	9.7%	2,445	13.6%	1,162	521.4%	3,607	54.1%
2004	26,243	5.0%	2,542	4.0%	1,600	37.7%	4,142	14.8%
2005‡	26,728	1.8%	2,646	4.1%	1,658	3.6%	4,304	3.9%
2006§	26,865	0.5%	2,695	1.9%	1,664	0.4%	4,359	1.3%

*This table excludes the following NIAID contributions to the Global Fund for AIDS, Malaria and TB to allow for better comparison of nonbiodefense research: 2002, $25M; 2003, $99M; 2004, $149M; 2005 (appropriated), $99M; 2006 (estimated), $100M. †The FY 2003 biodefense funding for NIAID does not reflect the $371M for biodefense in the FY 2003 NIH Buildings and Facilities (B&F) Appropriation. The biodefense B&F funds were realigned to support biodefense research as of FY 2004. ‡ Appropriated. § Estimated.

References
1. National Institute of Allergy and Infectious Diseases, Open Letter in *Science* Regarding NIH Biodefense Funding: Questions and Answers (available at www2.niaid.nih.gov/newsroom/Releases/scienceletter.htm).
2. The complete list can be viewed at www.niaid.nih.gov/Biodefense/bandc_priority.htm.

The Past and Future of Extant Amphibians

THE FIRST REACTION OF A PALAEOHERPETOLOGIST to the growing concern about the future of amphibians ("Status and trends of amphibian declines and extinctions worldwide," Reports, S. N. Stuart *et al.*, 3 Dec. 2004, p. 1783) is curiosity and perplexity. Those who work with fossils and bones of Neogene and Quaternary amphibians tend to consider these organisms as being morphologically so stable and conservative as to be practically unsuitable for biochronology. It is generally assumed that amphibian assemblages show little change over millions of years (*1*–*3*). This sharply contrasts with their high sensitivity to environmental factors, which, at least theoretically, should render them precise proxies of changes in biodiversity and good indicators of environmental health.

If this is the case, how does one explain the stability of amphibian communities and the dramatic turnover experienced, for example, by mammals and birds in North America during the Pleistocene? Eight families, 46 genera, and 191 species of mammals, in addition to 2 families, 19 genera, and a huge number of species of birds went extinct, but only about a half dozen species of amphibians (no families or genera) went extinct (*1*).

An impressive European example is offered by Valdemino, a Middle Pleistocene site in northwestern Italy (*4*). The herpetofauna is represented exclusively by modern species that lived in sympatry with, among others, Barbary apes, elephants, rhinoceroses, leopards, and sabre-toothed tigers.

Even taking into consideration the fact that the perception of such a persistence through time can be biased by the morphological uniformity of several taxa, which leads inevitably to the lack of recognition of evolutionary changes within cryptic species groups, the chronological range of some amphibian taxa is highly remarkable: Several living species of anurans have a fossil record that dates back to the Miocene or Pliocene (*5*), epochs that ended 5.3 and 1.8 million years ago, respectively.

Winning skills for long-term survival of several taxa could have been, and still could be, low metabolic rates; reproductive strategies; food-web relationships; and the ability to bypass climatic stress by hibernation and aestivation, to adapt to climatic and vegetation changes, to exploit ephemeral and unstable habitats, and to survive for generations in suboptimal conditions, despite facing severe genetic bottlenecks (*1*, *2*).

This tenacious capability of amphibians to survive suggests that any conservation effort, even if focused on nearly depleted populations with limited ranges, could be successful in granting long-term survival.

MASSIMO DELFINO

Earth Sciences Department, Florence University, Via G. La Pira, 4, I-50121 Florence, Italy. E-mail: delfino@geo.unifi.it

References

1. J. A. Holman, *Pleistocene Amphibians and Reptiles in North America* (Oxford Monogr. Geol. Geophys. No. 32, Oxford Univ. Press, New York, 1995).
2. J. A. Holman, *Pleistocene Amphibians and Reptiles in Britain and Europe* (Oxford Monogr. Geol. Geophys. No. 38, Oxford Univ. Press, New York, 1998).
3. M. Delfino, J.-C. Rage, L. Rook, *Deinsea* **10**, 153 (2003).
4. M. Delfino, *Herpetol. J.* **14**, 113 (2004).
5. B. Sanchiz, *Salientia* (Gustav Fischer Verlag, Stuttgart/New York, 1998).

Response

DELFINO'S LETTER REINFORCES THE PECULIARITY and seriousness of current amphibian declines and extinctions. The evidence we presented in our Report shows that the rate of amphibian extinctions is increasing very rapidly and now far surpasses that of mammals and birds.

Although amphibians have survived past climatic and ecological changes, many species appear to be unable to withstand current threats. We suspect that two factors are at play. First, current changes in both climate and habitats are probably much more rapid than was previously the case, at least over the Quaternary (*1*). Second, amphibians now face a larger number of complex threats that may be acting synergistically. Previously, amphibians have not been confronted simultaneously by rapid climate change and human-induced habitat loss, overexploitation, and disease (*2–4*).

If threats can be contained through effective conservation actions, then amphibian populations can be expected to rebound and be viable over long periods of time. However, because such a resilient group of species is in such rapid decline, the underlying causal changes taking place in the biosphere will probably have substantial adverse impacts extending well beyond amphibians.

SIMON N. STUART,[1]* JANICE S. CHANSON,[1] NEIL A. COX,[1] BRUCE E. YOUNG,[2] ANA S.L. RODRIGUES,[3] DEBRA L. FISCHMAN,[3] ROBERT W. WALLER[3]

[1]IUCN Species Survival Commission/Conservation International Center for Applied Biodiversity Science, Biodiversity Assessment Unit, 1919 M Street, NW, Suite 600, Washington, DC 20036, USA. [2]NatureServe, Apartado 75-5655, Monteverde, Puntarenas, Costa Rica. [3]Center for Applied Biodiversity Science, Conservation International, 1919 M Street NW, Suite 600, Washington, DC 20036, USA.

*To whom correspondence should be addressed. E-mail: s.stuart@conservation.org

References

1. Intergovernmental Panel on Climate Change, *Climate Change 2001: The Scientific Basis* (World Meteorological Organization and United Nations Environment Program, New York, 2001).
2. C. Weldon, L. H. du Preez, A. D. Hyatt, R. Muller, R. Speare, *Emerg. Infect. Dis.* **10**, 2100 (2004).
3. P. A. Burrowes, R. L. Joglar, D. E. Green, *Herpetologica* **60**, 141 (2004).
4. S. R. Ron, W. E. Duellman, L. A. Coloma, M. R. Bustamante, *J. Herpetol.* **37**, 116 (2003).

Don't Call Them Co-eds!

AS A GRADUATE OF PRINCETON'S UNDER-graduate engineering program and current faculty member at Smith College, I was pleased to see your coverage of the Princeton-Smith student exchange agreement ("Support group," Random Samples, 21 Jan., p. 351). At the same time, I was dismayed to find the use of the anachronism "co-eds" to refer to female Princetonians in your otherwise positive coverage. For many of us, that gender-biased term—referring to women as the reason a school has become "co-ed"—is a glaring reminder of Princeton's history as a men's school that admits women, rather than an institution equally committed to the education of all students. We welcome all Princeton engineering students to Smith as part of the exchange, not just women. Men would indeed benefit from experiencing engineering education in a program unique in its majority-women faculty and student body—and we promise not to demean their value in our community by referring to them as co-eds.

DONNA M. RILEY

Picker Engineering Program, Smith College, 51 College Lane, Northampton, MA 01063, USA.

The Source of the Lisbon Earthquake

IN HIS PERSPECTIVE "WHAT CAUSED THE Great Lisbon earthquake?" (27 Aug. 2004, p.1247) M.-A. Gutscher proposes an eastward-dipping subduction zone under the Straits of Gibraltar as a likely candidate responsible for the magnitude (*M*) 8.5 1755 Lisbon earthquake and associated tsunami (*1*), a suggestion that adds to a growing list of disparate source locations. Although H. F. Reid proposed a source off the western coast of Portugal (*2*), after an M_S 7.9 earthquake southwest of Portugal in 1969, it became common to associate the 1755 earthquake with the compressive structures of the Gorringe Bank (*3*). Recent tsunami research has led to the suggestion that the seismic rupture was closer to the western coast of Portugal and extended farther north toward Lisbon (*4*), which was in turn used to support the proposal that the western margin of Portugal is currently the locus of incipient subduction (*5*). Marine work on the southwest continental margin of Portugal revealed new active faults that were deemed responsible for the 1755 earthquake (*6*, *7*), and new analyses of the tsunami data led to a complex rupture model with a segment along the ENE-WSW Guadalquivir Bank on the Gulf of Cadiz (*8*). With the addition of the Gibraltar Straits, the span of the proposed epicentral regions for the Lisbon earthquake is about 600 km, a surprising uncertainty in view of the well-documented damage that the earthquake caused.

The distribution of damage, for which there is a wealth of documentation (*9*, *10*), points to a source location west or southwest of Portugal and is hard to reconcile with a rupture under the Gibraltar Straits. The much larger death toll in Portugal, when compared with that of Spain, should also rule out an epicentral region near the Gibraltar Straits. Irrespective of the merits

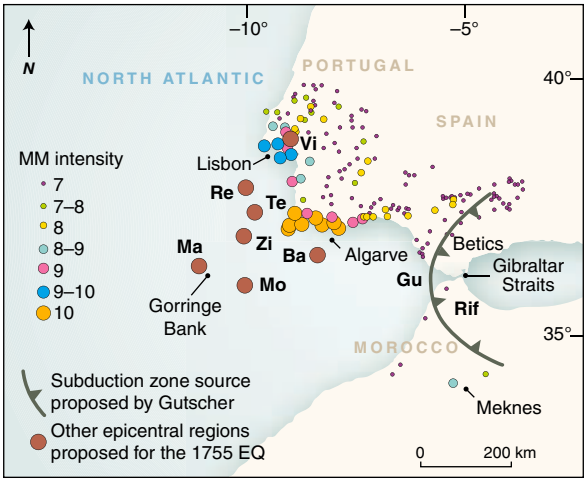

Intensities of the 1755 Lisbon earthquake (*9*–*11*) and indicative locations of epicentral regions proposed by different authors. Vi, (*11*) (partial source); Re, (*2*); Te, (*7*); Zi, (*6*); Ma, (*13*); Mo, (*14*); Ba, (*8*) (partial source); Gu, Gutscher. The Gibraltar Arc 1755 (partial) tsunami source was modeled as a 180 × 210 km^2 surface with 20 m of co-seismic slip (*15*), which is unwarranted by the intensity distribution.

or demerits of the proposed model of subduction underneath the Gibraltar Straits, any direct link between the Lisbon earthquake and such a tectonic process is very unlikely, in view of the evidence provided by the intensity data.

Intricacies in the available information render the 1755 source location a challenging problem. The region of high intensities around Lisbon [9-10 Mercalli (*11*)] is disconnected from that of the Algarve (see figure), possibly indicating a triggered secondary earthquake source near the Portuguese capital (*12*). Solving this complicated puzzle to a level that is satisfactory for hazard assessment requires the integration of data from different fields. Focusing only on an isolated type of observations, or on partial subsets of data, is not beneficial to a responsible hazard assessment effort.

JOAO F. B. D. FONSECA

Earthquake Engineering and Seismology Group, ICIST, Instituto Superior Tecnico, Avenida Rovisco Pais 1, Lisbon 1049-001, Portugal.

Response

FONSECA'S LETTER HELPS TO draw attention to the complex tectonic boundary between the African and Eurasian plates in southwest Iberia where the Great Lisbon earthquake nucleated. Fonseca takes exception to the proposition that this earthquake may have originated along an active east-dipping subduction zone in the Gulf of Cadiz. Although the subduction zone indeed passes beneath the Straits of Gibraltar, the potential rupture surface is not here, 600 km from Lisbon (as Fonseca states), but located roughly from 7° to 9°W and from 35° to 36°N. Thus, its northwest limit is some 100 km from the Algarve coast, where the highest shaking intensities were felt, and about 300 km from Lisbon. The Gulf of Cadiz coast (not including the highest intensity Algarve region) experienced high intensities—in northwest Morocco (*1*) and southwest Spain (*2*)—and roughly encircles the potential subduction fault plane.

Tsunami and seismic intensity modeling performed in collaboration with colleagues from Lisbon (*3*) suggests that although a subduction source alone is not able to successfully account for all historically observed seismic intensity and tsunami observations, it certainly does not contradict evidence from historical data. Indeed, in combination with a second potential fault zone triggered farther to the northwest (Gorringe Bank or Guadalquivir Bank, for instance), it represents an attractive source. The subduction fault plane offers two distinct advantages over most other suggested sources in the area. First, it has a large surface area, sufficient to generate an M8.6 to M8.8 earthquake for 10 to 20 m of seismic slip. Second, the expected subduction zone deformation rates (5 to 10 mm/year) are consistent with the available evidence concerning the recurrence time (1500 to 2000 years). Most other proposed sources, when taken individually, are far too small to generate the tremendous seismic moment and thus require unreasonably large co-seismic slips and extremely long recurrence times.

References

1. J. F. B. D. Fonseca, *1755—the Lisbon Earthquake* (Argumentum, Lisbon, 2004).
2. H. F. Reid, *Bull. Seismol. Soc. Am.* **4** (no. 2), 53 (1914).
3. E. Buforn, A. Udias, M. A. Colombas, *Tectonophysics* **152** (nos. 1-2), 89 (1988).
4. M. A. Baptista *et al.*, *J. Geodynam.* **25**, 159 (1998).
5. A. Ribeiro, *Soft Plate and Impact Tectonics* (Springer, Berlin, 2002).
6. N. Zitellini *et al.*, *Ann. Geofis.* **42** (no. 1), 49 (1999).
7. P. Terrinha *et al.*, *Mar. Geol.* **195**, 55 (2003).
8. M. A. Baptista *et al.*, *Nat. Hazards Earth System Sci.* **3**, 333 (2003).
9. F. L. P. Sousa, *O Terremoto Do 1° de Novembro de 1755* (Serviços Geológicos de Portugal, Lisbon, 1932).
10. J. M. Martinez-Solares, *Los effectos en España del terremoto de Lisboa* (Instituto Geografico Nacional, Madrid, 2001).
11. V. S. Moreira, Sismicidade Histórica de Portugal Continental (INMG, Lisbon, 1984).
12. S. P. Vilanova, A. C. F. Nunes, J. F. B. D. Fonseca, *Bull. Seismol. Soc. Am.* **93** (no. 5), 2056 (2003).
13. F. Machado, *Rev. Fac. Ciên. Lisboa Ser.* C **14**, 19 (1966).
14. V. S. Moreira, in *Earthquakes at North-Atlantic Passive Margins: Neotectonics and Postglacial Rebound*, S. Gregersen, P. W. Basham, Eds. (Kluwer Academic, London, 1989).
15. M. A. Baptista, M. A. Gutscher, J. M. Miranda, AGU 2003 Fall Meeting Abstract T51D-0197 (2003).

LETTERS

However, one or more of these structures may have contributed to the 1755 event.

I agree with Fonseca that a wide variety of additional data must be acquired and integrated to help understand this tectonically complex region. This process is already under way, and thanks to five marine oceanographic cruises in the past 5 years (including three this summer), bathymetric mapping of the Gulf of Cadiz–SW Iberia Margin is now complete. These data reveal several tectonically active structures and confirm the continued activity of the deformation front of the accretionary wedge related to the east-dipping subduction (*4*).

MARC-ANDRE GUTSCHER
Institut Universitaire Européen de la Mer, CNRS Unité Mixte de Recherche 6538, Domaines Oceaniques, Plouzané F-29280, France. E-mail: gutscher@univ-brest.fr

References
1. A. Levret, *Tectonophysics* **193**, 83 (1991).
2. J. M. Martinez-Solares, A. Lopez, J. Mezcua, *Tectonophysics* **53**, 301 (1979).
3. M.-A. Gutscher, M.-A. Baptista, J.M. Miranda, *Tectonophysics Spec. Vol.*, in press.
4. M.-A. Gutscher, presentation at the EuroMargins Meeting, Barcelona, Spain, 11 to 13 Nov. 2004.

TECHNICAL COMMENT ABSTRACTS

COMMENT ON "Oscillations in NF-κB Signaling Control the Dynamics of Gene Expression"

D. Barken, C. J. Wang, J. Kearns, R. Cheong, A. Hoffmann, A. Levchenko

Nelson *et al.* (Reports, 22 Oct. 2004, p. 704) argue that oscillations in nuclear factor kappa B (NF-κB) signaling control gene expression. However, we show that altering expression levels of fluorescently tagged signaling proteins can severely affect the dynamic behavior of the signaling pathway under study and caution against equating the signaling behavior of genetically engineered cells with that of normal cells.

Full text at
www.sciencemag.org/cgi/content/full/308/5718/52a

RESPONSE TO COMMENT ON "Oscillations in NF-κB Signaling Control the Dynamics of Gene Expression"

D. E. Nelson, C. A. Horton, V. See, J. R. Johnson, G. Nelson, D. G. Spiller, D. B. Kell, M. R. H. White

Our experimental data shows no correlation between NF-κB (RelA) expression level and oscillation dynamics. We show that a small change to the computational model used by Barken *et al.* to generate their theoretical data reduces the apparent discrepancies. Cell system differences and possible compensatory changes to normal signaling in their genetically engineered knockout cells may explain differences between the two studies.

Full text at
www.sciencemag.org/cgi/content/full/308/5718/52b

FOOD

Of Bubbles, Landscapes, and Vines

Stuart West

Wine enriches our lives, mixing perfectly with food, friends, and social occasions. That it also mixes well with science is shown by two recent books that explore how our understanding and appreciation of wine can be improved by considerations of physics and geology.

Champagne is a special wine. Dom Pérignon realized this with his first glass, calling to his fellow monks, "Come quickly, brothers, I am tasting stars!" However, the bubbles that caused this exclamation don't just make champagne, they save it. Still wine from the champagne region is thin and acid, and it is with good reason it doesn't appear on wineshop shelves. It is the bubbles that transform it into something sublime.

Uncorked: The Science of Champagne is about the physics of these bubbles. Gérard Liger-Belair (a physical chemist at the University of Reims Champagne-Ardenne) provides a highly entertaining introduction to the science of champagne bubbles that can be read in a couple of hours. After describing the history and methods of champagne production, he devotes most of the book to explaining how bubbles form and what happens when they do. He bursts the conventional wisdom that bubbles form on impurities in glass, and he shows how they are instead born out of debris stuck on the glass wall.

But it is after the bubbles form that the exciting things begin to happen. The bubbles "kiss and tumble" their way to the top of the glass, where they form galaxies (two-dimensional vortices) or bubble flowers before exploding and sending a concentrated burst of aromatic compounds toward the drinker. The author's account includes numerous asides, such as why one should not wear lipstick or eat chips when drinking champagne (fatty molecules deflate bubbles) and the suggestion that the best planet on which to drink champagne would be Jupiter (its high gravity would lead to smaller bubbles).

Uncorked: The Science of Champagne
by Gérard Liger-Belair
Princeton University Press, Princeton, NJ, 2004. 158 pp. $19.95, £12.95. ISBN 0-691-11919-8.

Great Wine Terroirs
by Jacques Fanet, translated by Florence Brutton
University of California Press, Berkeley, CA, 2004. 240 pp. $39.95, £26.95. ISBN 0-520-23858-3.

Uncorked is very readable, and Liger-Belair's clear and simple descriptions of the physics are superbly suitable for a general audience. The book is also very aesthetically pleasing, making it an ideal present for wine lovers and bores alike. Central to this success is a fine collection of photographs and illustrations (often from the author's own research) that depict the processes described. Many of these images were taken with high-speed photography, which reveals the surprising beauty that exists in the life of bubbles.

However, while the book brings bubbles to life, Liger-Belair doesn't explain why champagne is unique. What is it that makes devotees extol the delights of champagne to the detriment of other sparkling wines, even when those are made with the same grape varieties? The answer to this question is terroir, the elusively defined French term for the combination of factors that define the characteristics of a wine-growing area.

In *Great Wine Terroirs*, a translation of *Les Grands Terroirs du Vin* (Hachette Pratique, Paris, 2001), Jacques Fanet (a former assistant director of France's National Institute of Appellations) explains how the characteristics of wine regions have been formed over the last 200 million years. His aim is to link the wine that comes from an area with the geological processes that have shaped its landscape. The main part of the book moves through the various broad types of terroir, describing the intricacies of the related growing areas and their associated grape varieties. Fanet discusses some 70 terroirs, arranging them according to their geologic setting: the edge of faults (e.g., Alsace), sedimentary basins (Champagne), Quaternary terraces (Pomerol), ancient basement (Coonawarra), foothills of mountains (Napa), and volcanic terrain (Tokaj).

Fanet has packed a lot of information into the book, which will reward multiple readings. He does an excellent job conjuring up how the landscapes have been formed and the implications for wine production. Some of the points he makes are quite general—for example, the importance of Mesozoic marine deposits in France and how rivers provide not only irrigation and transport but also erosion that leads to high-quality terroirs such as stony terraces. But he also goes into such details as how the pinot noir grand crus of Burgundy are located on the stoniest, most limestone soils and the factors that produce differences among these grand crus.

Fanet's book contains an impressive collection of color maps, diagrams, and photographs that help bring the terroirs to life. These are important, because in places the text is quite dense, with lots of jargon, and thus difficult to follow. The strong bias in the geographic coverage is understandable, as hundreds of years of trial and error have revealed the details of French terroirs. There are, however, important omissions (such as Marlborough with its prize-winning sauvignon blancs) and imbalances in the space allotted to other European areas (for example, the rieslings of Alsace receive twice the space of those of Germany).

Vines on the rocks. Most Châteauneuf-du-Pape vineyards are established on the Quaternary terraces of rounded, polished cobbles deposited by the Rhône River.

CREDIT: J. GUILLARD/SCOPE (COURTESY UNIVERSITY OF CALIFORNIA PRESS)

Although Fanet provides a wealth of geological information on how the different terroirs are formed, he is less clear in explaining how the different terroirs lead to different wines. For example, what links the gravel terraces of the Gironde with the terra rossa of the Coonawarra in their ability to produce cabernet sauvignon that lacks its characteristic vegetal aroma? Or why does *Botrytis* mold develop differently on vines grown on Carboniferous terrains, Brioverian schists,

The reviewer is at the Institute of Evolutionary Biology, School of Biological Sciences, University of Edinburgh, West Mains Road, Edinburgh, EH9 3JT, Scotland, UK. E-mail: stu.west@ed.ac.uk

or Saint-Georges schists, and what are the consequences for the resultant wine? It isn't clear whether such details are gaps in our knowledge or gaps in the book's coverage. Consequently, one might gain the maximum benefit from the book by reading it alongside an existing wine encyclopedia or atlas.

Overall, *Great Wine Terroirs* left me wanting to travel to the areas Fanet describes, to use it as a guidebook while matching the wines and terroirs in person. In contrast, reading *Uncorked* gave me more reasons to crave champagne. Both books also have the potential to show nonscientists that scientific principles apply even to the simple pleasures of life.

10.1126/science.1111135

BIOMEDICINE

Cell Senescence in the Dock

Steven N. Austad

Normal human cells can divide in vitro only a limited number of times before permanently arresting their replication. This finding was huge news when first reported in 1961, because it overturned entrenched conventional wisdom that cells freed of the body could divide indefinitely in a dish. In early studies, these cells also died soon after ceasing replication, so the phenomenon came to be termed cellular senescence—in obvious parallel with the state of human senescence from which death shortly follows. Subsequent studies supported this interpretation by noting that cells harvested from older people reached "senescence" after fewer cell divisions than cells from younger people. A more precise parallel with aging was expressed by Leonard Hayflick, discoverer of cellular senescence, when he surmised that the "finite lifetime of normal cells constitute[s] a programmed mechanism that sets an overall limit on an organism's length of life" (*1*).

Cells, Aging, and Human Disease
by Michael B. Fossel
Oxford University Press, New York, 2004. 503 pp. $69.95, £43. ISBN 0-19-514035-4.

Over the next several decades, Hayflick's finding led to hosts of exciting discoveries about the complex web of molecular control over cell proliferation and its arrest, the role of telomere length in those processes, the enzyme telomerase, and a variety of cell cycle proteins. Even so, researchers studying senescence in whole animals rather than isolated cells grew dubious about the straightforward relationship between proliferative arrest and organismic senescence. Among the reasons for their doubt were that so many of the degenerative changes of later life occurred in cells such as neurons or cardiomyocytes (both of which replicate rarely or never in adulthood) and that people seem to die much more often because their cells replicate when they shouldn't (as in cancer) rather than cells not replicating when they should. Even those who initially embraced the equation of in vitro replicative cessation with senescence grew more guarded in their claims as it became evident that so-called senescent cells if properly cultured did not die but could live for years and that such cells were very rare even among those taken from the very elderly.

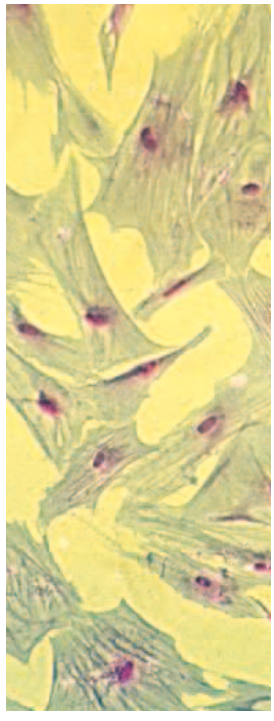

After arrest. The cells in this culture, which have been genetically engineered to age rapidly, are in a late phase of their life and no longer divide to produce new cells.

Given these developments, Michael Fossel is something of a throwback. *Cells, Aging, and Human Disease*, like an earlier trade book of his (*2*), shows him to be a proud true believer. He holds that cellular senescence underlies virtually every aspect of human senescence and that the appropriate activation of telomerase, which prevents senescence in human cells, will necessarily ameliorate or cure most problems that plague us as we age. The gist of Fossel's argument is that even though senescent cells are rare, they can—because of their loss of replicative ability and altered function—have far-reaching effects on their cellular neighbors, deleterious effects that cascade until a whole tissue or organ is compromised. As to the issue that some of the most serious maladies of aging humans affect primarily nondividing cells, he feels the underlying problem can still be traced to other, dividing cells such as support cells or cells that line nearby blood vessels. After introductory chapters on recent advances in aging research and mechanisms of cellular senescence, he provides a lengthy chapter devoted to the surmised impact of cellular senescence on cancer and a series of 10 short chapters that consider the pathology of aging skin, muscle, kidneys, eyes, and a host of bodily systems (cardiovascular, immune, etc.).

So how convincing are Fossel's arguments? "Arguments" is the operative word here, as the book makes no pretense of being a scientific review, which carefully sifts and interprets a corpus of evidence. It is instead a polemic, argued in the spirit if not the style of a legal document. Studies are selectively introduced to make a point: the ubiquitous influence of cellular senescence in aging. For a disease like cancer or a function (such as the immune system) in which robust cell division is self-evidently involved, the evidence Fossel adduces is compelling. Nearly everyone would agree that cellular senescence (by providing a telomere-based brake on cell division) acts as a potent antitumor mechanism. Cellular senescence's role in tumor suppression likely underlies the evolution of its mechanisms (*3*). By contrast, his case for interpreting Alzheimer's disease as a result of senescing cells requires a procrustean effort to force an unruly literature into a predetermined box that most researchers in the field would not recognize.

The book's target audience is not clear. The technical language, with a whole alphabet soup of gene names, suggests a work aimed at specialists in cellular and molecular biology. Nonspecialists will certainly find the book heavy going. However, Fossel (a clinical professor of medicine at Michigan State University) is not himself a researcher in the field but an enthusiastic and energetic spectator, and his grasp of the literature is broad rather than deep. This leads to an idiosyncratic, occasionally inaccurate, overview of current research in aging subdisciplines not directly related to cellular senescence. It is also reflected in his habit of invoking roles for telomeres or telomerase on the flimsiest pretext.

Readers interested in an account that places cellular senescence at the epicenter of human aging and assembles as much evidence as possible to support that view will find a great deal to satisfy them in *Cells, Aging, and Human Disease*. Those seeking a more general and balanced overview of recent progress in aging research should look elsewhere.

The reviewer is at the Barshop Center for Longevity and Aging Studies, University of Texas Health Science Center, 15355 Lambda Drive, San Antonio, TX 78245–3207, USA. E-mail: austad@uthscsa.edu

References
1. L. Hayflick, *Sci. Am.* **218**, 32 (March 1968).
2. M. Fossel, *Reversing Human Aging* (Morrow, New York, 1996).
3. J. Campisi, *Cell* **120**, 513 (2005).

10.1126/science.1109551

When Science Is Not Enough: Fighting Genetic Disease in Brazil

Mayana Zatz

In my country, Brazil, one out of five babies dies before their first birthday because of a gene-related disorder. The life-wrecking prevalence of these diseases is invisible only to those who close their eyes. It was during my undergraduate years in the 1960s, while pursuing my childhood dream of becoming a scientist who could cure some of these diseases, that I had a transformative experience.

All of us studying biology at the University of São Paulo at the time had read books by a professor there named Oswaldo Frota-Pessoa, an expert in human and medical genetics. More than his books, it was his example as a scientist that moved me. He became my teacher, scientific adviser, and intellectual father.

On one pivotal day, he ushered me into a world beyond books and laboratories by inviting me to take part in the genetic counseling of families with patients affected by genetic disorders such as Down syndrome or Huntington's chorea. I realized during that counseling session, which took place under Frota's supervision within the university's genetics department, that by entering the field of medical genetics I could do scientific research and simultaneously help those who are suffering from genetic diseases.

At that time, few people envisioned that genetics was destined to become such a consequential science with so many applications in human health. Even fewer people imagined the ethical implications and conundrums that advances in genetic science and technology would bring.

I began laying the groundwork for my own subsequent involvement in these controversial developments as a graduate student and a fledgling genetic counselor. One day I was faced with a young woman who sought genetic counseling because her sister had three sons affected with Duchenne muscular dystrophy, a muscle-wasting disease with no cure. She was getting married and was worried that any sons she might conceive would be destined to develop the disease.

It was heart-wrenching that all we could do for this woman was to recite the statistics to her. All we could tell her was that she would be taking a gamble with any sons she conceived, and that it was up to her if she wanted to take the gamble. Wanting to do more to help this woman and others like her, I decided to focus my research on the disease that had placed her in such a difficult situation.

This yearlong essay series celebrates 125 years of *Science* by inviting researchers from around the world to provide a regional view of the scientific enterprise. Series editor, Ivan Amato

Raging Against Dystrophy

The era of molecular medicine was just beginning. For my part, I analyzed the activity of the muscle enzyme creatine kinase in about 1000 individuals from families with a history of Duchenne muscular dystrophy. We learned that women with high serum levels of creatine kinase had an increased risk of having sons with Duchenne muscular dystrophy. I chose this subject initially for my master's degree, but it also became the focus of my doctoral studies and then my life's work.

Even as I was doing research, my genetic-counseling duties kept me intimately connected to the clinical and social benefits that such research could have. I met daily with families affected by genetic disorders, mostly Duchenne muscular dystrophy. I tried to explain to parents and sisters of affected patients what the disease was, what the prognosis was, what risk they had of having additional affected sons, and what could be done to improve the quality of life for those living with Duchenne muscular dystrophy.

Even after getting my Ph.D., I continued to

CREDIT: COURTESY OF MAYANA ZATZ

Mayana Zatz
Brazil

Mayana Zatz has had a lifelong calling to help those with genetic disorders, mainly progressive muscular dystrophies. She has done so on fronts ranging from investigating the biomolecular bases of such diseases to establishing social institutions dedicated to improving the lives of those who are living with these afflictions. Except for a 2-year stint of postdoctoral work in neuromuscular diseases at the University of California, Los Angeles, Zatz's academic training and professional life have unfolded at the University of São Paulo in Brazil, where she now directs the university's Human Genome Research Center. In 1981, she founded the Brazilian Muscular Dystrophy Association (ABDIM) to improve the lives of children afflicted with muscular dystrophy, particularly those whose hardship is magnified by poverty. Now with its own clinical center, ABDIM serves more than 100 such children, providing physical therapy, psychological counseling, and training in arts and computer skills. In addition to her biomedical research and ABDIM work, Zatz has long been active in genetic counseling, fully embracing the ethical ambiguities that come with the ability to test for the likely onset of diseases for which there are no cures. In addition, Zatz has become socially active in issues that include the ethical use of genetic tests and the use of embryonic stem cells in research and medicine. Among her awards are the TWAS (The Academy of Sciences for the Developing World) Prize in Basic Medical Sciences, in 2003, and UNESCO/L'Oreal "Women in Sciences" Award, in 2001.

All essays appearing in this series can be found online at www.sciencemag.org/sciext/globalvoices/

pursue parallel approaches to combating the disease—molecular studies with the goal of ultimately curing the disease and counseling to help those affected manage the disease. In 1978, I intensified my scientific studies by establishing a new research group at the University of São Paulo. At the same time, I was haunted by a nagging question: What had happened to the families I had counseled during my training period with Professor Frota? The answer, I suspected, would help me choose an area of research most likely to benefit those suffering from Duchenne muscular dystrophy.

Joined by my students, I started to visit my former counselees at their homes. By 1981, we had reestablished contact with about 300 families. During these visits I had two surprises. The good one was that very few children had been born to mothers who had a high genetic risk of having sons with Duchenne muscular dystrophy. Most of these mothers had understood the risks we had outlined in the genetic counseling sessions. To my dismay, however, we witnessed the terrible living conditions of those children with Duchenne muscular dystrophy who were born before the counseling sessions with their parents. Most of them could not leave their houses because they had no wheelchair. They were not accepted in schools because no one wanted to carry them from place to place. They had no access to physical therapy because there was no hope that they would regain mobility. They were completely excluded from society.

I decided that something had to be done for these children. So in 1981 I founded the Brazilian Muscular Dystrophy Association, or ABDIM. My goal was to improve the quality of life of these children and their families by providing education and counseling. The effort grew slowly and steadily, and in 1988, we inaugurated the ABDIM center so that we could directly provide services to at least some of Brazil's most needy children suffering from genetic disorders. Today we use our vans to pick up about 100 children from their homes and bring them to our facility, where they are attended to by a multidisciplinary team. Our staff provides many services for the boys, including physiotherapy, hydrotherapy, psychological support, and art and computer lessons. We are currently raising funds to enlarge the center so that we can serve up to 400 patients.

In the late 1980s, thanks to two former students, Rita Passos-Bueno and Mariz Vainzof, who are currently both faculty members in our department, we introduced molecular genetics technology in our laboratory. This action rekindled my interest in solving the long-term problem of finding a cure for Duchenne muscular dystrophy and other genetic disorders by uncovering the biological bases of these diseases. With these and other collaborators, I was able to publish more than 200 scientific papers, most of them related to neuromuscular disorders.

Few people envisioned that genetics was destined to become such a consequential science with so many applications in human health. Even fewer people imagined the ethical implications...

The Testing Dilemma

As we carried out our studies over the years—mapping new genes and trying to understand their role in the disease process—more genetic tests became available. The introduction of molecular technology brought great advances in the diagnosis and identification of couples at risk of having affected offspring. However, the same tests raised new ethical issues that called for the development of responsible protocols for their use. For many years we had tested the sisters of patients with Duchenne muscular dystrophy to determine if they carried the defective gene responsible for the disorder. Those identified as possible carriers were assured that they themselves would not develop the disease, but they were informed that they were at high risk of having sons who would. Although it is debatable whether the sisters of patients with Duchenne muscular dystrophy should be tested before child-bearing age, I felt that knowledge of the test results would give parents a basis for encouraging their daughters to have a profession and a broader role in life beyond motherhood. Although knowing that one is a carrier of a pathogenic mutation may have a negative emotional impact, our follow-up sessions with the women we counseled revealed that such information helped most of them in their reproductive decisions and, following prenatal diagnosis, in preventing the birth of affected children.

Testing for genetic disorders where asymptomatic carriers may themselves be affected later in life revealed a completely different ethical conundrum. The first example that we encountered was myotonic dystrophy, a disorder that may cause baldness, cataracts, and infertility, as well as muscle weakness and atrophy. For many years, understanding genetic anticipation, that is, the phenomenon in which certain genetic diseases such as myotonic dystrophy appear to become more severe in each successive generation, had been a puzzle. The discovery of dynamic mutations in which a specific short sequence in the gene increases in length from generation to generation was a breakthrough. We were eager to study this type of defective gene in the families of patients diagnosed with myotonic dystrophy. We contacted those who already had been diagnosed with the disease and asked them if they wanted to be tested. Most of them accepted and came with their young children to the laboratory at the University of São Paulo.

We analyzed blood samples from all of the family members, and surprisingly we found that many asymptomatic children carried an expanded form of the gene. This meant not only that they would have a 50% chance of having affected offspring but also that they themselves would develop the disease later in life. Because there is currently no cure or treatment for myotonic dystrophy, the genetic information carried a terrible price. Should we reveal test results to the parents of those children who tested positive if it meant they would be unable to help their

Tough choices. In genetic counseling sessions like the one shown here, the author helps prospective parents at risk of having children with genetic disorders to make reproductive decisions.

CREDIT: COURTESY OF MAYANA ZATZ

little ones?

We decided that this particular type of genetic information exacted too high of an emotional burden. It became our policy not to test children for myotonic dystrophy, Huntington's disease, or other disorders with a relatively late onset and for which there is no cure or treatment. Another ethical argument that we use to justify our policy is that when you test a child for a genetic disease, you deny him the option of deciding in the future whether he wants to be tested or not. Our experience has shown that most young at-risk people prefer not to be tested when we tell them that nothing can be done if they test positive for the disease.

Vote vigil. A group of patients and advocates for stem cell research in Brazil wait to hear the result of a vote by the country's legislators on whether to change a law forbidding such research.

The list of questions that a person needs to consider before deciding to be tested is growing all the time. What disorder are they being tested for? What are the implications of a positive or a negative result? What can and should be done in each case? What are the benefits of genetic testing? In the context of genetic counseling, a discussion of these issues may take hours, and new dilemmas appear all the time. For example, what should be done when the results of genetic tests reveal awkward information about paternity? Or when the test results of one person reveal the risk status of a relative who does not want to know this information?

Another acute dilemma is how to deal with prenatal diagnosis. With the exceptions of rape or to save the mother's life, abortion is forbidden by law in Brazil. Despite the legal restrictions, the reality is that in the past, many women who had close relatives with Duchenne muscular dystrophy or other genetic disorders chose to terminate their pregnancy, often at great danger to themselves, rather than risk passing the defective gene on to their child. Would it have been unethical to withhold the possibility of prenatal diagnosis to these women, even though the technology to do so was in hand?

For us, the pivotal ethical issue is this: If genetic testing were to reveal that a fetus did not carry the defective gene, we might prevent the termination of the pregnancy. Therefore, in the 1990s we decided to offer prenatal diagnosis to women who would interrupt their pregnancy if they feared their fetus might be affected. Since then, we have done hundreds of prenatal diagnoses. In most cases, the test revealed that the fetus had not inherited the pathogenic mutation present in their family. As a result, prenatal diagnosis has encouraged more women to carry their babies to term than to terminate their pregnancies.

I vividly remember a young pregnant woman who came to us for prenatal diagnosis because she had lost two brothers and three uncles to Duchenne muscular dystrophy. It had been an unplanned pregnancy, but she told us she wanted to have the child if we could assure her that the baby would not be at risk of contracting the disease. Unfortunately, our tests showed that the fetus had inherited the defective gene. Her mother, who had accompanied her, immediately said: "You have to interrupt this pregnancy! You don't have to go through what I did." With tears in her eyes, the woman turned to me and asked: "Do you think God wants me to abort this pregnancy?" For a nonreligious person like me, it was not an easy question to answer. "The only thing I can tell you," I said, " is that when your mother was pregnant she did not know she could pass this gene to you and to your affected brothers. But in your case, God wanted you to know. He is putting the decision in your hands."

I found out later that she had terminated the pregnancy, and I think that was the right decision. I believe that we have to keep fighting to change the law in Brazil to allow abortion of fetuses with genetic or untreatable disorders, mainly those incompatible with the ability to lead an independent life. The decision whether to keep or terminate a particular pregnancy has to be primarily the mother's because it is she who will bear all the burden of raising an affected child.

Stemming the Tide

Meanwhile, stem cell research and the prospect of being able to replace defective tissues through stem cell therapy offer enormous hope for patients with disorders such as Duchenne muscular dystrophy. Even so, in February 2004, the Brazilian Congress rejected the scientific or medical use of embryonic stem cells. With a group of scientists and patients' associations, we fought to have the law changed. We also have been waging a public awareness campaign through the media in which we have tried to explain what stem cells are, why research with embryonic stem cells is so important, and the difference between using stem cells from an aborted fetus and using stem cells from frozen embryos obtained as part of fertility procedures and that eventually would be discarded. On 2 March 2005, we learned that our efforts paid off: The legislators approved research with embryonic stem cells. It is hard to describe the emotion that we felt when the results of the vote were announced (352 for and 60 against), and we joined together in holding hands and singing the Brazilian national anthem.

Even as I continue to push for policy reform, I know that success will bring its own difficulties. If the research is permitted, hundreds of desperate patients will beg us to inject stem cells into their bodies, hoping to be cured. Explaining the difference between basic research, therapeutic trials, and proven treatment will be a hard and necessary task that will deflate many people's hopes of a timely cure. However, in my opinion, telling patients that there is no cure for their disease would be a worse frustration. I think people want to know that we scientists are doing our best to rid the world of terrible diseases.

If the research is permitted, hundreds of desperate patients will beg us to inject stem cells into their bodies, hoping to be cured.

The father of a boy with Duchenne muscular dystrophy once told me: "We are special! We have been blessed because we were chosen to take care of these children." I consider the ability to work as a scientist and as a genetic counselor also to be a great blessing.

The author is at the Biosciences Institute, University of São Paulo, Rua do Matão 277, sala 211, São Paulo 05508–090, Brazil.

CREDIT: VALENTINA FRAGOSO

PHYSIOLOGY

Walking Made Simple

R. McNeill Alexander

The obvious way to make a humanlike robot walk is to provide it with motors to drive every joint, and a computer to control them. The computer tells every joint what its angle should be, at every stage of the stride. Many successful robots have been made in this way. The best ones imitate a human walk quite well, but require complex, fast, precise control mechanisms, and use far more energy than a walking human would. In contrast, passive-dynamic walking robots are simple mechanical devices composed of rigid parts connected by joints that are able to walk in a stable fashion down a slope even though they have no motors or controllers. In a recent *Science* paper (*1*), Collins *et al.* describe their design of several new robots inspired by passive-dynamic walkers. These new robots have much simpler control systems than those of powered robots, but walk at least as well as they do, and at lower energy cost.

Enhanced online at www.sciencemag.org/cgi/content/full/308/5718/58

To understand and appreciate these new robots, we need to know something about human walking and its energy cost. The cost of transport for human (or animal) locomotion is defined as (energy cost)/(body weight × distance traveled). It may seem perverse to use weight rather than mass in this formula, but it makes the cost of transport dimensionless. The energy cost may be defined as the food energy consumed (giving the metabolic cost of transport), or as the mechanical work performed (the mechanical cost of transport). Measurements of oxygen consumption show that for humans walking at the most economical speed (about 1.3 m/s), the metabolic cost of transport is about 0.2. The corresponding mechanical cost of transport is about 0.05 (our muscles work with efficiencies of around 0.25) (*2*).

We have to do work, when we walk, to overcome friction in our joints (*3*) and to counter air resistance (*4*), but the work needed for these purposes is far too small to explain the observed costs of transport. In principle, no other work is needed to travel at constant speed over level ground. In the absence of friction and air resistance, a wheeled vehicle given an initial push would roll on for ever over rigid level ground. Why does walking require more energy than ideal locomotion on wheels?

A simple model will help us to answer that question (*5*). The figure depicts a biped with rigid legs of negligible mass. In each step, it rises and falls along an arc of a circle. Similarly, because we keep each leg straight while its foot is on the ground, we rise and fall in each step, more or less along an arc of a circle. The biped slows down as it rises and speeds up as it falls. Kinetic energy is converted to gravitational potential energy and back again, as in a swinging pendulum. No work is needed as the model moves from position (A_1) to position (A_3) in the figure. At position (A_3), however, the vertical component of the body's motion must be reversed; the downward movement of the body must be halted, then work must be done to propel it upward for the start of the next step. The mechanical cost of transport can be calculated from this work. To imitate human walking, assume a speed of 1.3 m/s, a leg length of 0.9 m, and an angle α of 25° (see the figure). With these values, the mechanical cost of transport is 0.02, even lower than the value actually observed for humans.

A first step toward the design of a new, simpler type of walking robot was taken by McGeer (*6*). He built a more sophisticated version of a familiar toy that walks passively down slopes, powered by gravity. As expected (since the toys work well), his robot walked down slopes with a stable gait. In contrast to the earlier powered robots, with their complex control mechanisms, here was a robot that walked stably without any control system. McGeer's work suggested the possibility of much simpler powered robots than had previously been made. However, as a model of bipedal walking, McGeer's model was perhaps a cheat. Instead of two legs it had four that were symmetrically arranged so that it was, in effect, two-dimensional. Kuo (*7*) showed that an equivalent three-dimensional biped would rock from side to side in an unstable way.

McGeer's walker was powered by the gravitational potential energy it lost as it walked downhill. Thus, the cost of transport was (potential energy loss)/(body weight × distance traveled), which is equal to the gradient. By this measure, it proved more economical energy-wise than conventional robots. It was not, however, as economical as the theoretical minimum calculated above, for a surprisingly subtle reason (*6*, *8*). In the figure, (B) represents McGeer's robot at the instant when its foot hits the ground. The force of the impact on this foot reduces the horizontal component of the body's velocity, as well as eliminating the vertical component. More kinetic energy is lost and has to be replaced than predicted by the simple theory in which only the vertical component is affected. As a consequence of this, the mechanical cost of transport is 4cosα times the cost predicted by the simple theory. Using the same values of speed, leg length, and angle α as before, it is 0.07 instead of 0.02. This penalty can be avoided in powered robots if the impulse on the body (the time integral of force) can be kept vertical. One possibility is an upward, forward push with the foot that is about to be lifted, simultaneous with or just before the landing of the other foot (see the figure, C).

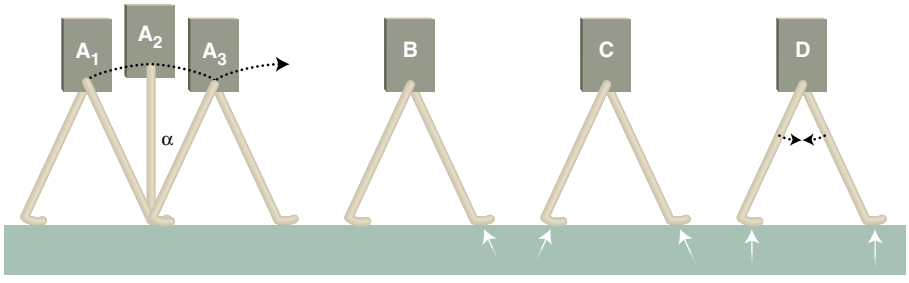

Principles of walking. The diagrams represent walking by a biped whose legs remain straight while the foot is on the ground. (**A**) shows successive stages of a step. (**B**), (**C**), and (**D**) show forces on the feet at the instant when the left (leading) foot hits the ground. In (B), the foot hits the ground before any muscle becomes active. In (C), the right foot pushes on the ground at the instant the left foot lands, making the resultant force on the body vertical. In (D), a torque at the hips has a similar effect.

CREDIT: PRESTON HUEY/*SCIENCE*

The author is in the School of Biology, University of Leeds, Leeds LS2 9JT, UK. E-mail: r.m.alexander@leeds.ac.uk

Another is torque applied at the hip joints, making the forces on the feet vertical (see the figure, D).

One of the new robots described by Collins *et al*. (*1*), the Cornell biped, has been designed to work like the robot in part (C) of the figure. It has a torso, arms with shoulder joints but no elbows, and legs with hip joints, knees, and ankles. An electric motor in the ankle makes one foot push on the ground, just before the other lands. This is remarkably effective, giving a mechanical cost of transport of only 0.055. This cost is approximately equal to the human value, and far better than the estimated mechanical cost of 1.6 for the robot Asimo, in which all joints are motorized and controlled. The hip joints have no motors, but a passive linkage ensures that the torso bisects the angle between the two thighs, and so is kept upright. Other passive linkages make each arm swing in phase with the opposite leg. The knees have no motors, but latches keep them straight while the foot is on the ground. Only the ankles are motorized. This astonishingly simple machine walks like a human and is remarkably economical with regard to energy expenditure.

The second of the new robots described by Collins and co-workers, the Delft biped, was not designed specifically for energy economy, but nevertheless achieves a mechanical cost of transport of only 0.08. It is powered by pneumatic actuators at the hips (see the figure, D). It has no other muscles but, like the Cornell biped, does have controlled latches at the knees. Clever ankle design, based on the principle of skateboard suspensions, improves lateral stability. The third new robot from the Massachusetts Institute of Technology group is based like the others on ramp-walking toys. It has motors only at the ankles. Its special feature is that it learns to control its own walking. Typically, the learning process takes about 10 min or 600 steps, and it can adapt to uneven terrain and different surfaces.

These new robots are important for three reasons. They give us new insight into human walking. They point a possible way to the design of more lifelike artificial legs for amputees. And they bring renewed excitement to the design of humanoid robots. They show us that bipedal robots far simpler than their predecessors work as effectively and far more economically, and can even be designed to teach themselves to walk.

References

1. S. Collins *et al.*, *Science* **307**, 1082 (2005).
2. R. Margaria, *Biomechanics and Energetics of Muscular Exercise* (Clarendon, Oxford, 1976).
3. R. M. Alexander, *Animal Mechanics* (Blackwell, Oxford, ed. 2, 1983).
4. L. G. C. E. Pugh, *J. Physiol.* **207**, 823 (1970).
5. R. M. Alexander, *Appl. Mech. Rev.* **48**, 461 (1995).
6. T. McGeer, *Int. J. Robotics Res.* **9**, 62 (April 1990).
7. A. D. Kuo, *Int. J. Robotics Res.* **18**, 917 (1999).
8. A. D. Kuo, *J. Biomech. Eng.* **124**, 113 (2002).

10.1126/science.1111110

GEOLOGY

The Calibration of Ediacaran Time

Alan J. Kaufman

More than a century ago, the last great geological period was formally ratified by an international committee. This was the final rocky step in the subdivision of deep time based on the evolutionary progression of animal fossils. However, recent years have seen the identification of an older and tumultuous new interval, the Ediacaran Period, during which Earth's earliest soft-bodied organisms emerged in the oceans. This interval was recently ratified (*1*), underscoring advances in the absolute dating (*2*–*6*) and worldwide correlation of geological strata that were deposited in isolated basins before true animals exploded onto the scene in the succeeding Cambrian Period.

On page 95 of this issue, Condon *et al.* (*7*) present precise age constraints for the Ediacaran Period. The authors have analyzed volcanic dust in two key depositional layers in the Doushantuo Formation of southern China. Their radiometric dates provide important insights into the rates of geological and evolutionary processes. The first layer, with an age of about 635 million years, is at the base of the new interval, whereas the second, at about 550 million years, may constrain the age of an environmental disaster (*8*–*10*) that is closely associated with the rapid diversification of the Ediacara biota (see the figure) that lend their name to the new Period.

Early animals? A pile of three-dimensionally preserved casts of the soft-bodied Ediacaran organism *Ernietta* from ~545 million-year-old sediments in the Nama Group of southern Namibia. The scale bar corresponds to 15 cm.

CREDIT: A. J. KAUFMAN

Convention previously focused on the evolutionary first appearance of a specific fossil or assemblage to define the beginning of new geological periods. In contrast, the beginning of the Ediacaran period is defined by the base of a marine carbonate rock, which formed in southern Australia in the aftermath of a distinctive and potentially global ice age (*11*, *12*). Equivalent glacial rocks occur immediately beneath similar carbonates at the base of the Doushantuo Formation.

In the area studied by Condon *et al.*, the new ages constrain the Doushantuo Formation, which represents most of the Ediacaran Period, to some 85 million years—a remarkably long interval for only about 100 m of rock. This observation begs the question: How much time may be missing in Ediacaran strata from southern China?

In the absence of dates between the two radiometric tie points, one must consider two possibilities: Either the sediments accumulated continuously, albeit slowly (some two orders of magnitude more slowly than in similar environments of the same age), or there are breaks in time (hiatuses or unconformities) hidden within the poorly exposed layers. On the basis of limited physical data, Condon *et al.* suggest the presence of two such unconformities in their study area near the Yangtze Gorges. The duration of these stratigraphic breaks with respect to the environmental anomaly—reflecting a dramatic change in the cycling of carbon on Earth's surface—and subsequent biological innovations form the cornerstone of their conclusions, and deserve closer examination.

The author is in the Geology Department and the Earth Science Interdisciplinary Center, University of Maryland, College Park, MD 20742, USA. E-mail: kaufman@geol.umd.edu

Spectacular fossil animal embryos (*13*, *14*) of great evolutionary importance are found at Weng'an (some 375 km to the southwest of the authors' study area), where the Doushantuo Formation accumulated closer to the shoreline and records only a single surface of unconformity. In such nearshore environments, oceanic sediments are often exposed above sea level, resulting in the removal of underlying sediments and hence the erasure of some fraction of geological time. Which of the two hiatal surfaces from the deeper-water sections at the Yangtze Gorges correlates to the single unconformity at Weng'an? The data are more equivocal than presented by Condon *et al.*, and the choice carries important evolutionary consequences.

At the Yangtze Gorges, the extraordinary carbon cycle anomaly recorded in marine carbonates near the top of the Doushanto Formation is truncated by the uppermost unconformity. Condon *et al.* suggest that there is little time missing across the surface, thereby preserving a causal relation between the environmental perturbation and the rapid diversification of Ediacara organisms and associated faunas around 550 million years ago. However, correlation of this surface and the intervening sediments back to Weng'an tells another story. At Weng'an, both the carbon cycle anomaly and the sediments typical of the uppermost Doushantuo Formation at the Yangtze Gorges are missing, implying a substantial hiatus.

Comparison of broadly equivalent strata in southern Australia and the western United States suggests a stratigraphic architecture similar to that in southern China, where similar carbon cycle anomalies are truncated by unconformities (*15*). In the western United States, the post-anomaly unconformity removes a minimum of 130 m of section, more than the entire thickness of the Doushantuo Formation. These observations suggest that the unconformity separating the Ediacaran faunas and the carbon cycle anomaly in southern China may, in fact, hide a lot of time, thereby decoupling the environmental and biological events that the authors wish to connect. This is not meant to detract from the important radiometric calibration that Condon *et al.* provide, but rather to note that the stratigraphic relations between these dates, and therefore their connection to evolutionary events, are far from straightforward.

According to Condon *et al.*, the rapid diversification of complex multicellular organisms in Ediacaran oceans forced the carbon cycle anomaly seen worldwide, but this seems possible only if there is no real time missing across the upper Doushantuo unconformity. If this is not the case, then this interpretation may be placing the cart before the horse. Alternative models suggest that environmental changes may have driven evolutionary transformations. In particular, atmospheric oxygen—long believed to be an external forcing factor to evolution—appears to have built up rapidly during the Ediacaran Period, not because of a discrete biological event but as a result of the tectonic forces that lift and erode mountain ranges (*16*).

Through precise radiometric clocks and clever stratigraphic connections, geoscientists can increasingly correlate Ediacaran sediments that are separated widely in space and time. These tools allow us to piece together a complex puzzle of unforgettable biological events against a background of repetitive climatic and environmental perturbations. However, even with exact dates, the cyclicity of these events and the specter of a fragmentary rock record add uncertainty to our picture of Ediacaran Earth history.

References

1. A. H. Knoll *et al.*, *Science* **305**, 621 (2004).
2. J. P. Grotzinger *et al.*, *Science* **270**, 598 (1995).
3. M. W. Martin *et al.*, *Science* **288**, 841 (2000).
4. J. E. Amthor *et al.*, *Geology* **31**, 431 (2003).
5. K.-H. Hoffmann *et al.*, *Geology* **32**, 817 (2004).
6. C. R. Zhou *et al.*, *Geology* **32**, 437 (2004).
7. D. Condon *et al.*, *Science* **308**, 95 (2005); published online 24 February 2005 (10.1126/science.1107765).
8. S. J. Burns, A. Matter, *Eclogae Geol. Helv.* **86**, 595 (1993).
9. C. R. Calver, *Precambrian Res.* **100**, 121 (2000).
10. F. A. Corsetti, A. J. Kaufman, *Geol. Soc. Am. Bull.* **115**, 916 (2003).
11. P. F. Hoffman *et al.*, *Science* **281**, 1342 (1998).
12. P. F. Hoffman, D. P. Schrag, *Terra Nova* **14**, 129 (2002).
13. S. H. Xiao *et al.*, *Nature* **391**, 553 (1998).
14. J. Y. Chen *et al.*, *Science* **305**, 218 (2004).
15. N. Christie-Blick *et al.*, *Am. J. Sci.* **290A**, 295 (1990).
16. A. J. Kaufman, F. A. Corsetti, *EOS Trans. AGU* **85**, Fall Meet. Suppl. Abstr. PP41A-0575 (2004).

10.1126/science.1111101

EVOLUTION

Where We're Hot, They're Not

Lynn B. Jorde

Homologous recombination, the exchange of material between chromosome pairs during meiosis, plays several key roles in diploid organisms. It produces new combinations of alleles, greatly increasing the potential for adaptive diversity. It is required for the normal separation of the two members of a chromosome pair during meiosis. It is an essential step in recombination-mediated repair of double-strand breaks in DNA. Defects in this crucial repair process can give rise to inherited diseases such as familial breast cancer.

The measurement of recombination frequencies has been the keystone of long-standing efforts to map the chromosomal locations of genes. As Winckler *et al.* (*1*) now report on page 107 of this issue, mapping of recombination hotspots in the human and chimpanzee genomes reveals a surprising finding. Despite 99% identity between human and chimpanzee DNA sequences, there is virtually no overlap between these two species in the locations of their recombination hotspots.

Traditionally, gene mapping in humans has relied on the direct observation of recombination events in families (linkage analysis). This approach, while enormously successful, is limited by the small number of generations during which meiosis can be observed in humans. An alternative approach, based on the once-obscure concept of linkage disequilibrium (LD), has gained widespread attention during the past couple of decades. To understand LD, imagine that a disease-causing mutation has just occurred in a population. The chromosome on which this mutation occurred contains specific DNA variants (alleles) in neighboring polymorphic (variable) loci. At first, the mutation will be observed only in conjunction with these alleles, so the association (or LD) between the mutation and the surrounding variants will be high. Through time, these associations will dissipate because of recombinations between the mutation and nearby loci, and LD will drop (see the figure, A). The closest loci will experience the fewest recombinations and hence retain higher levels of LD with the mutation. Thus, LD patterns can reveal the approximate locations of disease-causing mutations. LD analysis, in contrast to linkage analysis, reflects the effects of dozens or hundreds of past generations of recombination and may therefore confer improved resolution and statistical power to localize mutations. Although its merits are still debated (*2*), LD analysis may be especially useful in the detection of mutations that underlie complex diseases (*3*, *4*), and it has yielded some recent successes (*5*, *6*).

As with all explorations, gene hunting based on LD benefits from a good map. The principal goal of the much-discussed International Haplotype Map (HapMap)

The author is in the Department of Human Genetics, University of Utah School of Medicine, Salt Lake City, UT 84112, USA. E-mail: lbj@genetics.utah.edu

Project (*7*) is to generate such a map and to identify chromosomal regions, or "haplotype blocks," in which LD is maintained at a high level in populations (see the figure, B). By knowing which polymorphic loci are highly correlated with one another, investigators can avoid the wasteful collection of redundant information when searching for disease-causing mutations.

The LD patterns revealed by the HapMap Project and other studies have shown that recombinations appear to be concentrated in specific regions known as hotspots, which are found once every 50 to 200 kb in the human genome (*8*, *9*). A hotspot is defined as a 1- to 2-kb region in which the recombination rate, estimated here by LD, is at least 10 times that in the surrounding region (*9*). A better understanding of hotspots could have important implications for our ability to discover and exploit haplotype blocks (for example, determining how often haplotype blocks are defined by hotspots).

In their new work, Winckler *et al*. (*1*) have addressed this goal by using LD-based methods to compare hotspot locations in 1.5 megabases (Mb) of orthologous DNA sequences from the human and chimpanzee genomes. Human and chimpanzee DNA sequences are almost 99% identical. Thus, if hotspots are sequence-dependent, one might expect a high degree of concordance in their locations. Instead, Winckler *et al*. found that 18 recombination hotspots revealed in the human genome were absent from the chimpanzee genome. Hotspots in the human β-globin and human leukocyte antigen gene regions were also found to be absent in chimpanzees. The three recombination hotspots found in chimpanzees were absent in humans. Another recent study revealed the same lack of concordance (*10*).

What could account for this? One possibility is that LD, which can be affected by evolutionary processes such as natural selection, genetic drift, and admixture (*11*), is not a reliable indicator of recombination hotspots. Indeed, it is possible to generate haplotype blocks through genetic drift alone (*12*). However, Winckler *et al*. show that European and African populations, which have quite different demographic histories, reveal a high degree of concordance in the locations of hotspots (although, as in all such studies, there is generally more LD in the European than in the African sample). Other studies report generally similar findings (*9*, *13*). Even more convincingly, LD-based methods are quite successful in detecting hotspots previously documented by the direct assessment of recombination events in sperm cells (*8*, *14*).

Although the effects of human population history appear not to account for hotspot locations, it is possible that hotspot discordance could result from the substantial differences seen in the demographic histories or population structures of humans and chimpanzees (*15*). Winckler *et al*. used the well-known STRUCTURE algorithm to demonstrate a lack of population structure in the chimpanzee sample, but the number of loci they used (40) may be insufficient to detect meaningful population subdivision (*16*). Sperm typing in chimpanzees would allow a direct examination of recombination hotspots (at least in males) and would more conclusively exclude population structure and demographic history as explanatory factors.

As with any statistical analysis, the power to detect hotspots should be considered. Whereas the sample sizes on which most of the analyses are based are reasonably large (90 European-derived and 90 African individuals), the sample of 38 western chimpanzees is relatively small, as is the amount of DNA sequence (three 500-kb regions in the primary analysis). The authors have addressed this issue extensively and have shown that a lack of power would be unlikely to account for the startling absence of hotspot concordance. Also supporting their findings are the congruent results of Ptak *et al*. (*10*), which were based on an assessment of 14 Mb of DNA sequence in 71 humans but only eight chimpanzees.

Still another possible explanation for these results lies in genomic factors that are known to correlate with recombination rates. Recombination is elevated in GC-rich regions of the genome, and human recombination rates tend to be lower near centromeres and higher near telomeres (*17*, *18*). In addition, the overall human recombination rate is about 60% greater in female than in male meiosis. These factors, while related to recombination rates over relatively large regions, do not appear to correlate strongly with recombination hotspots in humans (*8*, *19*).

Lacking evidence that population history or local DNA sequence variation can account for hotspot location, Winckler *et al*. suggest that epigenetic factors that influence chromatin configuration (for example, acetylation and methylation) may be the key. Here it is useful to consider the budding yeast *Saccharomyces cerevisiae*, which has provided much of our knowledge about eukaryotic recombination. In yeast, meiotic recombination is initiated by DNA double-strand breaks, which occur in relatively open chromatin regions (*17*, *18*). The same appears to be true of mammalian recombination. Furthermore, many of the proteins necessary for this process, such as the DNA topoisomerase–related enzyme Spo11, are highly conserved from yeast to mammals (*19*). Yeast recombination hotspots occur roughly once every 50 kb (*20*), and, as in mammals, they do not appear to

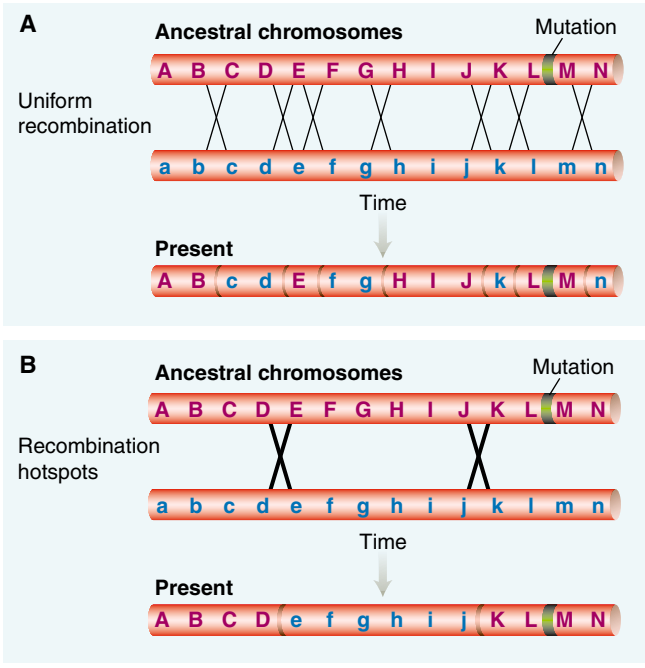

Mapping recombination hotspots. (**A**) Hypothetical ancestral chromosomes contain a series of polymorphic loci with alleles A, a; B, b; C, c and so on. If recombination occurs in a relatively uniform fashion, markers that are close to one another will maintain high levels of linkage disequilibrium (for example, loci A and B). In contrast, markers that are more distant will have low levels of linkage disequilibrium because of multiple intervening recombinations (for example, loci A and N). A mutation that occurs on the ancestral chromosome near loci L and M will be found in association only with those alleles in a chromosome sampled from the present population. (**B**) If recombination is concentrated in hotspots, linkage disequilibrium will be preserved over longer distances across the chromosome (haplotype blocks). Thus, loci A, B, C, and D will retain a high degree of linkage disequilibrium, but between loci D and E linkage disequilibrium will break down rapidly because of multiple recombinations that occur at the hotspot. The mutation located between loci L and M is associated with polymorphic loci over a longer chromosome distance (K, L, M, and N).

be consistently associated with specific DNA sequence motifs (*17*).

These comparisons suggest a number of potentially useful studies. Although technically challenging, it may prove fruitful to examine regional variation in chromatin accessibility in mammalian meiotic cells. How does this affect the action of recombination-related proteins such as Spo11? In addition to Spo11, at least 11 other proteins are involved in the initiation of double-strand breaks and recombination in yeast (*21*), and many of the responsible genes have orthologs in humans (such as, *RAD50*, *RAD51*, and *MRE11*). Comparisons of these genes in humans and chimpanzees could reveal differences that affect recombination patterns. In yeast, recombination hotspots can be eliminated by the insertion of the Ty transposable element, which suppresses recombination in nearby sequences (*22*). Thousands of *Alu* and *LINE1* mobile elements have been differentially inserted in humans and chimpanzees since their divergence 5 million to 6 million years ago (*23*). Could these elements act in a fashion similar to yeast Ty, contributing to the rapid divergent evolution of recombination hotspots in humans and chimpanzees?

Studies such as that by Winckler *et al.* demonstrate the value of comparative genomic analysis for understanding basic biological processes such as recombination, and for potentially improving the design of genetic association studies. Their work also demonstrates the utility of analyses of within-species diversity and underscores the need for DNA sequence information from large samples of humans and other species. As this information accumulates, our understanding of biology, as well as our ability to design well-conceived gene-mapping studies, will continue to evolve and improve.

References and Notes

1. J. D. Terwilliger, F. Haghighi, T. S. Hiekkalinna, H. H. Goring, *Curr. Opin. Genet. Dev.* **12**, 726 (2002).
2. L. B. Jorde, *Genome Res.* **10**, 1435 (2000).
3. C. S. Carlson, M. A. Eberle, L. Kruglyak, D. A. Nickerson, *Nature* **429**, 446 (2004).
4. T. Laitinen *et al.*, *Science* **304**, 300 (2004).
5. J. P. Hugot *et al.*, *Nature* **411**, 599 (2001).
6. International HapMap Consortium, *Nature* **426**, 789 (2003).
7. G. A. T. McVean *et al.*, *Science* **304**, 581 (2004).
8. D. C. Crawford *et al.*, *Nat. Genet.* **36**, 700 (2004).
9. W. Winckler *et al.*, *Science* **308**, 107 (2005); published online 10 February 2005 (10.1126/science.1105322).
10. S. E. Ptak *et al.*, *Nat. Genet.*, published online 18 February 2005 (10.1038/ng1529).
11. K. T. Zondervan, L. R. Cardon, *Nat. Rev. Genet.* **5**, 89 (2004).
12. K. Zhang *et al.*, *Hum. Genet.* **113**, 51 (2003).
13. D. M. Evans, L. R. Cardon, *Am. J. Hum. Genet.* **76**, 681 (2005).
14. A. J. Jeffreys, L. Kauppi, R. Neumann, *Nat. Genet.* **29**, 217 (2001).
15. A. Fischer, V. Wiebe, S. Paabo, M. Przeworski, *Mol. Biol. Evol.* **21**, 799 (2004).
16. M. J. Bamshad *et al.*, *Am. J. Hum. Genet.* **72**, 578 (2003).
17. T. D. Petes, *Nat. Rev. Genet.* **2**, 360 (2001).
18. B. de Massy, *Trends Genet.* **19**, 514 (2003).
19. L. Kauppi, A. J. Jeffreys, S. Keeney, *Nat. Rev. Genet.* **5**, 413 (2004).
20. J. L. Gerton *et al.*, *Proc. Natl. Acad. Sci. U.S.A.* **97**, 11383 (2000).
21. S. Prieler, A. Penkner, V. Borde, F. Klein, *Genes Dev.* **19**, 255 (2005).
22. S. Ben-Aroya, P. A. Mieczkowski, T. D. Petes, M. Kupiec, *Mol. Cell* **15**, 221 (2004).
23. D. J. Hedges *et al.*, *Genome Res.* **14**, 1068 (2004).

24. I thank NIH and NSF for financial support, and M. Bamshad, D. Carroll, A. Rogers, R. Toydemir, W. S. Watkins, D. Witherspoon, and S. Wooding for helpful comments.

10.1126/science.1110903

PSYCHOLOGY

Beyond a Joke: From Animal Laughter to Human Joy?

Jaak Panksepp

In the beginning was the word…but was the word funny? Research suggests that the capacity for human laughter preceded the capacity for speech during evolution of the brain. Indeed, neural circuits for laughter exist in very ancient regions of the brain (*1*), and ancestral forms of play and laughter existed in other animals eons before we humans came along with our *hahahas* and verbal repartee. Recent studies in rats, dogs, and chimps (*2*, *3*) are providing evidence that laughter and joy may not be uniquely human traits.

The capacity to laugh emerges early in child development, and perhaps in mammalian brain-mind evolution as well. Indeed, young children, whose semantic sense of humor is marginal, laugh and shriek abundantly in the midst of their other rough-and-tumble activities. If one looks carefully, laughter is especially evident during chasing, with the chasee typically laughing more than the chaser. As every aspiring comedian knows, success is only achieved if receivers exhibit more laughter than transmitters. The same behavior patterns are evident in the "play panting" of young chimps as they mischievously chase, mouth, and tickle each other (*2*).

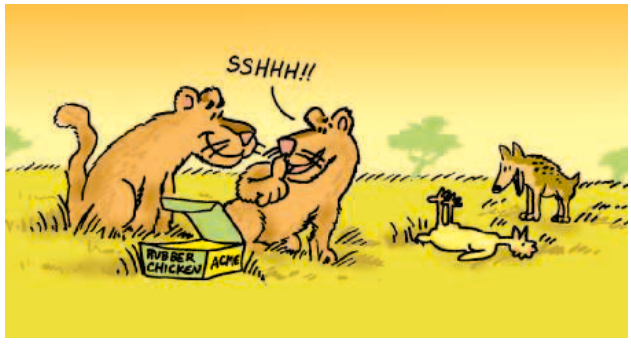

CREDIT: JOE SUTLIFF

Laughter seems to hark back to the ancestral emotional recesses of our animalian past (*3*, *4*). We know that many other mammals exhibit play sounds, including tickle-induced panting, which resembles human laughter (*2*, *4*, *5*), even though these utterances are not as loud and persistent as our sonographically complex human chuckles (*6*). However, it is the discovery of "laughing rats" that could offer a workable model with which to systemically analyze the neurobiological antecedents of human joy (*3*). When rats play, their rambunctious shenanigans are accompanied by a cacophony of 50-kHz chirps that reflect positive emotional feelings (*7*). Sonographic analysis suggests that some chirps, like human laughs, are more joyous than others.

Could sounds emitted by animals during play be an ancestral form of human laughter? We have shown that if rats are tickled in a playful way, they readily emit these 50-kHz chirps (*3*, *8*). The rats we tickled became socially bonded to us and were rapidly conditioned to seek tickles. They preferred spending time with other animals that chirped a lot rather than with those that did not (*3*). Indeed, chirping in rats could be provoked by neurochemically "tickling" dopamine reward circuits in the brain (*9*), which also light up during human mirth (*10*). Perhaps laughter will provide a new measure for analyzing natural reward/desire circuits in the brain, which are also activated during drug craving (*7*, *11*).

Deciphering the neural circuitry of play-

The author is at the J. P. Scott Center for Neuroscience, Mind and Behavior, Department of Psychology, Bowling Green State University, Bowling Green, OH 43403,USA, and at the Falk Center for Molecular Therapeutics, Department of Biomedical Engineering, Northwestern University, Evanston, IL 60201, USA. E-mail: jpankse@bgnet.bgsu.edu

ful chirping in rats is an important goal of future research. Such knowledge may help to reveal how joking and horsing around emerged in our expansive higher brain regions. Although no one has investigated the possibility of rat humor, if it exists, it is likely to be heavily laced with slapstick. Even if adult rodents have no well-developed cognitive sense of humor, young rats have a marvelous sense of fun. We have already bred rats that exhibit excess playful chirping (*12*), and thereby hope to track down some of the genes for joy. Perhaps we will even stumble on new molecules to alleviate depression as well as some excessive-exuberance disorders (*13*, *14*).

Research on rough-housing play in mammals, both sapient and otherwise, clearly indicates that the sources of play and laughter in the brain are instinctual and subcortical (*1*, *3*, *8*). Although our species-typical capacities for verbal joking surely reflect highly refined cortico-cognitive skills (*15*), those incoming words must somehow tickle the ancient playful circuits of our minds for joy to occur. As we learn "to rib" each other with words, as opposed to just rough-and-tumble horse-play, we may be developing new synaptic connections to joyous neural zones that reside far below our cerebral crowns. It has long been intimated that laughter has many health benefits as well (*16*).

Human laughter, however, has a dark and dominant side. According to the philosopher Thomas Hobbes, "Laughter is nothing else but a sudden glory arising from some sudden conception of some eminency in ourselves." Experts compiling the DSM-V psychiatric guidelines may wish to consider how excessive gloating laughter contributes to "eminent-domain" disorders worthy of more precise psychiatric diagnosis. New treatments for such disorders might include strengthening the capacity for internal silent laughter (*17*), one of the few remaining mental capacities that may be uniquely human.

Many still believe that emotional feelings, from joy to grief, are special capacities of the human brain, but as Darwin taught, it just ain't so (*18*). The recognition of emotional feelings in our fellow animals should no longer be reflexively deemed an anthropomorphic sin (*4*, *8*). Perhaps it is time for neuroscience to accept that animals are capable of many emotional feelings (*8*, *19*) (despite the consternation that may cause for investigators who treasure the study of fear behaviors more than joy).

We find ourselves at the tall-tale end of an intellectual era when the animal mind was deemed nonexistent or impenetrable. Gentle Darwin was prescient when he coaxed us to see our own emotional nature as continuous with that of our fellow animals (*18*). By studying the many emotional "instinctual" behaviors and related learning capacities of other animals, we may develop excellent ways to fathom the neuroemotional foundations of human consciousness. Weighty data are tipping the scales of evidence in favor of ever more subtle affective conceptions of animal minds, *H. sapiens* included (*8*). Although our emotional systems are neither uniquely nor intelligently designed, it is a blessing that we can finally understand their affective nature (*19*). As William Blake incomparably declared in *Auguries of Innocence* (1863):

> It is right it should be so;
> Man was made for joy and woe;
> And, when this we rightly know
> Through the world we safely go.
> Joy and woe are woven fine
> A clothing for the soul divine;
> Under every grief and pine
> Runs a joy with silken twine.

If the mental lives of other animals are also created from the neural threads of joy and woe (not to mention many other feelings), we may need to openly consider the nature of their affective brains in order to understand our own. This brings special responsibilities for the scientifically sapient savants among us (*20*, *21*). Although some still regard laughter as a uniquely human trait, honed in the Pleistocene, the joke's on them.

References

1. K. Poeck, in *Handbook of Clinical Neurology*, P. J. Vinken, G. W. Bruyn, Eds. (North Holland, Amsterdam, 1969), vol. 3.
2. T. Matsusaka, *Primates,* **45**, 221 (2004).
3. J. Panksepp, J. Burgdorf, *Physiol. Behav.* **79**, 533 (2003).
4. G. M. Burghardt, *The Genesis of Animal Play* (MIT Press, Cambridge, MA, 2005).
5. R. R. Provine, *Laughter* (Viking, New York, 2000).
6. J.-A. Bacharowski *et al.*, *J. Acoust. Soc. Am.* **110**, 1581 (2001).
7. B. Knutson *et al.*, *Psychol. Bull.* **128**, 961 (2002).
8. J. Panksepp, *Affective Neuroscience* (Oxford Univ. Press, New York, 1998).
9. J. Burgdorf *et al.*, *Behav. Neurosci.* **115**, 940 (2001).
10. D. Mobbs *et al.*, *Neuron,* **40**, 1041 (2003).
11. J. Panksepp *et al.*, *Addiction,* **97**, 459 (2002).
12. J. Burgdorf *et al.*, *Behav Genet.* **35**, 67 (2005).
13. J. Panksepp, Ed. *Textbook of Biological Psychiatry* (Wiley, Hoboken, NJ, 2004).
14. J. Panksepp *et al.*, *Neuroendocrinol. Lett.* **23** (suppl. 4), 105 (2002).
15. B. Wild *et al.*, *Brain*, **126**, 2121 (2003).
16. L. Joubert, *Treatise on Laughter* (Univ. of Alabama Press, Birmingham, AL, 1579/1980).
17. J. Panksepp, N. Gordon, *Consciousness & Emotion,* **4**, 197 (2003).
18. C. Darwin, *The Expression of Emotions in Man and Animals* (Oxford Univ. Press, New York, ed. 3, 1872/1998).
19. J. Panksepp, *Consciousness & Cognition* **14**, 22 (2005).
20. T. Grandin, *Animals in Translation,* (Scribner, New York, 2005).
21. F. D. McMillan, Ed., *Mental Health and Well-Being in Animals* (Blackwell, Boston, MA, 2005)

10.1126/science.1112066

MATERIALS SCIENCE

Playing Nature's Game with Artificial Muscles

Ray H. Baughman

Feel the pumping of your heart or leap to witness the wonder of some of nature's muscles. Skeletal muscles self-repair, provide billions of work cycles involving contractions of more than 20%, increase strength and change stiffness in response to need, generate stresses of ~0.35 MPa, contract at 50% per second, and can even transform to fuel for the starved body (*1*). They convert the energy of a safe, energetic fuel (adenosine triphosphate) to mechanical energy with higher maximum efficiency (~40%) than that achieved by a typical car engine (*1*).

Artificial muscles offering even higher performance are being sought for artificial and damaged hearts, artificial limbs, humanoid robots, and bird- or insect-like air vehicles that fly by flapping wings. How well do such artificial muscles compare with natural muscle, and what are the prospects for future advances? This Perspective focuses on artificial muscles that generate large strains (fractional changes of muscle length) of about 20%, rather than high force, high response rate, and/or high output power at low strain. Instead of mimicking nature by creating large macroscopic strains by the combined effects of trillions of molecular actuators, the artificial muscles use material deformations.

Electronically conducting polymers such as polyaniline and polypyrrole provide one type of high-strain actuator. In what is basically a battery, these muscles actuate by using dimensional changes produced by electrochemically inserting solvated dopant ions into a conducting-polymer electrode. Although first described almost two

The author is at the NanoTech Institute and Department of Chemistry, University of Texas at Dallas, Richardson, TX 75083, USA. E-mail: ray.baughman@utdallas.edu

decades ago (*2*), conducting-polymer muscles with strains matching those of natural muscles have only recently been realized (*3*). These advances are likely to accelerate commercialization efforts (*4*). Arrays of micrometer-scale conducting-polymer muscles have been made that undergo complex, coordinated motions. However, these devices (*5*, *6*) typically operate at a strain of 1% or less by using the cantilever effect to amplify displacements.

State-of-the-art conducting-polymer artificial muscles operate at voltages of a few volts and can generate high strains (26%), high strain rates (11% per second), and large stresses (7 to 34 MPa) (*1*, *3*, *7*). However, actuator performance typically degrades after a few thousand cycles when the actuator is operated at high actuator strains and high applied mechanical loads. Energy conversion efficiencies are low (typically <1%) but could be improved drastically by avoiding electrolyte electrolysis, harvesting stored electrical energy, and using doping-induced conformation changes (*1*, *2*, *8*).

Another type of artificial muscle is based on dielectric elastomers, which resemble the silicone rubbers used as sealants. These systems can generate higher actuator strains than do conducting-polymer artificial muscles, and they constitute capacitors rather than batteries (*9*). Actuation is mainly caused by "Maxwell stress," which results from the attraction between charges on opposite capacitor electrodes and the repulsion between like charges. Artificial Muscle Inc. (*4*) was recently founded to exploit the impressive performance of elastomeric actuators, which can generate strains of 120%, stresses of 3.2 MPa, and a peak strain rate of 34,000% per second for 12% strain (*1*). When elastomer stiffness is decreased, maximum stress generation decreases, but maximum actuator stroke and work-per-cycle increase. Operating voltages of several thousand volts have thus far limited application, but strategies for avoiding this problem are evolving (*10*).

A third type of artificial muscle uses the volume change of an electrolyte and electrostatic repulsion (*1*, *11*). One version, which amplifies low strains using the cantilever effect, is called the ionic polymer/metal composite actuator (*12*). These actuators, sold by Environmental Robots Inc. (*4*), consist of two metal-nanoparticle electrodes that are both filled with a solid electrolyte and separated by this electrolyte. The actuators act as supercapacitors: An applied interelectrode potential injects electronic charge into the high-surface-area electrodes. To balance this charge, solvated ions migrate between the electrodes, causing one electrode to expand relative to the other, thereby bending the cantilever actuator strip. Tensile strains of 40% have been produced by a related device in which an electrode-wrapped polymer gel yarn is separated from a counter electrode by a liquid electrolyte (*13*). Actuation results from a local pH change caused by electrolysis of the electrolyte and transport of hydrated ions and water into the yarn, but actuation rate and energy conversion efficiency are low.

Other high-strain artificial muscles include shape-memory alloys, which are commercially important and generate strains of up to 8%, but require conversion of electrical energy to thermal energy and the inefficient conversion of the latter to mechanical energy (*1*). Actuators that use electrochemically generated gases confined in carbon nanotubes provide strains of 300%, but energy conversion efficiency and cycle life are low (*14*).

All of these high-strain artificial muscles suffer from challenging problems that have delayed their commercial application. How might these problems be overcome for applications such as autonomous biomimetic robots?

A possible clue is provided by low-voltage, low-strain actuators that use electrochemical charge injection into a nanostructured electrode, resulting in electrostatically driven electrode expansion (*15*). One such device type, carbon nanotube artificial muscles, can generate 100 times the stress of natural muscle and provides comparable actuation rates (20% per second), but the actuator strain is at best 2%. These performance characteristics could be improved by replacing the carbon nanotubes with, for instance, a nanostructured elastomeric conducting polymer that has a comparable gravimetric surface area but is more easily deformable (by a factor of 100).

Another approach is to radically improve the ionic polymer/metal composite actuators by first replacing cantilever actuators that operate by bending with actuators that operate in tension. This could be done by separating the opposing electrodes by a liquid electrolyte, which would provide the solvated ions that cause actuation. The gravimetric capacitance of today's ionic polymer/metal composite actuators is less than one-tenth that of other supercapacitors. Increasing this capacitance by increasing the electrode surface area could provide a corresponding increase in actuator strains, as long as the electrode does not restrict movement in the actuator stroke direction. Highly twisted carbon nanotube yarns, with their high electrical conductivities and high surface area (*16*), seem ideal for use as this type of electrode (see the figure).

Nature's scheme of converting the chemical energy of a high-energy-density fuel to mechanical work has advantages, which can be partially achieved by driving electrical actuators with fuel cells. Because a fuel cell and fuel source can deliver more than three times as much electrical energy as a battery of the same weight, fuel cells are preferred for autonomous robots that use electrically powered artificial muscles. It would be very useful to have muscles for artificial hearts that use the same fuel and arterial fuel delivery system as natural muscle, or autonomous humanoid robots for hazardous environments that drink a shot of alcohol or hydrazine to continue work. Gel actuators and conducting-polymer actuators can be driven to provide high

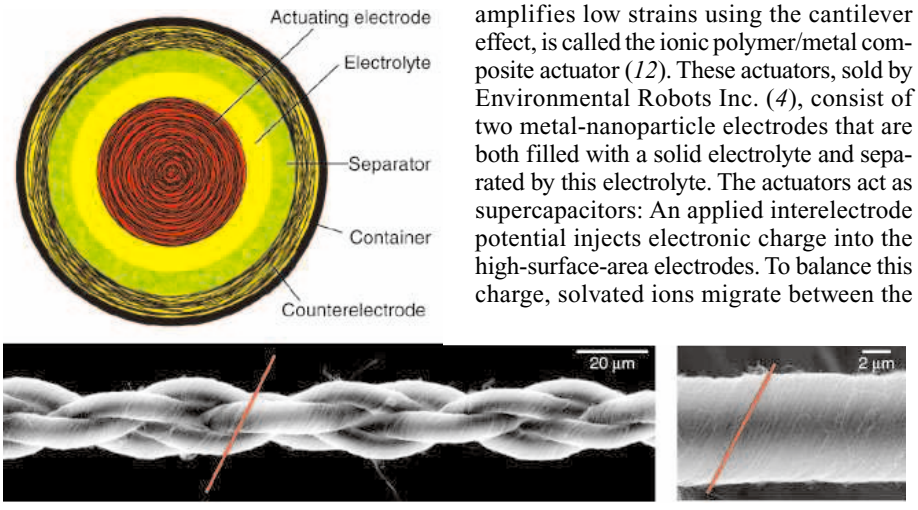

A proposed high-stroke artificial muscle. (Top) Cross section of the proposed actuator. A highly twisted nanofiber yarn electrode (black) is filled with a conducting polymer or gel electrolyte (red). The conducting polymer or electrolyte does the actuation. The nanofibers provide nanometer-scale electronic connections and giant surface area for electrochemical charge injection. A counterelectrode and a porous electrode separator are also included. A liquid electrolyte (yellow) provides the electrochemically inserted solvated ions that cause actuation when a voltage is applied between the electrodes. **(Bottom)** Scanning electron micrographs of highly twisted four-ply and single-ply multiwalled carbon nanotube yarns (*16*). The oblique nanotube alignment (red lines) enables large extension in the yarn direction.

CREDIT: BOTTOM LEFT FROM (*16*); BOTTOM RIGHT, MEI ZHANG/NANOTECH INSTITUTE, UNIVERSITY OF TEXAS AT DALLAS

actuator strains by means of chemical energy, but either the fuel energy density or the chemical-mechanical conversion efficiency is low (*1*, *11*).

If an artificial muscle could simultaneously serve as a fuel cell, then weight, volume, and cost reductions could result. Inactive muscles could be used as fuel cells to provide other electrical needs for the robot, or could be joined together in series to power high-rate actuation for active fuel-cell muscles. The concept of making a carbon nanotube–based fuel cell muscle is patented (*17*) and has been demonstrated in a primitive prototype (*18*). Yet humankind is still far behind in much of nature's game of providing high-strain muscles.

References and Notes

1. J. D. Madden *et al.*, *IEEE J. Ocean. Eng.* **29**, 706 (2004).
2. R. H. Baughman, *Synth. Metals* **78**, 339 (1996).
3. S. Hara *et al.*, *J. Mater. Chem.* **14**, 1516 (2004).
4. Y. Bar-Cohen posts periodic newsletters on artificial muscles at http://eap.jpl.nasa.gov.
5. E. Smela, O. Inganäs, I. Lundström, *Science* **268**, 1735 (1995).
6. E. Smela, *Adv. Mater.* **15**, 481 (2003).
7. S. Hara *et al.*, *Synth. Metals*, in press.
8. W. Lu *et al.*, *Science* **297**, 983 (2002).
9. R. Pelrine *et al.*, *Science* **287**, 836 (2000).
10. Q. M. Zhang, V. Bharti, X. Zhao, *Science* **280**, 2101 (1998).
11. D. Kaneko, J. P. Gong, Y. Osada, *J. Mater. Chem.* **12**, 2169 (2002).
12. S. Nemat-Nasser, Y. Wu, *J. Appl. Phys.* **93**, 5255 (2003).
13. H. B. Schreyer *et al.*, *Biomacromolecules* **1**, 642 (2000).
14. G. M. Spinks *et al.*, *Adv. Mater.* **14**, 1728 (2002).
15. R. H. Baughman, A. A. Zakhidov, W. A. de Heer, *Science* **297**, 787 (2002).
16. M. Zhang, K. R. Atkinson, R. H. Baughman, *Science* **306**, 1358 (2004).
17. R. H. Baughman *et al.*, U.S. Patent 6,555,945 (29 April 2003).
18. V. H. Ebron *et al.*, unpublished data.

19. This work was supported by Defence Advanced Projects Agency grant MDA 972-00-C-0032 and the Robert A. Welch Foundation.

10.1126/science.1099010

CELL BIOLOGY

Kinasing and Clipping Down the NF-κB Trail

Nicolai S. C. van Oers and Zhijian J. Chen

Cells of the innate and adaptive immune system recognize and respond to pathogenic insults with a diverse array of cell surface receptors. These distinct receptor complexes share one commonality: activation of the master transcription factor NF-κB. The basic mechanism of NF-κB activation involves the phosphorylation and ubiquitin-mediated degradation of its inhibitor IκB. Phosphorylation of IκB is carried out by a large kinase complex termed IKK, which integrates signals from multiple pathways. Some of the pathways leading to IKK activation are quite sophisticated, as exemplified by the T cell activation pathway (*1*). T cells express a cell surface receptor termed the T cell receptor (TCR) that recognizes foreign peptides embedded in host major histocompatibility complex (MHC) molecules. Research over the past decade has uncovered more than a dozen proteins that link the TCR to IKK, yet two recent papers in *Science* (*2*, *3*), including one on page 114 of this issue, teach us that our understanding of the NF-κB pathway is far from complete. These studies add two more players, a kinase and a caspase, to the NF-κB pathway that is set in motion by TCR activation. The new studies underscore how exquisitely the adaptive immune system is regulated.

The recognition of suitable peptide-MHC ligands by TCR activates a sequence of intracellular protein tyrosine phosphorylation events. These events are coordinated by three families of protein tyrosine kinases: Src, Syk, and Tec (*4*). Upon TCR ligation, Src protein tyrosine kinases (Lck in T cells) selectively phosphorylate two tyrosine residues present in the immunoreceptor tyrosine-based activation motifs (ITAMs) of the TCR subunits (see the figure). In a biphosphorylated state, the ITAMs are bound in a complex with the tandem Src homology 2 (SH2) domains of a Syk protein tyrosine kinase called ZAP-70. Catalytic activation of ZAP-70 depends on its autophosphorylation and transphosphorylation by Lck. Activated ZAP-70 then phosphorylates tyrosine residues on an essential adaptor protein termed LAT (linker of activated T cells). LAT is a type II transmembrane protein that is localized in the plasma membrane by addition of palmitoyl groups to its two cysteine residues. The phosphorylated tyrosine residues in LAT provide key docking sites for a number of SH2-containing adaptor and effector proteins, including phospholipase C–γ, SLP76, and guanine nucleotide exchange factors (GEFs) such as Vav (see the figure).

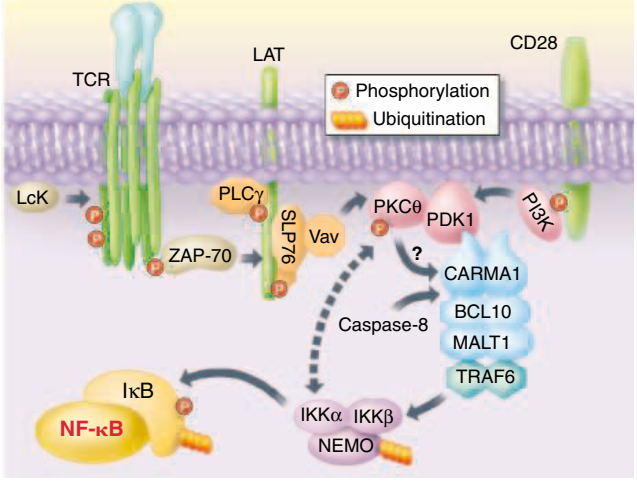

The NF-κB activation pathway in T cells. Stimulation of a T cell receptor (TCR) by a peptide-MHC complex and costimulation of CD28 by ligands on antigen-presenting cells activate a cascade of tyrosine phosphorylation. This cascade results in the activation of PI3K, PDK1, and PKCθ. PDK1 recruits IKK to the lipid rafts of the plasma membrane through PKCθ, and recruits BCL10 and MALT1 through CARMA1. PKCθ may also regulate the CARMA1-BCL10-MALT1 (CBM) complex through phosphorylation of its members. MALT1 mediates polyubiquitination of the IKK subunit NEMO directly or indirectly through the TRAF6 ubiquitin ligase. Caspase-8 is also required for IKK activation by facilitating the binding of IKK to the CBM complex in response to TCR stimulation. Membrane translocation and ubiquitination of IKK lead to its activation. Activated IKK phosphorylates IκB and targets this NF-κB inhibitor for ubiquitination and subsequent degradation by the proteasome. Degradation of IκB enables NF-κB to enter the nucleus and switch on expression of genes that are essential for the proliferation and function of activated T cells.

Through an unknown mechanism, SLP76 and Vav lead to the activation of the serine-threonine kinase PKCθ and the recruitment of this kinase to lipid rafts in the plasma membrane, where TCR bound to its ligand resides. According to the current model, PKCθ activates IKK through additional proteins including CARMA1 (also known as CARD11), BCL10, and MALT1, which form a complex [referred to as CBM, as suggested in (*2*)]. Each component of this complex is essential for NF-

N. S. C. van Oers is in the Department of Microbiology and the Center for Immunology, and Z. J. Chen is in the Department of Molecular Biology, University of Texas Southwestern Medical Center, Dallas, TX 75390, USA. E-mail: zhijian.chen @utsouthwestern.edu

κB activation in T cells (*5*). MALT1 activates IKK by promoting the ubiquitination of the IKK subunit NEMO directly (*6*), or indirectly through the RING domain ubiquitin ligase TRAF6 (*7*, *8*).

To elucidate the mechanism of PKCθ activation in T cells, Lee *et al*. (*3*) investigated the phospholipid-dependent kinase PDK1. As noted previously (*9*), PKCθ contains a putative PDK1 phosphorylation site at threonine 538 in its activation loop. PDK1 is a serine-threonine kinase regulated by phosphatidylinositol 3-kinase (PI3K), an enzyme that phosphorylates inositol phospholipids at the 3′ position of the inositol ring to produce phosphatidylinositol 4,5-bisphosphate (PIP_2) and phosphatidylinositol 3,4,5-trisphosphate (PIP_3). These phospholipids recruit selected effector proteins (including PDK1) that contain a pleckstrin-homology (PH) domain. The mechanism of PI3K activation through TCR requires further investigation. However, PI3K is known to be activated by a second cell surface molecule termed CD28, which provides a critical costimulatory signal for T cell activation by interacting with ligands expressed on antigen-presenting cells. Inhibitors of PI3K block the translocation of PKCθ to the lipid rafts in stimulated T cells, whereas constitutively active PI3K or overexpression of PDK1 enhance translocation of PKCθ to the lipid rafts (*10*). Thus, it is likely that the PI3K pathway is involved in PKCθ activation. One study, however, found no signal-dependent translocation of PDK1 to the lipid rafts in T cells (*10*), so the link between PI3K and PKCθ remained unclear.

Lee *et al*. now provide strong evidence that PDK1 is required for the activation of PKCθ and IKK in T cells. After stimulation of TCR and CD28, PDK1 moves to the lipid rafts and then binds to and phosphorylates (presumably directly) PKCθ at threonine 538 in its activation loop. Silencing of PDK1 expression in Jurkat T cells by RNA interference (RNAi) abrogated PKCθ phosphorylation, IKK and NF-κB activation, and interleukin-2 production in response to TCR stimulation. RNAi of PDK1 also prevented the binding of PKCθ to IKK and blocked the translocation of these two kinases to lipid rafts. With these results in hand, Lee and co-workers propose that PDK1 recruits PKCθ to plasma membrane lipid rafts and that PKCθ in turn recruits IKK.

If PKCθ's only job is to recruit IKK to the plasma membrane, then what are the members of the CBM complex (CARMA1-BCL10-MALT1) doing, given that they are clearly essential for IKK activation? It turns out that PDK1 also binds to CARMA1 and is required for the recruitment of CARMA1 and BCL10 to the lipid rafts. These findings prompted Lee *et al*. to propose a dual role for PDK1 in the TCR pathway. PDK1 recruits not only IKK to lipid rafts through PKCθ but also the CBM complex to lipid rafts, where MALT1 activates IKK through ubiquitination of NEMO.

The model proposed by Lee *et al*. is a substantial revision of the current linear model in which PKCθ operates upstream of CBM, which in turn recruits IKK to the lipid rafts. Although PKCθ is required for IKK activation in mature T cells, it is not clear whether it is also required for the recruitment of CBM. The requirement of CARMA1 for IKK recruitment needs further investigation. Lee *et al*. showed that CARMA1 deficiency did not affect the recruitment of IKK to PKCθ. However, two other groups—one using the same CARMA1-deficient cell line, the other using T cells derived from CARMA1-deficient mice—showed that CARMA1 is required for recruiting IKK to the lipid rafts (*11*, *12*). Although the exact biochemical mechanism of IKK activation by PKCθ remains to be resolved, the establishment of PDK1 as an essential upstream kinase of PKCθ has filled an important gap in the TCR pathway.

Another player in the TCR pathway is caspase-8, a cysteine protease that initiates apoptosis through "clipping" various cellular proteins. Surprisingly, T cells from patients carrying mutations in caspase-8 not only are defective in apoptosis, but also fail to activate NF-κB after TCR stimulation (*13*). In a recent study, Su *et al*. further investigated the mechanism by which caspase-8 mediates NF-κB activation in T cells, and they make several important observations (*2*). First, the enzymatic activity, but not autoprocessing, of caspase-8 is required for restoring NF-κB activation in a caspase-8–deficient cell line. Second, caspase-8 binds to CBM and IKK upon TCR stimulation. In cells lacking caspase-8, BCL10 still binds to MALT1, but this complex no longer recruits IKK in response to signals. Third, FADD, an adaptor protein known to interact with caspase-8, also binds to BCL10 and MALT1 in a signal-dependent manner. Taken together, these results suggest that FADD and caspase-8 bind to CBM and facilitate the recruitment and activation of IKK. Currently, it is not clear where caspase-8 is positioned in the IKK pathway in T cells. Caspase-8 may work upstream of CBM to facilitate the oligomerization and activation of CBM, thus promoting the recruitment of IKK. Alternatively, caspase-8 could bridge CBM and IKK, facilitating binding between these two complexes.

The signaling capabilities of caspase-8 appear to be an evolutionarily conserved mechanism in innate and adaptive immunity. Indeed, the *Drosophila* caspase-8 homolog Dredd is essential for the antibacterial response mediated by the NF-κB homolog Relish (*14*). In cells treated with caspase inhibitors or in Dredd-deficient cells, Relish cannot be cleaved into a mature subunit in response to bacterial challenge. Although Dredd is a putative protease of Relish, so far there is no biochemical evidence that Dredd cleaves Relish directly. Instead, there is now evidence that Dredd mediates the activation of *Drosophila* IKK, which phosphorylates and targets Relish for cleavage (*15*). Thus, the caspase-8 family of proteins has evolved to acquire dual roles in apoptosis and immunity, both of which are beneficial to the hosts in their battle against pathogens.

The revelation that PDK1 and caspase-8 play key parts in TCR-mediated activation of IKK sets the stage for unraveling the biochemical mechanisms of T cell signaling. Key questions remain to be addressed: How are PI3K and PDK1 activated by early signaling events in the TCR pathway? What are the physiological substrates of PKCθ? Does PKCθ help to recruit CBM? Is CBM required for the recruitment of IKK? What are the physiological targets of caspase-8 in the IKK pathway? How is caspase-8 activated by TCR stimulation? Answers to these and other questions will undoubtedly add to a more complete picture of T cell activation, which has been a core subject of immunology research. Because PDK1, PKCθ, and caspase-8 are enzymes that are amenable to chemical intervention, specific inhibitors of these enzymes could potentially become a new generation of immunosuppressive agents. The recent work on PDK1 and caspase-8 is a timely reminder that perhaps there are more treasures hidden down the NF-κB trail.

References

1. R. Weil, A. Israel, *Curr. Opin. Immunol.* **16**, 374 (2004).
2. H. Su *et al.*, *Science* **307**, 1465 (2005).
3. K.-Y. Lee *et al.*, *Science* **308**, 114 (2005).
4. L. A. Pitcher, N. S. van Oers, *Trends Immunol.* **24**, 554 (2003).
5. X. Lin, D. Wang, *Semin. Immunol.* **16**, 429 (2004).
6. H. Zhou *et al.*, *Nature* **427**, 167 (2004).
7. L. Deng *et al.*, *Cell* **103**, 351 (2000).
8. L. Sun, L. Deng, C. K. Ea, Z. P. Xia, Z. J. Chen, *Mol. Cell* **14**, 289 (2004).
9. C. E. Sedwick, A. Altman, *Mol. Immunol.* **41**, 675 (2004).
10. M. Villalba *et al.*, *J. Cell Biol.* **157**, 253 (2002).
11. D. Wang *et al.*, *Mol. Cell. Biol.* **24**, 164 (2004).
12. H. Hara *et al.*, *J. Exp. Med.* **200**, 1167 (2004).
13. H. J. Chun *et al.*, *Nature* **419**, 395 (2002).
14. N. Silverman, T. Maniatis, *Genes Dev.* **15**, 2321 (2001).
15. R. Zhou, T. Maniatis, personal communication

10.1126/science.1110902

Global Iron Connections Between Desert Dust, Ocean Biogeochemistry, and Climate

T. D. Jickells,[1] Z. S. An,[2] K. K. Andersen,[3] A. R. Baker,[1] G. Bergametti,[4] N. Brooks,[1] J. J. Cao,[2] P. W. Boyd,[5] R. A. Duce,[7] K. A. Hunter,[6] H. Kawahata,[8] N. Kubilay,[9] J. laRoche,[10] P. S. Liss,[1] N. Mahowald,[11] J. M. Prospero,[12] A. J. Ridgwell,[13] I. Tegen,[14*] R. Torres[15]

The environmental conditions of Earth, including the climate, are determined by physical, chemical, biological, and human interactions that transform and transport materials and energy. This is the "Earth system": a highly complex entity characterized by multiple nonlinear responses and thresholds, with linkages between disparate components. One important part of this system is the iron cycle, in which iron-containing soil dust is transported from land through the atmosphere to the oceans, affecting ocean biogeochemistry and hence having feedback effects on climate and dust production. Here we review the key components of this cycle, identifying critical uncertainties and priorities for future research.

Iron is an essential nutrient for all organisms, used in a variety of enzyme systems, including those for photosynthesis, respiration, and nitrogen fixation (*1*, *2*). However, iron is very insoluble under oxidizing conditions above pH 4 (*3*). For marine phytoplankton, separated from the iron-rich sediment of the ocean floor by considerable water depths, physiological iron requirements must be met from within the water column. Iron supply is a limiting factor on phytoplankton growth over vast areas of the modern ocean, although this may not have been so in the distant past, when prokaryotes first evolved in a less oxic ocean (*1*).

Iron supply reaches the oceans mainly from rivers as suspended sediment in a vast global transport system (Table 1). However, fluvial and glacial particulate iron is efficiently trapped in near-coastal areas (*4*), except where rivers discharge directly beyond the shelf. Hydrothermal inputs are rapidly precipitated at depth in the oceans. Hence, the dominant external input of iron to the surface of the open ocean is aeolian dust transport, mainly from the great deserts of the world. Currently hyper-arid areas such as the Sahara desert occupy 0.9 billion hectares and drylands occupy 5.2 billion hectares, which is one-third of global land area. These environments are particularly sensitive to global change pressures (*5*, *6*), and such changes could alter ocean productivity and hence climate. There are other possible contributors to atmospheric iron supply, including volcanic, anthropogenic, and extraterrestrial sources (*7*, *8*), whose iron may be more soluble than iron in soil aluminosilicates (*7*), and these merit further study.

Dust produced in arid areas has important and disparate effects throughout the Earth system, as illustrated in Fig. 1 and discussed below. These need to be incorporated into climate models to correctly predict impacts of global change pressures. We first consider each component of the system before attempting a global synthesis.

Climate Effects on Dust/Iron Fluxes

Satellite imagery has greatly increased our knowledge of large-scale dust source regions, emphasizing the importance of localized sources, which vary seasonally. There are similar climatic and geomorphological controls on many source regions (*6*), and dried-out lake systems such as the Bodele Depression in North Africa appear to be particularly important. Dust production depends on the supply of wind-erodible material, which ironically usually requires fluvial erosion, often from adjacent highlands, followed by subsequent drying out and the loss or absence of vegetative protection (*6*, *9*–*11*). Dust production arises from saltation or sandblasting, when winds above a threshold velocity transport soil grains horizontally, producing smaller particles, a small proportion of which get carried up into the atmosphere for long-range transport. These processes depend on rainfall, wind, surface roughness, temperature, topography, and vegetation cover, which are interdependent factors linked to aridity and climate in a highly nonlinear way. Wind tunnel studies show dust production to be proportional to the cube of wind speed (*5*).

Desert dust aerosol is dominated by particles of diameter 0.1 to 10 μm, with the mean size being around 2 μm. Such aerosols have a lifetime of hours to weeks, allowing long-range transport over scales of thousands of

Table 1. Global iron fluxes to the ocean (in Tg of Fe year^{-1}). From Poulton and Raiswell (*4*), with modified atmospheric inputs from Fig. 2. "Authigenic fluxes" refer to releases from deep-sea sediments during diagenesis. We distinguish only separately dissolved and particulate for fluvial inputs, because it is clear that fluvial particulate iron, along with iron from coastal erosion and glacial sediment sources, does not reach the oceans, whereas authigenic, atmospheric, and hydrothermal iron all reach the oceans regardless of their phase.

Source	Flux
Fluvial particulate total iron	625 to 962
Fluvial dissolved iron	1.5
Glacial sediments	34 to 211
Atmospheric	16
Coastal erosion	8
Hydrothermal	14
Authigenic	5

[1]School of Environmental Sciences, University of East Anglia, Norwich NR47TJ, UK. [2]State Key Lab of Loess and Quaternary Geology, Institute of Earth Environment, Chinese Academy of Sciences, AS, 10 Fenghui South Road, Post Office Box 17, China. [3]Niels Bohr Institute, University of Copenhagen, Juliane Maries Vej 30, 2100 Copenhagen, Denmark. [4]Laboratoire Interuniversitaire des Systèmes Atmospherique, Universités Paris 7 and Paris 12, UMR CNRS 7583, Paris, France. [5]National Institute of Water and Atmospheric Research Centre for Chemical and Physical Oceanography, Department of Chemistry; [6]Department of Chemistry, Post Office Box 56; University of Otago, Dunedin, New Zealand. [7]Departments of Oceanography and Atmospheric Sciences, Texas A&M University, TAMU 3146, College Station, TX 77843–3146, USA. [8]Geological Survey of Japan, National Institute of Advanced Industrial Science and Technology (AIST), Tsukuba-higashi 1-1-1, Ibaraki 305–8567, Japan. [9]Institute of Marine Sciences, Middle East Technical University, Post Office Box 28, Erdemli-Mersin 33731, Turkey. [10]Leibniz-Institute für Meereswissenchaften IFM-GEOMAR, Marine Biogeochemistry, Gebäude Westufer, Düsternbrooker Weg 20, 24105 Kiel, Germany. [11]National Center for Atmospheric Research. Post Office Box 3000, Boulder, CO 80307, USA. [12]Rosenstiel School of Marine and Atmospheric Sciences, University of Miami, 4600 Rickenbacker Causeway, Miami, FL 33149–1089, USA. [13]Department of Earth and Ocean Sciences, University of British Columbia, 6339 Stores Road, Vancouver, British Columbia V6T 1Z4 Canada. [14]Max-Planck-Institute for Biogeochemistry. Post Office Box 10, 01 64 07701 Jena, Germany. [15]Universidad de Conception, Departamento de Oceanografia, Casilla 160C, Chile.

*Present address: Institute for Tropospheric Research, Permoserstrasse 15 04318, Leipzig, Germany.

kilometers (*5*, *11*) but producing strong gradients of dust deposition and concentrations that vary substantially on time scales of ~1 day. Dust production, transport, and deposition to the oceans again depend on climatic factors, particularly atmospheric structure, which regulates uplift, and wind speed and precipitation, which influence removal. Much of the transport of dust occurs at altitudes of several kilometers, with subsequent removal by wet deposition. Hence, satellite images of dust may not reflect dust inputs to the oceans (*7*).

Dust removal occurs by wet and dry deposition, processes whose efficiency varies with aerosol particle size (*7*). Measurements at a limited number of sites and modeling studies suggest that 30 to 95% of total removal is by wet deposition (*7*, *12*). Wet deposition is spatially variable, reflecting several climatically sensitive factors, including aerosol size distribution, rainfall patterns, and transport altitude. This results in considerable uncertainties in estimating the contribution of wet deposition to total deposition.

Dust fluxes can be estimated from direct measurements and subsequent extrapolation (*13*), models (*11*, *14*, *15*), and satellite observations (*16*). The various approaches all yield similar dust deposition estimates of 1000 to 2000 Tg year^{-1} (1 Tg = 10^{12}g), varying substantially from year to year. However, models are usually tuned to match observations, and hence the agreement is not truly an independent validation.

Existing models of global dust transport (*14*, *15*) include only first-order physical representations of the key dust production processes, largely because of the lack of suitable data sets of global surface characteristics. Despite this, global models seem able to simulate dust deposition fluxes reasonably well. We estimate production at 1700 Tg year^{-1}, with almost two-thirds from North Africa and 26% of the dust reaching the oceans (Fig. 2). Changes in the hydrological cycle and/or vegetative cover affect global dust production (*10*) as recorded over glacial/interglacial cycles in loess, ice core, and marine sediment records. Dust fluxes were 2 to 20 times higher during the last glaciation (*17*–*19*) because of stronger winds, aridity, changes in vegetation cover, lowered sea level, and reduced precipitation. It has been suggested that changing land use practices over recent decades have altered dust fluxes by up to 50% (*14*, *20*), although recent work suggests lower values (*15*). Although the global importance of land use change as a dust source is currently uncertain, effects at a regional scale are clear, such as around the Aral Sea and the in the U.S. 1930s Dust Bowl storms (*6*). Dust storm frequency over the Sahel appears to have increased since 1950. This may be related to multidecadal-scale climate variability or land use change (*21*). Dust transport over China, the United States, and North Africa has been related to large-scale climatic cycles (*22*–*26*), and the variability in dust transport can be influenced by climatic cycles such as El Niño–Southern Oscillation and North Atlantic Oscillation (*23*, *24*). Some climate models suggest that enhanced greenhouse warming could ''green'' the Sahel and southern Sahara (*14*, *27*), drastically altering global dust production. Different models of global dust flux

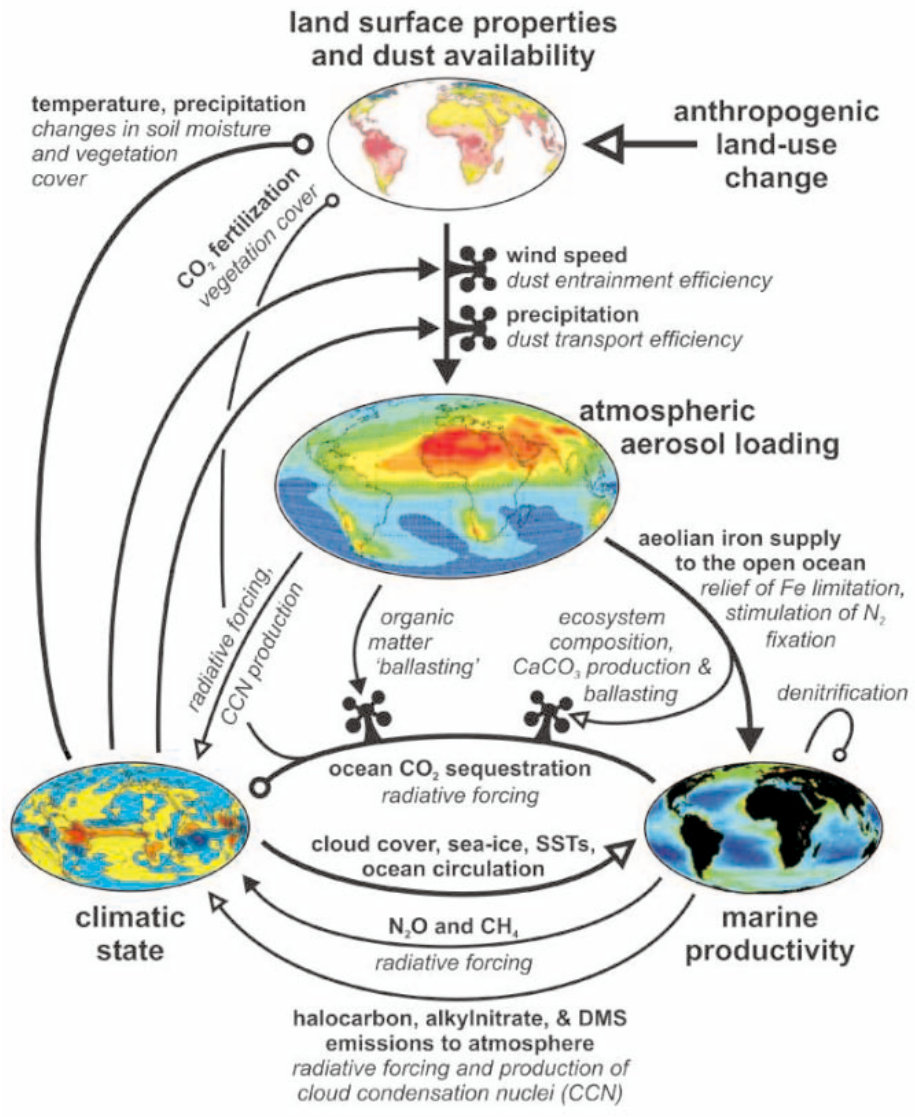

Fig. 1. Schematic view of global iron and dust connections. Highlighted are the four critical components (clockwise from top): the state of the land surface and dust availability, atmospheric aerosol loading, marine productivity, and some measure of climatic state (such as mean global surface temperature). The sign of the connections linking these varies; where the correlation is positive (for example, increased atmospheric aerosol loading → increased marine productivity), the line is terminated with a solid arrowhead. Where the correlation is negative (for example, increased marine productivity → lower CO_2 and a colder climate), the termination is an open circle. Connections with an uncertain sign are terminated with an open arrowhead. The mechanism by which the link acts (for example, the impact of a change in atmospheric CO_2 is via the radiative forcing of climate) is displayed in italics. Finally, the "water tap" symbols represent a secondary mechanism modulating the effect of a primary mechanism; for instance, a change in global precipitation strength and distribution will alter the efficiency with which entrained dust is transported to the open ocean. If a path of successive connections can be traced from any given component back to itself, a closed or feedback loop is formed. An even number (including zero) of negatively correlated connections counted around the loop gives a positive feedback, which will act to amplify a perturbation and tend to destabilize the system. Conversely, an odd number of negative correlations gives a negative feedback, dampening any perturbation and thus stabilizing the system. For instance, atmospheric aerosol loading → marine productivity → climatic state → dust availability → atmospheric aerosol loading contains two negative and two positive correlations and thus is positive overall. In contrast, marine productivity looping back onto itself contains a single negative correlation and thus represents a negative feedback.

Table 2. Effects of dust/iron (Fe) on ocean biogeochemistry. (In addition, there are dust effects on the climate system via albedo and the hydrological cycle; see text.)

Interaction	Mechanism	Area*	Reference
Primary productivity	Reduction in Fe limitation allows more efficient use of macronutrients and hence CO_2 uptake.	HNLC and other Fe-limited areas	(*36*, *42*)
N_2 fixation	Reduction in Fe limitation on nitrogen fixation increases primary production and hence CO_2 uptake.	Subtropical gyres	(*1*, *43*)
Changes in species composition	Species-selective relief of iron stress.	Global	(*42*)
Ballast effect	Increases sinking rate of organic matter, reducing organic matter regeneration within seasonal mixed layer; promotes CO_2 uptake.	Probably only significant in areas of high dust deposition	(*52*)
DMS	Increased productivity leads to increased DMS emissions and increased aerosol formation.	HNLC and other Fe-limited areas	(*54*)
N_2O and NO_3^-	Increased fluxes of organic matter to deep waters lower oxygen concentrations and promote denitrification, release N_2O, and lower oceanic nitrate inventory.	Upwelling systems	(*53*)
N_2O and CH_4	Increased productivity leads to changes in euphotic zone methane and N_2O concentrations.	HNLC and other Fe-limited areas	(*54*, *57*)
H_2S	Increased fluxes of organic matter to deep waters lower oxygen concentrations and promote sulfate reduction; sulphide production lowers iron inventory.	Upwelling systems	
Halocarbons and alkyl nitrates	Biogenic gases linked to primary productivity. These are greenhouse gases, linked to aerosol formation and to the ozone cycle.	As for DMS	(*54*)
Isoprene and CO	Biogenic trace gases linked to primary productivity. These gases influence atmospheric oxidizing capacity.	As for DMS	(*54*, *57*)

*Most impacts have effects throughout the oceans, but where appropriate, we identify here areas that are most sensitive to changes in dust/iron flux.

(*14*, *15*) predict similar present-day dust fluxes (Fig. 2), but their predictions for the next 100 years range from a modest increase (+12%) to a significant decrease (–60%), with different regional deposition patterns. These differences reflect variations in the relative importance of land use changes and CO_2 fertilization, as well as differences in climate predictions.

Dust has important but uncertain direct impacts on climate and radiative budgets (*20*, *28*) and possibly rainfall patterns (*29*). We note the importance of these physical effects but focus here on the biogeochemical effects. In a biogeochemical context, the key flux to the oceans is not dust, but soluble or bioavailable iron. Although the iron content of soil dust (average, 3.5%) is variable globally, the uncertainty introduced by this variability is small compared with other uncertainties in the iron cycle (*7*). Iron solubility from soil dust is low [<1 to 2% (*7*)]. Higher solubilities of aerosol iron have been reported (*12*). The controls on aerosol iron solubility include photochemistry (photoreduction of Fe III to Fe II) and acidity, particularly during aerosol cloud processing (*7*). Emissions of acid precursors (SO_2 and NO_x) have more than doubled from the preanthropogenic state, and NO_x emissions are expected to continue to increase (*20*). Organic complexation may play a role in regulating atmospheric iron solubility. Consequently, emissions of organic matter from natural sources (such as soil humic acids and plant terpenes) and anthropogenic sources (such as biomass burning and industrial/urban emissions) may influence atmospheric iron cycling (*7*). We know very little about the organic chemistry of aerosols or of the active microbial community identified in aerosols, which may influence iron solubility (*7*, *30*). All these factors (acidity, organic complexation, and photochemistry) will alter with global change pressures.

Dust/Iron Impacts on the Ocean

The physicochemical environment of atmospheric iron changes dramatically on entering the oceans. At a seawater pH of 8, soluble ferric iron rapidly reprecipitates, setting up a competition between adsorption to water column particulates, active biological uptake, and organic complexation, which evolves over the surface water residence time of dust [tens of days (*31*)]. Experimental measurements of the solubility of aerosol iron have generally been conducted over shorter time scales and hence may not adequately predict the solubility of aerosol iron.

Measuring total and speciated iron concentrations in the ocean is difficult, but global data are now emerging (*32*). Total dissolved iron shows nutrient-like oceanic profiles, with low surface water concentrations (0.03 to 1 nmol liter^{-1} where photochemically produced Fe II may be significant) increasing to deep water concentrations of 0.4 to 2 nmol liter^{-1} (*32*, *33*). Significant colloidal iron is present in the water column and is potentially biogeochemically labile (*32*). The impact of atmospheric deposition on surface water iron concentrations has been demonstrated (*34*), as has recycling from sediments and coastal regions (*35*, *36*). Within the oceans, dissolved iron is predominantly organically complexed, stabilizing it against rapid scavenging (*37*), although its residence time is still probably only decades (*32*, *33*). The source, biological function, and structure of these organic iron-complexing ligands are essentially unknown. Electrochemical titrations suggest that some have similar binding strength to that of true siderophores: strong iron-specific ligands (*3*, *33*, *37*). Siderophores have been found in marine bacteria and coastal seawater (*38*). Although many species may be able to use siderophore-bound iron, siderophore synthesis systems are not readily identifiable in the genomes of important picophytoplankton species such as *Synecochoccus* and *Prochlorococcus* (*39*, *40*), though they may be present in *Trichodesmium* and *Crocosphaera* (two marine diazotrophs) and in uncultured heterotrophic bacterial genomes from the Sargasso Sea (*41*).

Iron limitation reflects deep-water Fe/N concentration ratios that are inadequate to meet phytoplankton iron requirements (*36*) because of scavenging of iron regenerated from sinking organic matter in the deep ocean at faster rates than N. Thus, sustaining open ocean phytoplankton primary production requires an additional input of iron to that produced from upwelling, which is usually atmospheric. The relative importance of atmospheric and upwelling sources varies throughout the oceans (*36*). Iron limitation of phytoplankton primary production in as much as 30% of the oceans has now been suggested (*1*, *36*, *42*). In some areas, such as the Southern Ocean, this results in incomplete use of macronutrients (N, P, and Si) and relatively low algal abundance, hence the term "high-nutrient low-chlorophyll" (HNLC) regions. Recent studies emphasize more complex interactions within the ocean than simple iron limitation or sufficiency, with evidence in some areas of simultaneous limitation of primary production by iron, light,

macronutrients (*42*, *43*), and trace nutrients (such as Co and Zn) (*2*, *44*). Furthermore atmospheric inputs supply not only iron but also other nutrients and carbonate, which may influence ocean biogeochemistry (*45*, *46*).

Luxury iron uptake has been demonstrated for some phytoplankton, allowing them to better adapt to episodic atmospheric supply (*47*). Iron availability influences algal community structure as well as overall productivity. Open ocean phytoplankton generally need less iron than coastal species, which have evolved in a more iron-rich environment, although iron-limited coastal systems are known (*36*). A reduced iron requirement can be achieved by reducing cell size or minimizing the number of iron-containing enzymes (*39*). The success of *Prochlorococcus* in HNLC areas depends on both strategies. Relief of iron stress results in the growth of phytoplankton taxa characterized by larger cells, particularly diatoms with less dense opal skeletons (*36*). A similar process may arise for coccolithophores as a result of Fe/Zn co-limitation (*44*). Changes in skeleton density should influence sinking rates and hence carbon export to depth, although this has not been seen in field experiments (*48*). Changes in coccolithophore abundance directly affect atmospheric partial pressure of CO_2 (pCO_2), because their calcification produces CO_2 (*36*, *42*). In addition to direct limitation of primary production in the HNLC regions, iron may limit (or co-limit with P) nitrogen fixation by photosynthetic diazotrophs in tropical oceans, where stratification creates high temperature and irradiance and low nitrate concentrations in surface waters, which favor this process (*1*, *43*). The best characterized photosynthetic diazotroph, *Trichodesmium*, requires 5 to 10 times more iron for growth based on nitrogen fixation, as compared to ammonium (*47*).

The supply of dust to the oceans is very important in maintaining oceanic primary production and CO_2 uptake but is sensitive to climate change, although the overall effect will vary between ocean biogeochemical provinces (Table 2). In HNLC regions, changes in iron supply will directly affect primary production and species composition, whereas in subtropical/tropical oligotrophic regions, the impact will be mainly via changes in nitrogen fixation. The dust supply from the great North African and Asian deserts directly affects the tropical North Atlantic and temperate North Pacific, respectively, and effects in the two regions can be expected to be different. The largest HNLC region, the Southern Ocean (*36*), has the biggest potential to influence atmospheric CO_2. Here atmospheric dust supply is low (Fig. 2), originating from small dust sources in Argentina, Australia, and South Africa (*6*). Changes in these small and little-studied desert regions may have a disproportionately large global impact.

Because the solubility of iron from dust is low, it follows that there is a large flux of particulate iron through the deep ocean, particularly beneath the major dust plumes. If some of this dust dissolves at depth, it will increase abyssal dissolved iron concentrations and, over the long term, productivity in upwelling regions such as the Southern Ocean. Deep-water dust dissolution will depend on organic ligand concentrations and possibly sediment redox (*33*).

Martin (*49*) proposed that increased dust transport during the last glaciation reduced iron limitation in HNLC regions, increasing primary production and CO_2 uptake. The complexity of iron biogeochemistry and nutrient co-limitation means that higher glacial dust loadings need not necessarily cause increased productivity. Current models and ice core data yield very different results, predicting that glacial/interglacial changes in dust fluxes will change atmospheric pCO_2 by 5 to 45 parts per million (ppm) as a contribution to the total change of 80 to 100 ppm (*19*, *50*). Bopp *et al*. (*50*) reviewed much of the existing marine sediment core data on glacial/interglacial ocean productivity changes and found no simple global pattern of change. However, there are regional patterns (*51*) with increases in productivity in the northwest Pacific, South Atlantic, and Indian Oceans north of the polar front, with decreases south of it. South Pacific productivity appears to be little changed. Some of these patterns can be reproduced in ocean models (*50*).

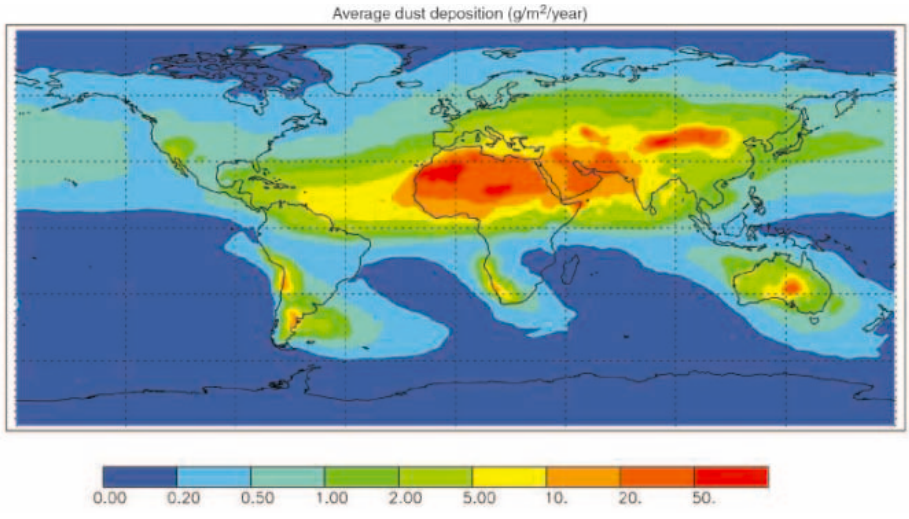

Fig. 2. Dust fluxes to the world oceans based on a composite of three published modeling studies that match satellite optical depth, in situ concentration, and deposition observations (*11*, *14*, *15*). The models have been extensively compared to observations, and although individual models show strengths and weaknesses, this composite appears to match observations well. Total atmospheric dust inputs to the oceans = 450 Tg year^{-1}. Percentage inputs to ocean basins based on this figure are as follows: North Atlantic, 43%; South Atlantic, 4%; North Pacific, 15%; South Pacific, 6%; Indian, 25%; and Southern Ocean, 6%.

Effect on Climate of Iron Inputs to the Oceans

The oceans clearly exert a major influence on climate via heat transport and related physical processes (*20*). Large-scale reorganization of oceanic circulation will also affect the transport of iron, effects driven predominantly from within the ocean. Climate change will induce a variety of physicochemical changes in the open ocean, particularly by changing stratification and nutrient supply ratios (*42*), with unpredictable effects. We acknowledge these important issues but focus on the dust cycle, considering now ways in which this can affect the oceans and climate, beside the direct iron limitation of primary production and nitrogen fixation discussed above (Table 2).

Changes in iron fluxes can result in species shifts and changes in phytoplankton size distribution, changing oceanic CO_2 uptake by altering the efficiency of organic carbon export to deep water. Dust may also play a direct role in regulating export via the ballast effect (*52*). In most areas, dust is a minor ballast component compared to opal and calcite, but their production is also influenced by dust/iron supply. Changes in ocean productivity and organic carbon export to deep water will influence subsurface oxygen levels and thereby denitrification in oxygen minima zones, oceanic nitrate inventories and productivity, and nitrous oxide emissions (*53*). Changes in sediment H_2S in such areas could affect deep-ocean iron concentrations and productivity.

Up to eightfold changes in dimethyl sulfide (DMS) concentrations are seen in iron addition experiments (*54*). DMS oxidizes in the atmosphere to form acidic sulfate aerosol, a highly effective scatterer of solar radiation. Modeling suggests that a twofold global rise in DMS fluxes produces a global temperature decrease of 1°C, proving a climate feedback and linking

the C, Fe, and S cycles (*55*). DMS is only one of a group of trace gases that can influence climate and whose emissions are sensitive to iron concentrations (*54*, *56*, *57*). These include gases that directly affect greenhouse gas forcing (nitrous oxide and methane), ozone cycling (halocarbons and alkylnitrates), and atmospheric oxidizing capacity (isoprene and carbon monoxide). Impacts on ozone are important in radiative forcing (*20*) and via ultraviolet-B impacts on phytoplankton community structure (*42*).

Global Iron Connections

Our analysis demonstrates the complexity of the global iron cycle (Fig. 1). Low iron solubility leads to limitation of marine productivity, with potentially large-scale feedbacks within the global climate system. These could act to either amplify future global climate change via a positive (destabilizing) feedback or diminish it via a negative (stabilizing) feedback. There are considerable uncertainties in our understanding of these interactions, requiring research that integrates across the whole Earth system. We suggest the following research priorities: (i) dust deposition processes, (ii) aerosol iron bioavailability, and (iii) the impact of iron on marine nitrogen fixation and trace gas emissions. These should lead to improvements in global models, allowing realistic predictive capability that can be tested against improved results from the paleo record of the biogeochemical response to changing dust fluxes.

There are discussions about changing terrestrial land uses to create carbon sinks to help mitigate global change. Such changes may reduce dust fluxes to the ocean and thereby reduce primary productivity, offsetting gains in terrestrial carbon storage (*58*). There is also discussion about fertilizing the ocean with iron to increase CO_2 uptake (*59*). Our analysis demonstrates that such a scheme could produce many changes in marine biogeochemical systems. Clearly, we need a comprehensive understanding of the current and future dust/iron cycle before we can contemplate such engineering of the Earth system.

References and Notes

1. P. G. Falkowski, R. T. Barber, V. Smetacek, *Science* **281**, 200 (1998).
2. F. M. M. Morel, N. M. Price, *Science* **300**, 944 (2003).
3. S. M. Kraemer, *Aquat. Sci.* **66**, 3 (2004).
4. S. W. Poulton, R. Raiswell, *Am. J. Sci.* **302**, 774 (2002).
5. R. A. Duce, in *Aerosol Forcing of Climate*, R. J. Charlson, J. Heintzenberger, Eds. (Wiley, Chichester, UK, 1995), pp. 43–72.
6. J. M. Prospero, P. Ginoux, O. Torres, S. E. Nicholson, T. E. Gill, *Rev. Geophys.* **40**, 1002 (2002).
7. T. D. Jickells, L. J. Spokes, in *The Biogeochemistry of Iron in Seawater*, D. R. Turner, K. Hunter, Eds. (Wiley, Chichester, UK, 2001), pp. 85–121.
8. K. S. Johnson, *Global Biogeochem. Cycles* **15**, 61 (2001).
9. N. Brooks, M. Legrand, in *Linking Climate Change to Land Surface Change*, S. McLaren, D. Kniveton, Eds. (Kluwer Academic, Dordrecht, Netherlands, 2000), pp. 1–25.
10. C. S. Zender, D. Newman, O. Torres, *J. Geophys. Res. Atmos.* **108**, 4543 (2003).
11. P. Ginoux *et al.*, *J. Geophys. Res. Atmos.* **106**, 20255 (2001).
12. J. L. Hand *et al.*, *J. Geophys. Res. Atmos.* **109**, D17205 (2004).
13. R. A. Duce *et al.*, *Global Biogeochem. Cycles* **5**, 193 (1991).
14. N. M. Mahowald, C. Luo, *Geophys. Res. Lett.* **30**, 1903 (2003).
15. I. Tegen, M. Werner, S. P. Harrison, K. E. Kohfeld, *Geophys. Res. Lett.* **31**, L05105 (2004).
16. Y. J. Kaufman *et al.*, *J. Geophys. Res. Atmos.* 10.1029/2003JD004436 (2004).
17. Z. S. An, G. Kukla, S. C. Porter, J. L. Xiao, *CATENA* **18**, 125 (1991).
18. D. K. Rea, *Rev. Geophys.* **32**, 159 (1994).
19. R. Röthlisberger *et al.*, *Geophys. Res. Lett.* **31**, L16207 (2004).
20. Intergovernmental Panel on Climate Change, *Climate Change 2001: The Scientific Basis. Contribution of Working Group1 to the Third Assessment Report of the Intergovernmental Panel on Climate Change* (Cambridge Univ. Press, Cambridge, 2001).
21. J. M. Prospero, R. T. Nees, *Nature* **320**, 735 (1986).
22. X. Y. Zhang *et al.*, *Geophys. Res. Lett.* **30**, 10.1029/2003GL018206 (2003).
23. J. M. Prospero, P. J. Lamb, *Science* **302**, 1024 (2003).
24. C. Moulin, I. Chiapello, *Geophys. Res. Lett.* **31**, L02107 (2004).
25. S. D. Schubert, M. J. Suarez, P. J. Pegion, R. D. Koster, J. T. Bacmeister, *Science* **303**, 1855 (2004).
26. C. S. Zhao, X. Dabu, Y. Li, *Geophys. Res. Lett.* **31**, L01103 (2004).
27. M. Claussen, V. Brovkin, A. Ganopolski, C. Kubatzki, V. Petoukhov, *Clim. Change* **57**, 99 (2003).
28. B. J. Huebert *et al.*, *J. Geophys. Res. Atmos.* **108**, 8633 (2003).
29. D. Rosenfeld, Y. Rudich, R. Lahav, *Proc. Natl. Acad. Sci. U.S.A.* **98**, 5975 (2001).
30. D. W. Griffin *et al.*, *Aerobiologia* **19**, 143 (2003).
31. T. D. Jickells, *Mar. Chem.* **68**, 5 (1999).
32. H. J. W. de Baar, J. T. M. de Jong, in *The Biogeochemistry of Iron in Seawater*, D. R. Turner, K. A. Hunter, Eds. (Wiley, Chichester, UK, 2001), pp. 123–253.
33. P. Parekh, M. J. Follows, E. Boyle, *Global Biogeochem. Cycles* **18**, GB1002 (2004).
34. G. Sarthou *et al.*, *Deep-Sea Res. I* **50**, 1339 (2003).
35. V. A. Elrod, W. M. Berelson, K. H. Coale, K. S. Johnson, *Geophys. Res. Lett.* **31**, L12307 (2004).
36. A. J. Watson, in *The Biogeochemistry of Iron in Seawater*, D. R. Turner, K. A. Hunter, Eds. (Wiley, Chichester, UK, 2001), pp. 9–39.
37. K. W. Bruland, E. L. Rue, in *The Biogeochemistry of Iron in Seawater*, D. R. Turner, K. Hunter, Eds. (Wiley, Chichester, UK, 2001), pp. 255–289.
38. M. Gledhill *et al.*, *Mar. Chem.* **88**, 75 (2004).
39. B. Palenik *et al.*, *Nature* **424**, 1037 (2003).
40. G. Rocap *et al.*, *Nature* **424**, 1042 (2003).
41. J. C. Venter *et al.*, *Science* **304**, 66 (2004).
42. P. W. Boyd, S. C. Doney, in *Ocean Biogeochemistry: A Synthesis of the Joint Global Ocean Flux Study (JGOFS)*, M. J. R. Fasham, Ed. (Springer, Berlin, 2003), pp. 157–193.
43. M. M. Mills, C. Ridame, M. Davey, J. La Roche, R. J. Geider, *Nature* **429**, 292 (2004).
44. K. G. Schulz *et al.*, *Nature* **430**, 673 (2004).
45. A. R. Baker, S. D. Kelly, K. F. Biswas, M. Witt, T. D. Jickells, *Geophys. Res. Lett.* **30**, 2296 (2003).
46. T. Oba, T. F. Pedersen, *Paleoceanography* **14**, 34 (1999).
47. A. B. Kustka *et al.*, *Limnol. Oceanogr.* **48**, 1869 (2003).
48. P. W. Boyd *et al.*, *Nature* **428**, 549 (2004).
49. J. H. Martin, *Paleoceanography* **5**, 1 (1990).
50. L. Bopp, K. E. Kohfeld, C. Le Quere, O. Aumont, *Paleoceanography* **18**, 1046 (2003).
51. Z. S. An, J. J. Cao, K. K. Anderson, H. Kawahata, in preparation.
52. R. Francois, S. Honjo, R. Krishfield, S. Manganini, *Global Biogeochem. Cycles* **16**, 1087 (2002).
53. M. A. Altabet, M. J. Higginson, D. W. Murray, *Nature* **415**, 159 (2002).
54. S. M. Turner, M. J. Harvey, C. S. Law, P. D. Nightingale, P. S. Liss, *Geophys. Res. Lett.* **31**, L14307 (2004).
55. G. Zhuang, Z. Yi, R. A. Duce, P. R. Brown, *Nature* **355**, 537 (1992).
56. P. S. Liss, A. Chuck, D. C. E. Bakker, S. Turner, *Tellus*, in press.
57. O. W. Wingenter *et al.*, *Proc. Natl. Acad. Sci. U.S.A.* **101**, 8537 (2004).
58. A. J. Ridgwell, M. A. Maslin, A. J. Watson, *Geophys. Res. Lett.* **29**, 1095 (2002).
59. S. W. Chisholm, P. G. Falkowski, J. J. Cullen, *Science* **296**, 467 (2002).

60. We acknowledge the leadership of the Surface Ocean–Lower Atmosphere Study project (www.solas-int.org) for conceiving this synthesis. We thank the International Council for Science, the United Nations Educational, Scientific and Cultural Organisation, NSF (grants GEO-0402845 and OCE 0228863), the International Geosphere-Biosphere Programme, and the Scientific Committee on Ocean Research for partial support of this work, and B. Sulzberger for her contribution to this work.

10.1126/science.1105959

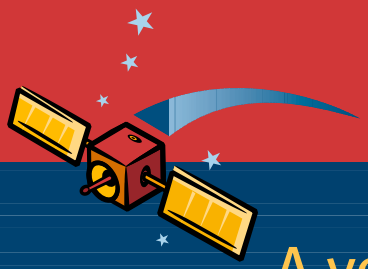

Thank you!

A very special "thank you" to all of the sponsors and supporters of the 2005 AAAS Annual Meeting.

SPONSORS

SUBARU

Premier Sponsor

NATIONAL SCIENCE FOUNDATION

L'ORÉAL

AFFYMETRIX

SUPPORTERS

- Apple Computer, Inc.
- Burroughs Wellcome Fund
- CommCore Consulting Group
- European Commission
- Johnson & Johnson Pharmaceutical Research and Development, L.L.C.
- Merck/AAAS Undergraduate Science Research Program
- Monsanto
- National Institute of Standards and Technology
- Pacific Northwest National Laboratory
- Sandia National Laboratories

Thanks also to GE Healthcare for generously supporting the AAAS Young Scientist Award, in cooperation with *Science*. The AAAS Science Journalism Awards are sponsored by Johnson & Johnson Pharmaceutical Research & Development, L.L.C. The Newcomb Cleveland Prize is supported by Affymetrix.

AAAS
ADVANCING SCIENCE, SERVING SOCIETY

Abundance of Cellular Material and Proteins in the Atmosphere

Ruprecht Jaenicke

Atmospheric aerosols play a crucial role in regulating the global climate and can either enforce or suppress anthropogenic forcing. Their influence on climate forcing (natural as well as anthropogenic) has been estimated (*1*), but a better understanding of the composition and sources of atmospheric aerosols is needed to improve climate models. Here we report evidence that particles injected directly from the biosphere constitute a major portion of atmospheric aerosols.

Cellular (and protein) particles injected directly into the atmosphere include fur fibers, dandruff, skin fragments, plant fragments, pollen, spores, bacteria, algae, fungi, viruses, protein "crystals," and more, ranging in size from tens of nanometers to millimeters. Knowledge about "dead" or fragmented biological particles in the atmosphere is greatly limited. Tropical forests have been proposed as sources (*2*), and filter samples (*3*) in western Siberia at ground and aloft show ~3 μg/m³ of protein, but cellulose and protein make up only a fraction of primary biological aerosol particles (PBAPs).

The meteorological relevance of cellular particles could be high. Pollen grains attract water at relative humidity well below 100% and thus might act locally as cloud condensation nuclei, influencing the formation of clouds. Other biological particles, including decaying vegetation (and associated bacteria) and marine plankton, are excellent ice nuclei. Ice nuclei trigger precipitation and thereby remove water from the atmosphere. One can easily imagine the influence on global cloud cover, climate forcing and feedbacks, and precipitation distribution if the source and distribution of cellular atmospheric particles varies on a regional to global scale.

Atmospheric chemists and modelers have previously considered the biosphere a minor source of primary particles (*4*), and bioaerosols were thought to occur only in minute concentrations, with insignificant global emissions (*1*) for the year 2000 [56 Tg/year of biogenic carbonaceous aerosols (>1 μm in size) compared with 3300 Tg/year for sea salt and 2000 Tg/year for mineral dust]. Recently, however, a greater contribution to the atmosphere of particles from biological activities of the oceans has been reported (*5*). Still, some surveys (*6*) report as much as 20 to 40% of the aerosol measured as compositionally unidentified.

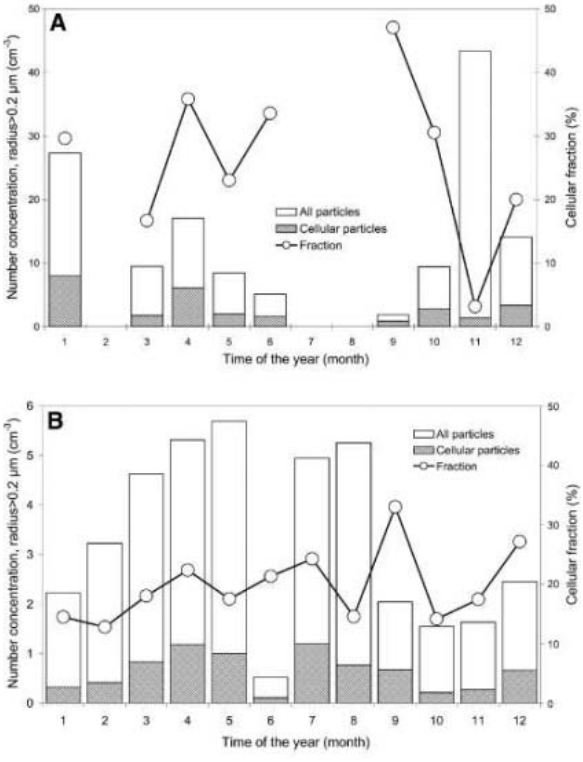

Fig. 1. Observation of PBAPs greater than 0.2 μm in radius. Particles were collected and stained with a protein dye; protein-containing particles then developed a bluish tint. The shape of the particles, the presence of characteristic elements, and their stability in an electron beam (microscope) were also used for identification. Cellular (and all) particles were individually sized and counted. (**A**) In Mainz, Germany (1990 to 1998, at a semirural location), a rather stable concentration plateau was observed. The PBAP fraction varied between 5% and almost 50%. The common assumption that, in winter, the biological fraction and its concentration are low was not confirmed. (**B**) Data from Lake Baikal, Russia (1996 to 1997, at a remote continental location) (*10*) support the year-round stable presence of PBAPs.

We observed PBAPs at several geographical locations and aloft, covering all seasons and many characteristic environments (Fig. 1). These data reveal the complete absence of a pronounced annual cycle, despite the common expectation that concentrations in spring or summer should be higher than in winter. A detailed analysis shows that the fractions of different biological compounds do vary, though: In spring, pollen is more abundant, whereas in winter, decaying cellular matter prevails. We have also observed that resuspension from exposed surfaces acts as a source in winter and in dry periods. This might be important for cellular particle production even from the cryosphere. Measurements in Ireland (1998, at a marine location) (*7*) also indicate a rather high portion for the PBAP fraction, on the order of 25%. Not surprisingly, recent measurements (2001) in a tropical forest reveal that particles smaller than 1 μm compose up to 40%, and particles larger than 1 μm up to 80%, of the total aerosol number concentration of PBAPs (*8*).

The biosphere is thus a major source (*9*) for primary aerosol particles, and cellular (protein-containing) particles are a major fraction of the atmospheric aerosol.

References and Notes

1. J. P. Penner *et al.*, in *Climate Change 2001: The Scientific Basis. Contribution of Working Group I to the Third Assessment Report of the Intergovernmental Panel on Climate Change*, J. T. Houghton *et al.*, Eds. (Cambridge Univ. Press, Cambridge, 2001), pp. 289–348.
2. P. E. Artaxo Netto, *J. Geophys. Res.* **93**, 1605 (1988).
3. A. I. Borodulin, A. S. Safatov, B. D. Belan, M. V. Panchenko, *J. Aerosol Sci.* **34**, S681 (2003).
4. T. E. Graedel, P. J. Crutzen, *Atmospheric Change: An Earth System Perspective* (Freeman, New York, 1993).
5. C. D. O'Dowd *et al.*, *Nature* **431**, 676 (2004).
6. E. Andrews *et al.*, *J. Air Waste Manage. Assoc.* **50**, 648 (2000).
7. C. M. Kenny, S. G. Jennings, *J. Aerosol Sci.* **29**, S779 (1998).
8. B. Graham *et al.*, *J. Geophys. Res.* **108**, 4765 (2003).
9. Our estimate of the strength of the "source biosphere" for atmospheric primary particles, based on observed concentrations, the strength of other sources, and atmospheric residence times, is presently roughly 1000 Tg/year. Earlier estimates reflected a limited view of aerosolized biological components and were focused on organic aerosols.
10. The measurements at Lake Baikal were carried out by T. Khodzer of the Limnological Institute of the Russian Academy of Science at Irkutsk, Russia.
11. This research has been supported over many years by several organizations, naming only the German Science Foundation as a long-time supporter.

13 October 2004; accepted 18 January 2005
10.1126/science.1106335

Institut für Physik der Atmosphäre, Universität Mainz, 55099 Mainz, Germany. E-mail: jaenicke@uni-mainz.de

Role of Marine Biology in Glacial-Interglacial CO_2 Cycles

Karen E. Kohfeld,[1]*† Corinne Le Quéré,[1]‡ Sandy P. Harrison,[1]§ Robert F. Anderson[2]

It has been hypothesized that changes in the marine biological pump caused a major portion of the glacial reduction of atmospheric carbon dioxide by 80 to 100 parts per million through increased iron fertilization of marine plankton, increased ocean nutrient content or utilization, or shifts in dominant plankton types. We analyze sedimentary records of marine productivity at the peak and the middle of the last glacial cycle and show that neither changes in nutrient utilization in the Southern Ocean nor shifts in plankton dominance explain the CO_2 drawdown. Iron fertilization and associated mechanisms can be responsible for no more than half the observed drawdown.

The causes of the 80- to 100-ppm atmospheric CO_2 fluctuations during glacial cycles remain elusive despite more than 20 years of research (*1*). Oceanic processes must account for the observed 80- to 100-ppm drawdown, as well as an additional 10 to 45 ppm resulting from decreased terrestrial carbon storage during glacial periods compared with interglacial periods (*2*). Current climate models are unable to reproduce the observed decrease in glacial atmospheric CO_2 using physical mechanisms alone (*3*), so changes in marine biology are often invoked as an additional mechanism to lower atmospheric CO_2. One family of explanations invokes changes in the sequestration of carbon in the deep ocean and ocean sediments resulting from the sinking of marine plankton and its detritus because of (i) iron fertilization of marine biota from increased atmospheric dust deposition to the ocean (*4*) and subsequent redistribution of limiting nutrients (*5*), (ii) increases in the oceanic nutrient content or the carbon/nitrogen/phosphorus (C/N/P) ratio (*6*), (iii) shifts in the dominant plankton types (*7*), and (iv) increased carbon and nutrient utilization in surface waters due to increased stratification (particularly in polar oceans) (*8*). Each of these processes is likely to affect specific oceanic regions and leave distinct imprints on the marine sediment record (Table 1). Here, we describe the various processes by which the marine biological pump could have changed, identifying the oceanic regions they are likely to affect and the signature they would leave in marine sediments. We evaluate each process by examining the global reconstructions of marine activity archived in the paleoceanographic record.

Both the iron-fertilization and the increased-nutrient hypotheses require an increase in export production, or the amount of carbon exported to the seafloor. According to the iron-fertilization hypothesis (*4*), an increased supply of iron-rich dust to the oceans during glacial periods could have alleviated the iron limitation observed in high-nutrient, low-chlorophyll (HNLC) regions. The process of iron fertilization has been observed to increase carbon fixation in surface waters today (*9*–*12*). Although these studies have not firmly established that iron fertilization increases export production, this process has been invoked as a means of increasing carbon flux to the deep ocean under conditions of high dust (*4*). This would have the strongest impact on the North Pacific, equatorial Pacific, and Southern Oceans (Fig. 1) and would be observed as higher dust-deposition rates and increased carbon and biogenic fluxes to marine sediments.

The increased-nutrient hypothesis suggests that carbon fixation and removal from surface waters could increase if the nutrient content of the whole ocean were increased or if the amount of carbon fixed per unit of nitrate and phosphate were greater (*6*, *13*). This process was initially proposed to address nutrient limitation in warm low- to mid-latitude regions but would affect any oceanic region where nutrients are limiting (Fig. 1) and would be observed as increased carbon and biogenic fluxes to marine sediments.

Although dictated by slightly different processes, the first two hypotheses both predict increases in export production. What does the sediment record show? Changes in export production have been inferred from the fluxes of specific biogenic components (organic carbon, biogenic opal, and alkenone biomarkers), from naturally occurring radionuclides (^{231}Pa and ^{10}Be), and from degradation products (barium, authigenic uranium, and/or cadmium) (*14*). None of these indicators provides an unequivocal signal, because the relationship between productivity and flux is influenced by multiple environmental factors. We have adopted an approach that assumes that changes in

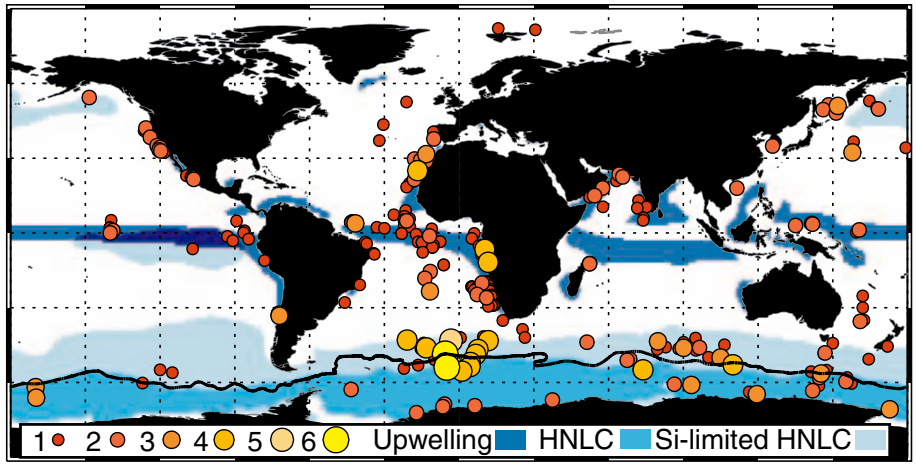

Fig. 1. Locations of ocean regions that are most critical for controlling uptake and sequestration of CO_2, including areas of wind-induced upwelling with annual values greater than 10 cm d^{-1} (dark blue) (*52*); HNLC regions where either N/chl or P/chl is above 20 μmol/kg per mg Chl/m^3, for an N/P ratio of 16 (intermediate blue); and HNLC regions with silica concentrations less than 20 μmol/kg per mg Chl/m^3 (light blue). Nutrient data are from (*53*). Solid line shows approximate location of the APF (*54*). Overlain dots show locations of cores that provide estimates of changes in export production used in this study. The size of the overlain dots indicates the number of export-production indicators available per core.

[1]Max Planck Institute for Biogeochemistry, Jena, Germany. [2]Lamont-Doherty Earth Observatory and Department of Earth and Environmental Sciences, Columbia University, Palisades, NY 10964, USA.

*To whom correspondence should be addressed. E-mail: office@kohfeld.com

†Present address: School of Earth and Environmental Sciences, Queens College of City University of New York, Flushing, NY 11367, USA.

‡Present address: University of East Anglia and the British Antarctic Survey, UK.

§Present address: School of Geographical Sciences, University of Bristol, Bristol, UK.

any specific indicator reflect changes in export production if several other indicators imply the same change. Carbonate accumulation responds more strongly than other indicators to chemical feedbacks associated with changes in ocean carbonate chemistry, as well as being affected by preservation overprints associated with deepwater circulation (*3*). It is therefore excluded from our overall assessment of changes in export production. We assess the relative change in export production between different time intervals using a five-point scale (lower, slightly lower, no change, slightly higher, and higher) (*15*). We evaluate the reliability of these qualitative assessments at each site on the basis of the quality of the age model and measurement methods, the number of sedimentary indicators, and the degree of consensus between them (*15*).

We obtained estimates of the change in export production (i) between the last glacial maximum (LGM) (~18,000 to 22,000 years ago) and the late Holocene (about the last 5000 years, which we use to define the modern state) from 258 cores; (ii) between marine isotope stages 5a to 5d (stage 5a-d) (80,000 to 110,000 years ago) and the LGM from 83 cores; and (iii) between stage 5a-d and the late Holocene from 80 cores. Stage 5a-d is a period when atmospheric CO_2 levels were ~50 ppm lower than late Holocene levels, but atmospheric dust deposition to the ocean was close to present-day levels (*16–21*) compared with the deposition rates observed during the LGM (*22*), which were two to three times as high. Long time-series records of dust deposition to the ocean demonstrate that the relatively low dust influx was not only observed in the Vostok ice core (*23*) but also represented a global phenomenon (fig. S1). Stage 5a-d therefore allows us to determine the impact of export production on atmospheric CO_2 in the absence of enhanced iron fertilization due to dust. We use the Holocene as an analog for the last interglacial period, stage 5e (130,000 to 115,000 years ago), assuming that Holocene conditions are representative of those that existed during stage 5e. We base this assumption on the fact that the change in external forcing (i.e., solar insolation) compared with the present was in the same direction during both periods (*24*). As a result, many regional climate changes affected by seasonal and latitudinal insolation patterns are likely to have occurred during both periods. Furthermore, the Vostok ice-core record reveals that the past four interglacial periods experienced very similar atmospheric CO_2 levels (*23*). Thus, we assume that conditions of the global carbon cycle must have been similar from one interglacial period to the next to have produced such consistency among peak interglacial CO_2 levels.

Export production during stage 5a-d is lower than during the late Holocene in the western Pacific, the South Atlantic gyre, the eastern Atlantic, and the Southern (south of 50°S) Oceans (Fig. 2A). The upwelling region in the eastern equatorial Atlantic and the present-day Antarctic Polar Front (APF) show slightly higher export production at stage 5a-d compared with the Late Holocene. These areas are relatively small and do not affect the overall picture that global export production was lower during stage 5a-d than during the late Holocene. Export production was globally higher during the LGM than during either stage 5a-d or the Late Holocene (Fig. 2, B and C). Only the Southern Ocean, south of the modern-day APF, had lower export production at the LGM than in the late Holocene or stage 5a-d. The northwest Pacific, the subantarctic, and equatorial regions of the Atlantic and Indian Oceans were all characterized by increased export production at the LGM. Export production to the north of the modern-day APF was higher during stage 5a-d than during the late Holocene, and this increase was further enhanced during the LGM. This suggests that changes in export production had already begun during stage 5a-d in the

Table 1. Mechanisms by which marine biota can reduce atmospheric CO_2 concentrations.

Hypothesis	Description	Oceanic regions influenced	Sediment impact (LGM compared to modern)	Ref.
Iron fertilization	Increased inputs of iron-rich dust increase marine productivity, carbon uptake in surface waters, and subsequent carbon flux to the deep ocean, which lowers atmospheric CO_2.	Regions influenced by eolian dust input and with underutilized nutrient (P, N, Si) inventories (Southern Ocean, North Pacific, equatorial Pacific).	Increased dust accumulation rates, increased accumulation of exported carbon.	(*4*)
Whole-ocean nutrient increase	Increased ocean nutrient reservoir alleviates nutrient limitation and allows global increase in marine biomass and carbon export to deep ocean.	Nutrient-limited regions (e.g., low-latitude gyres).	Increased export carbon flux globally.	(*6*, *13*)
Nutrient utilization	Increased utilization of carbon and nutrients in surface waters removes CO_2 from contact with the atmosphere and results in lower atmospheric CO_2. Increased nutrient utilization could occur either by increasing surface production or by decreasing vertical mixing and, therefore, the supply of nutrients and CO_2 to surface waters.	Regions with underutilized nutrient inventories (primarily the Southern Ocean, equatorial Pacific, and North Pacific, with the Southern Ocean containing a majority of unused nutrients and having a strong connection with CO_2-rich deep waters).	Higher nitrate uptake (increased ^{15}N of organic material in surface waters); lower surface-water phosphate concentrations (lower Cd/Ca ratios in planktonic foraminifera); higher surface-water silica uptake (increased $\delta^{30}Si$ in diatoms); lower surface-water CO_2 concentrations (relative increase in $\delta^{13}C$ of organic material).	(*8*)
$CaCO_3$/Corg rain ratio	Decreased export of $CaCO_3$ relative to organic carbon from surface to deep ocean maintains high surface-water alkalinity (CO_2 more soluble) and reduces deep-ocean carbonate burial. Associated whole-ocean alkalinity increase reduces atmospheric CO_2.	Mainly in regions dominated by coccolithophorid production today but a global shift expected.	Relative decrease in calcite-producing plankton; whole-ocean increase in carbonate preservation.	(*7*)
Silica leakage	Mechanism by which the rain ratio could change. Iron-fertilized diatoms in the Southern Ocean take up less silicic acid relative to nitrate. The unused silicic acid is exported to silicon-limited regions, increases diatom production at the expense of coccolithophorids, and decreases the $CaCO_3$ to organic carbon rain ratio.	Regions north of the APF that are silicon limited. Low latitudes influenced by mixing of subantarctic mode water into the thermocline.	Shift from calcite- to silicate-producing plankton; increased export production; increased deep-ocean alkalinity (whole-ocean increase in carbonate preservation; increased carbonate-ion content).	(*5*, *32*)

region of the modern-day APF, although the full increase was not realized until the LGM.

Figure 2 shows that export production decreased at the beginning of the glaciation (Fig. 2A, stage 5a-d minus late Holocene) and increased subsequently (Fig. 2B, LGM minus stage 5a-d). Thus, the 50-ppm drawdown that had occurred by stage 5a-d cannot be explained by increased export production resulting from increased nutrient content or changes in the C/N/P ratio. Increased export production during the LGM is synchronous with the observed maximum in dust concentration, thus lending support to the hypothesis of iron fertilization during glaciations. It is possible that iron fertilization could explain the last 30 to 50 ppm of atmospheric CO_2 drawdown during the glacial period. This is consistent with the observation that when an ocean-biogeochemistry model is forced to reproduce the observed LGM export-production patterns, there is only a slight increase in global export production (+6% or +0.7 PgC/year) (*14*). In this experiment and in other simulations, iron fertilization accounts for <40-ppm decrease in atmospheric CO_2 (*3*, *14*, *25*).

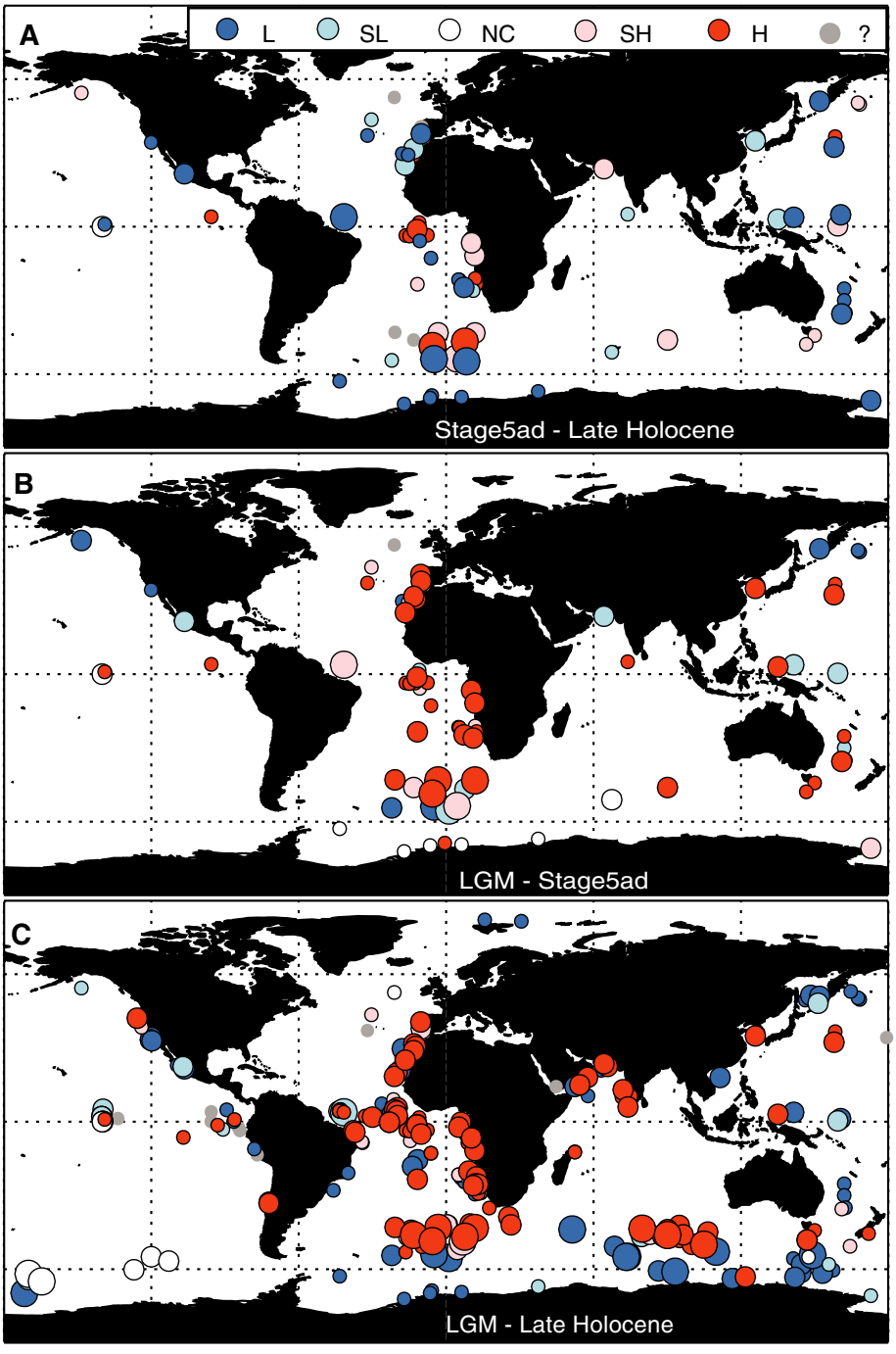

Fig. 2. Relative changes in export production for (**A**) stage 5a-d (80,000 to 110,000 years ago) minus Late Holocene (0 to 5000 years ago), (**B**) LGM (18,000 to 22,000 years ago) minus stage 5a-d, and (**C**) LGM minus Late Holocene. Dark and pale blue circles indicate lower (L) and slightly lower (SL) export production, respectively; dark and pale red circles indicate higher (H) and slightly higher (SH) export, respectively. White circles indicate no change (NC) between the two time periods. Gray circles represent sites where there is no unambiguous consensus between the different types of data. The size of the circle indicates the level of confidence (with small circles indicating low and large circles high confidence) in the assessment of the change in export production (*15*).

Increased surface-water nutrient and carbon utilization through the biological pump could also explain atmospheric CO_2 drawdown. This process could be particularly important in the Southern Ocean because of the large inventory of unused surface nutrients and the strong connection between surface waters and CO_2-rich deep waters. Increased nutrient utilization would occur if decreased vertical mixing south of the APF reduced the supply of nutrients and CO_2 to surface waters (*1*, *8*, *26*). Increased nutrient utilization south of the modern-day APF at the LGM compared with the late Holocene would bring about higher nitrate uptake, resulting in increased ^{15}N of organic material in surface waters (*8*); lower surface-water phosphate concentrations, causing lower Cd/Ca ratios in planktonic foraminifera (*27*); higher surface-water silica uptake, resulting in increased $\delta^{30}Si$ (*28*); and lower surface-water CO_2 concentrations, resulting in a relative increase in $\delta^{13}C$ of organic material (*29*). LGM records from south of the modern-day APF (fig. S2) do show higher $\delta^{15}N$ values, but proxy records indicate that phosphate concentrations (foraminifera Cd/Ca ratios) are higher, silica utilization ($\delta^{30}Si$) is lower, and surface-water CO_2 concentrations (organic $\delta^{13}C$) are higher than late Holocene values. Three of the four surface ocean indicators ($\delta^{13}C$, Cd/Ca, and $\delta^{30}Si$) are consistent with both a decrease in nutrient utilization and the observed decrease in export production. Recent improvements in measurement techniques have called the reliability of existing $\delta^{15}N$ data into question (*30*), so it is possible that future $\delta^{15}N$ data will prove more consistent with other nutrient indicators. Although we recognize that all of these paleonutrient indicators are affected by environmental factors that complicate their interpretation (*31*), the balance of evidence does not support the view that nutrient utilization accounted for a substantial part of the atmospheric CO_2 drawdown south of the modern-day APF.

The final explanation for changes in the marine biological pump invokes a shift in the dominant plankton types that would have decreased the export of carbonate relative to organic carbon (the rain ratio), resulting in an increase in the carbonate-ion content of seawater and thereby drawing down atmospheric CO_2 (*7*). Decreasing the relative export

of calcium carbonate to the seafloor could occur as a result of a global shift from primarily carbonate-producing plankton to siliceous (or other noncarbonate-producing) plankton. A mechanism that both decreases the rain ratio and reconciles the $\delta^{15}N$ and $\delta^{30}Si$ records in the Southern Ocean has recently been proposed (*5*, *32*), based on observations that diatoms take up substantially less silicic acid relative to nitrate under high-iron conditions (*32*, *33*). The "silica-leakage" hypothesis suggests that increased deposition of iron-rich dust during the last glacial period could account for high nitrate utilization while still leaving a pool of unused silicic acid in the Southern Ocean. This excess silicic acid could have been transported to the subantarctic and then to low-latitude thermocline waters by subantarctic mode waters. This would alleviate silicon limitation in both the subantarctic and the low-latitude HNLC regions (Fig. 1), thereby increasing diatom production at the expense of coccolithophorids.

The silica-leakage hypothesis would be registered as a shift from carbonate-producing to silicon-bearing plankton in marine sediments. Furthermore, the silica-leakage hypothesis constrains the timing and impact of this plankton shift to be coincident with increases in dust supply, and it would manifest itself as higher export production south of the APF. However, we have demonstrated that dust supply as well as export production in the Southern Ocean south of the APF were low during stage 5a-d compared with both the LGM and the late Holocene. Thus, the silica-leakage hypothesis as described above cannot be invoked to explain the initial 50-ppm decrease in atmospheric CO_2.

Records measuring specific molecular biomarkers demonstrate a shift from coccolithophorid to diatom assemblages in the Tasman Sea (*34*, *35*) and demonstrate that the contribution of coccolithophorids to the total flux of organic carbon in the South Atlantic (*36*), off northwest Africa (*37*, *38*), and in the Arabian Sea (*39*) was less important at the LGM than it is today. However, the decrease in the contribution of coccolithophorids occurs at the peak glacial period, well after stage 5a-d. Therefore, although the number of records is limited and more data are needed, especially from HNLC regions where silicon is limiting (in the Pacific Basin, Fig. 1), existing results are consistent with the hypothesis that a shift in phytoplankton taxa may have contributed to the lowering of atmospheric CO_2 from stage 5a-d to the LGM but not to the initial lowering of atmospheric CO_2 from stage 5e to stage 5d.

Both the rain-ratio hypothesis and the silica-leakage hypothesis also predict increases in the overall carbonate-ion content of deepwater, as well as a global increase in carbonate preservation in marine sediments [see (*1*) for review]. Although benthic foraminiferal boron isotope measurements of deepwater pH imply that carbonate-ion concentrations were 100 μmol/kg higher at the LGM compared with today (*40*), several other measures suggest very different conditions: (i) reconstructions of carbonate burial rates suggest little or no deepening of the lysocline required by an increase in carbonate-ion concentration (*41*), (ii) increases in foraminiferal size imply that carbonate-ion concentrations were only 4 to 8 μmol/kg higher (*42*), and (iii) foraminiferal assemblage dissolution indices estimate that carbonate-ion concentrations were a maximum of 5 μmol/kg higher in the Pacific and 20 μmol/kg lower in the Atlantic (*43*). Three of these four indicators suggest only a small change in deepwater carbonate-ion concentration. Thus, the evidence suggests that the expected change in deep-sea carbonate-ion concentration predicted by any form of the rain-ratio hypothesis is not observed.

We recognize limitations that could affect our conclusions. First, data coverage is poor in some regions, and nutrient utilization may occur in places other than the Southern Ocean. Figure 1 highlights key oceanic regions that remain relatively understudied with respect to the glacial-interglacial carbon cycle, and Fig. 2 demonstrates key regions where data do not agree. Second, vertical fluxes of biogenic components to the deep sea can be affected by other factors, such as sediment redistribution. Although we have corrected for these factors wherever possible (^{230}Th normalization was used in 77 out of 258 cores), further analyses may be needed to confirm our conclusions. Third, further research is required to improve our quantification of glacial-interglacial changes in deepwater carbonate-ion concentrations and carbonate burial. Finally, there may be interactions between physical and biological processes (such as the extent of vertical mixing and the impacts of interactive sea ice on polar biology) that might lead to a synergistic enhancement of the impact of ocean physics and biology on atmospheric CO_2 drawdown. Despite these potential limitations, our analysis shows that export production was low during stage 5a-d and increased afterward to reach its maximum at the LGM. Thus, we conclude that observational evidence does not support the idea that large-scale changes in the marine biological pump was the dominant influence on atmospheric CO_2 changes during glaciations.

Alternative hypotheses that can explain the initial 50-ppm decrease in atmospheric CO_2 without conflicting with biological data reconstructions include increased stratification of the glacial ocean (*1*, *44*), reduced ventilation of CO_2-rich deepwater resulting from increased sea-ice cover (*45*), and changes in the location and mechanisms of deepwater formation that alter deepwater composition (*46*). The first two mechanisms require that actual vertical mixing in the ocean be much smaller than the effective vertical mixing currently observed in global ocean circulation models (*47*, *48*); the third mechanism requires that ocean circulation models have stronger air-sea CO_2 equilibration in deepwater formation regions of the Southern Ocean than they do currently (*49*).

Current ocean general circulation models are unable to reproduce the observed variations in atmospheric CO_2 with the use of physical mechanisms alone; this is why the marine biological pump is often invoked as a probable mechanism to lower atmospheric CO_2. Our data analysis suggests that ocean biology contributed less than half of the observed glacial-interglacial variations in atmospheric CO_2 and therefore that physical processes must be responsible for most of the oceanic uptake of atmospheric CO_2 during glaciations. Our analysis thus suggests that ocean models should be more sensitive to changes in climate than they are currently, a conclusion supported by their inability to reproduce observed decadal variations in oceanic heat (*50*) and oxygen content (*50*, *51*).

References and Notes

1. D. M. Sigman, E. A. Boyle, *Nature* **407**, 859 (2000).
2. J. Kaplan, I. C. Prentice, W. Knorr, P. Valdes, *Geophys. Res. Lett.* **29**, 1079 (2002).
3. D. Archer, A. Winguth, D. Lea, N. Mahowald, *Rev. Geophys.* **38**, 159 (2000).
4. J. Martin, *Paleoceanography* **5**, 1 (1990).
5. K. Matsumoto, J. L. Sarmiento, M. A. Brzezinski, *Global Biogeochem. Cycles* **16**, 10.1029/2001GB001442 (2002).
6. W. S. Broecker, *Geochim. Cosmochim. Acta* **46**, 1689 (1982).
7. D. Archer, E. Maier-Reimer, *Nature* **367**, 260 (1994).
8. R. François *et al.*, *Nature* **389**, 929 (1997).
9. A. Tsuda *et al.*, *Science* **300**, 958 (2003).
10. P. W. Boyd *et al.*, *Nature* **407**, 695 (2000).
11. K. H. Coale *et al.*, *Science* **304**, 408 (2004).
12. K. H. Coale *et al.*, *Nature* **383**, 495 (1996).
13. M. B. McElroy, *Nature* **302**, 328 (1983).
14. L. Bopp, K. E. Kohfeld, C. Le Quéré, O. Aumont, *Paleoceanography* **18**, 10.1029/2002PA000810 (2003).
15. Materials and methods are available as supporting material on *Science* Online.
16. H. Kawahata, K. I. Ohkushi, Y. Hatakeyama, *J. Oceanogr.* **55**, 747 (1999).
17. H. Kawahata, T. Okamoto, E. Matsumoto, H. Ujiie, *Quat. Sci. Rev.* **19**, 1279 (2000).
18. R. Tiedemann, M. Sarnthein, N. J. Shackleton, *Paleoceanography* **9**, 619 (1994).
19. S. C. Clemens, W. L. Prell, *Paleoceanography* **5**, 109 (1990).
20. S. Schneider, *Ber. Fachber. Geowiss. Universit. Bremen* **187**, 134 (2002).
21. P. P. Hesse, *Quat. Sci. Rev.* **13**, 257 (1994).
22. K. E. Kohfeld, S. P. Harrison, *Earth Sci. Rev.* **54**, 81 (2001).
23. J. R. Petit *et al.*, *Nature* **399**, 439 (1999).
24. A. L. Berger, *Quat. Res.* **9**, 139 (1978).
25. A. J. Watson, D. C. E. Bakker, A. J. Ridgwell, P. W. Boyd, C. S. Law, *Nature* **407**, 730 (2000).
26. D. M. Sigman, M. A. Altabet, R. François, D. C. McCorckle, J.-F. Gaillard, *Paleoceanography* **14**, 118 (1999).
27. H. Elderfield, R. E. M. Rickaby, *Nature* **405**, 305 (2000).
28. C. L. De La Rocha, M. A. Brzezinski, M. J. DeNiro, A. Shemesh, *Nature* **395**, 680 (1998).
29. Y. Rosenthal, M. Dahan, A. Shemesh, *Paleoceanography* **15**, 65 (2000).
30. R. S. Robinson, B. G. Brunelle, D. M. Sigman, *Paleoceanography* **19**, PA3001 (2004); 10.1029/2003PA000996.

31. R. F. Anderson, Z. Chase, M. Q. Fleisher, J. P. Sachs, *Deep-Sea Res. II* **49**, 1909 (2002).
32. M. A. Brzezinski *et al.*, *Geophys. Res. Lett.* **29**, 1564 (2002).
33. D. A. Hutchins, K. W. Bruland, *Nature* **393**, 561 (1998).
34. M. Ikehara *et al.*, *Paleoceanography* **15**, 170 (2000).
35. E. Calvo, C. Pelejero, G. A. Logan, P. De Deckker, *Paleoceanography* **19**, 10.1029/2003PA000992 (2004).
36. P. J. Mueller, M. Cepek, G. Ruhland, R. R. Schneider, *Paleogeogr. Paleoclimatol. Paleoecol.* **135**, 71 (1997).
37. M.-A. Sicre *et al.*, *Org. Geochem.* **31**, 577 (2000).
38. P. Martinez *et al.*, *Org. Geochem.* **24**, 411 (1996).
39. D. Budziak *et al.*, *Paleoceanography* **15**, 307 (2000).
40. A. Sanyal, N. G. Hemming, G. N. Hanson, W. S. Broecker, *Nature* **373**, 234 (1995).
41. N. R. Catubig *et al.*, *Paleoceanography* **13**, 298 (1998).
42. J. Bijma, B. Hoenisch, R. E. Zeebe, *Geochem. Geophys. Geosys.* **3**, 10.1029/2002GC00038 (2002).
43. D. M. Anderson, D. Archer, *Nature* **416**, 70 (2002).
44. J. R. Toggweiler, *Paleoceanography* **14**, 571 (1999).
45. B. B. Stephens, R. F. Keeling, *Nature* **404**, 171 (2000).
46. J. R. Toggweiler, R. Murnane, S. Carson, A. Gnanadesikan, J. L. Sarmiento, *Global Biogeochem. Cycles* **17**, 1027 (2003).
47. D. E. Archer *et al.*, *Paleoceanography* **18**, 10.1029/2002PA000760 (2003).
48. W. Broecker *et al.*, *Global Biogeochem. Cycles* **13**, 817 (1999).
49. J. R. Toggweiler, A. Gnanadesikan, S. Carson, R. Murnane, J. L. Sarmiento, *Global Biogeochem. Cycles* **17**, 1026 (2003).
50. S. Levitus *et al.*, *Science* **292**, 267 (2001).
51. L. Bopp, C. Le Quéré, M. Heimann, A. C. Manning, P. Monfray, *Global Biogeochem. Cycles* **16**, 1022 (2002).
52. L. Xie, W. W. Hsieh, *Fish. Oceanogr.* **4**, 52 (1995).
53. M. E. Conkright *et al.*, *NOAA Atlas NESDIS 46* World Ocean Database 2001, vol. 5, *Temporal Distribution of Nutrient Profiles* (U.S. Government Printing Office, Washington, DC, 2002).
54. A. H. Orsi, T. Whitworth, W. D. Nowlin, *Deep-Sea Res. I* **42**, 641 (1995).
55. We thank A. Ridgwell, S. Kienast, I. Tegen, and two anonymous reviewers for helpful comments. We gratefully acknowledge the work of all authors cited in the Supporting Online Material for their invaluable data contributions. The ideas presented here emerged from stimulating discussions with I. C. Prentice and the participants of the Green Ocean Project: www.bgc-jena.mpg.de/bgc-synthesis/projects/green_ocean.

Supporting Online Material
www.sciencemag.org/cgi/content/full/308/5718/74/DC1
Materials and Methods
Figs. S1 to S5
Tables S1 to S3

17 September 2004; accepted 31 January 2005
10.1126/science.1105375

Getting to Know You: Reputation and Trust in a Two-Person Economic Exchange

Brooks King-Casas,[1] Damon Tomlin,[1] Cedric Anen,[3] Colin F. Camerer,[3] Steven R. Quartz,[3] P. Read Montague[1,2]*

Using a multiround version of an economic exchange (trust game), we report that reciprocity expressed by one player strongly predicts future trust expressed by their partner—a behavioral finding mirrored by neural responses in the dorsal striatum. Here, analyses within and between brains revealed two signals—one encoded by response magnitude, and the other by response timing. Response magnitude correlated with the "intention to trust" on the next play of the game, and the peak of these "intention to trust" responses shifted its time of occurrence by 14 seconds as player reputations developed. This temporal transfer resembles a similar shift of reward prediction errors common to reinforcement learning models, but in the context of a social exchange. These data extend previous model-based functional magnetic resonance imaging studies into the social domain and broaden our view of the spectrum of functions implemented by the dorsal striatum.

The expression and repayment of trust is an important social signaling mechanism that influences competitive and cooperative behavior (*1–6*). The idea of trust typically conjures images of complex human relationships, so it would seem to be a difficult part of social cognition to probe rigorously in a scientific experiment. Nevertheless, instances of trust can be stripped of complicating contextual features and encoded into economic exchange games that preserve its essential features (*7–9*). For example, in a game in which two players send money back and forth with risk, trust is operationalized as the amount of money a sender gives to a receiver without external enforcement (*9*). Such trust games now enjoy widespread use both in experimental economics (*10*) and neuroscience experiments (*11–17*).

To measure neural correlates of trust using functional magnetic resonance imaging (fMRI), we first made a simple modification to a single-exchange trust game in order to improve the ecological validity of the task (*10*). Specifically, we changed the single-round format to a multiround format in which the same two individuals (one designated the "investor," and the other the "trustee") played 10 consecutive rounds. This modification reflects the fact that significant social exchanges are rarely single-shot, and the assumption that algorithms in our brains are tuned to this fact (*1–6*). Thus, by adapting the multiround format, (i) trust becomes bidirectional, in that both the investor and trustee assume the risk that money sent might not be reciprocated by their partner; and (ii) reputation building can be probed, as players develop models of one another through iterated exchange (*10*, *11*). Participants were informed that individual rounds of the trust game would be implemented as follows: One player (investor) could invest any portion of $20 with the other player (trustee), the money appreciated (three times the investment), and the trustee then decided how much of the tripled amount to repay (Fig. 1) (*18*). Players maintained their roles throughout the entire 10-round game. Responses were encoded only in monetary units and player identities were never revealed, thus stripping away many of the confounding elements of context and communication known to influence trust (*10*). Volunteers were recruited from separate subject pools at Baylor College of Medicine in Houston, TX, and California Institute of Technology in Pasadena, CA. Volunteers were instructed identically, but separately, at each institution (instructors read a script describing the task).

We used event-related hyperscan-fMRI (h-fMRI) to monitor homologous regions of two subjects' brains simultaneously as they played the multiround trust game (*19*) (fig. S1). The motivating idea behind this approach is simple: To probe neural substrates of social interactions, we scan the brains of multiple subjects engaged in a social interaction. Social decision-making critically depends on internally represented models of social partners. In principle, such covert knowledge might be inferred from behavioral observations. However, behavioral signals are intrinsically lower dimensional than their underlying neural responses, and so behavior alone is an insufficient signal source for inferring neural representations. Put another way, an inference based only on the observable behavior of a social partner ignores many observable neural processes that give rise to that behavior. The measurement of both interacting brains directly sidesteps this problem and allows us to probe the cross correlation of internal models—replacing inference with a measurement.

Reciprocity predicts trust. Linear regression analyses of the behavior of 48 pairs of subjects identified reciprocity to be the strongest predictor of subsequent increases or decreases in trust (*20*). Reciprocity is defined as a fractional change in money sent across rounds by one

[1]Human Neuroimaging Laboratory, Department of Neuroscience, [2]Menninger Department of Psychiatry and Behavioral Sciences, Baylor College of Medicine, One Baylor Plaza, Houston, TX 77030, USA. [3]Social Cognitive Neuroscience Laboratory, Division of Humanities and Social Sciences 228-77, California Institute of Technology, Pasadena, CA 91125, USA.

*To whom correspondence should be addressed. E-mail: read@bcm.tmc.edu

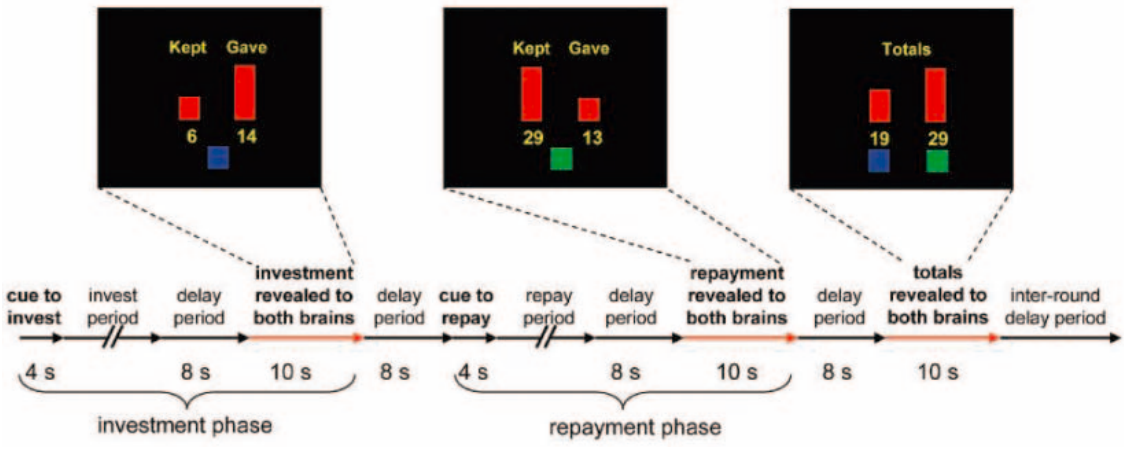

Fig. 1. Timeline for the two-person trust game. Trust experiments were carried out in 48 pairs of subjects. Each pair of subjects completed 10 consecutive trust exchanges. Each exchange began with a screen that indicated the beginning of the round, followed by a cue to invest. The investor then entrusted the trustee with any amount between 0 and 20 monetary units. During this first free response period, the trustee saw a blank screen for 8 s after the investor's decision was submitted. The investment was revealed to both players simultaneously. Amounts kept and given were represented both graphically (by a bar graph) and numerically. After the investor's decision was revealed, the trustee was then prompted to split three times the invested amount in any proportion between themselves and the investor. Eight seconds after the trustee repayment decision was submitted, the repayment was revealed to both players in the same graphical and numerical fashion. After another 8 s delay, the totals for the round were revealed using the same method. Rounds were separated by a variable 12- to 42-s interval. Except for the periods of free response, both players viewed the same visual stimuli simultaneously.

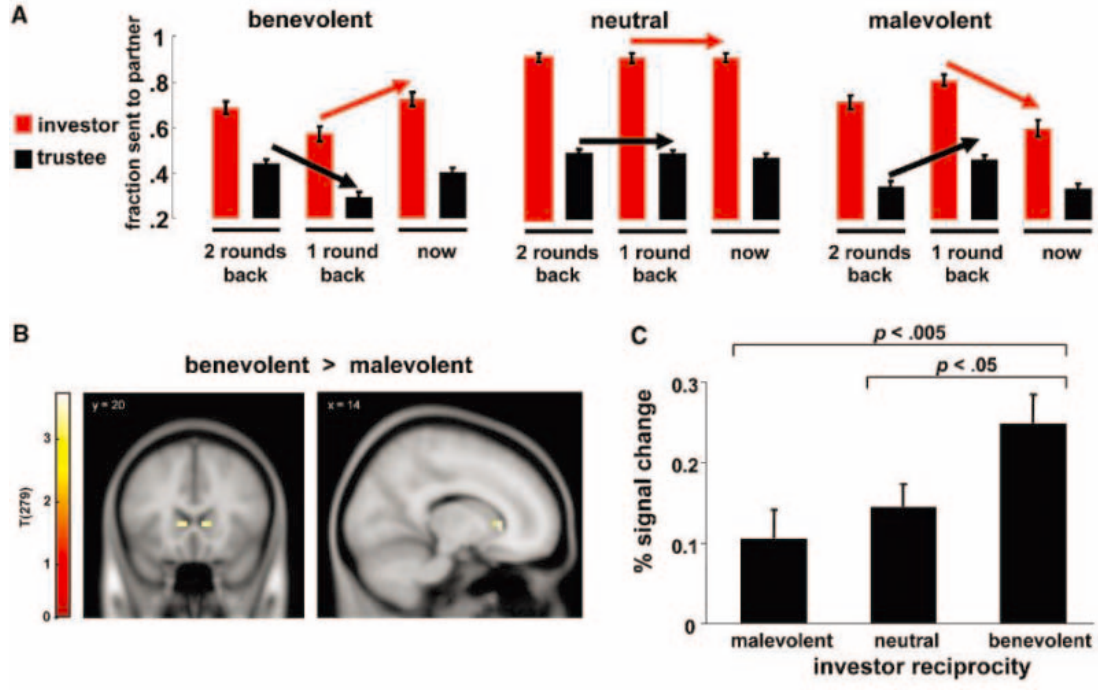

Fig. 2. Correlates of reciprocity in a multiround economic exchange. (**A**) Behavioral summary. Mean ± SE of investor (ΔI, red) and trustee (ΔR, black) behavior of rounds contributing to benevolent (n = 125), neutral (n = 134), and malevolent (n = 125) investor reciprocity categories. In each round j, investor reciprocity was defined as $r_j = \Delta I_j - \Delta R_{j-1}$; that is, the difference between the current change in payment ΔI_j by the investor in response to the previous change in repayment ΔR_{j-1} by the trustee. In the case of benevolent reciprocity, investors are being generous (sending more) in response to a defection by the trustee (decrease in repayment). Likewise, in the case of malevolent reciprocity, the investor repays the trustee's generosity (increase in previous repayment) with a breach of trust (*20*). (**B**) Response of trustee brain to investor reciprocity. A general linear model analysis identified four regions in the trustee brain that showed responses that were greater for the revelation of malevolent and benevolent investor reciprocity than for neutral reciprocity (*21*). Only one region, the head of the caudate nucleus, showed a response that was greater for benevolent relative to malevolent reciprocity (statistical parametric map shown alongside pseudo-color legend). No region showed greater responses to malevolent relative to benevolent investor reciprocity. (**C**) Region-of-interest analysis of head of caudate in trustee brain. Average activity 6 to 10 s after the investor's decision is revealed to trustee shows that the brain response to benevolent reciprocity was significantly greater from neutral (two-tailed t test, $P < 0.05$) and malevolent reciprocity (two-tailed t test, $P < 0.005$) (*21*).

player in response to a fractional change in money sent by their partner. This definition is simply an operationalized version of tit-for-tat, that is, a repayment in kind. Deviations from neutral reciprocity (perfect tit-for-tat) act as a strong social signal in the context of this game. In particular, strong deviation in investor reciprocity was the best predictor of changes in partner trust and became the primary focus of our analysis (*20*, *21*). Investor reciprocity on round j was quantified as $\Delta I_j - \Delta R_{j-1}$, where ΔI_j is the fractional change in investment from round $j - 1$ to j and ΔR_{j-1} is the last fractional change repayment ($R_{j-1} - R_{j-2}$).

Forty-eight subject pairs were scanned in this study (*21*), and we divided the exchanges into three approximately equal-sized groups: (i) benevolent reciprocity, (ii) neutral reciprocity, and (iii) malevolent reciprocity (*22*). These behavioral exchange data are summarized in Fig. 2A. For benevolent reciprocity, investors are actually being generous (sending more) in response to a defection by the trustee (decrease in repayment) (left panel). Conversely, for malevolent reciprocity, the investor repays the trustee's generosity with a breach of trust (right panel).

Using a general linear model analysis, we first sought trustee brain regions whose blood oxygenation level–dependent (BOLD) response was greater for benevolent or malevolent investor reciprocity than for neutral investor reciprocity (*21*). This analysis identified four significant regions: inferior frontal sulcus, superior frontal sulcus, thalamus, and inferior/superior colliculli (*23*). These findings

are consistent with a surprise signal—an unsigned response to deviations in the expected behavior of one's partner. A second analysis, comparing BOLD response for benevolent reciprocity to BOLD response for malevolent reciprocity, identified significant differences only in the head of the caudate nucleus (Fig. 2, B and C): (i) BOLD response was greater for instances of benevolent reciprocity relative to malevolent and neutral reciprocity; and (ii) responses to malevolent reciprocity did not differ from those to neutral reciprocity. These voxels were subsequently subjected to a region-of-interest (ROI) analysis (*21*).

"Intention to trust" signals. We expected to find a hemodynamic response in this ROI that correlated with the trustee's next choice to repay, and we expected that such signals might show strong cross-brain correlations. The reason for this expectation derived from the fact that reciprocity expressed by the investor ($\Delta I_j - \Delta R_{j-1}$) strongly predicted ($r = 0.56$) future changes in trust (repayment, ΔR_j) by the trustee. For example, benevolent reciprocity by the investor is expected to generate the intention to increase repayment (trust) in the brain of the trustee. A similar intention to decrease trust (repayment) would be expected in the trustee brain following malevolent reciprocity by the investor. Some part of the investor's brain should anticipate the neural consequences of changes in their own reciprocity on the trustee's brain; therefore, we also expected that such "intention to trust" signals would show strong cross-brain correlations. Indeed, they did.

Model building of partner: Cross-brain analysis. To carry out this analysis, we separated the hemodynamic responses in the caudate of the trustee brain into three groups according to whether their next repayment was larger, smaller, or the same as their last repayment. We were particularly interested in the net neural response to the intention to increase trust (repayment), because this act embodies risk on the part of the trustee and signals to the investor a degree of willingness to cooperate. We computed the net intent-to-trust signal in the ROI of the trustee caudate as

$$H(\text{increased repayment next round}) - H(\text{decreased repayment next round})$$

where H represents the hemodynamic response. Using this difference signal in the trustee brain, we computed cross-brain correlations with the investor brain and sought regions with the largest correlations. We were particularly interested in how the cross-brain correlations might change as the task developed and the subjects built better models of one another. Consequently, changes in this signal were examined across early (3 and 4), middle (5 and 6), and late (7 and 8) rounds using cross-brain and within-brain correlational analysis. Figure 3 illustrates the cross-correlograms of this signal with activity in two regions: the middle cingulate cortex (MCC) of investors and the anterior cingulate cortex (ACC) of trustees (*21*). The blue traces indicate that MCC activity in the investor brain and ACC activity in the trustee brain were most strongly correlated ($r > 0.59$) when the MCC signal was shifted forward in time by 14 s. The important point here is that the strongest cross-brain correlation did not shift significantly in time from early to late rounds; that is, neural responses in both brains to fiducial markers of the task did not change relative to each other. However, the peak of the cross-correlogram between investor MCC activity and the trustee "intention to trust" signal in the caudate showed a pronounced 14-s shift from early to late rounds (green traces). A similar finding resulted for the within-brain analysis of the trustee, using ACC activity and the same "intention to trust" signal in the caudate (red traces). These analyses show that a dramatic change in the relative timing of the measured BOLD signals was taking place either in the "intention to trust" signal of the trustee caudate or in both the trustee ACC and investor MCC. As shown in Fig. 4, the source of the shift is in the "intention to trust" signal of the trustee caudate.

Figure 4 shows the time traces of the hemodynamic responses in the head of the trustee caudate segregated according to future changes in trust (increases are shown in black,

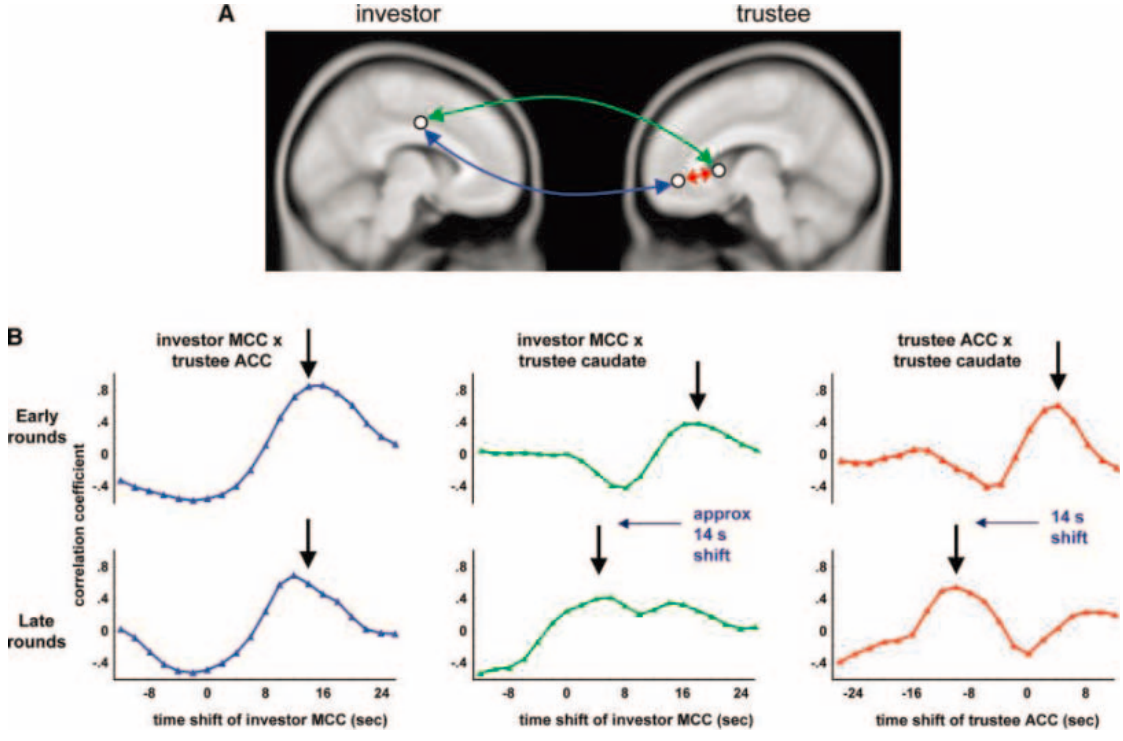

Fig. 3. Correlograms of the "intention to trust" with activity in investor MCC and trustee ACC. (**A**) Regions of correlation. The "intention to trust" signal in the trustee caudate was correlated within- and between-brains with regions that responded strongly to basic behavioral events within each round: The middle cingulate cortex (MCC) of the investor was strongly active when the investor lodged a decision, and the anterior cingulate cortex (ACC) of the trustee was strongly activated when an investor's decision was revealed (*21*). (**B**) Correlograms of caudate, ACC, and MCC. The caudate signal between rounds of increased and decreased repayment isolated an "intention to trust" signal in trustees. Average "intention to trust" signal was correlated with average ACC signal of trustee and average MCC signal of investors during the investment phase of each round (*21*) and is plotted with different time shifts. Correlograms are shown for early (rounds 3 and 4) and late (rounds 7 and 8) periods of the game. Blue traces indicate that the strongest cross-brain correlation for responses to basic behavioral events of the game did not shift significantly in time from early rounds to late rounds. The peak of the cross-correlogram between investor MCC activity and the trustee "intention to trust" signal in the caudate shows a pronounced 14-s shift from early to late rounds (green traces). A similar result is evident in the within-brain analysis of the trustee, using ACC activity and the same signal in the caudate (red traces).

decreases in red) (*21*). The amplitude and time effects associated with the 14-s time shift are shown in Fig. 4A and summarized in the bar graphs in Fig. 4B. In early rounds of the task (rounds 3 and 4), the peak of the response for intended increases in trust (i.e., an increase in next repayment) occurs after the investor's decision is revealed. In middle rounds (rounds 5 and 6), this response begins to drop back toward baseline and begins to grow at a time just before the revelation of the investor's decision. By late rounds (rounds 7 and 8), this peak is anticipatory and occurs before the revelation of the investor's decision. These data are consistent with a signal for intended increases in trust changing from being reactive to anticipatory and suggest that the trustee is building a model of the investor's likely next move. To test this model-building idea directly, we performed a separate version of the trust game and queried the trustees on each round about their expectation of the next investment.

Figure 5 illustrates the results of this additional experiment (n = 21 pairs, behavior only). On each round, both the investor and trustee were simultaneously prompted. The investor was cued to make their investment and the trustee was cued to guess the investor's decision (Fig. 5A). Timings were otherwise kept the same. The results of these experiments are summarized as the fraction of highly accurate guesses (to within ±$1) by the trustee as a function of round. Notice that the increase in the trustee's accuracy across rounds parallels the time during which the temporal transfer of the neural signal correlated with future increases in trust.

Discussion. We used an anonymous trust game in conjunction with event-related fMRI to probe neural correlates of the expression and repayment of trust between interacting human subjects. Important social relationships are rarely a single expression of trust between two strangers; thus, we made the game multiround instead of one-shot. Specifically, we sought to examine trust in a context in which (i) trust was expressed by both partners in the relationship, and (ii) trust could change over time and with experience (*25*).

Using a multiround trust game and a large sample of subjects (n = 48 pairs), we identified a social signal (reciprocity) expressed by the investor that strongly predicted changes in trust by the trustee. This social signal elicited two notable effects in the trustee brain: (i) brain regions whose activity correlated with large changes in reciprocity in a manner consistent with a surprise response; and (ii) a specific brain region, the head of the caudate nucleus, where the BOLD response was greater for benevolent reciprocity than for malevolent reciprocity. The strong relation between investor reciprocity and subsequent changes in trustee repayment led us to probe the "intention to trust" in the caudate nucleus. Rounds were segregated on the basis of whether trustees subsequently increased or decreased their repayment, representing a signal of the "intention to trust." Cross- and within-brain correlations of this intended-trust signal with neural responses to fiducial markers of the task (investment submitted and investment revealed) identified a remarkable temporal transfer of the "intention to trust" signal from a time just after the revelation of the investor's decision (a reactive signal) to a time just before this same revelation (an anticipatory signal). This shift suggested that the signal would correlate with the development of a model of the investor in the trustee's brain. To examine this latter possibility, we ran a separate behavioral experiment (n = 21 pairs) to test the trustee's ability to accurately guess (to within ±$1) the decision by the investor. The error rate of these accurate guesses dropped over the same time period during which the temporal transfer of the future trust signal shifted from reactive to anticipatory. This observation is consistent with the interpretation that the observed signals in the trustee caudate reflect the development of a reputation for their partner.

Lastly, we address an important detail about the amplitude differences between the caudate response to impending increases (black traces, Fig. 4) and impending decreases in trust (red

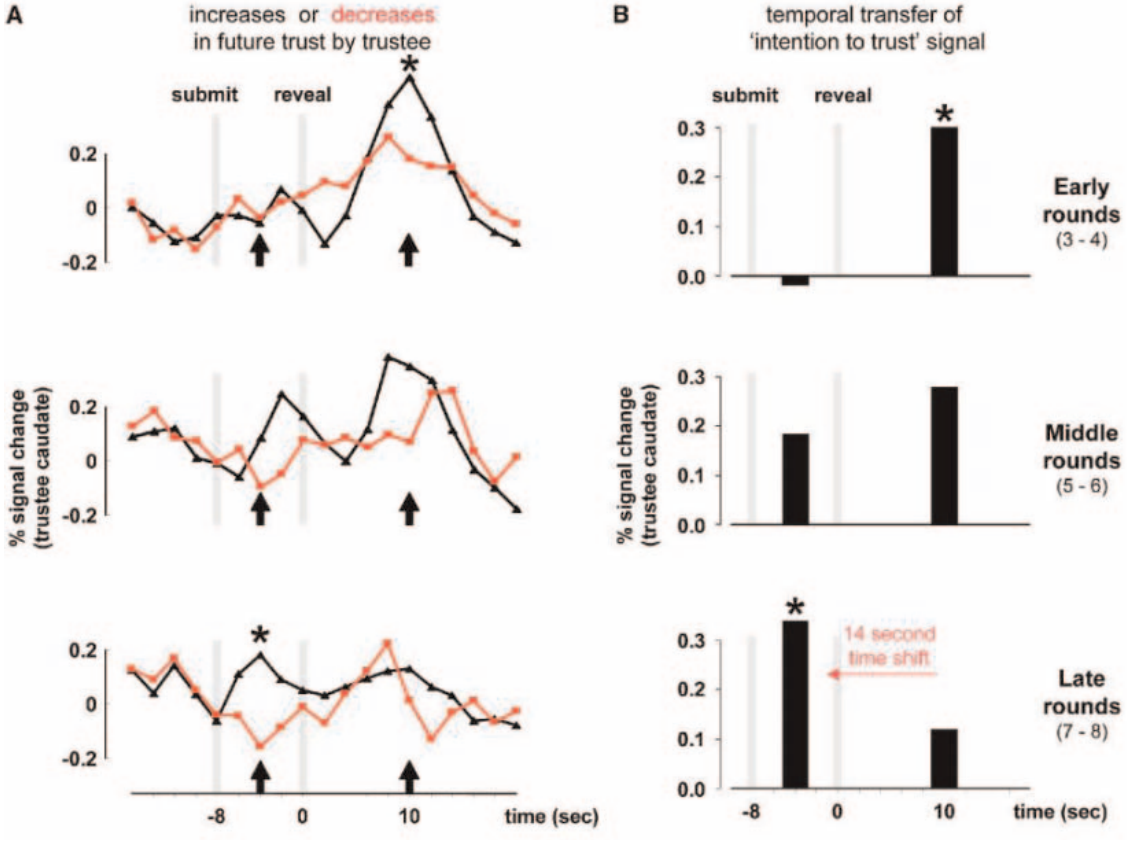

Fig. 4. Neural correlates of reputation building in trustee brain. (**A**) ROI time series. An ROI analysis was performed on voxels identified by the contrast illustrated in Fig. 2B (*21*). We segregated hemodynamic responses in response to the revelation of the investment (time = 0 s) according to the next decision made by the trustee (trustee's decision period begins at t = 22 s). Hemodynamic amplitudes for future increases in trust (ΔR > 5%; black trace) were greater (P < 0.05) than future decreases in trust (ΔR < −5%; red trace) in early rounds (top). As the game progressed (middle and bottom), the peak of this differentiated response underwent a temporal transfer from a time after the revelation of the investor's decision (t = 10 s; a reactive signal) to a time before this same revelation (t = −4 s; an anticipatory signal). Traces represent subsamples of 144 rounds in which repayment increased or decreased ≥5% (mean = 20; SD = 4.4). (**B**) ROI bar plot. The difference between the intention to increase trust [black trace of (A)] and the intention to decrease trust [red trace of (A)] is plotted for t = −4 s and t = 10 s. The 14-s temporal transfer from reactive to anticipatory is consistent with the development of a reputation for the investor within the trustee brain.

traces, Fig. 4). One explanation, supported by the behavioral data, is that increases in trust (ΔR) may have a greater effect on their partner's subsequent behavior (ΔI) than decreases in trust. If this were the case, an efficient computational system would devote more computational steps, and hence more energy, to deciding the magnitude of an increase in trust relative to a decrease. In this particular version of the trust game, increases in trust by the trustee were correlated positively with changes in investment on the subsequent round by the investor ($r = 0.27$) (fig. S6A). This was not true for decreases in trust, where there was no such correlation ($r = 0.00$) (fig. S6B). The absence of predictive information associated with a decrease in trust suggests that no analogous energetic investment should be made.

Taken together, these results suggest that the head of the caudate nucleus receives or computes information about (i) the fairness of a social partner's decision and (ii) the intention to repay that decision with trust. In early rounds of the game, the "intention to trust" is evident only after an investment is revealed. With experience, this signal shifts to a time preceding the revelation of the investment. This finding is reminiscent of analogous shifts of reward prediction error signals from reinforcement learning (*25*–*27*) that have recently been identified by fMRI in human caudate and putamen (*28*–*32*) and are thought to involve outputs of midbrain dopaminergic systems. These prediction error signals were identified using simple conditioning experiments in which lights predict the future delivery of rewards (e.g., squirt of juice or delivery of monetary return) (*33*, *34*). The scheme is simple: An initially neutral light is flashed; it causes no change in dopaminergic activity, but the later (surprising) arrival of juice causes a burst of activity in the dopamine neurons. Repeated pairing of light followed at a consistent time later by juice causes two dramatic changes: (i) The response to juice delivery drops back to baseline and (ii) a burst response occurs just after the light is flashed. This temporal transfer of the burst response to the light is thought to represent the future value predicted by the light. The simplicity of these experiments is somewhat beguiling.

The temporal transfer in the conditioning experiments is directly analogous to the temporal shift that we observe in the trustee brain as they build a model of the investor's response, but framed in the context of a social exchange. In the trustee brain, the analog to the light is the cue for the social partner to invest, and the "social juice" is change in investment. We know that positive changes in investment correlate with subsequent positive changes in repayment; a correlation that grows over the rounds of the task (fig. S5). Early in the exchange, the trustee's intention to increase trust occurs after revelation of the investor's decision to increase investment (Fig. 4A and fig. S5); that is, the increased investment is surprising. The intention to increase repayment therefore follows this revelation. As the game proceeds, this "intention to trust" response transfers to a time before the revelation of the investor decision to increase investment. The only open issue for this speculation is why the signal transferred to this particular time. There are several consistent predictors of the revelation of the investor's decision, but the signal backed up in time to occur just before this. This social prediction error interpretation is provocative and consistent but leaves this important question unanswered. The more general hypothesis is that the dopaminergic system can be used to establish more complex goal states ("rewards") and make more complex predictions through connections from prefrontal cortex onto midbrain and other subcortical structures (*35*).

It is possible that similar economic exchange tasks could be used to explore social processing deficits in a variety of neuropsychiatric disorders. These include populations that have faulty or missing capacities for building correct models of others (e.g., schizophrenia or autism spectrum disorders) (*36*, *37*), as well as individuals who misattribute motivations and intentions to others (e.g., borderline personality disorder) (*38*).

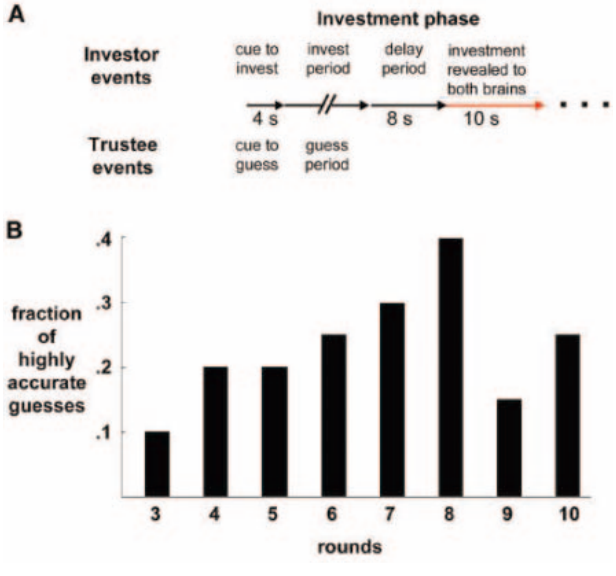

Fig. 5. Model building by trustee brain In a separate anonymous trust game (n = 21 pairs), trustees were queried to "guess the amount invested" just before the revelation of the investor's payment decision to both brains; otherwise, the task was identical to that of the original game (n = 48 pairs) from which scanning data were derived. (**A**) Timeline for queries to each player (investor and trustee). During the investment phase of the exchange, the trustees were prompted to guess the investor's decision. The trustee response to this query was not revealed to the investor. (**B**) Model building—highly accurate guesses by trustee of investor's next payment. A highly accurate guess was defined as ±1 monetary unit from the actual investment (±5%). These data show that a model of the investor's next move is available to the trustee by the middle to late rounds of the exchange and is not available in the early rounds.

References and Notes

1. R. L. Trivers, *Q. Rev. Biol.* **46**, 35 (1971).
2. R. Axelrod, W. Hamilton, *Science* **211**, 1390 (1981).
3. J. S. Coleman, in *Foundations of Social Theory* (Harvard Univ. Press, Cambridge, MA, 1990), pp. 177–179.
4. H. Rachlin, *Behav. Brain Sci.* **25**, 239 (2002).
5. R. Adolphs, *Nat. Rev. Neurosci.* **4**, 165 (2003).
6. E. Fehr, U. Fischbacher, *Nature* **425**, 785 (2003).
7. C. Camerer, K. Weigelt, *Econometrica* **56**, 1 (1988).
8. E. Fehr, G. Kirchsteiger, A. Riedl, *Q. J. Econ.* **108**, 437 (1993).
9. J. Berg, J. Dickhaut, K. McCabe, *Games Econ. Behav.* **10**, 122 (1995).
10. C. Camerer, *Behavioral Game Theory: Experiments in Strategic Interaction* (Princeton Univ. Press, Princeton, NJ, 2003), pp. 60–62.
11. K. McCabe, D. Houser, L. Ryan, V. Smith, T. Trouard, *Proc. Natl. Acad. Sci. U.S.A.* **98**, 11832 (2001).
12. D. J. de Quervain *et al.*, *Science* **305**, 1254 (2004).
13. J. Decetey, P. L. Jackson, J. A. Sommerville, T. Chaminade, A. N. Meltzoff, *Neuroimage* **23**, 744 (2004).
14. N. I. Eisenberger, M. D. Lieberman, K. D. Williams, *Science* **302**, 290 (2003).
15. P. Glimcher, A. Rustichini, *Science* **306**, 447 (2004).
16. J. Rilling *et al.*, *Neuron* **35**, 395 (2002).
17. A. G. Sanfey, J. K. Rilling, J. A. Aronson, L. E. Nystrom, J. D. Cohen, *Science* **300**, 1755 (2003).
18. "$20" refers to 20 monetary units (MU). Subject payment at the end of the experiment varied between $20 and $40, depending on the number of MU the subject accumulated over 10 rounds. Payment schedule was as follows: <68 MU = $20, 68 to 133 MU = $25, 134 to 200 MU = $30, 201 to 300 MU = $35, and >300 MU = $40. Before the game, participants were informed that they would receive between $20 and $40, scaled by their performance. However, they had no knowledge of the step payoff function until the game was completed. Notice that the perfectly selfish Nash equilibrium strategy (in which the investor keeps all $20 each round) results in 200 MU; no subject adopted this strategy.
19. P. R. Montague *et al.*, *Neuroimage* **16**, 1159 (2002).
20. Investments (I) and repayments (R) were scaled by the amount available to be sent ($20 for I; three times the amount invested for R). See fig. S2 for a description of investments and repayments over the course of the game. Linear regressions identified significant predictors of change in trust for investors (ΔI_j) and trustees (ΔR_j). Three predictors of ΔI_j were examined: (i) previous repayment (R_{j-1}; $r = 0.02$), (ii) change in repayment (ΔR_{j-1}; $r = 0.10$), and (iii) previous trustee reciprocity ($\Delta R_{j-1} - \Delta I_{j-1}$; $r = 0.31$). Three predictors of ΔR_j were examined: (i) previous investment (I_j; $r = 0.10$), (ii) change in investment (ΔI_j; $r = 0.26$), and (iii) previous investor reciprocity ($\Delta I_j - \Delta R_{j-1}$; $r = 0.56$). Thus, reciprocity was a stronger predictor than either amount previously sent (I_j or R_{j-1}) or change in amount previously sent (ΔI_j or ΔR_{j-1}). However, it is noteworthy that reciprocity expressed by the investor ($r = 0.56$) was more strongly related to change in trust than reciprocity expressed by the trustee ($r = 0.26$). This difference is likely accounted for by an asymmetry in the structure of the exchange: In each round, the investor can accumulate money ($20 endowment) without the cooperation of the trustee,

whereas the trustee is wholly dependent on the investor's cooperation. This dependency of the trustee on the investor likely results in greater responsivity by the trustee to changes in investor reciprocity.
21. A description of methods is available as supporting material in *Science* Online.
22. Each dyad contributed eight behavioral events to this analysis (48 pairs × 8 rounds = 384 rounds). Investor reciprocity cannot be calculated for the initial two rounds and was excluded. The 384 rounds had a mean ± SD of −0.01 ± 0.35, skewness of −0.19 (SE = 0.12), and kurtosis of 2.55 (SE = 0.25). Rounds were divided into approximately equal-sized categories: 125 malevolent reciprocity rounds ($x < -0.025$), 134 neutral reciprocity rounds ($-0.025 \leq x \leq +0.05$), and 125 benevolent reciprocity rounds ($x > +0.05$). For additional description of reciprocity categories, see figs. S3 and S4.
23. Regions with ≥10 significant voxels were identified using *t* tests. *Z* values and statistical parametric mapping (SPM) coordinates for each region are available in table S1.
24. The correlation of change in investment (ΔI_j) and subsequent change in repayment (ΔR_j) grew as experience between players accrued (fig. S5).
25. P. Dayan, L. F. Abbott, *Theoretical Neuroscience* (MIT Press, Cambridge, MA, 2001).
26. K. C. Berridge, in *The Psychology of Learning and Motivation*, D. L. Medin, Ed. (Academic Press, New York, 2000), pp. 223–278.
27. A. Dickinson, B. W. Balleine, in *Steven's Handbook of Experimental Psychology*, C. R. Gallistel, Ed. (Wiley, New York, 2002), vol. 3, pp. 26–72.
28. G. Pagnoni, C. F. Zink, P. R. Montague, G. S. Berns, *Nat. Neurosci.* **5**, 97 (2002).
29. S. M. McClure, G. S. Berns, P. R. Montague, *Neuron* **38**, 339 (2003).
30. J. P. O'Doherty, P. Dayan, K. Friston, H. Critchley, R. J. Dolan, *Neuron* **38**, 329 (2003).
31. J. O'Doherty *et al.*, *Science* **304**, 452 (2004).
32. B. Seymour *et al.*, *Nature* **429**, 664 (2004).
33. W. Schultz, P. Dayan, P. R. Montague, *Science* **275**, 1593 (1997).
34. P. R. Montague, S. E. Hyman, J. D. Cohen, *Nature* **431**, 760 (2004).
35. R. C. O'Reilly, T. S. Braver, J. D. Cohen, in *Models of Working Memory: Mechanisms of Active Maintenance and Executive Control*, A. Miyake, P. Shah, Eds. (Cambridge Univ. Press, New York, 1999), chap. 11, pp. 375–411.
36. K.-H. Lee, T. F. D. Farrow, S. A. Spence, P. W. R. Woodruff, *Psychol. Med.* **34**, 391 (2004).
37. E. L. Hill, U. Frith, *Philos. Trans. R. Soc. London Ser. B* **358**, 281 (2003).
38. P. A. Johnson, R. A. Hurley, C. Benkelfat, S. C. Herpertz, K. H. Taber, *J. Neuropsychiatry Clin. Neurosci.* **15**, 397 (2003).
39. This work was supported by the Center for Theoretical Neuroscience at Baylor College of Medicine (P.R.M.), National Institute on Drug Abuse (NIDA) grant DA11723 (P.R.M.), National Institute of Neurological Disorders and Stroke grant NS045790 (P.R.M.), National Institute of Mental Health grant MH52797 (P.R.M.), NIDA grant DA14883 (G. Berns), The Kane Family Foundation (P.R.M.), The David and Lucile Packard Foundation (S.R.Q.), and The Gordon and Betty Moore Foundation (S.R.Q.). We thank P. Dayan, J. Li, T. Lohrenz, C. Stetson, and two anonymous referees for comments on this manuscript. We thank the Hyperscan Development Team at Baylor College of Medicine for Network Experiment Management Object (NEMO) software implementation (www.hnl.bcm.tmc.edu/nemo) and G. Berns for early discussions and efforts leading to the development of hyperscanning. We also thank A. Harvey, S. Flaherty, K. Pfeiffer, R. Pruitt, and S. Gleason for technical assistance.

Supporting Online Material
www.sciencemag.org/cgi/content/full/308/5718/78/DC1
Materials and Methods
Figs. S1 to S6
Table S1
References

30 November 2004; accepted 7 February 2005
10.1126/science.1108062

Postsynaptic Receptor Trafficking Underlying a Form of Associative Learning

Simon Rumpel,[1] Joseph LeDoux,[2] Anthony Zador,[1] Roberto Malinow[1]*

To elucidate molecular, cellular, and circuit changes that occur in the brain during learning, we investigated the role of a glutamate receptor subtype in fear conditioning. In this form of learning, animals associate two stimuli, such as a tone and a shock. Here we report that fear conditioning drives AMPA-type glutamate receptors into the synapse of a large fraction of postsynaptic neurons in the lateral amygdala, a brain structure essential for this learning process. Furthermore, memory was reduced if AMPA receptor synaptic incorporation was blocked in as few as 10 to 20% of lateral amygdala neurons. Thus, the encoding of memories in the lateral amygdala is mediated by AMPA receptor trafficking, is widely distributed, and displays little redundancy.

Animals continually adapt their behavior in response to changes in the environment. It has long been held that selective modifications in synaptic efficacy represent the physical substrate for this behavioral plasticity (*1*, *2*). Long-term potentiation (LTP), a cellular model of synaptic plasticity, has emerged as a leading candidate mechanism underlying associative forms of learning in the central nervous system (*3*–*12*). Much is now known about the molecular mechanisms during LTP that translate a brief change in electrical activity patterns to a modification in synaptic efficacy (*13*–*23*). Recent studies indicate that synaptic addition of GluR1 subunit–containing AMPA-type glutamate receptors (GluR1-receptors) mediates the synaptic strengthening observed during LTP (*24*, *25*). An attractive

[1]Cold Spring Harbor Laboratory, Cold Spring Harbor, NY 11724, USA. [2]New York University, New York, NY 10003, USA.

*To whom correspondence should be addressed. E-mail: malinow@cshl.edu

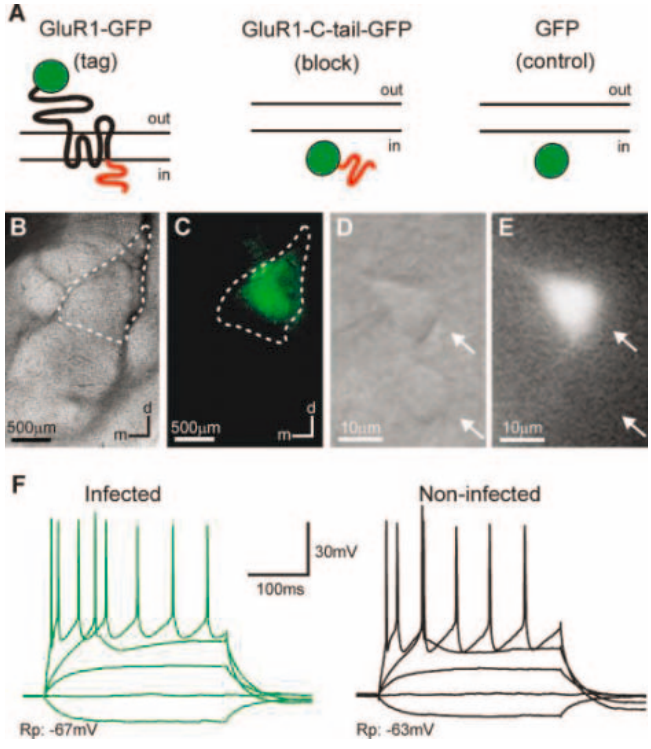

Fig. 1. Viral infection with amplicon vectors does not alter basic electrophysiological properties. (**A**) Schematic of recombinant proteins used in this study: GluR1-GFP, a fusion protein of GFP and the GluR1 subunit; GluR1-C-tail–GFP, a fusion protein of GFP and the last C-terminal 81 amino acids of the GluR1 subunit; and GFP alone. (**B** and **C**) Low magnification transmitted light (B) and epifluorescence (C) images of a coronal section of the right hemisphere including the amygdala. Note the area of GFP-expressing cells within the lateral amygdala (dotted line) 1 day after injection. d, dorsal; m, medial. (**D** and **E**) Highly magnified image of the lateral amygdala by infrared-differential interference contrast microscopy (D) and epifluorescence (E), which contains a neuron expressing (upper arrow) or not expressing (lower arrow) GFP. (**F**) Superimposed current-clamp recordings of an infected (green traces) and noninfected (black traces) neuron during 300-ms current injections of –100, 0, +100, +200, and +550pA. Rp, resting potential of neurons indicated next to traces.

proposal is that a learning-driven increase in GluR1-receptors at a selected group of synapses underlies associative memory.

We tested this proposal by using auditory fear conditioning, a well-characterized behavioral paradigm in which an animal learns to associate a tone with an electric shock and subsequently "freezes" when presented with a tone alone (*11*, *12*, *26*). The memory formed by fear conditioning is long lasting and can be easily assessed. Lesions and pharmacological treatments indicate a role of the amygdala in acquisition and storage of fear memory traces. Furthermore, LTP occurs at the synapses between the auditory thalamus to the lateral amygdala in vitro and in vivo. We have therefore studied the role of GluR1-receptor trafficking at thalamo-amygdala synapses in associative fear conditioning.

Amplicon vectors to tag or block plasticity. To investigate the role of GluR1-receptor trafficking in fear conditioning, we used an acute gene delivery technique to express recombinant proteins in a spatially and temporally controlled manner within a targeted brain region (*27*–*31*). In this way, we could monitor and perturb AMPAR trafficking. We injected amplicon vectors based on nonreplicating herpes simplex virus (*32*) into the lateral amygdala of juvenile rats (*33*) (Fig. 1A). Infected cells could be identified by amplicon-driven coexpression of the green fluorescent protein (GFP). Expression was rapid and robust, so that infected cells were clearly visible in amygdala brain slices prepared 24 hours after in vivo injection (Fig. 1, B through E). The basic electrophysiological properties of infected neurons, including input resistance and firing properties, were indistinguishable from those of noninfected control neurons (*34*) (Fig. 1F).

The first amplicon vector we used (Fig. 1A) encodes GluR1 fused with GFP. This vector drives expression of homomeric AMPARs that display greater rectification (i.e., a greater conductance when passing inward than outward current) than endogenous AMPARs (*35*). Synapses undergoing plasticity by incorporation of recombinant GluR1-receptors show increased rectification compared with synapses with only endogenous AMPARs. These receptors thus act as a "plasticity tag" for modified synapses that can be detected with an electrophysiological assay (*36*). The second amplicon vector encodes the carboxyl cytoplasmic tail (81 amino acids) of GluR1 fused with GFP. The resulting protein acts as a dominant-negative construct to prevent synaptic incorporation of endogenous GluR1-receptors and thereby blocks several forms of synaptic plasticity in vitro and in vivo (*36*, *37*); we designate this the "plasticity-block" vector. A third amplicon vector (the "infection-control" vector) drives expression of only GFP and serves as a control for infection.

There is little synaptic incorporation of GluR1-receptors in the absence of strong plasticity-inducing stimuli (*38*). We thus first assessed trafficking of GluR1-receptors in the lateral amygdala of animals that were not subjected to fear conditioning. We prepared brain slices from naïve animals 36 hours after in vivo infection of the lateral amygdala with the plasticity-tag vector. Rectification of AMPAR-mediated transmission between auditory thalamus and lateral amygdala (*11*) was similar in infected and noninfected neurons (Fig. 2, A to C), which indicated no detectable synaptic incorporation of recombinant GluR1-receptors in naïve rats. In a second series of experiments, we injected the plasticity-block

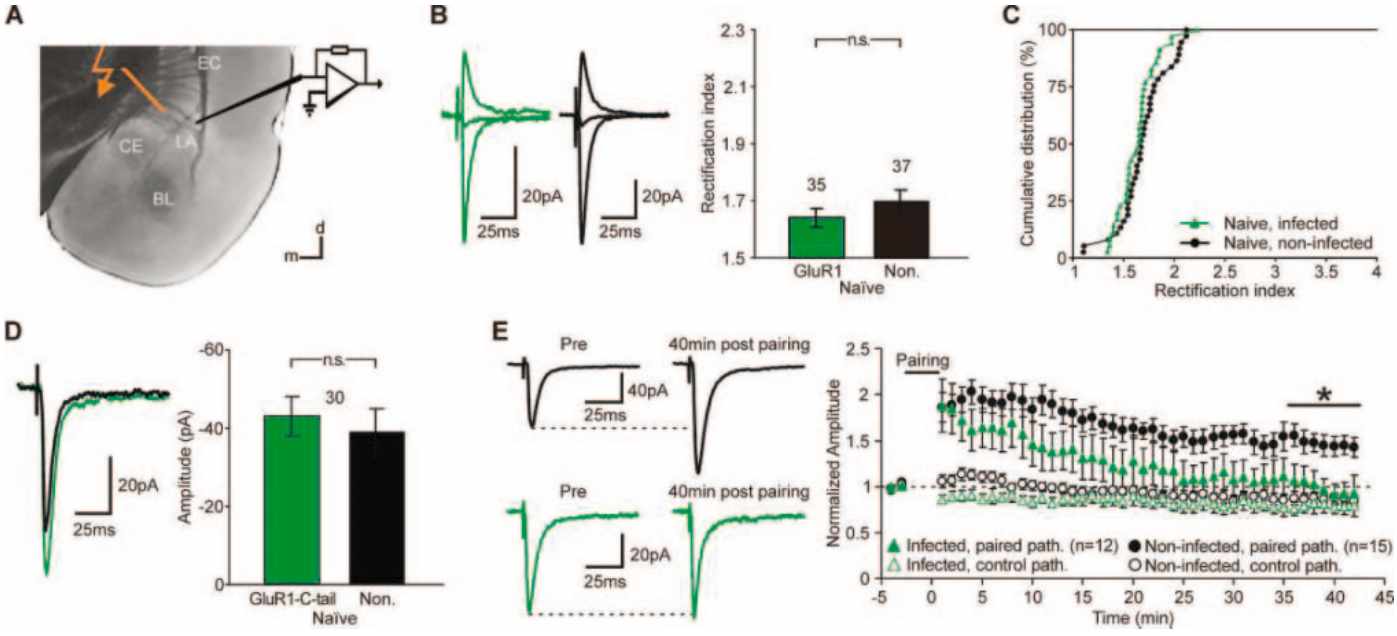

Fig. 2. Trafficking of GluR1 subunit–containing AMPARs in the lateral amygdala of naïve rats. (**A**) Transmitted light image of an acute amygdala slice preparation. Placement of stimulation and recording electrodes indicated. LA, lateral nucleus of the amygdala; BL, basolateral nucleus of the amygdala; CE, central nucleus of the amygdala; EC, external capsule; d, dorsal; m, medial. Note bundles of thalamo-amygdala fibers in the ventral striatum. (**B**) (Left) Evoked AMPAR-mediated postsynaptic currents (AMPA PSCs; 25 to 40 responses averaged) at –60, 0, and +40 mV holding potential recorded from a neuron infected with the plasticity-tag vector (green traces) and noninfected neuron (black traces). (Right) Mean rectification indices of synaptic pathways [RI, (amplitude at –60 mV holding potential)/(amplitude at +40 mV holding potential)] onto neurons infected with the plasticity-tag vector and noninfected neurons showed no statistically significant differences (*t* test, $P = 0.34$; n.s.), which suggests no incorporation of recombinant receptors in naïve animals. (**C**) Cumulative distribution plot of data shown in (B). (**D**) (Left) Superimposed averages (25 to 40 responses) of evoked AMPA PSCs recorded simultaneously in a neuron infected with the plasticity-block vector (green trace) and noninfected neuron (black trace) at –60 mV holding potential. (Right) Mean amplitude of evoked AMPA PSCs recorded simultaneously in pairs of neurons infected with the plasticity-block vector and not infected showed no statistically significant difference (*t* test, $P = 0.67$; n.s.). (**E**) (Left) Evoked AMPA PSCs (12 responses averaged) recorded in a noninfected neuron (black traces) and a neuron expressing plasticity-block vector (green traces) before and 40 min after LTP induction. (Right) Mean AMPA PSC amplitudes in neurons infected with the plasticity-block vector and noninfected neurons before and after the pairing protocol. Amplitudes were normalized to levels before pairing. Transmission in paired pathways from infected neurons returned to basal levels 40 min after LTP induction and was significantly lower than in paired pathways in control neurons (*t* test, $^*P < 0.01$). Error bars in this and all other figures are SEM.

vector into the lateral amygdala of rats to probe the trafficking of endogenous GluR1-receptors. Brain slices were prepared 14 to 20 hours after injection, to allow sufficient time to detect expression of the construct in neurons. The amplitude of basal AMPAR-mediated transmission was not affected by the plasticity-block construct, as assessed by simultaneous recordings of evoked transmission in nearby infected and noninfected neurons (Fig. 2D). Had there been synaptic incorporation of endogenous GluR1-receptors during the expression of the plasticity-block construct, synaptic currents would have been smaller in infected neurons (*39*). We then used the plasticity-block vector to assess the role of GluR1 trafficking during LTP in lateral amygdala neurons (Fig. 2E). In non-infected neurons, an LTP-inducing protocol led to persistent enhanced transmission. However, in neurons expressing the plasticity-block construct, the same stimulus protocol led only to a brief increase in transmission, similar to the results in hippocampus (*38*). Taken together, these results suggest that there was little or no synaptic incorporation of GluR1-receptors in the lateral amygdala of naïve rats during the expression period we examined.

Associative learning drives AMPARs into synapses. We next tested the first key prediction of the trafficking hypothesis: Conditioning should induce the incorporation of GluR1-receptors into thalamo-amygdala synapses. We injected the plasticity-tag vector into the lateral amygdala to monitor synapses undergoing plasticity. Thirty-six hours after injection, in one group of animals, we paired tones with shocks; in a second group, which

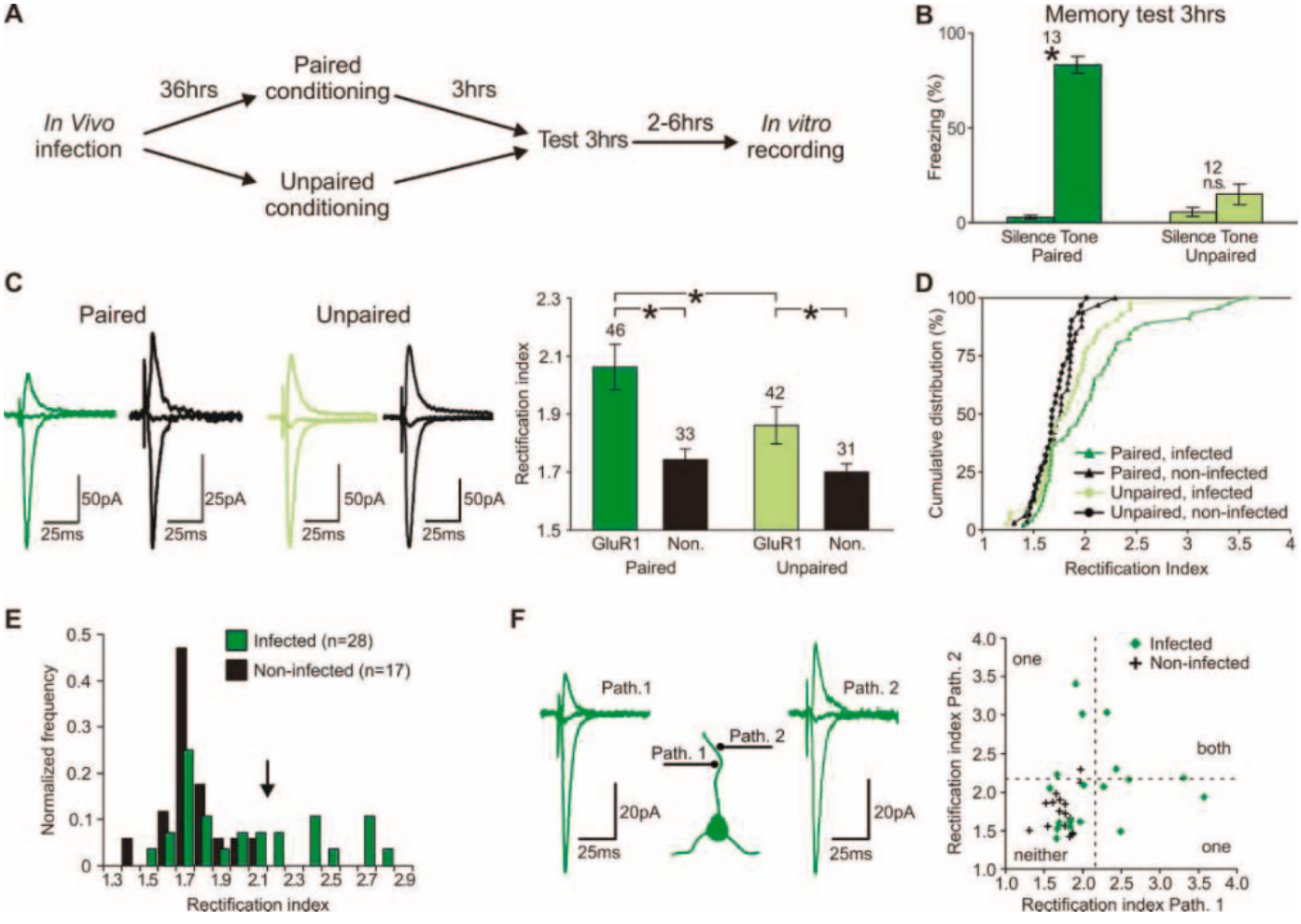

Fig. 3. Fear conditioning induces synaptic incorporation of recombinant GluR1 subunit–containing AMPA receptors. (**A**) Schematic of the experimental protocol. (**B**) Behavioral analysis of animals infected with the plasticity-tag vector 3 hours after either a paired conditioning protocol (solid green bars) or as control an unpaired conditioning protocol (hatched green bars). Freezing behavior was scored in testing cage during 1 min of silence and 1 min of tone presentation, as indicated. Animals from the paired group showed significantly increased freezing during tone presentation (*t* test, $*P < 0.01$). (**C**) (Left) Superimposed averages of evoked AMPA PSCs recorded at –60, 0, and +40 mV holding potential from neurons infected with the plasticity-tag vector (green) and noninfected (black) neurons from animals that underwent paired or unpaired conditioning. Note the strongly increased rectification in infected neuron from paired animal. (Right) Mean RIs of synaptic pathways from neurons infected with the plasticity-tag vector (GluR1) and noninfected neurons (non) from paired and unpaired animals (Paired, GluR1 versus non, *t* test, $P < 0.01$; unpaired, GluR1 versus non, *t* test, $P < 0.05$; GluR1, paired versus unpaired, *t* test, $P < 0.05$; significant differences indicated by asterisks). (**D**) Cumulative distribution of RIs from (C). Note the divergence of distributions for RI values >1.7. (**E**) Histogram of RIs in infected and noninfected neurons from paired animals (RIs have been averaged in case two synaptic pathways have been obtained from one neuron). Of tested lateral amygdala neurons, 36% showed learning-induced synaptic delivery of GluR1-receptors as estimated by determining the number of infected neurons that show RIs larger than two standard deviations of the distribution from noninfected neurons (arrow). (**F**) Learning-induced delivery of GluR1-receptors occurs at subsets of synapses and is not neuron-wide. (Left) Superimposed averages of evoked AMPA PSCs recorded at –60, 0, and +40 mV holding potential in a single neuron expressing the plasticity-tag construct. Two individual synaptic pathways onto the neuron had been probed by interleaved stimulation of two separate bundles of thalamo-amygdala fibers (see Fig. 2A). Note strong differences in rectification between pathways. (Right) Scatter plot of RIs from two pathways recorded in single neurons infected with the plasticity-tag vector (green diamonds) and single noninfected neurons (black crosses). RIs from pathways in infected neurons were not significantly correlated ($R^2 = 0.014$).

served as control for nonassociative learning, we delivered the same number of tones and shocks, but in an unpaired fashion (Fig. 3A). As expected (*11*, *12*), the paired group showed robust freezing in response to a test tone presented 3 hours later, whereas the unpaired control group did not (Fig. 3B). After behavioral testing, we prepared brain slices from both groups and examined synaptic transmission between auditory thalamus and lateral amygdala. In slices from each group, we measured rectification of transmission onto neurons expressing the plasticity-tag construct, as well as onto noninfected neurons.

Infected neurons from the paired group showed significantly more rectification than infected neurons from the unpaired group (Fig. 3, C and D), indicating synaptic delivery of GluR1-receptors during this form of associative learning. About 36% of infected neurons in the paired group displayed rectification values more than two standard deviations above the mean rectification of the noninfected cells (Fig. 3E). This suggests that about one-third of neurons in the lateral amygdala undergo plasticity after formation of the memory of the tone-shock pairing.

Rectification indices in infected neurons from unpaired animals were slightly but significantly higher than in noninfected neurons from unpaired animals (Fig. 3, C and D) and infected neurons from naïve animals (*t* test, $P < 0.01$) (Fig. 2, B and C). This result may be due to the occurrence of some forms of learning in the lateral amygdala (such as contextual learning, or learning that the tone predicts no shock) in the unpaired group that may drive GluR1-receptor incorporation but is not measured by our behavioral assay (*40*–*42*). In summary, our findings demonstrate that associative fear conditioning is a powerful stimulus for the incorporation of GluR1-receptors into synapses of auditory input to lateral amygdala neurons.

Learning-induced receptor trafficking is pathway-specific. One of the hallmarks of LTP is that it is pathway-specific: Only synapses that meet the conditions for induction undergo potentiation (*43*). We therefore examined whether learning-induced receptor trafficking in vivo occurred at all synapses onto a cell, or at only a subset of synapses. We compared rectification of two synaptic pathways onto infected lateral amygdala cells from the paired group. Synaptic responses were evoked by stimulation of two individual thalamo-amygdala fiber bundles (Fig. 3F). In general, rectification indices from two auditory thalamic pathways onto the same infected lateral amygdala cell showed no significant correlation ($R^2 = 0.014$). Most cells displaying plasticity showed significantly increased rectification in only one pathway (7 out of 10). These results indicate that receptor trafficking induced by fear conditioning can be restricted to a subset of synapses and is not a cellwide phenomenon.

Synaptic incorporation of AMPARs is necessary for learning. We next tested a second key prediction of the trafficking hypothesis: Synaptic delivery of endogenous GluR1-receptors is necessary to acquire the conditioned response. Our approach was to test whether molecular block of GluR1-receptor synaptic incorporation impaired memory formation. We first established a moderate conditioning protocol that did not saturate learning (Fig. 4A). We reasoned that such a protocol would increase our ability to detect an effect on learning if only a small fraction of neurons were infected. We also wished to avoid possible compensation of partial memory impairment by overtraining (*44*). To probe the role of GluR1-receptor delivery in fear memory formation, we infected one group of animals with the plasticity-block vector, the amplicon that showed no effect on basal transmission in naïve animals (Fig. 2D) but can block plasticity-induced synaptic delivery of GluR1-receptors (*38*) (Fig. 2E). A control group was infected with the infection-control vector (Fig. 4B). To maximize the number of lateral amygdala neurons infected, animals received robust bilateral injections (1 to 2 μl total per amygdala). After allowing 14 to 20 hours for expression of constructs, we exposed animals to the moderate conditioning protocol and then later tested them for the conditioned response as a measure of memory. To avoid possible bias, we performed injections and testing blindly (i.e., the experimenter did not know the identity of the injected vector).

In memory retention tests 3 or 24 hours after training, animals that received robust injections of the plasticity-block vector showed significantly less freezing in response to the tone than did the group that received robust injections of the infection-control vector (Fig. 4C). This finding suggests impairment of fear acquisition that led to disruption of both short-term (3-hour) and long-term (24-hour) memory of the conditioning experience. During the conditioning protocol, the two groups of animals showed similar levels of freezing after the footshock. Since lesions of the amygdala disrupt postshock freezing (*11*), the differences in learning and the consequent effects on memory cannot be explained by a simple impairment of basic sensorimotor systems as might be expected, for example, from impairment of normal synaptic transmission rather than of plasticity. Thus, blockade of synaptic GluR1-receptor incorporation in lateral amygdala neurons can disrupt the learning processes that led to the formation of a lasting form of associative memory.

Disabling plasticity in few neurons impairs learning. We wished to determine the fraction of neurons in the lateral amygdala that must exhibit plasticity in order to

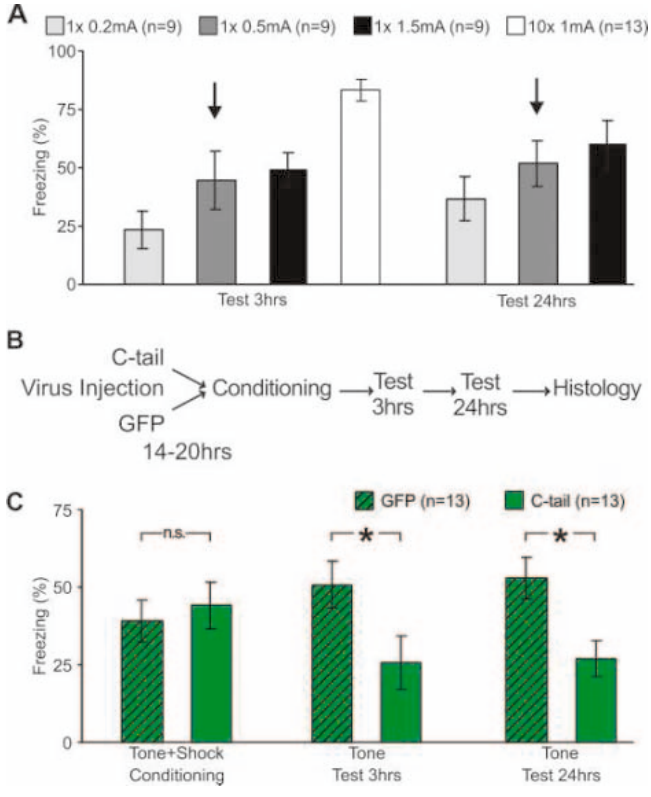

Fig. 4. Blocking synaptic incorporation of GluR1-receptors by overexpression of the plasticity-block construct impairs memory formation. (**A**) Behavioral analysis of noninfected animals 3 hours and 24 hours after single pairing of a tone and a footshock of varying intensity (protocols indicated). White bar illustrates freezing in animals conditioned with a protocol involving multiple pairing of tones and footshock (same data as Fig. 3B). The moderate conditioning protocol that was used in later experiments is indicated by arrows. (**B**) Schematic of the experimental protocol. (**C**) Behavioral analysis of animals infected either with the plasticity-block vector or the infection-control vector. Animals infected with the plasticity-block vector show significantly reduced freezing compared with control animals during memory retention tests (3 hours, *t* test, $P < 0.05$; 24 hours, *t* test, $P < 0.01$, significant differences indicated by asterisks), but not during the conditioning protocol (conditioning, *t* test, $P = 0.81$, n.s.).

support fear conditioning. We therefore used histological methods to estimate the proportion of neurons that were infected with the plasticity-block vector in the two lateral amygdalas of each animal (Fig. 5, A and B). After behavioral testing, the brain of each animal was removed, fixed, and sectioned serially, permitting three-dimensional analysis. For each brain section, we measured the fractional area of the lateral amygdala showing GFP fluorescence. By measuring fluorescence in all sections, the fraction of the two lateral amygdalas infected was calculated for each animal.

In order to estimate the fraction of infected neurons within each slice, we labeled several sections with a neuron-specific NeuN antibody (Fig. 5B). With dual-wavelength confocal imaging, individual neurons could readily be identified as infected or noninfected. The fraction of neurons displaying GFP in an infected region was measured [$\kappa = 0.58 \pm 0.04$ (mean ± SEM); $n = 5$ sections, two animals]. By multiplying this conversion factor κ by the fraction of the two lateral amygdalas infected, we could estimate the fraction of infected neurons in the two lateral amygdalas of each animal.

In animals that received robust injections with the plasticity-block vector, on average 27 ± 4% ($n = 13$) of lateral amygdala neurons were infected, indicating that blockade of synaptic GluR1 incorporation in as few as a quarter of neurons is sufficient to disrupt learning (Fig. 5C). We observed the same (27 ± 3%, $n = 13$) average rate of infection in control animals that received robust injections with the infection-control vector and showed normal learning, which indicated that expression of the plasticity-blocking construct, rather than variable infection levels, was responsible for the effect on learning.

Does abolishing plasticity in less than one-quarter of lateral amygdala neurons reduce learning? To obtain a lower bound on the fraction of lateral amygdala neurons required to produce an effect on learning, we tested an additional group of animals that received sparse bilateral infections of the plasticity-block vector or the infection-control vector (0.3 to 0.6 μl per amygdala). In these animals, the fraction of neurons infected was low (plasticity-block vector, 8 ± 1%, $n = 7$; infection-control vector, 7 ± 2%, $n = 6$; n.s.), and learning was normal (Fig. 5, C and D). Thus, if trafficking of GluR1-receptors is blocked in fewer than 10% of lateral amygdala neurons, then the animal displays normal learning. We pooled the data from the animals receiving robust and sparse infections and plotted the amount of freezing as a function of the fraction of infected neurons for each animal. We observed that most animals with 20% or more of lateral amygdala neurons infected with the plasticity-block vector showed diminished learning, whereas animals with less than 10% of neurons infected showed on average no effects on learning (Fig. 5E). Assuming that the amplicon vector does not preferentially infect neurons participating in encoding of the memory, these results indicate that blocking GluR1-receptor trafficking in ~10 to 20% of neurons undergoing plasticity is sufficient to impair memory formation in animals receiving moderate conditioning.

Cellular mechanisms of memory. We have shown that fear conditioning drives synaptic incorporation of GluR1-receptors in lateral amygdala neurons. It is noteworthy that not all synapses onto these plastic cells are modified, which suggests that learning-induced synaptic incorporation of GluR1-receptors is, like LTP, regulated in a synapse-specific manner. We find that interference with GluR1-receptor trafficking impairs amygdala LTP as well as fear conditioning, which indicates an essential contribution of this molecular process to memory formation. This view is supported by studies on genetically modified mice completely lacking the GluR1 subunit (*45*) that demonstrate impaired associative fear conditioning. Mice expressing GluR1 subunits with subtle mutations in phosphorylation sites (*46*) that block synaptic incorporation of recombinant GluR1-receptors (*47*) also show deficits in some associative forms of memory. Our findings establish the addition

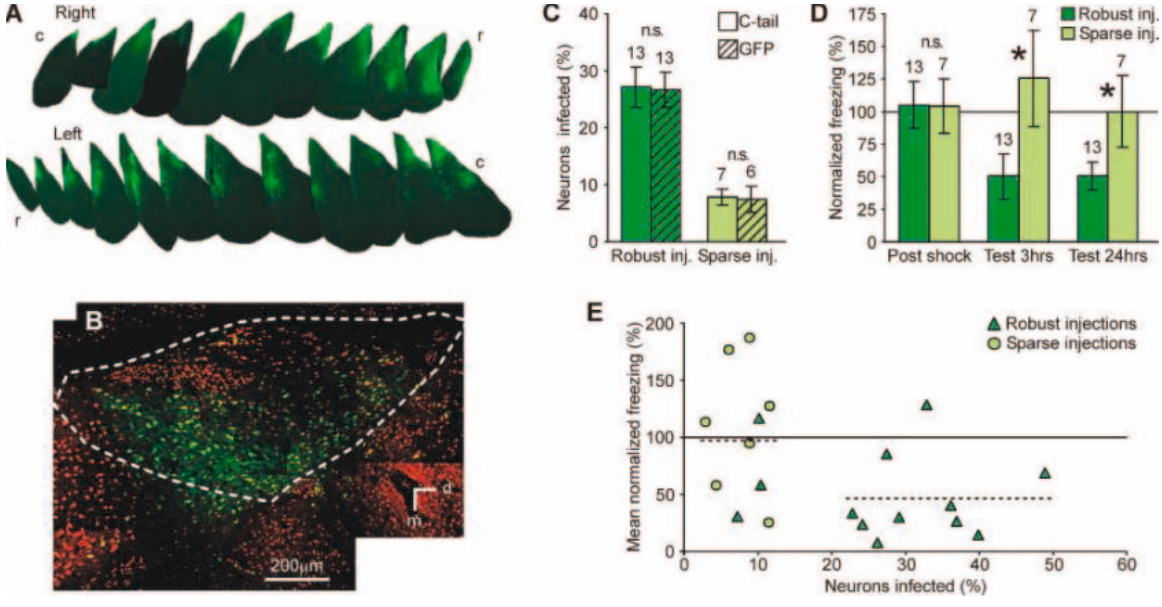

Fig. 5. Histological analysis of infection efficacy allows estimation of minimal fraction of plasticity-blocked neurons necessary to cause memory defects. (**A**) Montage of epifluorescence images of the lateral amygdala and basolateral nucleus of the amygdala taken from serial sections of the right (top) and left (bottom) hemisphere from an animal having received injections with the infection-control vector. r, rostral; c, caudal. (**B**) Combined dual-channel image of an injection site in the lateral amygdala by confocal laser scanning microscopy. Red channel, immunohistochemical labeling of neuronal marker NeuN; green channel, GFP expression from infected cells. Within the site of injection, 58% of neurons showed green fluorescence. Dotted line circumscribes lateral amygdala. d, dorsal; m, medial. (**C**) Fraction of amygdala neurons in animals infected with the plasticity-block vector (solid bars) and infection-control vector (hatched bars) for robust and intentionally sparse injections from a separate series of experiments; no statistically significant differences were observed between infection rate for the plasticity-block vector and the infection-control vector (robust, *t* test, $P = 0.92$; sparse, *t* test, $P = 0.89$, n.s.). (**D**) Behavioral analysis of animals with robust (same data as Fig. 4C) and sparse injections. Freezing of animals expressing the plasticity-block construct was normalized to control animals expressing only GFP. In memory retention tests, animals with sparse injections of the plasticity-block vector showed freezing levels similar to control animals and significantly higher freezing as animals with robust injections of the plasticity-block vector (3 hours, 24 hours, *t* test, $P < 0.05$, significant differences indicated by asterisks). (**E**) Freezing of animals expressing the plasticity-block construct was averaged across both test sessions, normalized to control animals, and plotted against the fraction of infected cells in the lateral amygdala [same data as in (D)]. Each symbol represents values from a single animal. Dotted lines indicate average freezing in animals with infection levels of 0 to 15% and 15 to 50%.

of postsynaptic receptors, as a form of synaptic plasticity, to be a key element in associative memory formation.

Circuit mechanisms of memory. By using molecular tagging techniques, we estimate that about a third of lateral amygdala neurons undergo plasticity during the formation of a memory driven by a single conditioning block. Because not all synapses on a plastic neuron undergo modification, one neuron may potentially participate in many memories, which allows combinatorial storage of a large number of memories (*48*–*50*). Perturbing plasticity in a small fraction of lateral amygdala neurons appears to be sufficient to reduce memory function, which suggests little robustness or redundancy. Memory formation may require coordinated changes in synaptic strength, and perturbing a few plastic units may corrupt integrated function, much as the inability of a few violinists to change key properly can detectably offset a symphonic performance. Finding such sensitivity to small perturbation is striking given that large lesions (*51*) or advanced brain pathology (*52*) produce little disturbance of memory formation.

References and Notes

1. S. Freud, in *The Origins of Psychoanalysis*, M. Bonaparte, A. Freud, E. Kris, Eds. (Basic Books, New York, 1895), pp. 356–359.
2. D. O. Hebb, *Organization of Behavior* (Wiley, New York, 1949).
3. M. S. Rioult-Pedotti, D. Friedman, J. P. Donoghue, *Science* **290**, 533 (2000).
4. P. Andersen, *Philos. Trans. R. Soc. London B Biol. Sci.* **358**, 613 (2003).
5. G. Lynch, *Philos. Trans. R. Soc. London B Biol. Sci.* **358**, 625 (2003).
6. B. L. McNaughton, *Philos. Trans. R. Soc. London B Biol. Sci.* **358**, 629 (2003).
7. R. G. Morris, *Philos. Trans. R. Soc. London B Biol. Sci.* **358**, 643 (2003).
8. S. Tonegawa, K. Nakazawa, M. A. Wilson, *Philos. Trans. R. Soc. London B Biol. Sci.* **358**, 787 (2003).
9. J. Lisman, *Philos. Trans. R. Soc. London B Biol. Sci.* **358**, 829 (2003).
10. H. Eichenbaum, *Neuron* **44**, 109 (2004).
11. J. E. LeDoux, *Annu. Rev. Neurosci.* **23**, 155 (2000).
12. S. Maren, *Annu. Rev. Neurosci.* **24**, 897 (2001).
13. R. A. Nicoll, *Philos. Trans. R. Soc. London B Biol. Sci.* **358**, 721 (2003).
14. G. L. Collingridge, J. T. Isaac, Y. T. Wang, *Nature Rev. Neurosci.* **5**, 952 (2004).
15. R. C. Malenka, M. F. Bear, *Neuron* **44**, 5 (2004).
16. R. Malinow, *Philos. Trans. R. Soc. London B Biol. Sci.* **358**, 707 (2003).
17. M. Sheng, M. J. Kim, *Science* **298**, 776 (2002).
18. I. Song, R. L. Huganir, *Trends Neurosci.* **25**, 578 (2002).
19. D. Johnston *et al.*, *Philos. Trans. R. Soc. London B Biol. Sci.* **358**, 667 (2003).
20. K. M. Harris, J. C. Fiala, L. Ostroff, *Philos. Trans. R. Soc. London B Biol. Sci.* **358**, 745 (2003).
21. C. Pittenger, E. R. Kandel, *Philos. Trans. R. Soc. London B Biol. Sci.* **358**, 757 (2003).
22. S. Choi, J. Klingauf, R. W. Tsien, *Philos. Trans. R. Soc. London B Biol. Sci.* **358**, 695 (2003).
23. D. Zamanillo *et al.*, *Science* **284**, 1805 (1999).
24. Y. Hayashi *et al.*, *Science* **287**, 2262 (2000).
25. M. Passafaro, V. Piech, M. Sheng, *Nature Neurosci.* **4**, 917 (2001).
26. C. F. Stevens, *Neuron* **20**, 1 (1998).
27. W. A. Carlezon Jr. *et al.*, *Science* **277**, 812 (1997).
28. A. Bahi, F. Boyer, T. Kafri, J. L. Dreyer, *Eur. J. Neurosci.* **19**, 1621 (2004).
29. Z. Dong *et al.*, *Proc. Natl. Acad. Sci. U.S.A.* **100**, 12438 (2003).
30. J. R. Goss *et al.*, *Methods Mol. Biol.* **246**, 309 (2004).
31. V. M. Sandler *et al.*, *J. Neurosci. Methods* **121**, 211 (2002).
32. R. L. Neve, A. I. Geller, *Adv. Neurol.* **79**, 1027 (1999).
33. S. A. Josselyn *et al.*, *J. Neurosci.* **21**, 2404 (2001).
34. E. S. Faber, R. J. Callister, P. Sah, *J. Neurophysiol.* **85**, 714 (2001).
35. J. Boulter *et al.*, *Science* **249**, 1033 (1990).
36. R. Malinow, R. C. Malenka, *Annu. Rev. Neurosci.* **25**, 103 (2002).
37. A. J. Watt, P. J. Sjostrom, M. Hausser, S. B. Nelson, G. G. Turrigiano, *Nature Neurosci.* **7**, 518 (2004).
38. S. Shi, Y. Hayashi, J. A. Esteban, R. Malinow, *Cell* **105**, 331 (2001).
39. T. Takahashi, K. Svoboda, R. Malinow, *Science* **299**, 1585 (2003).
40. K. A. Goosens, S. Maren, *Learn. Mem.* **8**, 148 (2001).
41. C. B. Sananes, M. Davis, *Behav. Neurosci.* **106**, 72 (1992).
42. P. S. Bellgowan, F. J. Helmstetter, *Behav. Neurosci.* **110**, 727 (1996).
43. P. Andersen, S. H. Sundberg, O. Sveen, H. Wigstrom, *Nature* **266**, 736 (1977).
44. S. Maren, *Eur. J. Neurosci.* **12**, 4047 (2000).
45. M. A. Good, A. Johnson, D. Bannerman, N. Rawlins, R. Sprengel, paper presented at the Annual Meeting of the Society for Neuroscience, San Diego, 23 to 27 October 2004.
46. H. K. Lee *et al.*, *Cell* **112**, 631 (2003).
47. J. A. Esteban *et al.*, *Nature Neurosci.* **6**, 136 (2003).
48. D. Marr, *Philos. Trans. R. Soc. London B Biol. Sci.* **262**, 23 (1971).
49. P. Andersen, M. Trommald, *J. Neurobiol.* **26**, 396 (1995).
50. M. B. Moser, E. I. Moser, *J. Neurosci.* **18**, 7535 (1998).
51. M. B. Moser, E. I. Moser, E. Forrest, P. Andersen, R. G. Morris, *Proc. Natl. Acad. Sci. U.S.A.* **92**, 9697 (1995).
52. D. A. Snowdon, *Ann. Intern. Med.* **139**, 450 (2003).

53. This project was supported by DFG Ru 900/2-1 (S.R.), NIH (J.L., A.Z., R.M.), Mathers Charitable Foundation and Sloane Foundation (A.Z.), and Ale Davis and Maxine Harrison Foundation (R.M.). We thank G. Di Cristo for help with confocal microscopy; R. Neve for help and materials for viral expression system; N. Dawkins-Pisany for technical assistance; R. Tsien, G. Buzsaki, J. Hopfield, and Z. Mainen for comments on an earlier version of this manuscript; and M. Moita for helpful discussions.

Supporting Online Material

www.sciencemag.org/cgi/content/full/1103944/DC1
Materials and Methods
Figs. S1 and S2
Reference and Notes

8 November 2004; accepted 8 February 2005
Published online 3 March 2005;
10.1126/science.1103944
Include this information when citing this paper.

REPORTS

Spin-Charge Separation and Localization in One Dimension

O. M. Auslaender,[1]* H. Steinberg,[1] A. Yacoby,[1]† Y. Tserkovnyak,[2] B. I. Halperin,[2] K. W. Baldwin,[3] L. N. Pfeiffer,[3] K. W. West[3]

We report on measurements of quantum many-body modes in ballistic wires and their dependence on Coulomb interactions, obtained by tunneling between two parallel wires in an GaAs/AlGaAs heterostructure while varying electron density. We observed two spin modes and one charge mode of the coupled wires and mapped the dispersion velocities of the modes down to a critical density, at which spontaneous localization was observed. Theoretical calculations of the charge velocity agree well with the data, although they also predict an additional charge mode that was not observed. The measured spin velocity was smaller than theoretically predicted.

Coulomb interactions have a profound effect on the behavior of electrons. The low-energy properties of interacting electronic systems are described by elementary excitations, which interact with each other only weakly. In two- and three-dimensional disordered metals, they are dubbed quasiparticles (*1*), as they bear a strong resemblance to free electrons (*2*), which are fermions carrying both charge and spin. However, the elementary excitations in one-dimensional (1D) metals, known as Luttinger liquids (*3*, *4*), are utterly different. Each is collective and highly correlated and carries either spin or charge.

We determined the dispersions of the elementary excitations in one dimension by measuring the tunneling current, I_T, across an

[1]Department of Condensed Matter Physics, Weizmann Institute of Science, Rehovot 76100, Israel. [2]Lyman Laboratory of Physics, Harvard University, Cambridge, MA 02138, USA. [3]Bell Labs, Lucent Technologies, 700 Mountain Avenue, Murray Hill, NJ 07974, USA.

*Present address: Geballe Laboratory for Advanced Materials, Stanford University, Stanford, CA 94305, USA.
†To whom correspondence should be addressed. E-mail: amir.yacoby@weizmann.ac.il

extended junction between two long, ballistic, parallel wires in a GaAs/AlGaAs heterostructure created by cleaved edge overgrowth (CEO) (*5*). In this geometry, tunneling conserves both energy and momentum. Each tunneling event creates an electron-hole pair with total momentum $\hbar k = eBd \equiv \hbar q_B$ and total energy $E = |eV_{SD}|$, where $2\pi\hbar$ is Plank's constant, $-e$ is the electron charge, B is the magnetic field applied perpendicular to the plane of the wires, d is the distance between their centers, and V_{SD} is the voltage bias between them (supporting online text).

The rate of tunneling between the wires depends on the ease of adding an electron to one wire and a hole to the other, determined by the electron-hole spectral function, $A_{k,E}$. For weak interwire interactions, $A_{k,E}$ is a convolution of the individual particle spectral functions, which encode the overlap of electrons (or holes) with the many-body modes of the coupled wires. Near $V_{SD} = 0$, in the limit of temperature $T \to 0$, tunneling is appreciable only if $|q_B| = |k_{FU} \pm k_{FL}|$, allowing exchange of electrons between the Fermi points $k_{Fi} = \pi n_i/2$, where n_i is electron density in sub-band i and i = U or L stands for sub-bands in the upper or lower wires. At finite energies, interactions broaden the peaks of the individual particle spectral functions, in particular giving them a distribution of momenta. In spite of this, at $E = 0$, $A_{k,E}$ is sharply peaked at $k = |k_{FU} \pm k_{FL}|$ for homogeneous wires (*6*). Thus, as long as momentum is conserved in the wires and in the tunnel junction, tunneling near $V_{SD} = 0$ is enhanced at the same $B \geq 0$ values as without interactions

$$B_{\pm} = \frac{\hbar}{ed}|k_{FU} \pm k_{FL}| \qquad (1)$$

For inhomogeneous wires, the $V_{SD} = 0$ line shape of the spectral function encodes information on the low-energy momentum distribution of the many-body states (*7*).

Interactions become more important as the energy associated with them increases relative to kinetic energy. To increase this ratio, we reduced electron density in the wires by applying negative voltage, V_G, to a 2-μm top gate lying on the surface of the device. Figure 1A shows a typical low-energy measurement of $\partial I_T/\partial V_G$, as a function of V_G and B (supporting online text). The derivative was measured in order to be sensitive only to the signal from the section of the device where density was controlled by the gate. This was done by adding a small ac component to V_G. A zero-bias anomaly (*5*, *7*) was avoided by setting V_{SD} = 100 μV. This measurement, as well as all those reported here, was performed at 0.25 K.

Figure 1B shows the typical behavior of $B_{\pm}$. At high values of V_G, tunneling was appreciable only in a narrow range around $B_{\pm}$. As a function of V_G, $B_{\pm}$ evolved continuously, following the behavior of k_{FU} and k_{FL}, which allowed us to invert Eq. 1 and extract the density in each sub-band (Fig. 1C) (*5*) (supporting online text). In practice, each wire contained several sub-bands for most of the V_G range. Tunneling was observed only between sub-bands with the same number of nodes (e.g., between sub-band 1 in the upper wire and sub-band 1 in the lower wire or between 2 in the upper wire and 2 in the lower wire). Tunneling within each pair of sub-bands, one sub-band in each wire, gave rise to a similar set of features.

The dispersions of the modes can be determined for every density in the regime where we observed the $B_{\pm}$ peaks. The dispersions are traced by the singularities of $A_{k,E}$ at finite energy and momentum (Fig. 2, A and B). For noninteracting electrons (Fig. 2A), the curves resulting from tunneling either from or to a Fermi point produce four curves: two shifted copies of the dispersion in each of the two wires (*5*).

Finite interactions split the singularities of $A_{k,E}$ (Fig. 2B) because of two effects. The first is spin-charge separation, caused by intrawire interactions, which creates two modes for each noninteracting mode. The second effect is mode mixing, caused by interwire interactions. Generally, the mixed modes are carried by both wires, giving rise to four independent velocities (supporting online text). This results in three identical copies of each of the four dispersions. At the limit of weak tunneling, the spin modes do not couple, and as a result each dispersion branch in Fig. 2A splits into a spin mode and two coupled charge modes, creating four curves near $|q_B| = |k_{FU} - k_{FL}|$ and two sets of three curves near $|q_B| = |k_{FU} + k_{FL}|$ (Fig. 2B).

The tunneling current, $I_T(V_{SD},B)$, is proportional to $A_{k,E}$, the singularities of which are peaks for the parameters of our experiment (*6*). During a scan of V_{SD} and B, $I_T(V_{SD},B)$ changes abruptly with a change in the number of modes that can be excited with the available energy and momentum, where $A_{k,E}$ is peaked. The curve along which this happens gives the dispersion of a mode, $E(k)$. In particular, the slope at $V_{SD} = 0$ gives the dispersion velocity, $v = \hbar^{-1}\partial E/\partial k$. For the experimentally relevant case of weak tunneling, we expected ten such

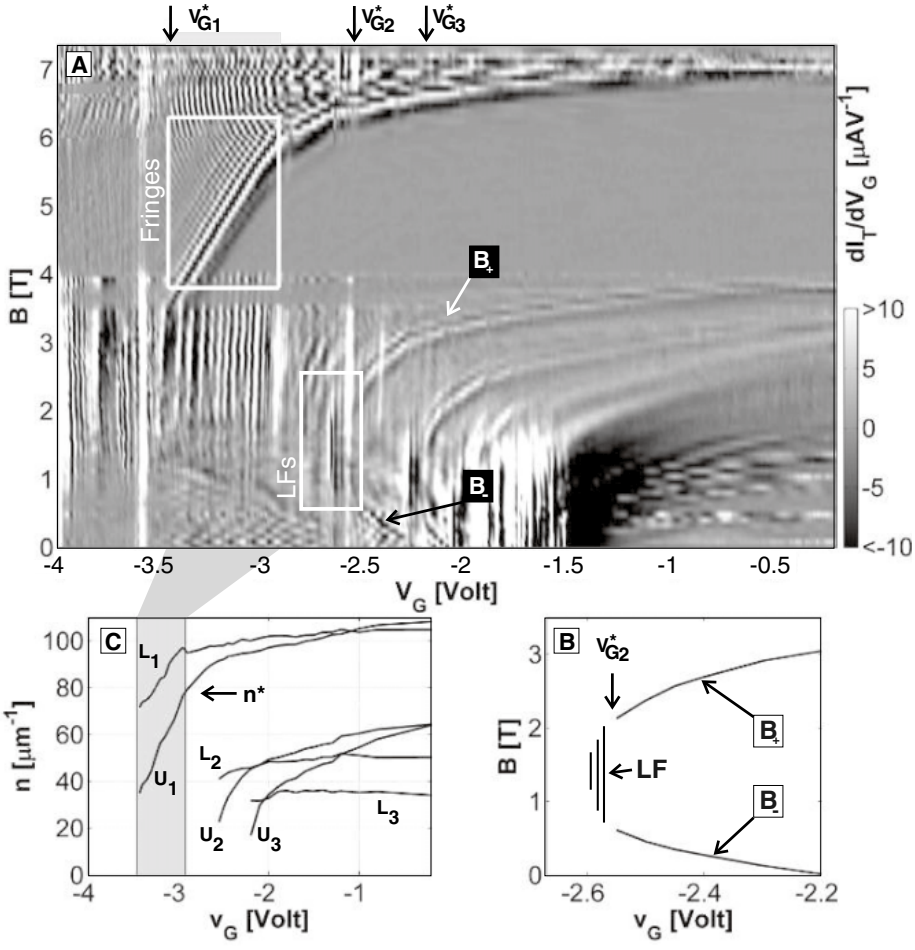

Fig. 1. (**A**) Gray-scale plot of $\partial I_T(V_G,B)/\partial V_G$. Onset of LFs for $V_G < V^*_{Gi}$ are marked by arrows; Fringes are finite-size fringes. (**B**) Zoom on the trace of $B_{\pm}$ for sub-band 2. At V^*_{G2}, $B_{\pm}$ are replaced by LFs, drawn schematically. (**C**) Dependence of density in sub-bands 1 to 3 on V_G. U_i and L_i represent the upper- and lower-wire sub-band i. The gray box marks the regime with a single occupied sub-band in each wire ($-3.45\ V < V_G < -2.90$ V), which starts below upper-wire density n^*.

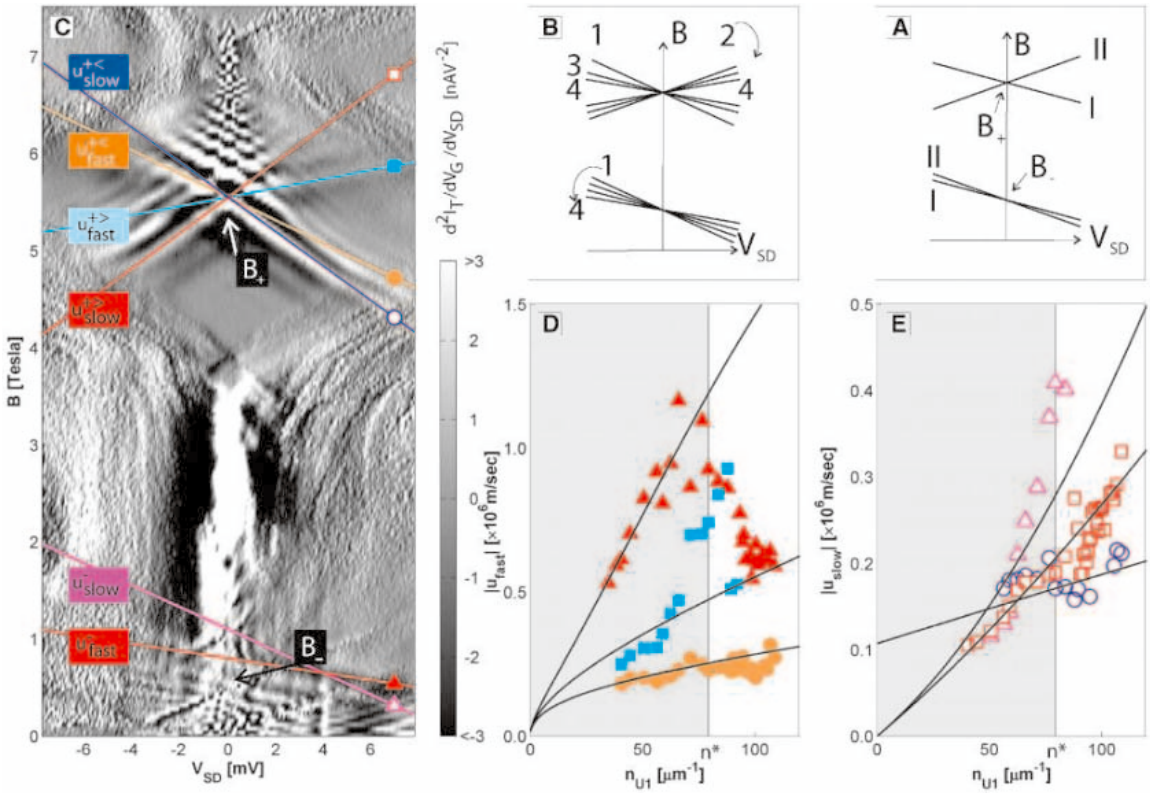

Fig. 2. (**A** and **B**) Illustration of the position of the singularities of $A_{k,E}$, with eV_{SD} replacing E and B replacing k. (**A**) For noninteracting electrons, there are four curves. *I*, copies of lower wire dispersion; *II*, copies of upper wire dispersion. (**B**) With interactions, there are 10 curves: three duplicates of each mixed charge mode (marked 3 and 4) and two copies of each spin mode (marked 1 and 2). (**C**) Numerical derivative, with respect to B, of the measured $\partial I_T(V_{SD},B)/\partial V_G$ at $V_G = -3.00$ V. Finite-size fringes appear for $B > B_+$ and $B < B_-$. All extracted slopes are marked and offset for clarity. Triangles represent slopes extracted near B_-, giving $|u^-_{fast}|$ (filled) > $|u^-_{slow}|$ (empty); squares represent positive slopes near B_+, giving $u^{+>}_{fast}$ (filled) > $u^{+>}_{slow}$ (empty); circles represent negative slopes near B_+, giving $|u^{+<}_{fast}|$ (filled) > $|u^{+<}_{slow}|$ (empty). (**D** and **E**) Apparent velocities, u, versus density, n_{U1}. Each wire has a single occupied sub-band in the shaded region. (**D**) Dependence of u values calculated for small slopes on density. Overlayed curves were calculated by setting v in Eq. 2 to v_{c-} from Eq. 4 and solving for $u^{\pm}$. (**E**) Dependence of u values calculated for large slopes on density. Overlayed curves were calculated by setting $v_{sU,L} = v_{FU,L}/1.25$ in Eq. 2.

intercepts (Fig. 2B) but only four different magnitudes of slope.

To determine the dependence of the dispersions on density, we measured $\partial I_T(V_{SD},B)/\partial V_G$ for different values of V_G, ranging from 0 V to −3.45 V. A typical result from the regime where each wire had a single sub-band, $-3.45 < V_G < -2.9$ V, is shown in Fig. 2C. The peaks that appeared in Fig. 1A at $B_\pm$ split and move with a slope that gives an apparent velocity $u = d^{-1}(\partial B/\partial V_{SD})^{-1}_{V_{SD}=0}$. Accompanying these peaks are finite-size fringes (*8*).

Six slopes appear in Fig. 2C, two near B_- and four near B_+. Both B_- slopes are negative, giving $|u^-_{slow}| < |u^-_{fast}|$. Near B_+ there are two negative slopes, giving $|u^{+<}_{slow}| < |u^{+<}_{fast}|$, and two positive slopes, giving $|u^{+>}_{slow}| < |u^{+>}_{fast}|$. For each scan, we extracted all discernable slopes. The results are summarized in Fig. 2, D and E, where they are plotted versus the density of electrons in the first sub-band of the upper wire, n_{U1}. In the shaded area, which extends up to $n^* \approx 80\ \mu m^{-1}$, as extracted from Fig. 1A, only one sub-band is occupied per wire.

The unexpected presence of six different branches of u in Fig. 2, D and E, wrongly suggests that the coupled wires have more than four independent modes. The error lies in assuming that the band-filling induced by a finite V_{SD} is negligible (*9*). In reality, V_{SD} induces charge transfer between the wires, which is controlled by the mutual capacitance, endowing k_{FU} and k_{FL} with a V_{SD} dependence. Thus, the actual excitation velocity is given by

$$v = \frac{|u^{\pm}|}{1 \pm \gamma_{\pm} u^{\pm}} \qquad (2)$$

where ± refers to the crossing point, $B_\pm$, near which $u^\pm$ is extracted. The value of $\gamma_\pm$ depends on the capacitance matrix of the wires and was calculated with a simple model (supporting online text). The model consisted of two wires of radius r, separated from each other by a distance $d \gg r$ and from a nearby gate by a distance $D_G/2 \gg d$. Because we applied V_{SD} to the upper wire, keeping the lower wire grounded, the energetic cost of adding charge to the wires is given to quadratic order in excess electron density, δn_i, by $\Sigma_i(E_{Fi}\delta n_i + e^2 c_i^{-1}\delta n_i^2) + \frac{1}{2}\Sigma_{i,j} e^2 \delta n_i c_{ij}^{-1} \delta n_j - e\delta n_U V_{SD}$, where i,j run over wire indices U and L; $E_{Fi} = \hbar^2 k_{Fi}^2/(2m)$ is the Fermi energy, $c_i^{-1} = \pi\hbar/(2e^2 v_{Fi})$; m is the band mass of electrons; $v_{Fi} = \hbar k_{Fi}/m$ is the Fermi velocity in wire i; and c_{ij}^{-1} are elements of the inverse capacitance matrix. In the random phase approximation (*1*), the first term in this expression is kinetic energy, and the second is Coulomb interaction energy. By assumption, the inverse capacitance of each wire to the gate (c_{UU}^{-1} and c_{LL}^{-1}) is identical: $c_G^{-1} = (2\pi\varepsilon)^{-1} \log[D_G/r]$. The inverse capacitance between the wires $c_{UL}^{-1} = c_{LU}^{-1}$ is $c_M^{-1} = (4\pi\varepsilon)^{-1} \log[1 + (D_G/d)^2]$. Here $r = 10$ nm and $d = 30$ nm. $D_G = 70$ nm is the distance of the wires to a parallel layer of dopants. Using $D_G = 500$ nm, the distance to the top gate, has only minor influence because of the log. The dimensions are roughly the molecular beam epitaxy growth parameters of the heterostructure and were not adjusted. The result of applying Eq. 2 is presented in Fig. 3. Clearly, the model is successful when each wire has only one occupied sub-band: All three fast branches collapse on a single curve for $n_{U1} < n^*$, and all slow branches collapse on two curves (supporting online text).

The same model for interactions that corrects for band-filling allows identifying the branches in Fig. 3. For this, we turn to the Hamiltonian of the coupled wires, which consists of a free electron part and an interacting part. Taking a long length approximation and bosonizing (*10*), we get

$$H = \sum_{i=1}^{N} \sum_{s=\uparrow\downarrow} \int_0^\infty dx \left[\frac{p_{is}^2(x)}{2mn_{is}} + \frac{m}{2} n_{is} v_{Fis}^2 q_{is}'^2(x) \right] + \sum_{i,j=1}^{N} \frac{e^2 c_{ij}^{-1}}{2} \sum_{s,s'=\uparrow\downarrow} n_{is} n_{js'} \int_0^\infty dx q_{is}'(x) q_{js'}'(x) \qquad (3)$$

The sums run over all N occupied sub-bands and over both spin orientations. The density

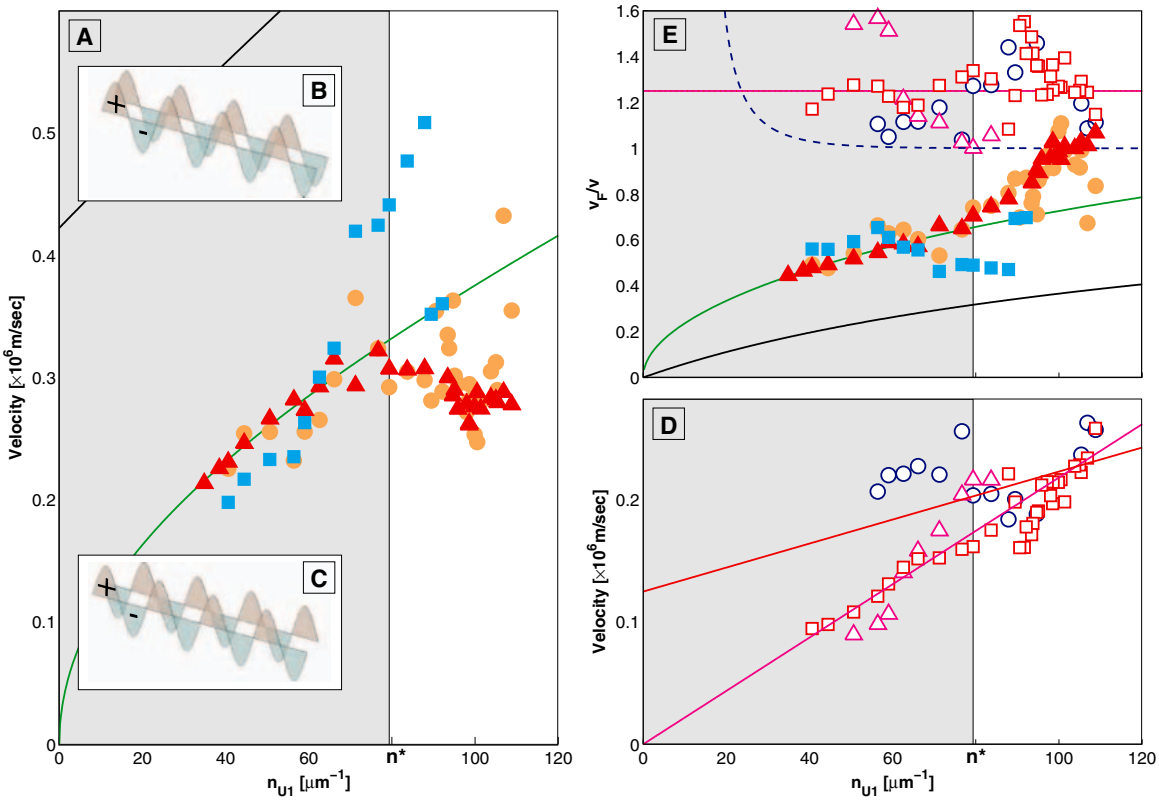

Fig. 3. Excitation velocity versus density. (**A**) Velocities obtained from Fig. 2D. Curves are the charge velocities v_{c-} (green) and v_{c+} (black) (Eq. 4). (**B** and **C**) Illustration of the symmetric/antisymmetric coupled-wire mode (+, excess positive charge; −, excess negative charge). (**D**) Velocities obtained from Fig. 2E. The lines are $v_{sU} = v_{FU}/1.25$ (magenta) and $v_{sL} = v_{FL}/1.25$ (red). The scale is the same as in (A). (**E**) Plot of v_F/v for the velocities in (A) and (D). v_F was calculated from n_{U1} in all cases except for $v_F/v_{slow}^{+<}$ and v_F/v_{sL}. In the latter two cases, v_F was calculated from the density in the first sub-band in the lower wire. The red and magenta curves from (D) overlap here.

of spin orientation s in sub-band i is $n_{is} = n_i/2$, q'_{is} is the gradient of the displacement operator, and p_{is} is the conjugate momentum.

Within this model, which neglects back-scattering, the velocities of the coupled-wire modes are found by diagonalizing Eq. 3 with a canonical transformation. This yields spin velocities equal to the Fermi velocities. For a single mode in each wire, $N = 2$, the two charge velocities are (*10*)

$$v_{c\pm}^2 = \frac{v_{cU}^2 + v_{cL}^2}{2} \pm \left[\left(\frac{v_{cU}^2 - v_{cL}^2}{2} \right)^2 + v_{FU} v_{FL} \left(\frac{2e^2}{\pi\hbar} c_M^{-1} \right)^2 \right]^{1/2} \quad (4)$$

Here v_{ci} is the charge velocity in each individual wire (*11*): $v_{ci}/v_{Fi} = \sqrt{1 + U_i/(2E_{Fi})}$, where $U_i = e^2 n_i / c_G$ is the interaction energy. Physically ± corresponds to symmetric or antisymmetric excitations (Fig. 3, B and C). When the wires are identical, both modes are carried equally by both wires, but when the densities differ, as in the experiment, the symmetric mode is carried primarily by the more occupied wire, the lower wire, whereas the antisymmetric mode is carried primarily by the upper wire.

We have overlaid the result of Eq. 4 on the corrected velocities in Fig. 3, A and E. The fast velocities follow the calculated v_{c-} closely for $n_{U1} < n,*$ attesting to the validity of the model and leading us to associate them with the antisymmetric charge mode. The faster v_{c+}, on the other hand, is completely absent from the data. This is to be expected near B_-, where tunneling creates interacting electron-hole pairs that propagate together, excitations that are almost completely antisymmetric. On the other hand, near B_+ none of the excitation branches should be suppressed, as they are all excited by tunneling, leaving the issue of the complete absence of the symmetric mode unresolved.

Turning to the slow branches in Fig. 3, D and E, we find linear dependence on the bare Fermi velocities, $v_{si} = v_{Fi}/f_i$, where $f_U = f_L = 1.25$. The linearity and the fact that $f_i > 1$, suggest that these modes are the spin modes. Theoretically, one expects a spin velocity equal to v_F as long as back-scattering is weak, whereas stronger back-scattering reduces it below v_F (*12*–*17*). For example, one group (*14*, *15*), using Monte Carlo simulations, found that the expression $f_{pert} = 1/\sqrt{1 - V_{2k_F}/(\pi\hbar v_F)}$ (supporting online text) gives an upper bound to the ratio between the v_F and v_S. However, a plot of f_{pert}

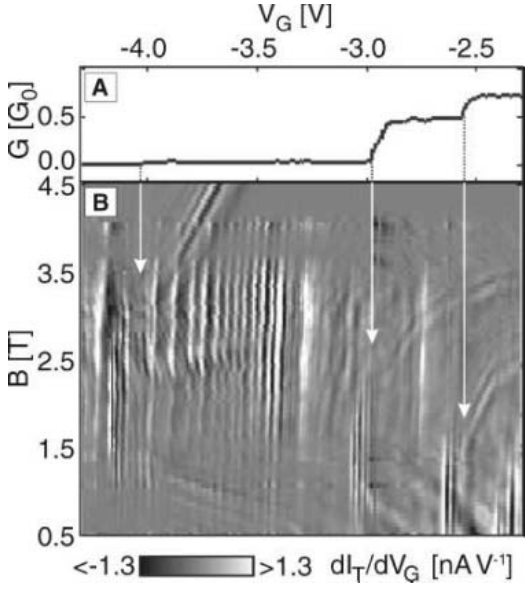

Fig. 4. (**A**) Two-terminal conductance of the upper wire as a function of V_G, measured by applying a dc voltage bias of 100 μV along the wire. The step height deviates from the universal $2e^2/h$ because of the indirect upper wire contact (*27*, *28*). This measurement depends very weakly on B, which is 1.3 T here. (**B**) Simultaneous measurement $\partial I_T(V_G,B)/\partial V_G$, showing that localization is concurrent with the conductance drops.

in Fig. 3E shows that f_{pert} does not account for the deviation of f_i from unity.

Further examination of Fig. 1A down to the depletion of each sub-band in the upper wire reveals that the continuous evolution of each set of $B_{\pm}$ peaks is replaced by a series of vertical streaks, dubbed localization features (LFs). These occur in a small range of V_G below $V^*_{Gi} = -3.45$, -2.55, and -2.20 V, for each of the three upper-wire sub-bands we observed. Each set of LFs signals an abrupt change in the momentum-space content of the wave function in the depleting sub-band.

Above V^*_{Gi}, finite-size fringes for $B < B_-$ and $B > B_+$ accompany the $B_{\pm}$ peaks, signifying that the states in both wires contain only wave numbers higher than the Fermi wave number and implying that they are extended (*8*). The location of the fringes at $B < B_-$ and $B > B_+$ indicates that the potential along the nonuniform upper wire has a hump, with a typical length given by the period $h/(e\Delta B_{fringe}d) \approx 0.75$ μm, consistent with the barrier the surface gate induces.

Below V^*_{Gi}, we find that each LF fills a broad range in B, lying roughly between the extrapolations of $B_{\pm}$. This implies that the wave function of the state along the upper wire is localized. We are thus led to conclude that the B streaks signify a qualitative change in the self-consistent potential at V^*_{Gi}, which marks a transition between an extended state and a localized state. The localized states appear while the more occupied sub-bands are still fully conducting, in contrast to a recent study of inhomogeneous wires (*18*).

The localization transition affects transport along the upper wire. Figure 4A shows the two-terminal conductance along this wire, $G(V_G,B)$, which is quantized. The stepwise decrease of $G(V_G,B)$ with density is a hallmark of ballistic transport in a wire (*19*). We were able to measure $G(V_G,B)$ simultaneously with $\partial I_T(V_G,B)/\partial V_G$, by recording both the dc current along the upper wire and the ac component of the tunneling current (supporting online text). The positions of the steps in $G(V_G,B)$, which have a very weak dependence on B, are concurrent with the localization transitions apparent in Fig. 4B. We thus conclude that electrons in a sub-band cease to conduct because of localization while their density is still finite.

The localization transition hints that bound states come into existence over the barrier induced by the top gate, which we used to vary the density. The possibility of this occurring has been addressed in the context of the 0.7-anomaly in point contacts (*20–23*). Using a variety of theoretical tools, it was found that, when the density is low enough, a bound state may exist over the barrier (*16*, *24–26*). Our measurements show clear evidence for this scenario in long 1D channels. Finally, 0.7-anomaly-like features are observed regularly in the conductance steps of CEO wires similar to ours (*23*). Further work is needed to show a direct link between the 0.7-anomaly and the observed localization features.

References and Notes

1. P. Nozières, D. Pines, *The Theory of Quantum Liquids* (Perseus, Cambridge, MA, 1999), ed 3.
2. B. L. Altshuler, A. G. Aronov, *Electron-Electron Interaction in Disordered Systems*, A. L. Efros, M. Pollak, eds. (North-Holland, Amsterdam, 1985), pp. 1–153.
3. S.-I. Tomonaga, *Prog. Theor. Phys.* **5**, 544 (1950).
4. J. M. Luttinger, *J. Math. Phys.* **4**, 1154 (1963).
5. O. M. Auslaender *et al.*, *Science* **295**, 825 (2002).
6. D. Carpentier, C. Peça, L. Balents, *Phys. Rev. B* **66**, 153304 (2002).
7. Y. Tserkovnyak, B. I. Halperin, O. M. Auslaender, A. Yacoby, *Phys. Rev. B* **68**, 125312 (2003).
8. Y. Tserkovnyak, B. I. Halperin, O. M. Auslaender, A. Yacoby, *Phys. Rev. Lett.* **89**, 136805 (2002).
9. D. Boese, M. Governale, A. Rosch, U. Zülicke, *Phys. Rev. B* **64**, 085315 (2001).
10. K. A. Matveev, L. I. Glazman, *Phys. Rev. Lett.* **70**, 990 (1993).
11. C. L. Kane, M. P. A. Fisher, *Phys. Rev. B* **46**, 15233 (1992).
12. C. F. Coll, *Phys. Rev. B* **9**, 2150 (1974).
13. H. J. Schulz, *Phys. Rev. Lett.* **71**, 1864 (1993).
14. C. E. Creffield, W. Häusler, A. H. MacDonald, *Europhys. Lett.* **53**, 221 (2001).
15. W. Häusler, L. Kecke, A. H. MacDonald, *Phys. Rev. B* **65**, 085104 (2002).
16. K. A. Matveev, *Phys. Rev. Lett.* **92**, 106801 (2004).
17. V. V. Cheianov, M. B. Zvonarev, *Phys. Rev. Lett.* **92**, 176401 (2004).
18. K. J. Thomas *et al.*, *J. Phys. Condens. Matter* **16**, L279 (2004).
19. C. W. J. Beenakker, H. van Houten, in *Solid State Physics*, H. Ehrenreich, D. Turnbull, eds. (Academic Press, San Diego, CA, 1991), vol. 44, pp. 1–228.
20. K. J. Thomas *et al.*, *Phys. Rev. Lett.* **77**, 135 (1996).
21. S. M. Cronenwett *et al.*, *Phys. Rev. Lett.* **88**, 226805 (2002).
22. D. J. Reilly *et al.*, *Phys. Rev. Lett.* **89**, 246801 (2002).
23. R. de Picciotto, L. N. Pfeiffer, K. W. Baldwin, K. W. West, *Phys. Rev. Lett.* **92**, 036805 (2004).
24. Y. Meir, K. Hirose, N. S. Wingreen, *Phys. Rev. Lett.* **89**, 196802 (2002).
25. K. Hirose, Y. Meir, N. S. Wingreen, *Phys. Rev. Lett.* **90**, 026804 (2003).
26. O. P. Sushkov, *Phys. Rev. B* **67**, 195318 (2003).
27. A. Yacoby *et al.*, *Phys. Rev. Lett.* **77**, 4612 (1996).
28. R. de Picciotto, H. L. Stormer, L. N. Pfeiffer, K. W. Baldwin, K. W. West, *Nature* **411**, 51 (2001).

29. We thank G. Fiete, Y. Oreg, and J. Qian for discussions. Supported in part by the U.S.-Israel Binational Science Foundation, European Commission Research Training Network contract no. HPRN-CT-2000-00125, and NSF grant no. DMR 02-33773. Y.T. is supported by the Harvard Society of Fellows.

Supporting Online Material

www.sciencemag.org/cgi/content/full/308/5718/88/DC1
SOM Text
Fig. S1
References and Notes

23 November 2004; accepted 22 February 2005
10.1126/science.1107821

Simultaneous Tomography and Diffraction Analysis of Creep Damage

A. Pyzalla,[1]* B. Camin,[2] T. Buslaps,[3] M. Di Michiel,[3] H. Kaminski,[1] A. Kottar,[1] A. Pernack,[2] W. Reimers[2]

Creep damage by void nucleation and growth limits the lifetime of components subjected to loading at high temperatures. We report a combined tomography and diffraction experiment using high-energy synchrotron radiation that permitted us to follow in situ void growth and microstructure development in bulk samples. The results reveal that void growth versus time follows an exponential growth law. The formation of large void volumes coincides with texture evolution and dislocation density, reaching a steady state. Creep damage during a large proportion of sample creep life is homogeneous before damage localization occurs, which leads to rapid failure. The in situ determination of void evolution in bulk samples should allow for the assessment of creep damage in metallic materials and subsequently for lifetime predictions about samples and components that are subject to high-temperature loading.

The efficiency of electricity-generating plants and gas turbines depends strongly on their components' sustainability of loading at high temperatures. The service lifetime of these components in most cases is controlled by creep-induced cavity growth. In order to quantify the remnant lifetime of creep-loaded components, models have been proposed that have their basis in parameters characterizing microstructure damage (*1–4*). Microscopic methods have been used to determine, for example, the fraction of grain boundaries damaged by cavities. Creep damage has thus only been determined from two-dimensional images. Because microscopy also necessitates

[1]Technische Universität (TU) Wien, Institute of Material Science and Technology, Karlsplatz 13-308, A-1040 Wien, Austria. [2]TU Berlin, Institute of Material Science and Technology, Sekr. BH18, Ernst-Reuter-Platz 1, D-10587 Berlin, Germany. [3]European Synchrotron Radiation Facility (ESRF), BP220, F-38043 Grenoble, France.

*To whom correspondence should be addressed. E-mail: anke.pyzalla@tuwien.ac.ot

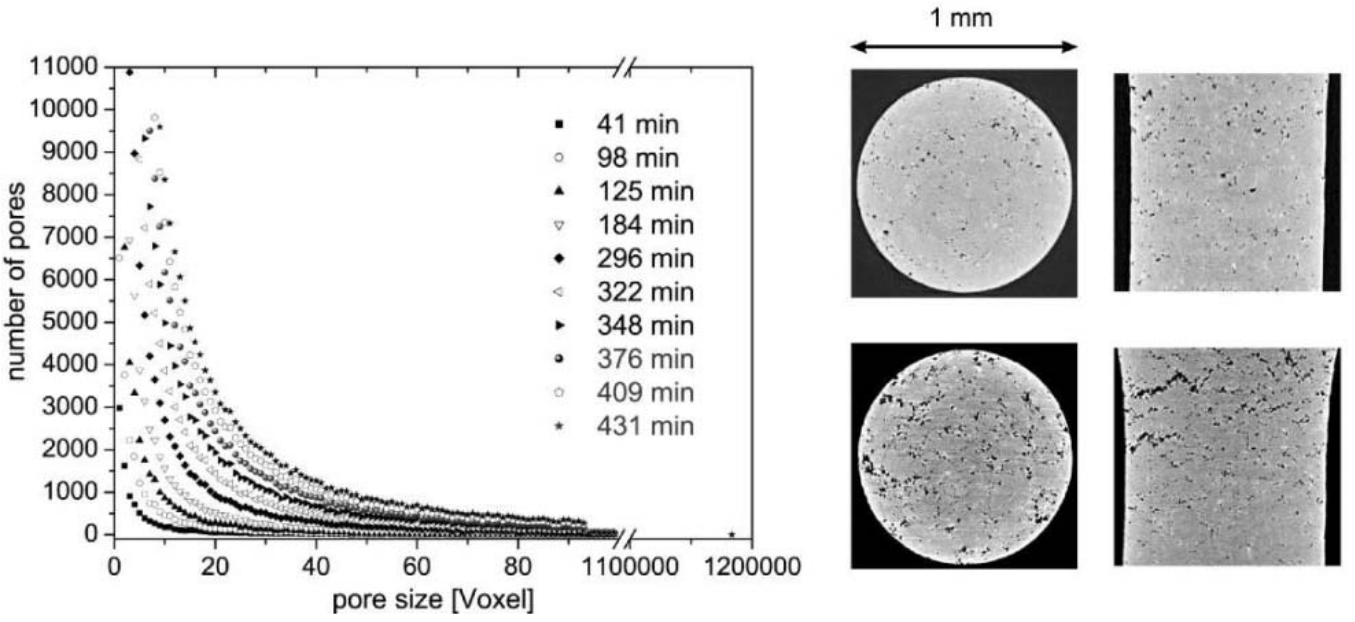

Fig. 1. (**Left**) Development of number and size of voids during the creep process. (**Right**) Slice of the sample after 348 min creep (top) and 431 min creep (bottom). One voxel is about 4 μm³.

cutting the sample, only a snapshot of the damage evolution was available. Synchrotron x-ray tomography provides data of damage in the bulk, which often substantially differs from damage at the surface (*5*), and it reveals the chronology of damage events and shows damage location in a defined volume.

X-ray microtomography has been restricted to imaging of samples in static conditions or those that evolve over very long time scales. This is because of the comparatively long data acquisition time, in the range of several tens of minutes or hours. Recently a fast-tomography technique has been developed at beamline ID15A at the European Synchrotron Radiation Facility (ESRF), Grenoble, France. It achieves an unprecedented speed by combining a high-efficiency phosphorus screen, a reflecting microscope objective, and a fast charge-coupled device (CCD) detector with the very intense high-energy white beam radiation provided by a wiggler source. The spatial resolution achieved is 2 μm (*6*, *7*).

Diffraction provides complementary information to tomography, e.g., about texture (orientation distribution of the crystallites), changes in domain size, dislocation density, and internal strains respectively internal stresses. Normally, x-ray diffraction is performed with use of monochromatic radiation where the intensity is recorded versus the diffraction angle 2θ. In an alternative experimental setup, white synchrotron radiation is used and the intensity is recorded versus energy, thus allowing a fast simultaneous recording of several reflections. High-energy synchrotron radiation, because of its large penetration depth, gives bulk information even for strongly absorbing samples (*8*). By using conventional tomography with a monochromatic beam, subsequent tomography and diffraction have been carried out on fiber-reinforced TiAl6V4 samples, which had been fatigue-tested beforehand (*9*).

However, combined and continuous tomography and diffraction experiments can provide a much deeper understanding of the microstructural changes during time-dependent processes (e.g., fatigue and creep), where it is important to characterize the dynamics in the early stages of the process. We studied the creep void evolution in brass and its correlation to texture and microstructure development, which are important parameters for understanding the lifetime of components subjected to high temperature loading. The experimental conditions were selected in such a way that the time scale of the creep process is much longer than the time required for collecting the microtomography data and the diffraction data.

We chose a common, easily machined brass alloy, $CuZn_{40}Pb_2$ [~58 weight % (wt. %) Cu, 40 wt. % Zn, and 2 wt. % Pb], which contains three phases: α-brass, β-brass, and Pb (*10*) (fig. S1). The α and β phase differ strongly in crystallographic structure, diffusivity, stacking fault energy, and atomic order (*11*). Pb shows a strong absorption contrast to both brass phases; thus, we could follow a certain location in the sample throughout the experiment. In order to provide the conditions for as realistic a creep experiment as possible during the limited beamtime available, we tensile deformed the sample (4.47% in total) before the creep experiment according to the results given in (*12*).

We developed a creep device in order to avoid artifacts during the tomography (*10*) (fig. S2). The path of the incoming and the emerging x-rays over a complete 360° turn of the sample is identical. The tensile load (25 MPa) was applied by using a spring in order to avoid vibrations. The sample was heated to 375°C ± 2°C by an induction-heated loop around the bottom of the sample. Because the camera has a restricted field of view of 1.6 mm by 1.6 mm and a spatial resolution of 2 μm (full width at half maximum, FWHM, of the point spread function), we had to miniaturize the samples to a diameter of 1 mm and an active length of 2 mm (1 mm was recorded by tomography).

The experiment was carried out on beamline ID15A at ESRF (*13*). The experimental setup consisted of three detection systems, which allowed us to sequentially perform tomography, energy-dispersive diffraction, and angle-dispersive diffraction without further alignment or calibration procedures during the experiment (*10*) (fig. S3). The gauge volume within the sample was defined by tungsten carbide slits. A Si-monochromator provided 80-keV radiation with 50 mm offset from the white beam. Several reflections of the α- and the β-brass were recorded. For the fast-tomography and the energy-dispersive diffraction, we used the white beam, which penetrated the monochromator crystal. In order to reduce coarse grains effects, the sample was rotated continuously. The tomograms were collected in about 3 min, which allowed us to study the dynamics of the creep process.

Data processing was performed in two steps: image preprocessing (*13*) and tomographic reconstruction. The tomographic reconstruction was performed by using a standard filtered back projection algorithm,

yielding a three-dimensional (3D) representation of the effective attenuation coefficient of the sample in terms of gray levels (*14*).

Volume elements of the 3D data sets (voxels) are identified as belonging to voids or alloy material with the use of an algorithm based on interactive data language (IDL) (*15*). This is done by applying an intensity threshold corresponding to 50% of the average gray level. Each voxel represents a volume of 1.6 μm by 1.6 μm by 1.6 μm. A void is defined by connected voxels that share a common face, edge, or corner. The number of voxels of each void is counted to obtain the void volume. Void volume histograms with a class width of one voxel are then calculated.

The results of the tomography experiment are summarized (Fig. 1); a corresponding macroscopic creep curve is shown in (*10*) (fig. S4). Initially after prestraining 4.47% at room temperature, the sample contains some small voids that are oriented in the longitudinal direction of the sample (*10*) (fig. S5). With increasing creep time, voids nucleate near the Pb and the number and the size of the voids increase (*10*) (movies S1 and S2). Tomographic reconstruction of sample slices and the corresponding void distributions show that after about 296 min void sizes strongly increase. In the slices, void chains are visible that form void networks preferentially oriented about 90° to the sample longitudinal axis, presumably along the phase boundaries between α- and β-brass (*11*). The increase in void size often is due to coagulation of voids within these void chains, and subsequently, microcracks become visible. Up to about 322 min, the voids are completely inside the sample. In the later tomograms, an increasing number of open voids become noticeable at the sample boundary. After 431 min, a large crack is visible, which leads to failure after 445 min (Fig. 2). The void volume versus creep time (Fig. 2) obeys an exponential growth law (quality of the fit $R^2 = 0.9969$):

$$y = y_0 + A\exp(t/B) \qquad (1)$$

with $y_0 = 0$, $A = 47 \times 10^3 \pm 7 \cdot \times 10^3$ voxel, $B = 5.4 \times 10^3 \pm 0.2 \times 10^3$ s.

With increasing creep time, the FWHMs of all reflections decrease (Fig. 2); however, more sophisticated profile reflection analysis is not possible because of the low resolution of the Ge detector. The decrease in FWHM indicates a decrease in dislocation density, which is strongest in the early stage of creep because of the 4.47% deformation of the sample before the creep test. In the final stage of the creep process after about 296 min, the reflection width appears to remain almost constant, which coincides roughly with the first formation of rather large voids.

An energy-dispersive diffraction pattern of the sample some minutes before failure is shown in Fig. 3. Although α and β-phase differ in their crystal structure, no significant phase-specific internal microstresses could be determined from peak shifts. The decrease in the integrated intensity values of the β_{420} and β_{422} reflections and the strong increase of the α_{440} reflections of the brass reveal texture formation during the creep process. Because under these experimental conditions the scattering vector is perpendicular to the longitudinal axis of the samples, the measured intensity changes versus time comply with the development of a <111>/<100>-fiber texture of the α-phase and a <110>-fiber texture of the β-phase in longitudinal direction of the sample. The <111>- or <111>/<100>-fiber texture in α-brass and the <110>-fiber texture in β-brass are the typical tensile deformation textures as well as the recrystallization textures of α- and β-brass (*16*). The large slope in the intensity of the α_{440} reflection coincides roughly with the time when large void formation starts (about 296 min). The texture formation presumably is caused by local load increase due to the strong decrease in supporting cross section when large voids are formed.

The reflection profiles of the angle-dispersive diffractograms recorded immediately after the

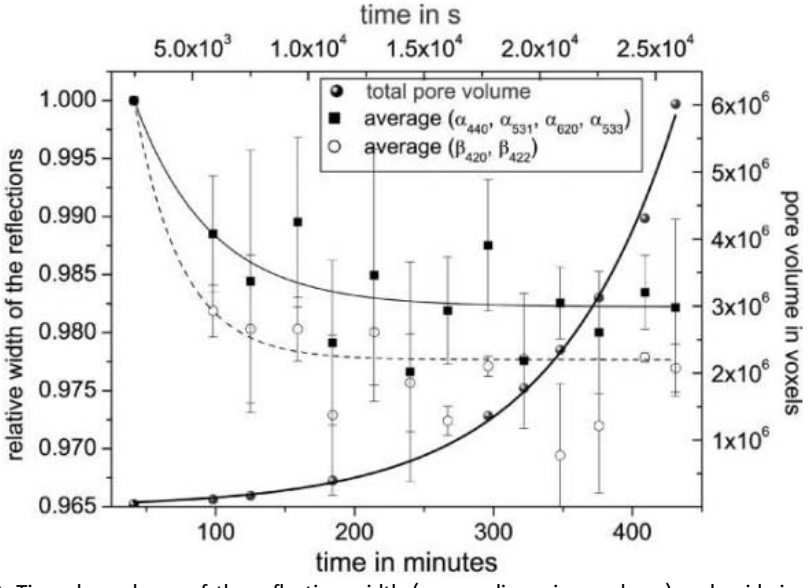

Fig. 2. Time dependence of the reflection width (energy dispersive analyses) and void size. One voxel is about 4 μm³. Error bars represent uncertainty of fit with Gaussian function.

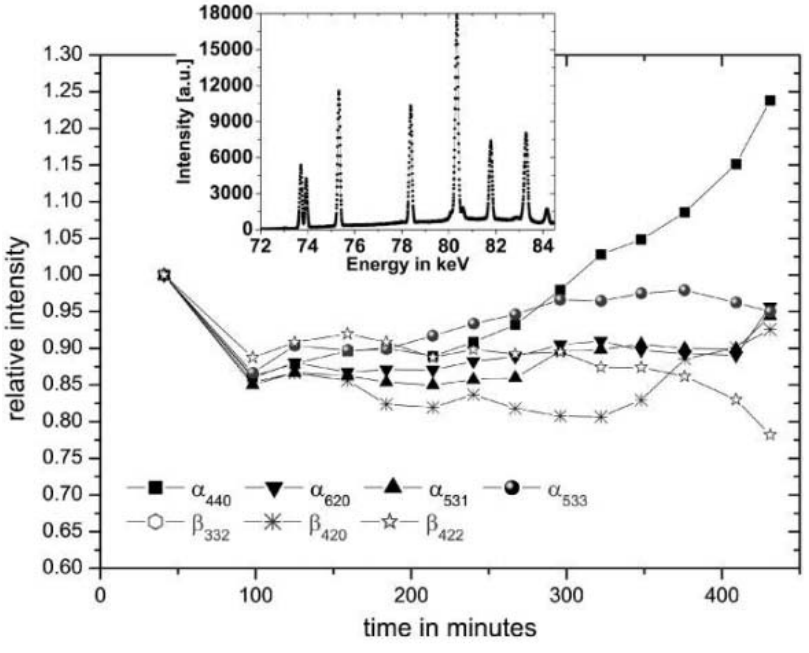

Fig. 3. Time dependence of the reflection intensities (energy dispersive analyses); scattering vector is perpendicular to the longitudinal axis of the sample. a. u., arbitrary units.

energy-dispersive measurement (the sample had to be translated 50 mm to reach the monochromatic beam) are not smooth (*10*) (fig. S6). Instead they reveal grain growth, which is stronger in the β-brass than in the α-brass.

The experiment revealed that void growth kinetics during creep could be studied in the bulk material in situ. The access to 3D bulk information further provided access to a quantitative determination of void size and void shape evolution during creep. This comprehensive 3D representation of creep damage in the sample confirms the proposition that the transition from homogeneous to localized creep damage occurs late in creep life (*4*, *17*). In the system studied, the increase of pore volume versus time obeys an exponential growth law. The evolution of large pores coincides with texture formation in α-brass.

Diffraction and tomography performed in one single experiment should also make it possible to observe changes in the stress field and plastic zone around growing cracks, load partitioning and deformation in reinforced cellular and porous materials, the delamination in fiber-reinforced materials, and the resulting changes in strain respectively stress partitioning between the fibers and the matrix.

References and Notes

1. H. Riedel, *Fracture at High Temperatures* (Springer-Verlag, Berlin, 1987).
2. L. M. Kachanov, *Izv. Akad. Nauk SSSR Otd. Tekh. Nauk* **8**, 27 (1958).
3. Y. N. Rabotnov, *Creep Problems in Structural Members* (North Holland, Amsterdam, 1969).
4. G. Eggeler, *Acta Metall. Mater.* **39**, 221 (1991).
5. J.-Y. Buffière, E. Maire, P. Cloetens, G. Lormand, R. Fougères, *Acta Mater.* **47**, 1613 (1999).
6. M. Di Michiel *et al.*, *Rev. Sci. Inst.*, in press.
7. O. Lame, D. Bellet, M. Di Michiel, D. Bouvard, *Nucl. Instrum. Methods Phys. Res. B* **200**, 287 (2003).
8. W. Reimers *et al.*, *J. Mater. Sci. Lett.* **19**, 581 (1999).
9. R. Sinclair *et al.*, *Acta Mater.* **52**, 1423 (2004).
10. Materials and methods are available as supporting material on *Science* Online.
11. K. Mäder, E. Hornbogen, *Scripta Metall.* **8**, 979 (1974).
12. M. R. Willis, J. P. Jones, *Scripta Mater.* **44**, 31 (2001).
13. Information about the ESRF ID15A high-energy scattering beamline can be found at www.esrf.fr/UsersAndScience/Experiments/MaterialsScience/ID15.
14. A. C. Kak, M. Slaney, *Principles of Computerized Tomographic Imaging* (IEEE Press, New York, 1988), p. 186.
15. *IDL Reference Guide, Version 5.4,* (Research System Incorporated, Boulder, CO, 2000).
16. J. Grewen, G. Wassermann, *Z. Metallkde.* **45**, 498 (1954).
17. G. Eggeler, J. C. Earthman, N. Nilsvang, B. Ilschner, *Acta Metall.* **37**, 49 (1989).

18. The authors are grateful to H. M. Mayer for the tensile deformation of the samples before the experiment and D. Fernandez-Carreiras from the ESRF for the imaging detector control system. We acknowledge the ESRF for beamtime on ID15A and financial support of travelling expenses. A.P. and W.R. acknowledge the Deutsche Forschungsgemeinschaft (DFG) for financial support of project Py9/1-2.

Supporting Online Material

www.sciencemag.org/cgi/content/full/308/5718/92/DC1
Materials and Methods
Figs. S1 to S6
Movies S1 and S2

26 October 2004; accepted 10 February 2005
10.1126/science.1106778

U-Pb Ages from the Neoproterozoic Doushantuo Formation, China

Daniel Condon,[1]* Maoyan Zhu,[2] Samuel Bowring,[1] Wei Wang,[2] Aihua Yang,[2] Yugan Jin[2]

U-Pb zircon dates from volcanic ash beds within the Doushantuo Formation (China) indicate that its deposition occurred between 635 and 551 million years ago. The base records termination of the global-scale Marinoan glaciation and is coeval with similar dated rocks from Namibia, indicating synchronous deglaciation. Carbon isotopic and sequence-stratigraphic data imply that the spectacular animal fossils of the Doushantuo Formation are for the most part younger than 580 million years old. The uppermost Doushantuo Formation contains a pronounced negative carbonate carbon isotopic excursion, which we interpret as a global event at circa 551 million years ago.

The Neoproterozoic Doushantuo Formation (South China), deposited after a global-scale glaciation, contains fossil embryos, algae, achritarchs, and small bilaterians that are purportedly the Earth's earliest animals. This formation also contains a chemostratigraphic record of environmental change during its deposition with distinct $\delta^{13}C$ anomalies occurring at its base and top. Here, we report previously undetermined U-Pb zircon ages for volcanic ash beds from the lower and uppermost Doushantuo Formation (Yangtze Gorges area, South China), each of which is associated with globally correlated negative $\delta^{13}C$ anomalies.

In its type area along the Yangtze Gorges, the Doushantuo Formation comprises a succession of carbonate, shale, and phosphatic shale that is about 100 m thick. It can be correlated over 8000 km^2 to the south and west (*1*). The Doushantuo Formation is characterized by two transgressive sequences. The lower sequence begins above a distinctive Lower Dolomite Member (cap carbonate), which is overlain by black shale and phosphorite that grade upward into increasingly dolomitic micrite and grainstone. The upper sequence is characterized by a basal black shale and phosphorite unit that grades into dolomitic micrite. These two sequences are separated by an interbasinal sequence boundary, which in the more proximal Weng'an successions occurs as a karstic unconformity (*2*, *3*). The well-preserved animal embryos, algae, and small bilaterians of the Doushantuo Formation are from the phosphorites of the Upper Sequence (*2*, *3*) at Weng'an, Guizhou Province. The uppermost part of the Doushantuo Formation (Miaohe Member) is considered to be correlative to the lower part of a third transgressive cycle grading into carbonates of the Dengying Formation. Abundant macroscopic multicellular algae fossils known as the Miaohe biota are found in the black shale (*4*).

The Lower Dolomite Member overlies the Nantuo Tillite and is equated with other Marinoan-type cap carbonates worldwide because of its distinctive carbonate facies and associated negative $\delta^{13}C$ values (*5*). Fossils from the overlying Dengying Formation consist of large horizontal traces and the weakly mineralized metazoan *Cloudina* considered characteristic of the <10 million years (My) preceding the Ediacaran/Cambrian boundary (*6*). An ash bed below the Nantuo Formation (i.e., Datangpo Formation) has a U-Pb zircon age (±SEM) of 663 ± 4 million years ago (Ma) (*5*). The overlying Cambrian Meishucunian phosphorite unit (the Zhongyicun Member), which contains abundant phosphatized small shelly fossils, provides a minimum age of 538 ± 1.5 Ma (*7*). Barfod *et al.* (*8*) reported Lu-Hf and Pb-Pb whole-rock isochron ages on phosphorites from the lower part of the Upper Sequence of the Doushantuo Formation of 602 ± 48 Ma [mean square of weighted deviates (MSWD) = 2] and 599 ± 4 Ma (MSWD = 2.9), respectively. Chen *et al.* (*9*) reported Pb-Pb isochron dates of 598 ± 26 Ma (MSWD = 2.7) and 576 ± 14 Ma (MSWD = 0.4) from the lower and upper parts, respectively, of the same sequence.

[1]Department of Earth, Atmospheric, and Planetary Sciences, Massachusetts Institute of Technology, Cambridge, MA 02139, USA. [2]Nanjing Institute of Geology and Paleontology, Chinese Academy of Sciences, Nanjing 210008, China.

*To whom correspondence should be addressed. E-mail: dcondon@mit.edu

We collected three volcanic ash samples from the Doushantuo Formation in the type sections of the Yangtze Gorges area. Sample YG-04-15 comes from a 1-cm-thick clay-rich ash bed 2.3 m above the base of the Doushantuo Formation (Wuhe-Gaojiaxi Section) within the Lower Dolomite Member. Zircons from this sample are variably discordant and define a linear array on a concordia diagram anchored by three concordant points (fig. S2). All points (n = 11) yield a weighted mean $^{207}Pb/^{206}Pb$ date of 635.4 ± 1.3 Ma (MSWD = 0.31), and the four concordant points yield a U-Pb "concordia age" (*10*) of 635.23 ± 0.57 Ma (MSWD of concordance and equivalence = 0.55) (*11*). The Lower Dolomite Member is the cap carbonate to the Nantuo Tillite (*5*, *12*–*14*). More specifically, ash bed YG-04-15 occurs at the transition from laminated limestone-dolostone (displaying sheet-crack and tepee-like structures) to laminated limestone-dolostone micrite [transition from C2 to C3 facies in the sense of (*13*)]. Most models for cap carbonate precipitation invoke high accumulation rates (*15*). Therefore, we consider the age of sample YG-04-15 to date to the end of the Nantuo glaciation.

A second ash bed (YG-04-2) occurs 9.5 m above the base of the Doushantuo Formation (Jijiawan Section) and 5 m above the top of the Lower Dolomite Member (Nantuo Cap Carbonate). Zircons from this ash bed yield variably discordant data (n = 9) that define a linear array on a concordia diagram anchored by three concordant data points (fig. S2). The U-Pb concordia age of 632.50 ± 0.48 Ma (MSWD of concordance and equivalence = 0.38) is indistinguishable from the weighted mean $^{207}Pb/^{206}Pb$ age of 632.4 ± 1.3 Ma (MSWD = 0.36). Comparing this age with YG-04-15 constrains the time interval between these two beds to between 1.7 and 3.8 My, and in the Jijiawan section this interval is represented by 3 m of dolomite overlain by about 5 m of black shale (*16*).

The age of the uppermost Doushantuo Formation (Miaohe Member) is constrained by the age of a third ash bed, JIN-04-2 (Jijiawan Section) that occurs at the top of the black shale member containing the Miaohe biota. Zircons from this ash bed yield variably discordant dates (n = 10) that define a linear array on a concordia diagram anchored by two concordant analyses (fig. S2). All data yield a weighted mean $^{207}Pb/^{206}Pb$ date of 550.55 ± 0.75 Ma (MSWD = 0.48). The two concordant analyses yield a U-Pb

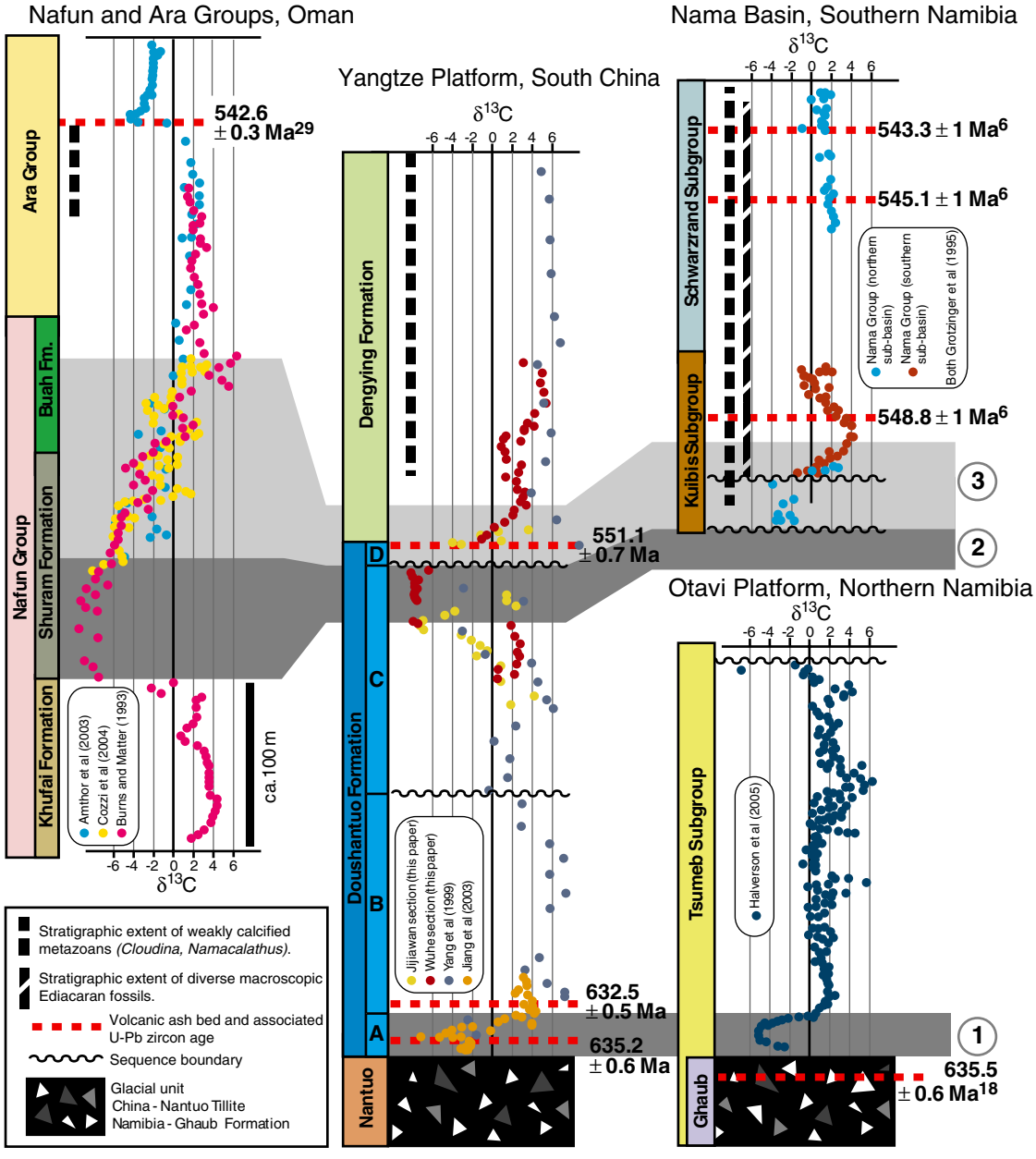

Fig. 1. Correlation of Doushantuo Formation (Yangtze Platform) with the Nama Group (Nama Basin) and Nafun/Ara Groups (Oman) successions. Three distinct sections are identified in each succession on the basis of magnitude of $\delta^{13}C$ and nature (increasing, decreasing, or invariant) of stratigraphic trend. (1) Correlation of cap carbonate excursion ($\delta^{13}C$ starting at –2‰, going to a nadir of –5‰, and returning to +2‰). (2) Invariant negative $\delta^{13}C$ excursion in the range of –7‰. (3) Transition from negative to positive (about 1‰) values after the upper Doushantuo/Shuram/Kuibis anomaly. Nama Group (Kuibis Formation) carbonates record values as low as –4‰. However, correlation with the Doushantuo Formation is based on stratigraphic proximity to the 549 Ma ash bed. Internal stratigraphy of the Doushantuo Formation: A, Lower Dolomite Member; B, Lower Sequence; C, Upper Sequence; and D, Miaohe Member. Superscripted numbers next to dates correspond to reference numbers.

concordia age of 551.07 ± 0.61 Ma (MSWD of concordance and equivalence = 0.48). This ash bed occurs about 85 cm below the base of the Dengying Formation (within the Miaohe Member) at the interface between a black shale unit and overlying carbonates that record a progressive increase in $\delta^{13}C$ values [from –4 to +0.5 per mil (‰)] over a thickness of 2.3 m. Negative $\delta^{13}C$ values occur both above and below the sequence boundary separating the Upper Sequence and Miaohe Member (fig. S1). Below this boundary a pronounced $\delta^{13}C$ excursion (with values as low as –8‰) occurs; in the Wuhe section it is characterized by invariant $\delta^{13}C$ values of –8‰, whereas in the Jijiawan section there is a return to positive $\delta^{13}C$ values before the base Miaohe Member sequence boundary is encountered. This local variation is most likely related to variable preservation below the sequence boundary and/or lateral variation in sediment accumulation and preservation. In both sections, the lowermost Dengying Formation dolomites have values of –3 to –1‰, which increase to about +3‰ over about 5 m. This trend is interpreted as being the top of the pronounced $\delta^{13}C$ excursion (with values as low as –8‰) that characterizes the top of the Doushantuo Formation (Fig. 1), thus constraining the age of the sustained negative excursion to (just) older than 551.1 ± 0.7 Ma, the time at which $\delta^{13}C$ values increase to positive values. This interpretation assumes that any period of nondeposition across this sequence boundary has a duration that is less than the duration of the negative $\delta^{13}C$ excursion itself.

The Doushantuo Formation contains two prominent $\delta^{13}C$ features, a negative (–5‰) to positive (up to 2‰) excursion in the Lower Dolomite Member (*5*, *13*) and a pronounced negative (down to –8‰) excursion in the uppermost Doushantuo Formation (Fig. 1 and fig. S1). The Nantuo Tillite–Lower Dolomite Member has been correlated with other Marinoan-type glacial successions recorded worldwide (*5*, *17*). Our age for the termination of the Marinoan glaciation is nearly identical to a concordant U-Pb age of 635.51 ± 0.54 Ma (*18*, *19*) marking the top of glacial deposits in the Ghaub Formation, Namibia. Termination of the Marinoan glaciation and cap carbonate deposition was thus essentially synchronous, within the age uncertainty, worldwide. These data support the hypothesis that cap carbonates were deposited very quickly after deglaciation (*20*).

It has been commonly assumed that the negative $\delta^{13}C$ anomaly at the top of the Doushantuo Formation was related to the Gaskiers glaciation (*21*, *22*), albeit with no sedimentological evidence for glaciation. If the lowermost Dengying Formation with its negative-to-positive $\delta^{13}C$ trend represents the top of this anomaly, this correlation is no longer viable because the 551.1 ± 0.7 Ma age from the uppermost Doushantuo ash bed (JIN-04-2, Jijiawan Section) postdates the circa 580 Ma Gaskiers glaciation. This age does reveal that much of the Upper Sequence and associated isotopic excursion occurred during a time when macroscopic Ediacaran Fauna are preserved in other successions worldwide [e.g., Mistaken Point Fauna (*23*); White Sea Fauna, and inferentially Australian Fauna (*24*)] and that their absence in the Doushantuo Formation is likely an artifact of paleoecological context (*25*).

Given that the top of the Doushantuo is not correlative with the Gaskiers glaciation, we suggest that the sequence boundary separating the Lower and Upper sequences (Fig. 1) within the Doushantuo reflects glacio-eustatic sea-level fluctuation associated with it. In the Yangtze Gorge region, there is no distinct evidence of a sea-level fluctuation. However, the more proximal succession at Weng'an, the corresponding surface, is karstic with evidence for subaerial exposure (*2*, *3*). An age of circa 580 Ma for this surface is at odds with the data from Barfod *et al.* (*8*), but given the complexity of diagenesis in phosphorites and the use of leached whole-rock samples that span several meters of section, it is difficult to evaluate the accuracy of the calculated dates. This interpretation would imply that the animal embryos and small bilaterian of the Weng'an Phosphorite Member (*2*, *3*) postdate the last extensive glaciation (circa 580 Ma) of the Neoproterozoic (*26*).

In Southern Namibia, carbonate rocks of the Schwarzrand and Kuibis subgroups (Southern and Northern Nama Basin) display a $\delta^{13}C$ excursion above a sequence boundary (*6*, *27*, *28*) and 500 m below an ash bed dated at 548.8 ± 1.0 Ma (*6*). Estimates of sediment accumulation rates in the Nama basin are about 100 to 200 m per 10^6 years, so the shift in $\delta^{13}C$ values is estimated to be about 551 Ma. In Oman, a distinct negative $\delta^{13}C$ anomaly in the lower half of the Shuram Formation (*29*–*31*) lies about 200 m below ash beds in the Ara Group dated at 542 Ma (*29*) and above the Fiq Formation, which is interpreted as a Marinoan-type glacial deposit (*32*). Given that in Namibia, Oman, and China, these similar sequences are overlain by rocks containing the Ediacaran/Cambrian boundary and their $\delta^{13}C$ curves display similar trends, we suggest correlation of the Shuram, Kuibis, and upper Doushantuo excursions. Halverson and colleagues (*17*) also correlated the Kuibis/Shuram anomalies with those of similar magnitude and stratigraphic position (i.e., post-Marinoan and pre-Cambrian) in Australia

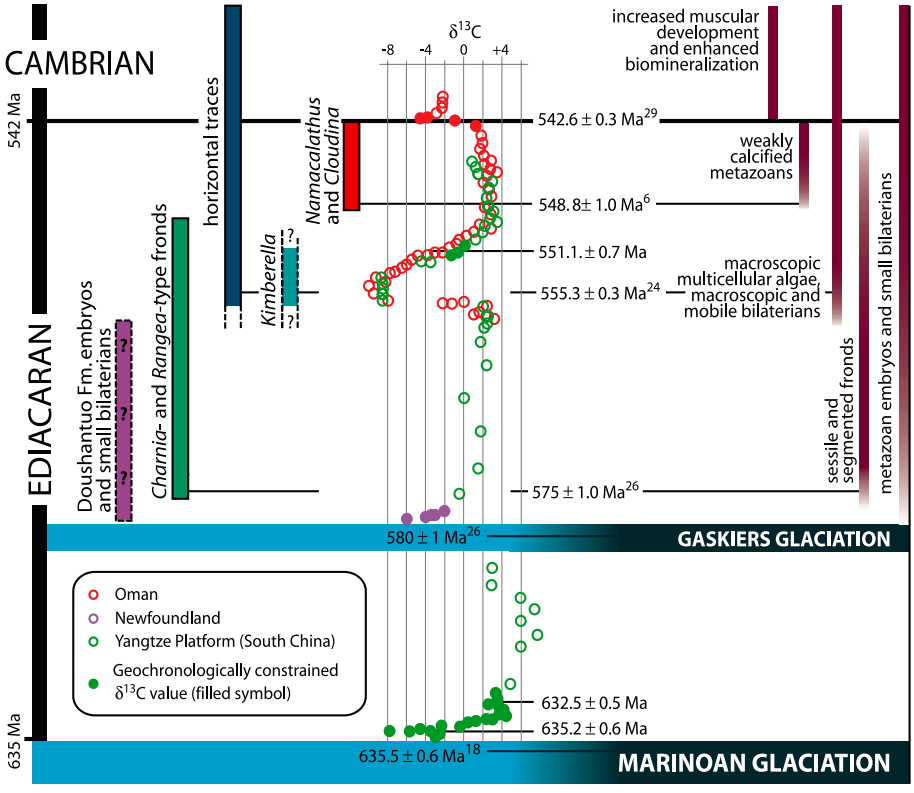

Fig. 2. Schematic diagram comparing fossil occurrences, evolutionary developments, and globally correlated $\delta^{13}C$ excursions within the context to a temporal framework constrained by U-Pb ages from sequences in Namibia, Oman, China, and Newfoundland. Newfoundland carbonate carbon $\delta^{13}C$ data are from Myrow and Kaufman (*35*). The absolute age of the –8‰ nadir is unconstrained except that it must be older than 551.1 ± 0.7 Ma. Superscripted numbers next to dates correspond to reference numbers.

[the Wonoka Formation (*33*)] and the western United States [Rainstorm Member, Johnnie Formation (*34*)] but chose to equate it with a postulated Gaskiers-related $\delta^{13}C$ excursion from circa 580 Ma (*35*). Instead, our data indicate that this globally correlated negative $\delta^{13}C$ excursion is not related to any known glaciation (*36*). The duration of this excursion is unconstrained; however, given that it is captured within over 100 m of section in Oman (Fig. 1) combined with approximate sediment accumulation rates calculated with our constraints, we suggest a duration of >1 and <10 My.

The Doushantuo and correlative strata record a fundamental shift from an interval of large carbon isotopic anomalies corresponding to glacial episodes (750 to 580 Ma) to an interval of anomalies unrelated to obvious glacial episodes (i.e., the anomalies from circa 551 and 542 Ma), as well as subsequent large fluctuations in the lower Cambrian. These new geochronological data allow us to calibrate that shift as being synchronous with the appearance of larger and more complex metazoans; this suggests possible feedback relationships between evolutionary innovation and seawater chemistry (Fig. 2).

Our ages indicate that the Doushantuo Formation spans more than 90% of the Ediacaran Period. These constraints are consistent with the upper Doushantuo/Shuram/Kuibis excursion being broadly coincident with the first appearance of complex trace fossils and mollusk-like bilaterian *Kimberella* (*37*), dated as slightly older than 555.1 ± 1.0 Ma (*24*). The advent of large pelagic bilaterians with unidirectional guts would have increased the flux of organic carbon to the deep ocean (*38*). Additionally, the radiation of algae containing resistant biopolymers in cell wall and cysts (i.e., Miaohe Biota) and the advent of biomineralization (*Namacalathus* and *Cloudina*, >549 Ma) would have also resulted in an increased organic carbon and carbonate carbon flux (*39*). These changes would have resulted in a downward flux of organic carbon with a possible coupled oxidation of the organic reservoir (*38*, *39*) driving the negative $\delta^{13}C$ excursion. This feedback loop would lead to an increase in marine oxygen levels and stimulate productivity and inferentially predation. It may be no coincidence that the first reefs inhabited by abundant weakly calcified and rare fully calcified metazoans appeared at about the same time as the isotopic anomaly [i.e., before 549 Ma in Namibia (*6*, *40*)].

References and Notes

1. M. Y. Zhu *et al.*, *Prog. Nat. Sci.* **13**, 951 (2003).
2. J. Y. Chen *et al.*, *Science* **305**, 218 (2004).
3. S. H. Xiao, Y. Zhang, A. H. Knoll, *Nature* **391**, 553 (1998).
4. S. H. Xiao, X. L. Yuan, M. Steiner, A. H. Knoll, *J. Paleontol.* **76**, 347 (2002).
5. C. M. Zhou *et al.*, *Geology* **32**, 437 (2004).
6. J. P. Grotzinger, S. A. Bowring, B. Z. Saylor, A. J. Kaufman, *Science* **270**, 598 (1995).
7. R. J. F. Jenkins, J. A. Cooper, W. Compston, *J. Geol. Soc. London* **159**, 645 (2002).
8. G. H. Barfod *et al.*, *Earth Planet. Sci. Lett.* **201**, 203 (2002).
9. D. F. Chen, W. Q. Dong, B. Q. Zhu, X. P. Chen, *Precambrian Res.* **132**, 123 (2004).
10. Materials and methods are available as supporting material on *Science* Online.
11. Age uncertainties are stated at the 2σ level.
12. J. D. Yang, W. G. Sun, Z. Z. Wang, Y. S. Xue, X. C. Tao, *Precambrian Res.* **93**, 215 (1999).
13. G. Jiang, M. J. Kennedy, N. Christie-Blick, *Nature* **426**, 822 (2003).
14. M. Macouin *et al.*, *Earth Planet. Sci. Lett.* **224**, 387 (2004).
15. P. F. Hoffman, D. P. Schrag, *Terra Nova* **14**, 129 (2002).
16. This corresponds to approximate sediment accumulation rates of about 1.5 to 3 m/My.
17. G. P. Halverson, P. F. Hoffman, D. P. Schrag, A. C. Maloof, A. H. N. Rice, *Geol. Soc. Am. Bull.*, in press.
18. K.-H. Hoffmann, D. J. Condon, S. A. Bowring, J. L. Crowley, *Geology* **32**, 817 (2004).
19. This is the analytical uncertainty on the U-Pb concordia age (excluding tracer calibration uncertainty) calculated from Hoffmann *et al.* (*18*).
20. P. F. Hoffman, A. J. Kaufman, G. P. Halverson, D. P. Schrag, *Science* **281**, 1342 (1998).
21. W. Wang *et al.*, *Acta Micropalaeontol. Sin.* **19**, 382 (2002).
22. S. H. Xiao *et al.*, *Precambrian Res.* **130**, 1 (2004).
23. G. M. Narbonne, J. G. Gehling, *Geology* **31**, 27 (2003).
24. M. W. Martin *et al.*, *Science* **288**, 841 (2000).
25. D. Grazhdankin, *Paleobiology* **30**, 203 (2004).
26. S. Bowring, P. Myrow, E. Landing, J. Ramezani, J. Grotzinger, *Geophys. Res. Abstr.* **5**, 13219 (2003).
27. The Schwarzrand Subgroup is characterized by a +2 plateau (*6*,*28*). In the northern subbasin, the underlying Kuibis Subgroup records a decrease from +3 down to 0 in upper Mooifontein Member with values of −3 obtained on carbonates from the underlying Mara Member. In the southern subbasin the Kuibis Subgroup has values of about 0 at the top that gradually increase toward the bottom of the section to +4 and then decrease down to −1.
28. B. Z. Saylor, A. J. Kaufman, J. P. Grotzinger, F. Urban, *J. Sediment. Res.* **68**, 1223 (1998).
29. J. E. Amthor *et al.*, *Geology* **31**, 431 (2003).
30. S. J. Burns, A. Matter, *Eclogae Geol. Helv.* **86**, 595 (1993).
31. A. Cozzi, J. P. Grotzinger, P. A. Allen, *Geol. Soc. Am. Bull.* **116**, 1367 (2004).
32. P. A. Allen *et al.*, in *16th International Sedimentological Congress Abstract Volume* (International Association of Sedimentologists, Johannesburg, South Africa, 2002), pp. 7–8.
33. C. R. Calver, *Precambrian Res.* **100**, 121 (2000).
34. F. A. Corsetti, A. J. Kaufman, *Geol. Soc. Am. Bull.* **115**, 916 (2003).
35. P. M. Myrow, A. J. Kaufman, *J. Sediment. Res.* **69**, 784 (1999).
36. G. Q. Jiang, L. E. Sohl, N. Christie-Blick, *Geology* **31**, 917 (2003).
37. M. A. Fedonkin, B. M. Waggoner, *Nature* **388**, 868 (1997).
38. G. A. Logan, J. M. Hayes, G. B. Hieshima, R. E. Summons, *Nature* **376**, 53 (1995).
39. D. H. Rothman, J. M. Hayes, R. E. Summons, *Proc. Natl. Acad. Sci. U.S.A.* **100**, 8124 (2003).
40. R. A. Wood, J. P. Grotzinger, J. A. D. Dickson, *Science* **296**, 2383 (2002).

41. This work was supported by NASA's Astrobiology Program (NCC2-1053 to S.B.), National Natural Science Foundation of China, the Chinese Academy of Sciences (KZCX3-SW-141), and Ministry of Science and Technology of China (G2000077700 and 2002CCA03300). We thank J. Zhang and X. Chen for fieldwork and C-O isotope analyses, respectively, and D. Fike, J. Grotzinger, G. P. Halverson, P. Hoffman, A. Knoll, A. Maloof, T. Prave, R. Summons, and two anonymous reviewers for comments. We thank D. Rothman for comments and discussion.

Supporting Online Material

www.sciencemag.org/cgi/content/full/1107765/DC1
Materials and Methods
Figs. S1 and S2
Tables S1 and S2
References

22 November 2004; accepted 14 February 2005
Published online 24 February 2005;
10.1126/science.1107765
Include this information when citing this paper.

Mortality and Greenhouse Gas Impacts of Biomass and Petroleum Energy Futures in Africa

Robert Bailis,[1] Majid Ezzati,[2]* Daniel M. Kammen[1,3]*

We analyzed the mortality impacts and greenhouse gas (GHG) emissions produced by household energy use in Africa. Under a business-as-usual (BAU) scenario, household indoor air pollution will cause an estimated 9.8 million premature deaths by the year 2030. Gradual and rapid transitions to charcoal would delay 1.0 million and 2.8 million deaths, respectively; similar transitions to petroleum fuels would delay 1.3 million and 3.7 million deaths. Cumulative BAU GHG emissions will be 6.7 billion tons of carbon by 2050, which is 5.6% of Africa's total emissions. Large shifts to the use of fossil fuels would reduce GHG emissions by 1 to 10%. Charcoal-intensive future scenarios using current practices increase emissions by 140 to 190%; the increase can be reduced to 5 to 36% using currently available technologies for sustainable production or potentially reduced even more with investment in technological innovation.

Biomass fuels (wood, charcoal, dung, and agricultural residues) are vital to basic welfare and economic activity in developing nations, especially in sub-Saharan Africa (SSA), where they meet more than 90% of household energy needs in many nations. Combustion of biofuels emits pollutants that currently cause over 1.6 million annual deaths globally (400,000 in SSA) (*1*). Because most of these deaths are among children and women, biomass use is

directly or indirectly related to multiple Millennium Development Goals of the United Nations (UN), including environmental sustainability, reducing child mortality, and gender equity.

We developed a database of current fuel use and a range of scenarios of household energy futures up to 2050 in SSA (Table 1). Current national-level energy production and consumption (Fig. 1) were estimated from the UN Food and Agriculture Organization's (FAO's) forest products database and the International Energy Agency's (IEA's) statistical database of countries not in the Organisation for Economic Cooperation and Development (*2*, *3*). FAO records woodfuel (defined as wood or wood transformed into charcoal) production and trade from 41 countries in SSA, including separate estimates for charcoal. Charcoal is widely used in Africa, even in countries with large endowments of fossil fuels, such as Gabon, Angola, and Nigeria (*2*). IEA maintains information on biomass and fossil fuels used in the residential sectors of 20 countries in the region and an aggregate estimate for the remaining countries in the region. Data were analyzed for consistency of each fuel type between FAO and IEA and for consistency across fuel types from IEA (*4*). We estimated that in 2000, households in SSA consumed nearly 470 million tons of woodfuels (0.72 tons per capita) in the form of wood and charcoal. By comparison, FAO estimates that India and China, with a combined population nearly 3.5 times larger than that of SSA, used 340 million tons of woodfuels in the same year (*5*).

The fraction of households using each fuel was derived from nationally representative household-welfare surveys conducted in the 1990s and compiled by the World Bank for 20 countries (*4*, *6*). These nations contained 47% of the region's urban population and 63% of its rural population. For countries not surveyed, we applied population-weighted estimates from surveyed nations, separately for rural and urban populations. South Africa was excluded from the weighted averages, because it has a distinct pattern of household fuel consumption. These extrapolations are consistent with the observed low variability of fuel-use patterns across the 20 countries with data, especially for rural areas, which form 64% of SSA's population (excluding South Africa, the fraction of households using woodfuels varied from 86 to 99% in rural areas and from 26 to 96% in urban areas in the 20 countries with data) (*6*). Overall, 94% of the African rural population and 73% of the urban population use woodfuels as their primary source of energy, mainly in the form of wood in rural areas and an equal split of wood and charcoal in urban centers. Most remaining households use a combination of kerosene, liquefied petroleum gas (LPG), and, to a very limited extent, electricity (*7*).

The scenarios for future household energy sources and use (Table 1) examined the role of two factors: (i) household fuel choice (Fig. 2) and (ii) sustainability of biomass harvesting and charcoal production techniques. Economic growth and energy infrastructure development have lagged in SSA compared with other world regions, limiting a large-scale shift to commercial sources of energy in the residential sector (*8*), which we present in the business-as-usual (BAU) scenario. Furthermore, economic growth and infrastructure expansion do not automatically create a parallel and simultaneous shift to commercial energy for household needs. Even in China, where rapid economic growth and infrastructure expansion have contributed to near-universal access to electricity (*9*), solid fuel use for cooking and heating among households has persisted; 80% of Chinese households continue to rely on biomass (mainly crop residues) and/or coal as their primary cooking and heating fuels (*10*).

In addition to the secular BAU trends, in which population growth and urbanization are the main drivers of change in household fuel use, we examined two additional categories of scenarios for household fuel choice. The first group examines a systematic shift from wood to charcoal (C, charcoal; RC, rapid charcoal). Charcoal is a popular fuel in many countries in SSA because it is relatively clean, safe, affordable, and storable and requires no expensive equipment to use. The second group of scenarios envisions large-scale adoption of petroleum-based fossil fuels (kerosene and LPG), which are currently commercial alternatives to biomass fuels in many mid- and high-income nations (F, fossil fuel; RF, rapid fossil fuel) (*11*). Like charcoal, kerosene can be purchased in small quantities and used with relatively inexpensive equipment. It has a reasonably well-developed supply chain and is used throughout the region for lighting, as well as for cooking in urban areas. In contrast, LPG must be purchased in relatively large quantities and requires much more expensive

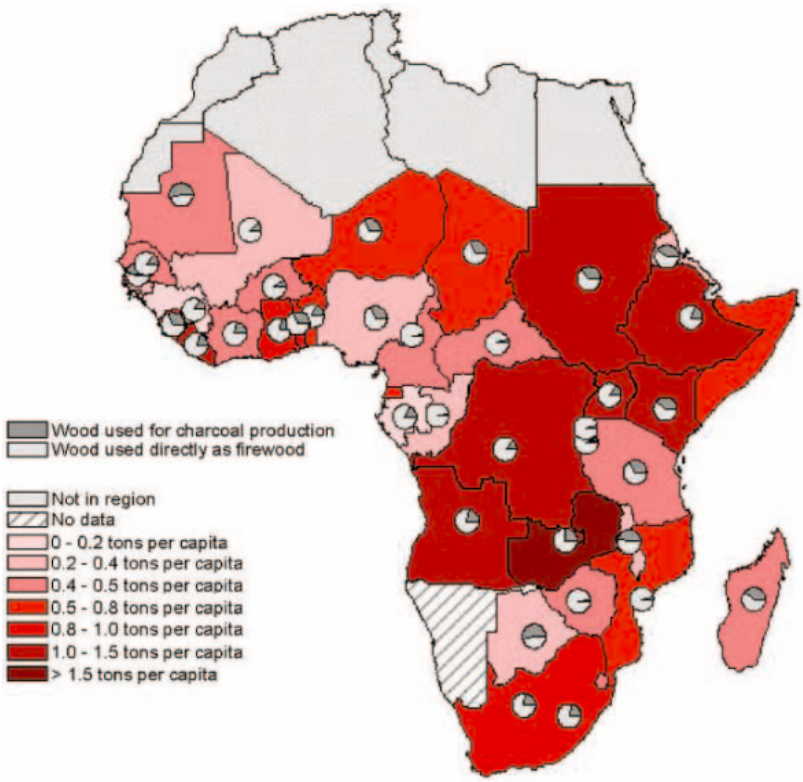

Fig. 1. Current per-capita biomass production in SSA. The colors show total wood fuel consumption, and the pie charts show the fraction of wood that is used for charcoal, based on multiple sources. FAO biomass estimates (including charcoal) (*3*) were roughly consistent with IEA estimates and were used for all countries except Angola, Kenya, South Africa, Sudan, and Zambia (20% of the region's population). For these countries, FAO biomass estimates would have been too low to meet minimal household energy needs when considered with energy use from fossil fuels and other energy sources reported by IEA (*2*). In all of these countries except Kenya, IEA estimates were used; for Kenya, data from a detailed national household fuel consumption study were used (*26*).

[1]Energy and Resources Group, University of California, Berkeley, CA 94720–3050, USA. [2]Harvard School of Public Health, Boston, MA 02115, USA. [3]Goldman School of Public Policy, University of California, Berkeley, CA 94720–3050, USA.

*To whom correspondence should be addressed. E-mail: mezzati@hsph.harvard.edu (M.E.); kammen@berkeley.edu (D.M.K.)

Table 1. Scenarios of household energy futures in SSA. All scenarios begin from the same year 2000 baseline. In 2000, 64% of the population lived in rural areas. Forty-one, 34, 13, 8, and 4% of urban households used wood or crop residues, charcoal, kerosene, LPG, and electricity as their primary source of household energy, respectively; 94, 4, and 2% of rural households used wood or crop residues, charcoal, and kerosene. Future population and urbanization estimates are from the UN Population Division (*30*). Future household energy use and production scenarios examine the role of two factors: (i) household fuel choice and (ii) biomass harvesting and charcoal production techniques. The rate of adoption of alternative fuels and sustainability practices were also examined (gradual versus rapid scenarios).

Scenario	Household fuel choice pattern	Woodfuel harvest and charcoal production	Definitions
Group 1: Business as usual scenarios			
Business-as-usual (BAU)	No change from current patterns in rural and urban areas of each country	Unsustainable	The proportion of people in rural and urban areas using each fuel remains unchanged from the baseline year. However, differential rates of population growth and urbanization in different countries in the region result in regional changes in household fuel choice during the period of analysis. No changes occur in woodfuel harvesting practices or in charcoal production techniques, in which 20% of trees removed for charcoal and 80% of those removed for wood regenerate (*4*).
Sustainable BAU (BAU-S)		Fully sustainable by 2050	Identical fuel consumption as in BAU, but there is a gradual linear increase in the proportion of trees harvested sustainably as well as in the use of improved (high-efficiency) charcoal kilns. By 2050, tree regeneration reaches 80% for charcoal harvesting and 100% for firewood harvesting. Also by 2050, 100% of charcoal production takes place in high-efficiency kilns.
Group 2: Charcoal intensive scenarios			
Charcoal (C)	Large shift from wood to charcoal with minimal use of fossil fuels	Unsustainable	Between 2000 and 2050, there is a gradual linear transition from wood to charcoal in both urban and rural areas By 2050, the fraction of households using wood decreases by 40% in rural areas and 100% in urban areas, with both groups shifting to charcoal. As a result, in 2050 approximately 80% of urban households and 40% of rural households use charcoal (61% of the total population). There are no changes in woodfuel harvest practices or in charcoal production methods.
Sustainable charcoal (C-S)		Fully sustainable by 2050	Identical trend in fuel consumption as in C, but there is a simultaneous shift in the fraction of harvested trees allowed to regenerate as well as in the use of improved (high-efficiency) charcoal kilns. By 2050, tree regeneration reaches 80% for charcoal production and 100% for firewood harvest; 100% of charcoal production takes place in high-efficiency kilns.
Rapid charcoal (RC)		Unsustainable	As in scenario C, the fraction of firewood users decreases by 40% in rural areas and by 100% in urban areas in as a result of a shift to charcoal. However, the switch occurs much more rapidly so that it is complete by 2010. In 2010, 40% of rural households and 75% of urban households use charcoal (52% of the total population). The rural and urban fractions remain constant through the rest of the analysis, but the total fraction of charcoal users continues to increase because of a demographic shift to urban areas. By 2050, the fraction of the total population using charcoal increases to 64%.
Rapid sustainable charcoal (RC-S)		Fully sustainable by 2010	Identical fuel consumption patterns as in RC, but there is also a rapid increase in the proportion of harvested trees allowed to regenerate as well as the use of improved (high-efficiency) charcoal kilns. The increase in tree regeneration and improved kilns is driven by a policy of aggressive dissemination of improved kiln technologies and improved land management. By 2010, tree regeneration reaches 80% for charcoal production and 100% for firewood harvest; 100% of charcoal production takes place in high-efficiency kilns.
Group 3: Fossil fuel intensive scenarios			
Fossil-fuel (F)	Large shift from wood and charcoal to petroleum-based fossil fuels	Unsustainable	Firewood and charcoal users in both urban and rural areas switch gradually to LPG and kerosene. By 2050, the proportion of households using wood or charcoal decreases by 40% in rural areas and 80% in urban areas. In rural areas, the shift is primarily to kerosene; in urban areas, the shift is to both kerosene and LPG. As a result, in 2050, 30% of households in rural areas use kerosene and 10% use LPG. In urban areas, 30% use kerosene and 50% use LPG. In total, 63% of the population uses fossil fuels.
Rapid fossil-fuel (RF)		Unsustainable	RF follows a similar pattern as scenario F, but at an accelerated pace. By 2010, approximately 40% of the rural population and 80% of the urban population (54% of total population) use fossil fuels. The rural and urban fractions remain constant up to 2050, but the total fraction of fossil fuel users continues to increase because of a demographic shift to urban areas. By 2050, the total fraction of people using fossil fuels increases from 54% to 63%.

stoves, both of which are barriers to its use in the urban poor and rural households. The use of LPG is currently limited to wealthier urban families in a small number of countries, with the exception of Senegal, where there have been substantial efforts to promote LPG use (*6*, *9*). These characteristics were the basis for choosing distinct household fuel-use patterns for rural and urban areas in our scenarios.

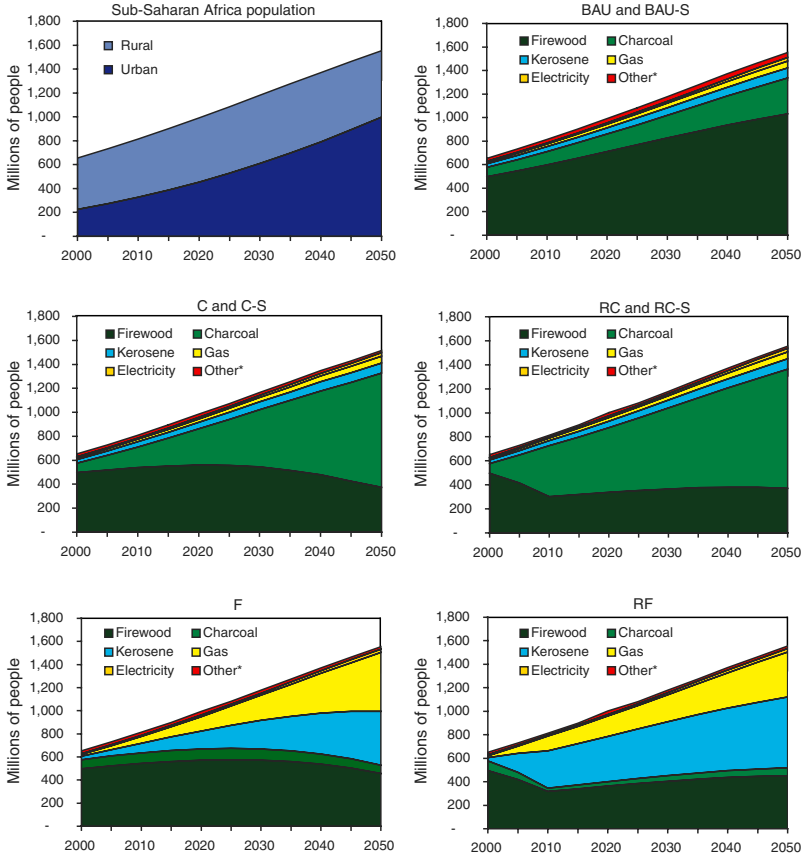

Fig. 2. Number of people in SSA using each fuel in BAU, charcoal (C and RC), and fossil fuel (F and RF) scenarios. For C between 2000 and 2050, the absolute number of people using charcoal increases more than 10-fold, partly driven by population growth and urbanization and partly by a shift to charcoal. This is a large but empirically realistic shift. For example, between 1980 and 2000, the number of households using charcoal as a primary source of energy in Kenya increased by about 250%, despite frequent attempts by the Kenyan government to restrict charcoal production (*26*). "Other" includes crop residues, dung, and mineral coal. Rural-urban breakdown until 2030 is based on UN estimates, and after 2030 is based on projections (*4, 30*).

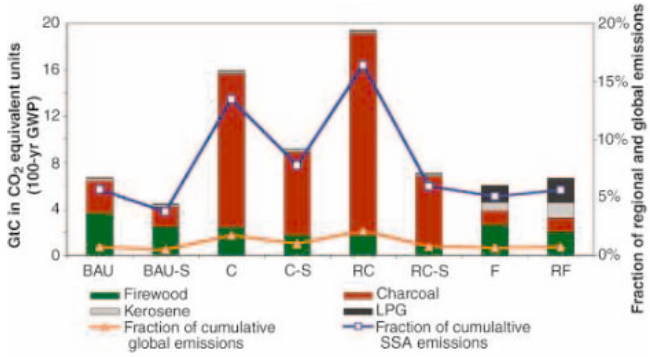

Fig. 3. Cumulative GHG emissions from 2000 and 2050 from CO_2, CH_4, and N_2O converted to CO_2 equivalent units, weighted by 100-year GWP for each scenario of household energy futures. Totals are disaggregated by emissions from each fuel. The figure also shows cumulative emissions as fractions of regional and global cumulative emissions [118 GtC and 917 GtC, respectively, based on the median emissions scenario reported in the Special Report on Emissions Scenarios to inform policy makers during the Intergovernmental Panel on Climate Change's Third Assessment period (*13*)]. See fig. S5 for annual emissions from each scenario. The figure presents the sum of emissions of GHGs targeted by the Kyoto Protocol (KP): CO_2, CH_4, and N_2O. This omits the warming effects of CO, non-methane hydrocarbons, and aerosols or particulate matter. These nonKP GHGs were included in the sensitivity analysis, along with sensitivity analysis based on a 20-year GWP (*4*).

For each biomass-based scenario, we examined the impacts of sustainably harvested (S) biomass (*4*) and charcoal production technology on greenhouse gas (GHG) emissions (BAU-S, C-S, and RC-S) (Table 1). Nearly all charcoal in SSA currently is produced in traditional kilns, which have suboptimal conversion efficiency and no emission controls. Technological shifts in charcoal production include indigenous or exotic multipurpose tree crops, alternative inputs such as biomass waste products, and efficient kilns with emission controls. For each scenario, we estimated emissions of CO_2 and non-CO_2 GHGs from both production and consumption of all fuels. Both charcoal and fossil fuels are associated with significant upstream (production) emissions. In contrast, wood has negligible upstream emissions. Both upstream and end-use emissions were converted into CO_2 equivalent units using 100-year global warming potential (GWP) to account for the differential warming effect (radiative forcing) of each emitted GHG (*4*, *12–14*).

The net GHG emissions from residential energy use in SSA in 2000 were 79 million tons of carbon (MtC) (61% from wood, 35% from charcoal, 3% from kerosene, and 1% from LPG). In the absence of systematic changes in fuel-use patterns and in production and harvesting techniques (BAU scenario), cumulative emissions between 2000 and 2050 will be an estimated 6.7 GtC. The two fossil fuel–intensive scenarios (F and RF) have the second and third lowest cumulative emissions, after the BAU fuel scenario with sustainable harvesting and charcoal production (BAU-S). The highest estimated cumulative emissions were from two charcoal-intensive scenarios with unsustainable biomass harvesting and traditional inefficient charcoal production (C and RC) (Fig. 3). However, if these household fuel scenarios are accompanied by sustainable harvesting and a transition to cleaner and higher efficiency charcoal production technologies (C-S and RC-S), emissions will be reduced by 45 and 66% for gradual and rapid transitions, respectively.

We also estimated the impacts of future fuel-use scenarios on the two most common diseases associated with household fuel use: mortality from lower respiratory infections (LRIs, mainly pneumonia) among children (<5 years of age) and chronic obstructive pulmonary disease (COPD) among adult women. In 2000, there were 690,000 LRI deaths among children and 53,000 COPD deaths among adult females in SSA (*15*). An estimated 51% of child LRI deaths (350,000 deaths) and 63% of adult female COPD deaths (34,000 deaths) were caused by household use of wood and charcoal (*4*, *16*). Without systematic changes in urban and rural fuel-use patterns, household biomass use will result in an estimated 8.1 million LRI deaths among young children and 1.7 million COPD deaths

of adult women between 2000 and 2030 (50% of all childhood LRI deaths and 63% of all adult female COPD deaths in the 30-year interval). Of these 9.8 million premature deaths, 1.0 and 1.3 million are avoidable with gradual transitions to charcoal (C) and fossil fuels (F), respectively; 2.8 and 3.7 million are avoidable with more rapid transitions to the two energy futures (RC and RF) (*17*). Eighty-three to 85% of avoidable deaths are in children, and the remaining are among adult women (Fig. 4).

This integrated assessment of GHG emissions and health impacts of the household fuel use in SSA, the world's poorest region with the lowest per-capita energy consumption and worst health status, reflects the substantial disease burden and GHG consequences if current land- and energy-management practices continue. A shift to sustainable biomass harvesting without a shift in household fuel-use patterns can reduce GHG emissions by 36% but will have no health or direct welfare benefits for the region. Transition to petroleum-based fuels provides the next largest climate-change benefits, with substantial reductions in childhood and adult female mortality (*11*). This transition is already underway among wealthier urban households in some countries of the region. However, for many people, this is not a feasible option over the next 2 to 3 decades. Obstacles include fuel affordability for individual households, high capital costs for fuel processing and delivery infrastructure, and volatility in both price and supply as a consequence of national energy policies and international markets.

The sustainable charcoal scenarios presented here define alternatives for significant health benefits in SSA and address regional and global environmental issues. A shift from firewood to either charcoal or fossil fuels can reduce indoor air pollution by 90% or more (*18*). Therefore, charcoal can capture much of the health benefits of fossil-fuel use without the economic burden and infrastructure requirements (*19*, *20*). In Kenya, the initial cost of a charcoal stove lasting 1 to 2 years is only $3 to $5; LPG stoves and gas tanks cost $30 to $50. In urban centers, where charcoal markets are well developed and firewood must be purchased, the operating cost of charcoal stoves per unit of useful energy delivered is similar to that of wood and substantially cheaper than fossil fuels (*20*). Therefore, a shift to charcoal among SSA households can be equally as or more cost effective than some of the commonly cited health interventions in developing countries (*15*, *21*). Charcoal is already a preferred fuel among many consumers and has a well-established production and marketing network in place in many countries. Therefore, charcoal resolves the important concern about "intervention scaling-up" in sustainable development and health technology evaluation.

Widespread charcoal use in Africa as a health intervention presents major policy and research challenges and opportunities. Widespread use of charcoal without changes in technology and land management will lead to substantially higher GHG emissions (Fig. 3). Charcoal use has large, though poorly characterized, impacts on forest cover, soil fertility, and biodiversity. Currently feasible sustainable practices, similar to past efforts in Thailand and Brazil (*22*, *23*), can substantially reduce these emissions. A real opportunity also exists to develop new harvesting and production methods, possibly with even fewer environmental impacts than those in the sustainable scenarios considered here (e.g., charcoal production from alternative feedstocks) (*24*). However, these advances require investment in technology R&D and in technology transfer and dissemination within and between countries. In addition to technological needs, the barriers to sustainable charcoal production are rooted in a lack of coherent energy policies specifically addressing residential energy needs and in biases toward industrial energy resources, as well as outdated forest policies that put control of forest resources in the hands of centralized agencies, which rarely recognize energy as an important forest product. If these technological, funding, and institutional challenges are met, transitioning to sustainable charcoal would create domestic jobs, boost rural economies, lessen the need for imported fossil fuels, and save foreign exchange. This integration of health outcomes into energy and resource technologies and policies offers an opportunity to reduce child mortality, promote gender equality, and improve environmental sustainability.

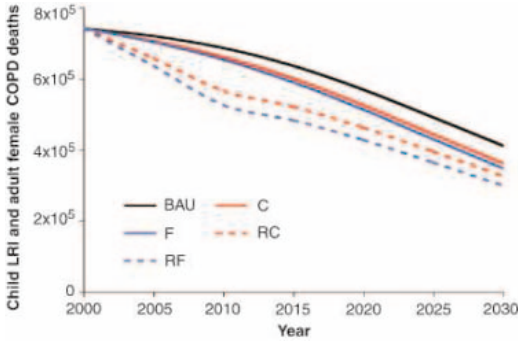

Fig. 4. Estimated mortality for scenarios of household energy futures in SSA. Diseases included are LRIs among children <5 years of age and COPD among adult women. Estimates account for forecasted demographic change (population growth and aging) and secular trends in background disease and mortality levels. The observed secular (BAU) decline in childhood LRI mortality is a result of factors such as increased coverage and efficacy of pneumonia case management using antibiotics; increased awareness and practice of breastfeeding, which increases child immunity and survival; and other secular trends caused by economic and technological factors (*29*). Secular (BAU) trends in COPD are upward mainly because of population aging (COPD mortality increases with age). There has been a slight increase in age-specific COPD mortality rates at older ages, possibly due to small increases in smoking among women in Africa, and a slight decrease in age-specific rates in middle ages, possibly due to competing causes of death (mainly human immunodeficiency virus/acquired immunodeficiency syndrome). Similar directions are seen for lung cancer, another disease affected by smoking, which is the main driver of secular COPD rates in Africa. See fig. S11 for separate estimates by disease.

References and Notes

1. M. Ezzati *et al.*, *Lancet* **360**, 1347 (2002).
2. IEA, *Energy Statistics of Non-OECD Countries* (IEA Publications, Paris, 2004).
3. FAOSTAT data (UN FAO, 2004) are available at http://faostat.fao.org/faostat/collections?version=ext&hasbulk=0&subset=forestry.
4. Materials, methods, and sensitivity analyses are available as supporting material on *Science* Online.
5. This estimate for China and India applies to woodfuels only. Households in China and India use more solid fuels than households in SSA but in forms other than woody biomass. In China, crop residues are common fuels in rural areas, and in India, crop residues and dung are each used by roughly 10% of households (*25*). Many households in China and India use coal as their primary fuel, which is also important for health and GHG impacts (*10*).
6. World Bank, *Africa Development Indicators Series* (World Bank, Washington, DC, 2000 and 2004).
7. In addition, approximately 3% of households in the region use nonwoody biomass such as crop residues or dung, and, according to data from national censuses, approximately 3% of the combined population in South Africa, Zimbabwe, and Botswana (about 0.4% of the regional population) relies on fossil coal.
8. S. Karekezi, *Energy Policy* **30**, 915 (2002).
9. IEA, in *World Energy Outlook* (IEA Publications, Paris, 2002), pp. 365–407.
10. K. R. Smith, S. Mehta, M. Maeusezahl-Feuz, in *Comparative Quantification of Health Risks: Global and Regional Burden of Disease Attributable to Selected Major Risk Factors*, M. Ezzati, A. Lopez, A. Rodgers, C. Murray, Eds. [World Health Organization (WHO), Geneva, 2004], pp. 1435–1493.
11. K. R. Smith, *Science* **298**, 1847 (2002).
12. Intergovernmental Panel on Climate Change, *Climate Change 2001: The Scientific Basis*, J. T. Houghton *et al.*, Eds. (Cambridge Univ. Press, Cambridge, 2001).
13. R. Bailis, M. Ezzati, D. Kammen, *Environ. Sci. Technol.* **37**, 2051 (2003).
14. T. Bond, C. Venkataraman, O. Masera, *Energy Sustainable Dev.* **8**, 20 (2004).
15. WHO, *World Health Report 2002: Reducing Risk, Promoting Health Life* (WHO, Geneva, 2002).
16. For comparison, in the same year in SSA, 1.8 million deaths were caused by protein-energy malnutrition; 270,000 by iron deficiency anemia; 470,000 by vitamin A deficiency; 390,000 by zinc deficiency; 610,000 by unsafe water, sanitation, and hygiene; and 960,000 by malaria (*1*, *15*). Most of these deaths were among children and women. Deaths caused by individual risk factors are not additive because of multicausality. Recent studies have established exposure to biomass smoke during pregnancy as a risk factor for low birth weight (*27*, *28*). Although this relationship requires further confirmation and better quantification, if even a small fraction of the 260,000 low–birth weight deaths in SSA are caused by biomass use, it would increase the total disease burden substantially.
17. The rapid transitions are particularly effective in reducing mortality for two reasons. First, the transition to cleaner fuels has immediate benefits for child LRI

mortality, because LRI is an acute disease. The projected secular trend of LRI mortality in SSA is declining, mainly because of expectations of improved access to clinical case management using antibiotics (*29*). Therefore rapid transitions to cleaner fuels promptly save lives when the background rates are at their worst (i.e., in the early part of the projection period). Second, rapid transition to cleaner fuels also reduces adult female deaths from COPD significantly. Because COPD is a chronic disease, the health benefits of cleaner fuels accrue gradually over time (fig. S10). With rapid transitions to clean fuels, a larger number of adult women will witness complete benefits by 2030. Coupled with the increasing number of older women in Africa because of population growth and aging (*30*), the benefits of rapid transition in reducing COPD are amplified in the later part of the projection period.

18. These are reductions in particulate matter, which is the pollutant consistently associated with the most substantial negative health impacts (*31*). Carbon monoxide (CO) is also a harmful pollutant associated with biomass fuels. In measurements in Kenya, CO concentrations from charcoal were not significantly different from those from wood stoves (*31*). Promoting charcoal as a household fuel should be accompanied with education about safe practices.
19. In practice, a large number of future energy paths may be taken. Examples include transitions to improved ceramic wood stoves among wood users and to mixed fossil and biomass fuels among biomass users. Because ceramic stove and mixed-fuel use are less precisely defined alternatives, both interventions have substantial heterogeneity in health hazards. Under a specific definition, gradual and rapid transitions to ceramic wood stoves would avoid 400,000 and 1.2 million deaths, respectively; gradual and rapid transitions to mixed fossil and biomass fuels would avoid 900,000 and 2.8 million deaths. Well-designed and well-maintained ventilated stoves with chimneys may provide health benefits that are comparable to those from charcoal, but they have not been widely disseminated in Africa.
20. The cost of cooking with wood is highly variable because wood can be obtained for free, although in urban areas this not usually the case. Market prices for split fuel wood (*26*) indicate that annual cooking costs would be at least $200 if all wood were purchased. For comparison, using a combination of field observations and fuel prices reported in (*26*), we estimate a range of annual cooking costs for charcoal ($116 to $271), kerosene ($149 to $273), LPG ($274 to $374), and electricity ($230 to $467). The range in costs is a function of fuel prices, which depend on the quantity purchased, the cost of the stove (amortized over its expected lifetime using a 12% discount rate), and stove efficiencies [reported, for example, in (*32*)].
21. Estimates of child deaths that could have been avoided worldwide in 2000 if the coverage of a number of nutritional, environmental, and treatment interventions were increased to 99% of children at need show that various interventions ranged between 1 and >10% (*33*). Interventions with particularly large benefits include oral rehydration therapy, insecticide-treated bed nets, clean water and sanitation, antibiotics for treating pneumonia, micronutrient supplementation, and exclusive breastfeeding (*33*). If the same assumption of 99% coverage is applied, in 2000, charcoal (99% of current wood users switching to charcoal) would save 250,000 childhood LRI deaths (6% of all SSA child deaths) and petroleum-based fossil fuels (99% of all biomass users) would save 350,000 childhood LRI deaths (8% of all SSA child deaths).
22. K. R. Smith *et al.*, *Greenhouse Gases from Small-Scale Combustion in Developing Countries: Charcoal Kilns in Thailand* [Technical Report No. EPA-600/R-99-109, U. S. Environmental Protection Agency (EPA), Washington, DC, 1999].
23. O. C. Ferreira, *Economy and Energy* **20** (May-June 2000).
24. Charcoal can be made from many forms of biomass, including agricultural and timber-processing residues. There are some attempts to market such products in several countries in SSA, but market penetration is currently very low.
25. Government of India, *Census of India: 2001* (Central Statistical Office, Delhi, 2001).
26. Ministry of Energy (Kenya), *Study on Kenya's Energy Demand, Supply and Policy Strategy for Households, Small Scale Industries and Service Establishments: Final Report* (KAMFOR Company Limited, Nairobi, 2002).
27. E. Boy, N. Bruce, H. Delgado, *Environ. Health Perspect.* **110**, 109 (2002).
28. V. Mishra, X. Dai, K. R. Smith, L. Mika, *Ann. Epidemiol.* **14**, 740 (2004).
29. C. J. L. Murray, A. D. Lopez, in *The Global Burden of Disease*, C. J. L. Murray, A. D. Lopez, Eds. (Harvard School of Public Health on behalf of WHO and World Bank, Boston, 1996), pp. 325–395.
30. UN, *World Population Prospects: The 2002 Revision* (Population Division of the Department of Economic and Social Affairs of the UN Secretariat, 2004) available at www.un.org/popin/data.html.
31. M. Ezzati, B. Mbinda, D. Kammen, *Environ. Sci. Technol.* **34**, 578 (2000).
32. K. R. Smith *et al.*, *Greenhouse Gases From Small-Scale Combustion Devices in Developing Countries Phase IIa: Household Stoves in India* (Technical Report No. EPA-600/R-00-052, EPA, Washington, DC, 2000) available at: www.teriin.org/climate/emission.htm.
33. G. Jones *et al.*, *Lancet* **362**, 65 (2003).
34. This research was supported by the EPA Office of Atmospheric Programs, the Energy Foundation, and NIH (grant PO1-AG17625). The authors thank B. H. Singer for comments on early drafts of this article; K. R. Smith and D. M. Pennise for discussions on GHG methods; and R. E. Black, A. D. Lopez, and E. K. Mulholland for discussions on mortality and mortality projections.

Supporting Online Material
www.sciencemag.org/cgi/content/full/308/5718/98/DC1
Materials and Methods
Figs. S1 to S11
Tables S1 to S7
References

28 October 2004; accepted 10 February 2005
10.1126/science.1106881

A Late Jurassic Digging Mammal and Early Mammalian Diversification

Zhe-Xi Luo* and John R. Wible

A fossil mammal from the Late Jurassic Morrison Formation, Colorado, has highly specialized teeth similar to those of xenarthran and tubulidentate placental mammals and different from the generalized insectivorous or omnivorous dentitions of other Jurassic mammals. It has many forelimb features specialized for digging, and its lumbar vertebrae show xenarthrous articulations. Parsimony analysis suggests that this fossil represents a separate basal mammalian lineage with some dental and vertebral convergences to those of modern xenarthran placentals, and reveals a previously unknown ecomorph of early mammals.

The Late Jurassic was a time of rapid diversification of mammals. Insectivorous eutriconodontans, symmetrodontans, and dryolestoids, and the omnivorous multituberculates dominated the Late Jurassic mammalian faunas of Laurasia, displacing several more primitive mammaliaform lineages (*1*–*3*). Most mammals of the Jurassic and Early Cretaceous with preserved skeletal elements are generalized terrestrial mammals (*4*–*7*), except docodontans (*2*). Here, we report a new mammal with dental specializations like those known only from early Tertiary palaeanodonts and extant xenarthran and tubulidentate placental mammals, in addition to numerous fossorial (digging) skeletal features.

Carnegie Museum of Natural History, Pittsburgh, PA 15213, USA.

*To whom correspondence should be addressed. E-mail: luoz@carnegiemnh.org

Fruitafossor windscheffeli gen. et sp. nov. (*8*) is represented by relatively complete lower jaws (Fig. 1), incomplete cranium, and nearly 40% of the postcranial skeleton, including complete forelimb and manus (Fig. 2), several elements of the hindlimb and hindfoot (pes) (Fig. 3), and most of the thoracic, complete lumbar and sacral, and some caudal vertebrae. The new taxon is distinguishable from all known Mesozoic mammaliaforms in having tubular and single-rooted molars with open-ended roots (Fig. 1) and in that the molar crown lacks enamel. It differs from all known Mesozoic mammaliaforms in that the posterior opening of the mandibular canal is located anterior to the pterygoid crest in a broad meckelian groove. It differs from all Jurassic mammals (except *Hadrocodium*) (*9*) in having an inflected mandibular angle that is continuous with the pterygoid crest (Fig. 1). *Fruitafossor* is also distinguishable from and more primitive than the well-established and successively more inclusive hierarchies of eutherians (*10*, *11*), the crown therian clade of eutherians and metatherians (*7*, *12*, *13*), the trechnotherian clade (*Zhangheotherium* and crown therians) (*14*–*17*), and the theriiform clade (multituberculates and trechnotherians) (*18*), and is more plesiomorphic (*19*, *20*) than each of these clades by many characteristics.

The most prominent feature of *Fruitafossor* is its single- and open-rooted tubular molars with elliptical cross section, which suggests that the molars had a sustained and continuous growth in life and are similar to the teeth of extant armadillos (dasypodids), which feed primarily on insects and small invertebrates, supplemented with plants (*21*). We thus infer that *Fruitafossor* had a similar diet. Tubular molars of *Fruitafossor* also bear some resemblance to the living aardvark (*Orycteropus*) that is specialized for feeding on ants and termites, although some aardvark teeth are bilobed. Among early Tertiary mammals, palaeanodonts also developed similar (although fewer) single-rooted cheek teeth with elliptical cross section.

Fruitafossor was a fossorial mammal, with forelimb and manual structures for scratch digging (*22*, *23*) (Fig. 2). The scapular glenoid is saddle-shaped and formed by both the scapula and a separate coracoid. This suggests that the range of mobility of the shoulder joint was similar to that of monotremes, rather than that of moles. The large infraspinous fossa occupies much of the lateral aspect of the scapula, and the incipient supraspinous fossa is represented by a small area on the cranial border of the scapula. The acromion is platelike and forms a rigid articulation with the clavicle. The scapula is similar to those of monotremes (Fig. 3), *Morganucodon*, and *Haldanodon* in most characteristics. The humerus (Fig. 2) has a large deltopectoral crest and a hypertrophied tuberosity for the insertion of a large teres muscle that also has an extensive area of origination from the prominent posteroventral angle of the scapula. The distal portion of the humerus is very wide with well-developed epicondyles. The ectepicondyle has a hypertrophied supinator/extensor crest typical of small digging mammals (*22*, *23*). The ratio of epicondylar width to humeral length is about 65%, above the average of all extant fossorial mammals in this index (*22*). The ulna has an elongate and medially pointed olecranon process, presumably for very large triceps, dorsoepitrochlearis, and digital flexor muscles. The olecranon length is 66% that of the ulnar portion anterior to the semilunar notch, also above the average of all extant fossorial mammals (*22*).

The manus has only four digits. The carpals are all proximo-distally shortened, as are metacarpals 2 to 4 and phalanges of digits 2 to 4. The proximal phalanges of digits 2 and 3 are the shortest. However, metacarpal 1 and digit 1 phalanges are more gracile than the short and blocklike metacarpals and phalanges of digits 2, 3, and 4. The terminal (claw-bearing) phalanx is the longest on each digit; it has a large flexor tubercle. The distal portion of the terminal phalanx is dorso-ventrally flat, broad, and nearly spatulate, although its apex is not bifid. A very large sesamoid bone for the digital flexor muscle is present on the plantar aspect of the manus, and a single sesamoid is also present ventral to the metacarpo-phalangeal joint (Fig. 2). Shortened and robust metacarpals and phalanges, the proportion of phalanges within the digit (*22*), and the main features of the terminal phalanx (*24*) are all typical of fossorial mammals.

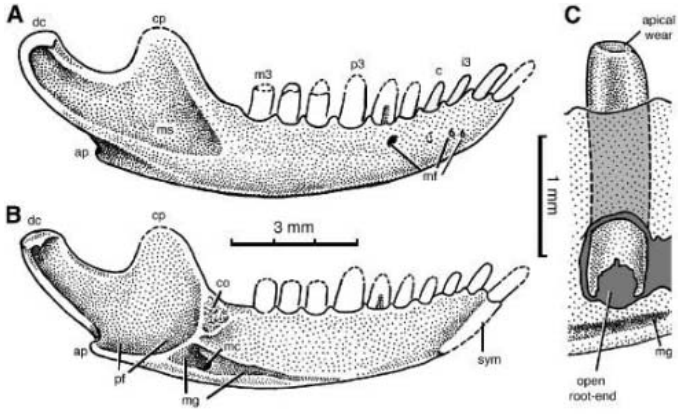

Fig. 1. *Fruitafossor windsheffeli* gen et sp. nov. (Holotype: LACM 150948): Reconstruction of left mandible and lower dentition (i3, c1, p3, m3) in (**A**) lateral and (**B**) medial views. (**C**) Tubular lower molar (m1) in medial view with open root-end exposed in the broken mandible [tubular structure of the molar is also corroborated by computerized tomography (CT) scans]. Abbreviations: ap, inflected angular process; co, facet for coronoid bone; cp, coronoid process; dc, dentary condyle; mc, posterior opening of mandibular canal; mf, anterior mental foramina; mg, meckelian groove; ms, masseteric fossa; pf, pterygoid fossa; sym, mandibular symphysis.

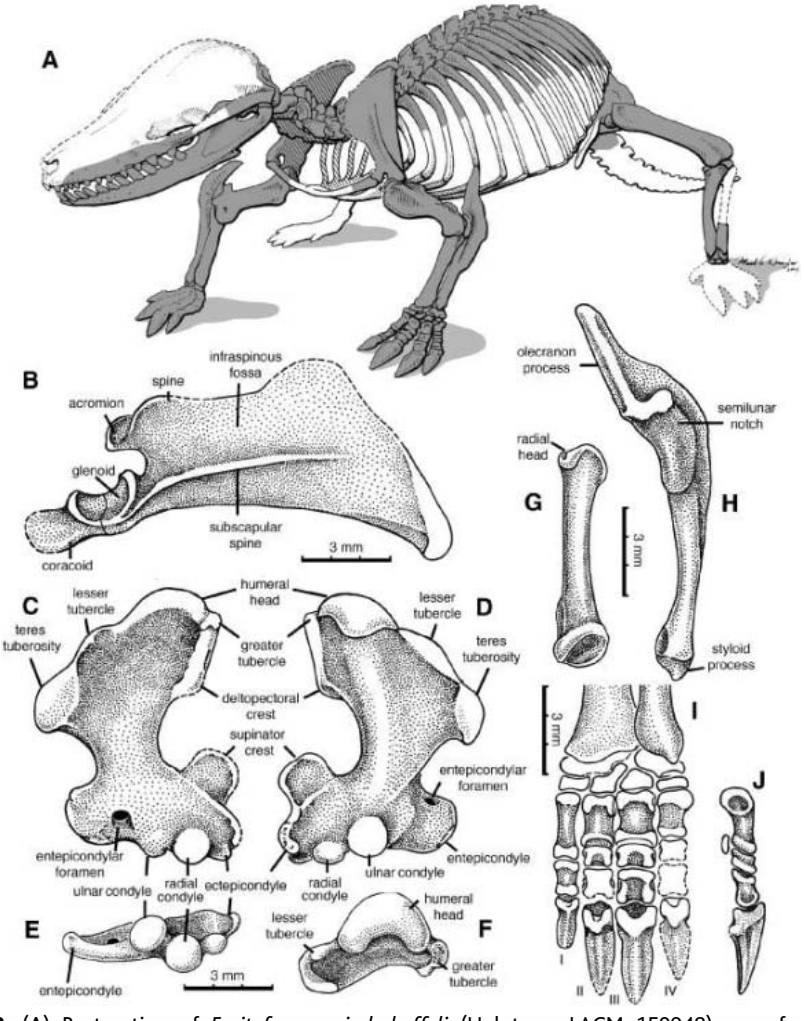

Fig. 2. (**A**) Restoration of *Fruitafossor windscheffeli* (Holotype: LACM 150948) as a fossorial mammal with forelimb and manual features for scratch digging and a dentition specialized for feeding on termites, other insects, and supplemented with plants (shaded parts of the skeleton are preserved in the type specimen); (**B**) left scapula in ventrolateral (tilted "posterolateral") view; (**C** to **F**) left humerus in ventral ("anterior"), dorsal ("posterior"), distal, and anteromedial views; (**G**) posteromedial view of left radius; (**H**) anterior view of left ulna; (**I**) plantar (ventral) view of left manus; and (**J**) lateral view of metacarpal and phalanges of digit 3.

However, many manual and digital features are also unique to *Fruitafossor*. The new taxon is distinctive from monotremes in the width-length proportion of metacarpal 1, which has nearly the same broad width as that of other metacarpals. Its short and broad metacarpals and phalanges differ from the gracile metacarpals and phalanges of eutriconodonts (*7*, *25*), multituberculates (*26*, *27*), and trechnotherians (*5*, *28*–*30*), which have less specialized terrestrial and other locomotory adaptations. The absence of a bifid claw differs from many (but not all) Cenozoic and extant placental mammals with digging adaptations (*22*, *23*).

Fruitafossor is characterized by a mixture of many plesiomorphies of premammalian mammaliaforms, a large number of eutriconodontan-like and monotreme-like features that are typical of basal mammals, and some derived features of tubulidentate and xenarthran placentals. Most of the scapular features are plesiomorphic and similar to those of morganucodontids, *Haldanodon*, and living monotremes (Fig. 3). The humerus lacks a distinctive humeral head but has a broad intertubercular groove; the two distal humeral condyles for the radius and ulna are spherical, widely separated, and arranged obliquely. In these features of the humerus, *F. windscheffeli* is similar to tritylodontids (*31*), tritheledontids (*32*), and morganuocodontids (*4*).

Fruitafossor shares plesiomorphic carpal features with eutriconodontans, multituberculates, and *Zhangheotherium* in the proportion of the hamate, lunate, and scaphoid, and lacks the derived features of the hypertrophied hamate

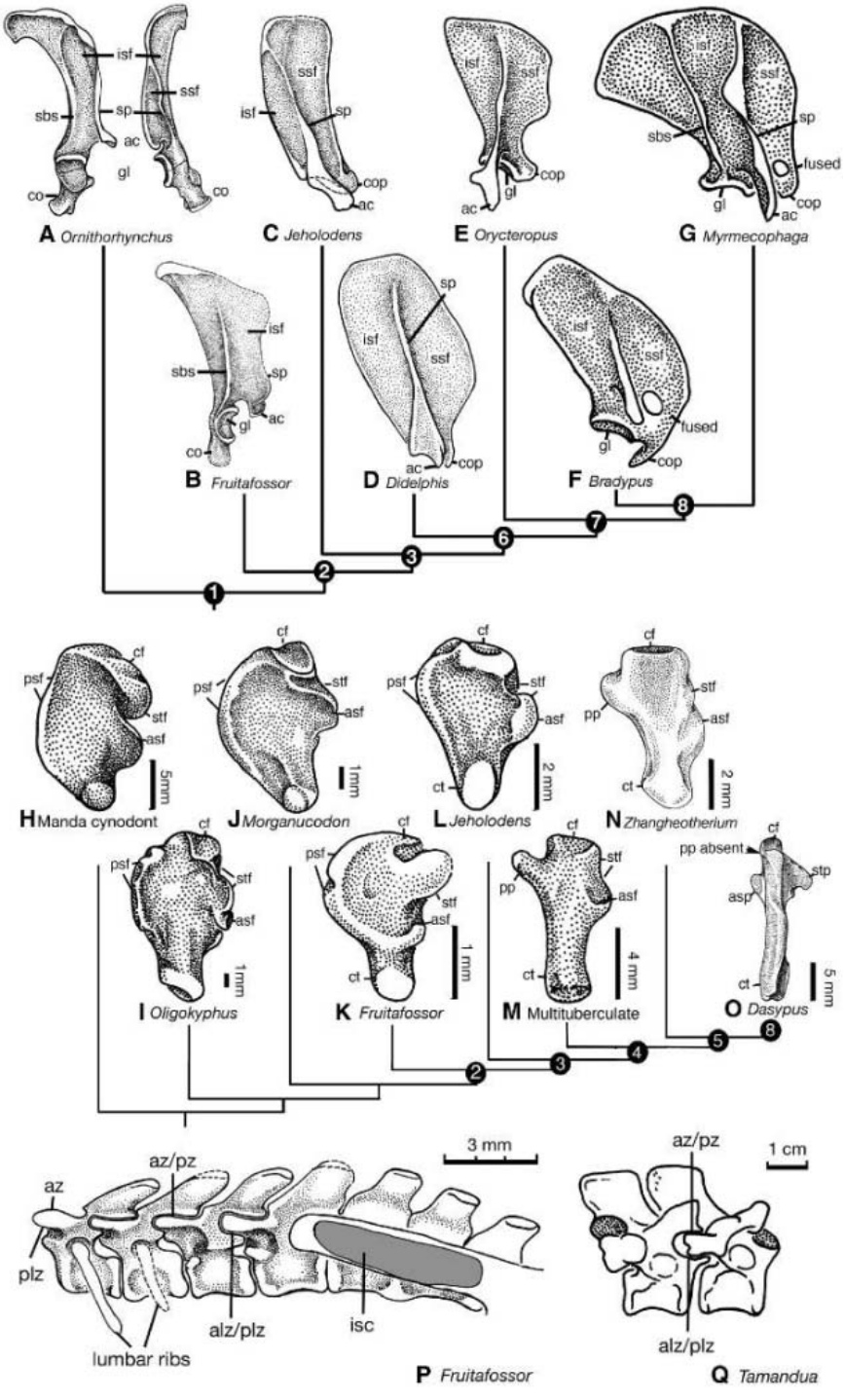

Fig. 3. Comparison of *Fruitafossor* with other mammals and premammalian cynodonts. (Top) Right scapulae of (**A**) monotreme *Ornithorhynchus* (platypus, lateral and anterior views); (**B**) basal mammal *Fruitafossor* (ventrolateral view); (**C**) eutriconodontan *Jeholodens* (lateral view); (**D**) marsupial *Didelphis* (opossum, lateral view); (**E**) placental *Orycteropus* (aardvark, lateral view); (**F**) placental *Bradypus* (sloth, ventral or plantar view); and (**G**) placental *Myrmecophaga* (giant anteater, lateral view). Abbreviations: ac, acromion process; co, coracoid bone; cop; coracoid process (reduced coracoid bone fused to scapula); gl, scapular glenoid joint surface; isf, infraspinous fossa; sbs, subscapular spine; sp, scapular spine; ssf, supraspinous fossa. (Middle) Calcanei (right, all in ventral view) of (**H**) the Manda cynodont; (**I**) mammaliamorph *Oligokyphus*; (**J**) mammaliaform *Morganucodon*; (**K**) *Fruitafossor*; (**L**) eutriconodontan *Jeholodens*; (**M**) a Late Cretaceous multituberculate; (**N**) trechnotherian *Zhangheotherium*; and (**O**) placental *Dasypus* (armadillo). [(H), (I), and (J) are redrawn from (*12*).] (Bottom) (**P**) Lumbars, mobile lumbar ribs, and sacral region of *Fruitafossor*. (**Q**) Lumbar vertebrae of placental *Tamandua* [after (*34*)]. Abbreviations: asf, astragalar facet; asp, astraglar process (astragalar facet is on the dorso-medial aspect of this process); alz/plz, lateral zygapophyseal vertebral articulation (derived xenarthran condition); az, prezygapophysis; az/pz, primitive mammalian zygapophyseal articulation; cf, calcaneocuboid facet; ct, calcaneal tuber; isc, ilio-sacral contact; pp, peroneal process; psf, peroneal shelf; stf, vertically oriented sustentacular facet; stp, sustentacular process (the horizontally oriented sustentacular facet is on the dorsal aspect of this process). Node (1) Crown Mammalia; Node (2) clade defined by common ancestor of *Fruitafossor* and crown Theria; Node (3) clade defined by ancestor of *Jeholodens* and crown Theria: enlargement of supraspinous fossa; acromial process extending beyond the glenoid; glenoid uniformly concave (not saddle-shaped); Node (4) Theriiformes, with synapomorphies of distinctive peroneal process (instead of a broad peroneal shelf), elongation of calcaneal tuber; Node (5) Trechnotherians; Node (6) Crown Theria with synapomorphies of shelflike sustentacular structure and a partial dorsal placement of sustentacular facet (instead of a medial placement); Node (7) Crown placental synapomorphy: loss of peroneal process or shelf; Node (8) Xenarthra: coracoid process fused with cranial border of scapula.

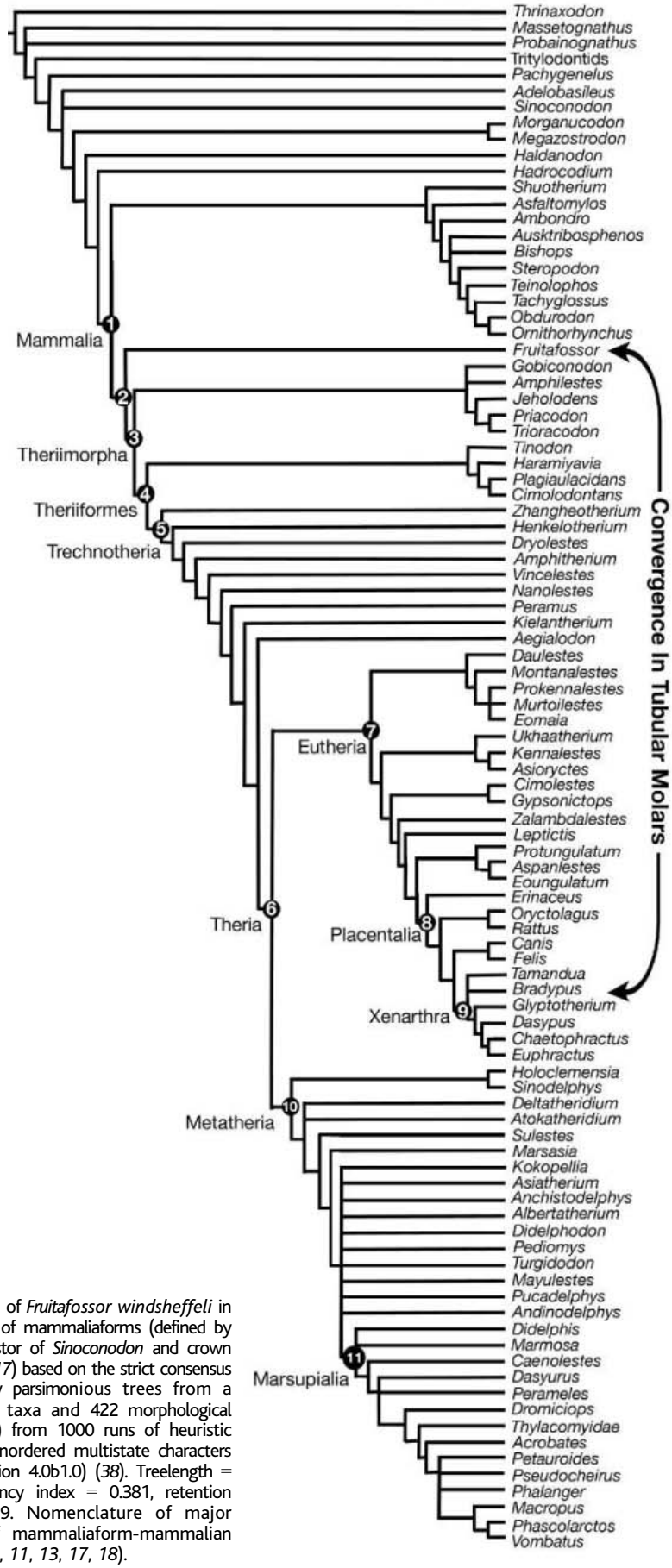

Fig. 4. Position of *Fruitafossor windsheffeli* in the phylogeny of mammaliaforms (defined by common ancestor of *Sinoconodon* and crown mammals) (*3*, *17*) based on the strict consensus of 184 equally parsimonious trees from a matrix of 96 taxa and 422 morphological characters (*20*) from 1000 runs of heuristic search, with unordered multistate characters by PAUP (version 4.0b1.0) (*38*). Treelength = 2111, consistency index = 0.381, retention index = 0.789. Nomenclature of major hierarchies of mammaliaform-mammalian clades after (*7*, *11*, *13*, *17*, *18*).

of metatherians or the enlarged trapezium of eutherians (*7*, *11*, *12*). The exposed portion of the scapula is similar to that of docodontans (*2*). Its calcaneus, although autapomorphic in some regards, bears strong similarities to those of *Morganucodon* and tritylodontids (*4*, *12*) and is far more primitive than the calcanei of multituberculates (*26*, *27*), *Zhangheotherium* (*29*), metatherians, and eutherians (*7*, *11*) (Fig. 3). Its lumbar vertebrae bear unfused and mobile lumbar ribs down to the penultimate lumbar vertebra (Fig. 3P), a feature of cynodonts (*31*) and monotremes.

Fruitafossor is similar to eutriconodontans and some spalacotheriid symmetrodontans in the rounded posteroventral margin of the mandible that is continuous with the dentary condyle (Fig. 1). The medial side of the mandible has a distinctive pterygoid fossa, a plesiomorphic feature of many other Late Jurassic mammals. However, the mandible has an anteriorly placed and inflected angle. The posterior opening of the mandibular canal is placed in a very broad meckelian groove, and anterior to the pterygoid fossa. These features are not known for any Jurassic and Cretaceous mammals and are autapomorphic for this new mammalian lineage.

Fruitafossor is similar to tubulidentates (aardvark) and armadillos (dasypodids) in its tubular molars, each with a single and open root (Fig. 1). Its lumbar vertebrae have a lateral anterior- and posterior-zygapophyseal articulation, in addition to the typical pre- and postzygapophyseal intervertebral articulations of most mammals (Fig. 3, P and Q). These are similar to the xenarthrous thoracic and lumbar vertebrae that are otherwise unique features for the placental order of Xenarthra (sloths, anteaters, and armadillos) (*33*, *34*). Given that *Fruitafossor* is not closely related to xenarthrans (Fig. 4), it must have independently developed this type of intervertebral articulation, including the anterior and posterior lateral zygapophyseal joints.

Fruitafossor differs from tubulidentates and armadillos in a long list of osteological characters (*20*). The presence of a broad meckelian groove indicates that the middle ear bones were still connected with the lower jaw in *Fruitafossor*. The round posterior margin of the mandible is different from the posteriorly positioned angle of most placentals, including aardvarks, sloths, and armadillos. *Fruitafossor* lacks the fusion of proximal caudal vertebrae with the sacral vertebrae, and the fusion of ischium with the caudals that are important apomorphies of xenarthrans. The medially placed sustentacular and astragalar facets, as well as the broad peroneal shelf on the calcaneus, indicate that *Fruitafossor* lacked the superpositional relationships of the calcaneus and astragalus of modern placentals. No trechnotherian mammals (including marsupials and placentals) have any of the primitive characteristics of the forelimbs seen in *Fruitafossor*.

We incorporated the dental and vertebral similarities of *Fruitafossor*, tubulidentates, and xenarthrans into global parsimony analysis of morphological features known for Mesozoic mammals and the major groups of extant mammals (*3*, *7*, *17*). *Fruitafossor* is resolved to be a basal mammal emerging in the Late Jurassic mammalian diversification and has no closer relationship to placental xenarthrans than have other nonplacental trechnotherians (Fig. 4), and is not a eutherian, let alone a xenarthran.

Xenarthrous intervertebral articulations help the vertebral column resist torsion produced by digging (*35*). We suggest that the open and single-rooted tubular molars and the xenarthrous lumbar vertebrae in *Fruitafossor* are convergent features to those of some modern placentals. So that it should not be misconstrued, we emphasize that *Fruitafossor* is not related to modern placental xenarthrans and has no bearing on the timing of the divergence of xenarthran placentals (*36*, *37*).

References and Notes

1. G. G. Simpson, *Mem. Peabody Mus. Yale Univ.* **3**, 1 (1929).
2. T. Martin, B. Krebs, Eds., *Guimarota: A Jurassic Ecosystem* (Verlag Dr. Friedrich Pfeil, Munich, 2000).
3. Z. Kielan-Jaworowska, R. L. Cifelli, Z.-X. Luo, *Mammals from the Age of Dinosaurs: Origins, Evolution and Structure* (Columbia Univ. Press, New York, 2004).
4. F. A. Jenkins Jr., F. R. Parrington, *Philos. Trans. R. Soc. London* **273**, 387 (1976).
5. Y.-M. Hu, Y.-Q. Wang, C.-K. Li, Z.-X. Luo, *Vertebr. PalAsiat.* **36**, 102 (1998).
6. A. Weil, *Nature* **416**, 798 (2002).
7. Z.-X. Luo, Q. Ji, J. R. Wible, C.-X. Yuan, *Science* **302**, 1934 (2003).
8. Etymology: "*Fruita*," for provenance of this new mammal near the town of Fruita, Colorado; "*- fossor*," after the fossorial (digging) specialization of the forelimbs and vertebrae; the specific name "*windscheffeli*" is in honor of Wally Windscheffel, who discovered the holotype specimen. Systematics: Class Mammalia, Order and Family *incertae sedis*, Genus et Species nov. *Fruitafossor windscheffeli*. Holotype: Natural History Museum of Los Angeles County (LACM) 150948 (Figs. 1 and 2), an individual represented by lower jaws, incomplete cranium, and about 40% of the postcranial skeleton. Locality and age: the Fruita Paleontology Area, Fruita, Colorado, USA; mudstones of the Morrison Formation, Kimmeridgian, about 150 million years (ma).
9. Z.-X. Luo, A. W. Crompton, A.-L. Sun, *Science* **292**, 1535 (2001).
10. M. J. Novacek *et al.*, *Nature* **389**, 483 (1997).
11. Q. Ji *et al.*, *Nature* **416**, 816 (2002).
12. F. S. Szalay, *Evolutionary History of the Marsupials and an Analysis of Osteological Characters* (Cambridge Univ. Press, Cambridge, 1994).
13. G. W. Rougier, J. R. Wible, M. J. Novacek, *Nature* **396**, 459 (1998).
14. D. R. Prothero, *Bull. Am. Mus. Nat. Hist.* **167**, 277 (1981).
15. Y.-M. Hu, Y.-Q. Wang, Z.-X. Luo, C.-K. Li, *Nature* **390**, 137 (1997).
16. M. C. McKenna, S. K. Bell, *Classification of Mammals above the Species Level* (Columbia Univ. Press, New York, 1997).
17. Z.-X. Luo, Z. Kielan-Jaworowska, R. L. Cifelli, *Acta Palaeontol. Pol.* **47**, 1 (2002).
18. T. B. Rowe, *J. Vertebr. Paleontol.* **8**, 241 (1988).
19. Diagnosis. Lower dentition: i3, c1, p3, m3. Upper dentition: I?, C1, P3, M3. Differs from all known Mesozoic mammaliaforms and most Cenozoic mammals (except some xenarthans and tubulidentates) in molars with a single and open-ended root and without enamel. Differs from all known mammaliaforms (except xenarthrans) in having an extra ("xenarthrous") articulation between lumbar vertebrae. More derived than most mammaliaforms in lacking the medial ridge above the postdentary trough and in the presence of a medial pterygoid fossa on the mandible. Distinguishable from multituberculates, eutriconodontans, and spalacotheriids in having a mandibular angle. Differs from mammaliaforms (except *Hadrocodium*) and Jurassic and Cretaceous cladotherians (except *Montanalestes* and metatherians) in the inflection of this angle. Differs from monotremes in the absence of a deeply excavated masseteric fossa, in having gracile metacarpal and phalanges of digit 1, and in the absence of the parafibular process of the fibula. Differs from all Cenozoic fossil therians (including palaeanodonts) and extant placentals (including tubulidentates and xenarthrans) in retaining a long list of plesiomorphies [full differential diagnosis in (*20*)].
20. Supporting material is available on *Science* Online.
21. R. M. Nowak, J. L. Paradiso, *Walker's Mammals of the World* (Johns Hopkins Univ. Press, Baltimore, MD, ed. 4, 1983).
22. M. Hildebrand, in *Functional Vertebrate Morphology*, M. Hildebrand, D. M. Bramble, K. F. Liem, D. B. Wake, Eds. (Belknap, Cambridge, MA, 1985), pp. 89–109.
23. K. D. Rose, in *Encyclopedia of Paleontology*, R. Singer, Ed. (Fitzroy Dearborn, Chicago and London, 1999), vol. 1, pp. 220–226.
24. N. McLeod, K. D. Rose, *Am. J. Sci.* **293**, 300 (1993).
25. Q. Ji, Z.-X. Luo, S.-A. Ji, *Nature* **398**, 326 (1999).
26. D. W. Krause, F. A. Jenkins, *Bull. Mus. Comp. Zool.* **150**, 199 (1983).
27. Z. Kielan-Jaworowska, P. P. Gambaryan, *Fossils Strata* **36**, 1 (1994).
28. G. W. Rougier, Q. Ji, M. J. Novacek, *Acta Geol. Sin.* **77**, 7 (2003).
29. Z.-X. Luo, Q. Ji, *J. Mamm. Evol.*, in press.
30. B. Krebs, *Berl. Geowiss. Abh.* **A133**, 1 (1991).
31. H.-D. Sues, thesis, Harvard University (1983).
32. C. E. Gow, *Palaeontol. Afr.* **37**, 93 (2001).
33. K. D. Rose, R. J. Emry, in *Mammal Phylogeny: Placentals*, F. S. Szalay, M. J. Novacek, M. C. McKenna, Eds. (Springer, Berlin, 1993), pp. 81–101.
34. T. J. Gaudin, *Fieldiana (Geol. New Ser.)* **41**, 1 (1999).
35. T. J. Gaudin, A. A. Biewener, *J. Morphol.* **214**, 63 (1992).
36. S. Kumar, S. B. Hedges, *Nature* **392**, 917 (1998).
37. W. J. Murphy *et al.*, *Science* **294**, 2348 (2001).
38. D. L. Swofford, *PAUP*: Phylogenetic Analysis Using Parsimony (and Other Methods)*, version 4.0b1.0 (Sinauer, Sunderland, MA, 2000).

39. We thank W. Windscheffel and C. Safris for discovering this fossil; W. Windscheffel and A. Henrici for preparation; T. Ryan and A. Grader for access to the CT Scanning Facility at the Pennsylvania State University; G. Callison and the Grand Junction office of the Bureau of Land Management for support; T. Gaudin, T. Martin, and J. Rawlins for numerous discussions; S. McLeod, X.-M. Wang, and L. Chiappe for access to research collections; anonymous reviewers for their improvement of the manuscript; and M. Klingler for illustrating Fig. 2A. Supported by NSF (USA) and Carnegie Museum (Z-X.L. and J.R.W.), National Geographic Society (USA), and National Natural Science Foundation (China) (Z.-X.L.).

Supporting Online Material

www.sciencemag.org/cgi/content/full/308/5718/103/DC1
SOM Text
Matrix S1
PAUP Search Results
References
Movies S1 and S2

20 December 2004; accepted 7 February 2005
10.1126/science.1108875

Comparison of Fine-Scale Recombination Rates in Humans and Chimpanzees

Wendy Winckler,[1,3,5]* Simon R. Myers,[6]* Daniel J. Richter,[5] Robert C. Onofrio,[5] Gavin J. McDonald,[1,5] Ronald E. Bontrop,[7] Gilean A. T. McVean,[6] Stacey B. Gabriel,[5] David Reich,[3,5] Peter Donnelly,[6]†,‡ David Altshuler[1–5]†,‡

We compared fine-scale recombination rates at orthologous loci in humans and chimpanzees by analyzing polymorphism data in both species. Strong statistical evidence for hotspots of recombination was obtained in both species. Despite ~99% identity at the level of DNA sequence, however, recombination hotspots were found rarely (if at all) at the same positions in the two species, and no correlation was observed in estimates of fine-scale recombination rates. Thus, local patterns of recombination rate have evolved rapidly, in a manner disproportionate to the change in DNA sequence.

Recombination shapes genomic diversity, breaking up ancestral linkage disequilibrium (LD) and creating new combinations of alleles on which natural selection can act. As in yeast (*1*), recombination in the human genome principally occurs at so-called "hotspots" of recombination (*2*, *3*); experimentally characterized examples include the β-globin (*4*) and human leukocyte antigen (HLA) regions (*5*, *6*). Because direct observation of recombination hotspots is laborious, only with the recent development of statistical methods to estimate recombination rates from population genetic (polymorphism) data (*2*, *3*) has it become practical to study fine-scale recombination rates on a genomic scale.

The molecular determinants of hotspot location and activity are largely unknown. In yeast, chromatin structure influences initiation of double-strand breaks (DSBs) at hotspots (*7*). Directed mutagenesis of single nucleotides can disrupt hotspot activity (*8*), and different alleles of the same locus can show differences in recombination (*9*–*11*), indicating strong sequence specificity. However, no sequence motif has been identified as causing recombination hotspots. The observation of meiotic drive at hotspots has led to the hypothesis that hotspots

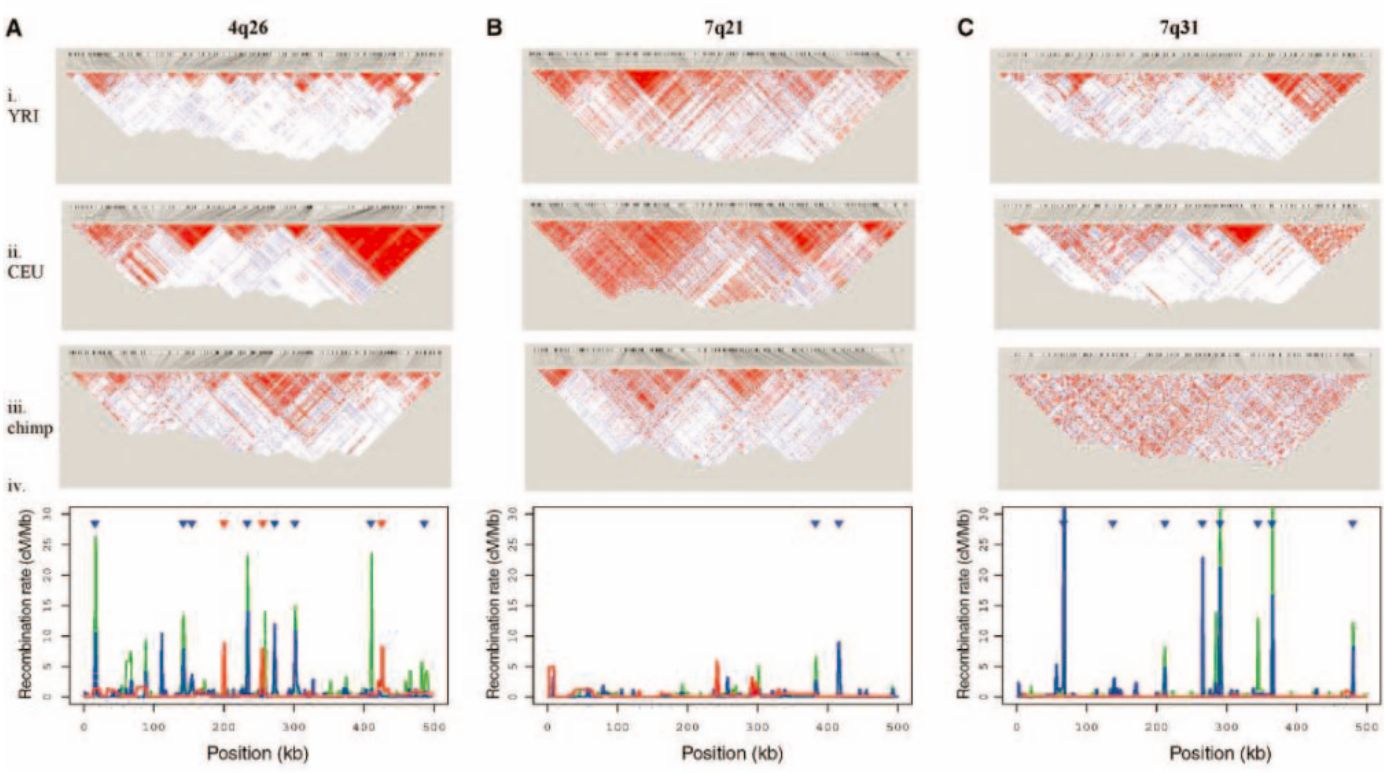

Fig. 1. Comparison of LD patterns and recombination rates for three 500-kb ENCODE regions (**A** through **C**). Pairwise LD of common SNPs (frequency > 0.05) in Yoruba sampled in Ibadan, Nigeria (YRI) (row i), CEU (row ii), and western chimpanzee (row iii) is expressed as D′, with red indicating LD that is strong (D′ > 0.8) and statistically significant [logarithm of the odds ratio for linkage (LOD) score > 2.0] (*14*). For comparability, genotype data for CEU and YRI were thinned to match the spacing in the chimpanzee data. Locations of SNPs are shown as lines above each plot. Comparison of estimated recombination rates (row iv from the complete data) for YRI (green), CEU (blue), and chimpanzees (red). Blue arrows indicate positions of human hotspots with statistical significance $P < 0.01$ in one human population and $P < 0.05$ in both human populations. Red arrows indicated positions of chimpanzee hotspots with statistical significance $P < 0.01$.

may be short-lived because of evolutionary selection against sites that initiate DSBs (*9*, *12*).

We compared fine-scale recombination patterns inferred from polymorphism data at orthologous loci in western chimpanzees and in two human population samples. Information about the DNA samples, regions examined, and polymorphisms studied is in table S1; details about experimental and analytic methods are provided online (*13*). Briefly, single-nucleotide polymorphisms (SNPs) were ascertained by resequencing in both species and by querying public databases. To validate SNPs and to expand the sample, we genotyped SNPs in a larger panel of humans and chimpanzees. Patterns of LD among SNPs were expressed using the pairwise metric |D′|, representing the extent of historical recombination among alleles (*14*). Statistical evidence for hotspots of recombination, as well as quantitative estimates of local rates of recombination, was calculated as in (*2*). Informally, recombination rates are estimated from polymorphism data by fitting an approximation to the coalescent model. Recombination rate estimates were obtained from the program LDhat by allowing a different recombination rate between each adjacent pair of SNPs and using Bayesian Markov chain Monte Carlo methods; statistical significance of a putative hotspot was calculated by comparing the fit of empirical genotype data to models that incorporate a constant recombination rate and those that allow variation in recombination rates (LDhot). The validity of this approach was previously confirmed empirically and through simulation (*2*). Whereas sperm typing estimates

Table 1. Recombination rates estimated from population genetic data at known human hotspots. Rates estimated using LDhat (*2*) in Utah residents with ancestry from northern and western Europe from the CEPH resource (CEU), Beni sampled from Nigeria (BEN), and western African chimpanzees. *P* values were obtained by performing a one-sided test for the presence of a 2-kb hotspot centered at the position of the known human hotspot (*2*), based on 10,000 simulations. "Chimp sites" indicates the number of SNPs found solely by resequencing in the region of the human hotspots. The estimated rates are centered at the positions of the known human hotspots. NA, not applicable.

Hotspot	Hotspot width (kb)	Statistical significance for test of hotspot presence (*P* value)			Estimated rate (cM/Mb)		Chimp sites
		CEU	BEN	Chimp	CEU	Chimp	
DNA2	1.3	0.107	0.127	1	6.38	0.46	12
DNA3	1.2	<0.001	0.003	NA	20.73	0.44	2
DMB1	1.8	0.009	0.057	0.182	11.83	1.54	7
DMB2	1.2	<0.001	0.007	1	58.08	1.50	10
TAP2	1.2	<0.001	<0.001	0.028	23.78	0.25	14
β-Globin	1.7	<0.001	<0.001	1	46.08	1.37	16

[1]Department of Molecular Biology and Center for Human Genetic Research, [2]Diabetes Unit, Department of Medicine, Massachusetts General Hospital, Boston, MA 02114–2622, USA. [3]Department of Genetics, [4]Department of Medicine, Harvard Medical School, Boston, MA 02115, USA. [5]Program in Medical and Population Genetics, Broad Institute of Harvard and MIT, Cambridge, MA 02141–2023, USA. [6]Department of Statistics, University of Oxford, Oxford OX1 3TG, UK. [7]Department of Comparative Genetics and Refinement, Biomedical Primate Research Centre, 2280 GH Rijswijk, Netherlands.

*These authors contributed equally to this work.
†These authors jointly directed the project.
‡To whom correspondence should be addressed. E-mail: donnelly@stats.ox.ac.uk (P.D.); altshuler@molbio.mgh.harvard.edu (D.A.)

Table 2. Summary of findings for identified ENCODE hotspots. Each row corresponds to a different hotspot identified using LDhot *P* values and requiring $P < 0.01$ in one human population, $P < 0.05$ in both (human hotspots), or $P < 0.01$ (chimpanzee hotspots). Throughout, we assume the effective population size (N_e) = 10,000 (CEU), 16,000 (YRI), 12,000 (chimpanzees) (*13*). Estimated hotspot intensity: LDhat estimates of rates of hotspot intensity in humans (averaged over CEU and YRI rates) and chimpanzees are averaged over the 2 kb around the hotspot center. Rate estimates by Hotspotter (*3*) are based on fitting a two-rate model, using the parameters above. Statistical significance for hotspots: *P* values were estimated using LDhot (*2*) or Hotspotter. Hotspotter *P* values are based on data phased using PHASE v2.0, obtained by fitting a two-rate model with a 2-kb hotspot centered at the position identified by LDhot, using data for the 25 sites on either side of the hotspot center. *P* values are calculated based on a one-sided likelihood ratio test, assuming a standard mixture of chi-squared distributions for the test statistic. Estimated power: For the hotspots discovered in humans, estimated power in chimpanzee to detect a hotspot of the same intensity with $P < 0.05$, and the probability of obtaining a *P* value lower than that observed in chimps ($P < P_{obs}$). For hotspots discovered in chimpanzee, the estimated power to detect a human hotspot of the same intensity for the CEU population (estimates of power based on the YRI data were very similar), as above. E stands for $\times 10$ to the value stated after it (e.g., 1.28×10^{-9}).

Hotspot information			Estimated hotspot intensity (cM/Mb)				Statistical significance for hotspots (*P* value)						Estimated power	
			Human (average)		Chimp		YRI		CEU		Chimp		Other species	
Chromosomal location	Nucleotide position (kb)	Species	LDhat	Hotspotter	LDhat	Hotspotter	LDhot	Hotspotter	LDhot	Hotspotter	LDhot	Hotspotter	LDhot ($P < 0.05$)	LDhot ($P < P_{obs}$)
4q26	16.00	Human	16.942*	13.092*	1.438	4.430	0.001*	1.28E-09*	0.001*	1.25E-05*	0.120	0.007*	0.802	0.864
4q26	141.96	Human	10.673*	26.479*	0.099	0.000	0.001*	3.84E-10*	0.005*	7.09E-14*	1.000	1.000	0.577	0.948
4q26	154.25	Human	3.005	6.719*	0.099	0.000	0.050*	0.002*	0.003*	0.010*	1.000	1.000	0.229	0.793
4q26	233.21	Human	17.739*	12.351*	0.120	0.000	0.001*	6.46E-13*	0.001*	2.34E-04*	1.000	1.000	0.807	0.988
4q26	272.50	Human	9.151*	8.417*	0.086	2.039	0.020*	6.44E-07*	0.003*	4.41E-06*	1.000	0.036*	0.521	0.938
4q26	301.25	Human	13.171*	11.438*	0.082	0.478	0.001*	8.99E-08*	0.002*	3.62E-04*	1.000	0.186	0.670	0.965
4q26	409.96	Human	10.517*	4.053*	0.463	0.000	0.001*	5.51E-09*	0.030*	0.038*	1.000	1.000	0.571	0.947
4q26	485.96	Human	1.486	1.182	0.650	3.322	0.001*	0.371	0.007*	0.204	1.000	0.116	0.132	0.633
7q21	382.37	Human	4.578	2.834	0.073	0.000	0.002*	0.001*	0.030*	0.179	1.000	1.000	0.321	0.918
7q21	415.87	Human	7.107*	10.531*	0.207	0.091	0.007*	3.93E-07*	0.020*	3.84E-07*	0.290	1.000	0.435	0.590
7q31	67.00	Human	35.995*	28.649*	0.111	2.915	0.001*	3.79E-11*	0.001*	9.36E-19*	0.160	0.007*	0.922	0.952
7q31	137.25	Human	0.831	1.743	0.054	1.069	0.001*	0.007*	0.008*	0.229	1.000	0.173	0.090	0.564
7q31	211.75	Human	4.971	7.192*	0.049	0.716	0.001*	0.002*	0.002*	3.04E-07*	0.290	0.217	0.339	0.479
7q31	265.25	Human	15.546*	13.410*	0.027	0.457	0.001*	2.26E-07*	0.001*	2.11E-12*	0.270	0.248	0.758	0.834
7q31	290.25	Human	31.250*	8.810*	0.003	0.145	0.001*	1.74E-09*	0.001*	0.002*	1.000	0.366	0.892	0.995
7q31	344.50	Human	6.501*	5.408*	0.091	1.149	0.001*	8.34E-06*	0.050*	0.306	1.000	0.306	0.408	0.925
7q31	364.50	Human	28.034*	12.880*	0.081	0.000	0.001*	4.85E-17*	0.001*	4.60E-05*	1.000	1.000	0.872	0.993
7q31	479.75	Human	11.202*	6.392*	0.051	0.000	0.001*	1.05E-09*	0.001*	3.12E-07*	1.000	1.000	0.597	0.952
4q26	200.00	Chimp	0.195	0.459	9.036*	9.977*	1.000	0.444	1.000	0.441	0.003*	1.51E-08*	0.926	0.994
4q26	255.50	Chimp	0.314	0.693	7.928*	14.631*	0.380	1.000	1.000	0.464	0.002*	6.97E-07*	0.878	0.987
4q26	425.25	Chimp	0.204	0.553	9.033*	8.859*	0.060	0.329	1.000	1.000	0.001*	2.88E-05*	0.926	0.994

male recombination rates in the present, coalescent approaches estimate rates that are averaged over sexes and over many generations.

We first collected polymorphism data spanning known human recombination hotspots in HLA and β-globin (*5*, *6*, *15*, *16*) and at the orthologous loci in western chimpanzees. As expected, estimated recombination rates were markedly increased in humans at the sites of known hotspots (Table 1 and fig. S1). At the orthologous locations in chimpanzee, however, there was no significant evidence for a hotspot ($P > 0.01$), and the estimated recombination rate was low (Table 1, fig. S1). We did detect ($P < 0.005$) a hotspot in the chimpanzee ~1.7 kb away from, but not overlapping with, the β-globin hotspot in humans (fig. S1). Two of the six hotspots described here had previously been studied in chimpanzee (*17*, *18*) with similar results (*19*).

To determine whether the lack of correspondence in the location of hotspots was general and to increase the power to detect correlation in fine-scale recombination rates across species, we examined three contiguous 500-kb regions (on chromosomes 4q26, 7q21, and 7q31) studied by the HapMap and ENCODE projects (*20*). These regions were selected without prior knowledge of LD or diversity in either species.

Qualitatively similar patterns of LD were observed in human and chimpanzee: Both had regions of strong LD (haplotype "blocks") (*21*) interspersed with sites of LD breakdown. Although overall patterns were similar, there was little alignment in the locations and extent of LD breakdown (Fig. 1, fig. S2). In humans, there is extensive LD in ENCODE region 7q21, but much less in chimpanzee. Conversely, in chimpanzee there is extensive LD in ENCODE region 7q31, but not in the human samples. The ENCODE region on chromosome 4 shows similar overall extent of LD in both species, but little alignment where LD is extensive and where it breaks down.

Statistical support was obtained for 18 hotspots in humans and 3 in chimpanzees ($P < 0.01$). In both species, most recombination events were estimated to occur over a small fraction of the overall sequence, with greater concentration of recombination activity in the two human samples than in the chimpanzee (fig. S3).

Although hotspots were detected in both species, there was little concordance in the location of hotspots in humans and in chimpanzee. At the site of a recombination hotspot in one species, the recombination rate in the other species is typically lower by a factor of 10 to 60 and not above baseline.

We analyzed the genotype data using a second analytic method (*3*) and obtained very similar estimates (Table 2). This second method provided statistical evidence ($P < 0.05$) for a hotspot in chimpanzee at 3 of the 18 human hotspots. Examination of obligate recombination events at these hotspots indicates that one of the 18 human hotspots may be a site of historical recombination in chimpanzee, and the other two are likely false positives of the method (fig. S4). Moreover, given 21 hotspots, two species, and two analytical methods, some overlap in the sites of recombination might occur by chance.

Finally, we estimated recombination rates in both species, averaged over 10-kb windows across these three 500-kb regions and 14 additional 160-kb regions previously described (*13*). No evidence for correlation in recombination rates was observed across the two species using the Spearman rank correlation test ($P > 0.1$).

We considered three possible artifacts that could erroneously cause a lack of correspondence in the estimated locations of hotspots: first, that the regions we studied were unusual, with low rates of sequence similarity between humans and chimpanzees; second, that population structure in the chimpanzee sample might confound analysis; and third, that the data and analytic methods provide insufficient statistical power to detect hotspots even where present.

Sequence identity ranged from 98.4 to 98.8%, with a mean of 98.6%, similar to previous estimates (*22*, *23*). The three 500-kb regions occur at nearly identical chromosomal positions in both species, which makes it unlikely that rearrangements (e.g., centromeric to telomeric) explain differences in recombination rates.

We genotyped 40 loci to assess population structure in the chimpanzee sample (*13*). Analyzed with Structure 2.0 (*24*), the best-fitting demographic model was that of a single population. When genotypes from two central African chimpanzees were added, two subpopulations were predicted, and the confounding individuals were identified. Analysis of chimpanzee pedigrees and genotype data ruled out cryptic relatedness.

Low power to detect hotspots, or a high rate of false positives, could cause a lack of overlap in the observed locations of hotspots in two species, although sensitivity and/or specificity would have to be extremely poor to explain the nearly complete lack of correspondence across 21 hotspots. Both sensitivity and specificity are thought to be good when analyzing human data, on the basis of hotspot analysis previously validated by sperm typing. We assessed power to detect hotspots in chimpanzee (where we lack sperm-typing data) in several ways. First, we used the standard coalescent to simulate genotype data based on hotspots of the same intensity as the human HLA and β-globin hotspots, matching the chimpanzee data in terms of sample size, ascertainment, and number of sites. In these simulations, rates as low as those seen in the actual chimpanzee data were observed less than 2% of the time.

Second, we evaluated power using the empirical genotype data from human and chimpanzee by juxtaposing collections of genotypes separated by different distances on the estimated fine-scale genetic map, artificially creating hotspots of known intensities. Figure 2 shows the relation between the estimated hotspot intensity and the fraction of simulations in which statistically significant evidence for recombination hotspots was obtained (table S2). Power in the chimpanzee is >80% for 8 of the human hotspots and >50% for 14 hotspots. At the sites of the chimpanzee hotspots, power in humans is >87%. These analyses make it extremely unlikely that the limited correspondence observed across 21 hotspots is an artifact of low power [(*13*); figs. S3 and S5].

It is unlikely that the hotspots identified are false positives of the methods used, for a number of reasons: Hotspot detection results are highly congruent across both human population samples when analyzed with two computational methods (Table 2), and hotspots align well with patterns of LD breakdown (Fig. 1). Perhaps the strongest argument that claimed hotspots are not false positives is that a completely model-free approach that makes no assumptions about demography (*25*) confirms that for both human and chimpanzee there is a clustering of obligate recombination events at detected hotspots (fig. S4).

The lack of correlation in recombination patterns between humans and chimpanzees demonstrates that fine-scale recombination rates evolve rapidly, to an extent disproportionate to the change in nucleotide sequence. Rapid evolution of hotspots has previously been hypothesized on the basis of examples of meiotic drive at hotspots and the mechanism of DSB repair (*9*, *12*). Our observations argue against models in which hotspots are directed solely by short, neutrally evolving DNA motifs, which would almost always be identical between the two species. Epigenetic factors, which are known to play a role in recombination hotspots (*7*), may vary more substantially across closely related species than does DNA sequence. Alternatively, if the trans-acting molecular machinery that initiates crossover events has nucleotide site preferences, then it is possible that substitutions in these components could dramatically alter site preference across the genome. Although DNA sequence is typically shared across human and chimpanzee, the polymorphisms in each species are not (*26*). It is intriguing to speculate that polymorphisms could themselves play a role in shaping fine-scale recombination; this could also explain why different alleles of a given locus can have substantially different recombination rates (*9*). Finally, we note that if recombination rates evolve rapidly, then in some cases, rates from "historical" polymorphism data might truly differ from contemporaneous rates in sperm.

By applying these analytical methods to genome-wide polymorphism surveys, an extensive collection of recombination hotspots will soon be available across the human genome. Studying these hotspots should ultimately illuminate the as yet mysterious factors that direct the location and frequency of recombination in our species.

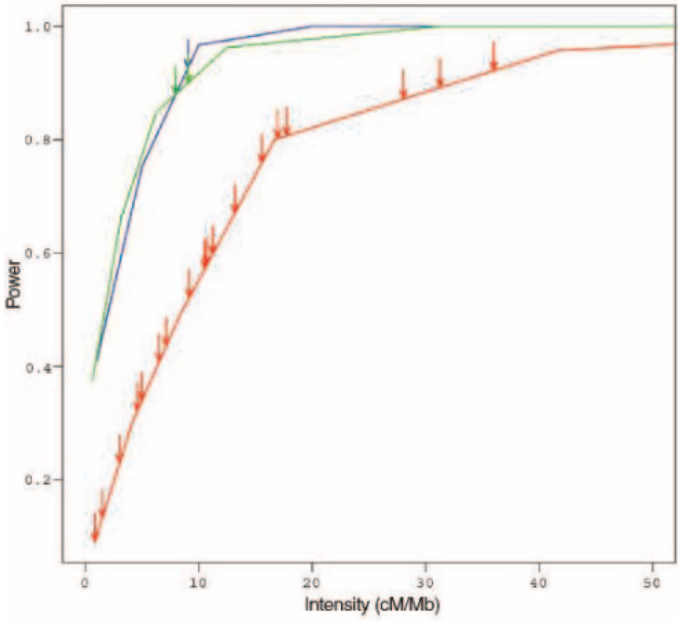

Fig. 2. Power to detect hotspots in two human populations and chimpanzee. "Power" indicates the likelihood of observing statistical support for a hotspot ($P < 0.05$) of a given intensity in centimorgans per megabase for YRI (green), CEU (blue), and chimpanzee (red). Arrows indicate the estimated intensity of the hotspots detected in each species, using the color scheme above. Power in chimpanzee ranges from 40 to 95% for hotspots of intensity >5 cM/Mb observed in the human data and, in human, is >87% for each hotspot observed in chimpanzee. For full details of the simulations, see (*13*).

References and Notes

1. J. L. Gerton *et al.*, *Proc. Natl. Acad. Sci. U.S.A.* **97**, 11383 (2000).
2. G. A. McVean *et al.*, *Science* **304**, 581 (2004).
3. D. C. Crawford *et al.*, *Nat. Genet.* **36**, 700 (2004).
4. A. Chakravarti *et al.*, *Am. J. Hum. Genet.* **36**, 1239 (1984).
5. A. J. Jeffreys, A. Ritchie, R. Neumann, *Hum. Mol. Genet.* **9**, 725 (2000).
6. A. J. Jeffreys, L. Kauppi, R. Neumann, *Nat. Genet.* **29**, 217 (2001).
7. T. C. Wu, M. Lichten, *Science* **263**, 515 (1994).
8. P. Schuchert, M. Langsford, E. Kaslin, J. Kohli, *EMBO J.* **10**, 2157 (1991).
9. A. J. Jeffreys, R. Neumann, *Nat. Genet.* **31**, 267 (2002).
10. C. L. Yauk, P. R. Bois, A. J. Jeffreys, *EMBO J.* **22**, 1389 (2003).
11. A. Nicolas, D. Treco, N. P. Schultes, J. W. Szostak, *Nature* **338**, 35 (1989).
12. A. Boulton, R. S. Myers, R. J. Redfield, *Proc. Natl. Acad. Sci. U.S.A.* **94**, 8058 (1997).
13. Materials and methods are available as supporting material on *Science* Online.
14. J. C. Barrett, B. Fry, J. Maller, M. J. Daly, *Bioinformatics* **21**, 263 (2005).
15. R. A. Smith *et al.*, *Blood* **92**, 4415 (1998).
16. J. A. Schneider *et al.*, *Hum. Mol. Genet.* **11**, 207 (2002).
17. S. E. Ptak *et al.*, *PLoS Biol.* **2**, e155 (2004).
18. J. D. Wall, L. A. Frisse, R. R. Hudson, A. Di Rienzo, *Am. J. Hum. Genet.* **73**, 1330 (2003).
19. We note that the previous study (*18*) that did not find evidence for a hotspot in the chimpanzee β-globin region did not examine the adjacent region in which

we found an elevated rate of recombination in the chimpanzee.
20. www.hapmap.org/.
21. S. B. Gabriel *et al.*, *Science* **296**, 2225 (2002).
22. I. Ebersberger, D. Metzler, C. Schwarz, S. Paabo, *Am. J. Hum. Genet.* **70**, 1490 (2002).
23. H. Watanabe *et al.*, *Nature* **429**, 382 (2004).
24. D. Falush, M. Stephens, J. K. Pritchard, *Genetics* **164**, 1567 (2003).
25. S. R. Myers, R. C. Griffiths, *Genetics* **163**, 375 (2003).
26. M. K. Halushka *et al.*, *Nat. Genet.* **22**, 239 (1999).

27. We thank the members of the Altshuler, Daly, and Donnelly laboratories and the participants in the International Haplotype Map Project for helpful discussions. D.A. is a Charles E. Culpeper Scholar of the Rockefeller Brothers Fund and a Burroughs Wellcome Fund clinical scholar in translational research. P.D. is supported by NIH, Wellcome Trust, Nuffield Trust, the SNP Consortium, and Wolfson Foundation. G.A.T.M. is supported by NIH, The Royal Society, and the SNP Consortium. D.R. is the recipient of a Career Development Award in Biomedical Science from the Burroughs Wellcome Fund.

Supporting Online Material
www.sciencemag.org/cgi/content/full/1105322/DC1
Materials and Methods
Tables S1 and S2
Figs. S1 to S5
References and Notes

16 September 2004; accepted 1 February 2005
Published online 10 February 2005;
10.1126/science.1105322
Include this information when citing this paper.

Neuronal Coherence as a Mechanism of Effective Corticospinal Interaction

Jan-Mathijs Schoffelen,[1,2]* Robert Oostenveld,[1,3] Pascal Fries[1,2]

Neuronal groups can interact with each other even if they are widely separated. One group might modulate its firing rate or its internal oscillatory synchronization to influence another group. We propose that coherence between two neuronal groups is a mechanism of efficient interaction, because it renders mutual input optimally timed and thereby maximally effective. Modulations of subjects' readiness to respond in a simple reaction-time task were closely correlated with the strength of gamma-band (40 to 70 hertz) coherence between motor cortex and spinal cord neurons. This coherence may contribute to an effective corticospinal interaction and shortened reaction times.

Within the central nervous system, the main occupation of a given group of neurons is to interact with other groups. It is commonly assumed that the influence of one neuronal group on another is primarily determined by the mean rate of action potentials generated (*1*). However, recent evidence suggests that a postsynaptic neuron actively compensates for slow changes in mean input rate and primarily responds to precisely synchronous input barrages (*2*–*5*). Studies in awake and behaving animals suggest that neuronal groups increase their impact on target groups through precise oscillatory synchronization (*6*, *7*), and it has been hypothesized that this might constitute a general mechanism for regulating the flow of information in the nervous system (*8*).

Here, we propose a mechanism that might greatly amplify the effects of oscillatory synchronization. Activated groups of neurons typically oscillate in the beta or gamma frequency bands (*9*, *10*) and thereby undergo temporally predictable excitability fluctuations. Synaptic input to an oscillating neuronal target group will be maximally effective if it arrives within a few milliseconds of the excitability peaks of the target (*11*). Thus, for a neuronal group to provide maximally effective input, it should be coherent with the target group.

We tested whether this potential mechanism has a functional role in human cognition and whether this role can be demonstrated through a behavioral correlate of coherence between distant groups of neurons. We studied coherence between motor cortex and spinal alpha-motoneurons (*12*–*15*) (Fig. 1). Because a spinal motoneuron and the corresponding muscle fibers form a motor unit with one-to-one correspondence of their action potentials, we used the electromyogram (EMG) of the right musculus extensor carpi radialis longus to indirectly measure the activity of the corresponding spinal neuronal group. Activity in the corresponding left motor cortex was assessed with magnetoencephalography (MEG). Corticospinal coherence (coherence between motor cortex and spinal cord) could then be assessed with standard analysis methods (*16*).

We investigated the effect of a manipulation of corticospinal interaction on corticospinal coherence. We used the well-studied behavioral effect that in simple reaction-time tasks, the hazard rate of the go-cue (*17*) determines the subjects' readiness to respond as operationalized by shortened reaction times (*18*, *19*). Subjects extended their right wrist to elevate their hand against the lever of a force meter to bring the measured force into a specified window. After a baseline period, a visual stimulus appeared and subjects had to keep the wrist extension until the stimulus changed speed at an unpredictable moment in time (fig. S1). The crucial experimental manipulation was to systematically modulate the hazard rate of the stimulus' speed change. In the UP-schedule, a stimulus change became more and more likely the longer the stimulus was on without change. In the DOWN-schedule, a stimulus change became less and less likely. A given subject was trained in three sessions on one of the schedules before neuronal activity was recorded in a fourth session. After several days' break, the same was done for the other sched-

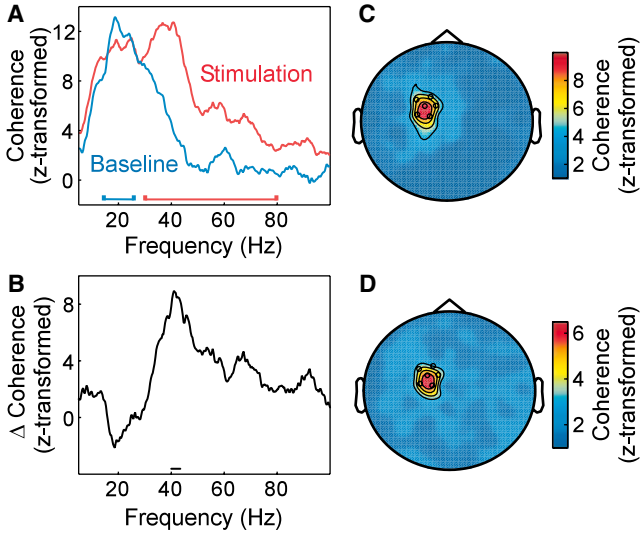

Fig. 1. (**A** and **B**) Readiness to respond induces corticospinal gamma-band coherence. In (A), corticospinal coherence [z-transformed (*30*), averaged over the six sensors highlighted in (C) and (D)] is shown before (blue) and after (red) onset of the visual stimulus; (B) shows the difference. Horizontal bars in (A) indicate frequency ranges used in (C) (blue bar) and (D) (red bar). Horizontal bar in (B) indicates frequency band with significant difference ($P < 0.05$, nonparametric randomization test). (**C**) Topography of beta-band coherence before the onset of the visual stimulus. (**D**) Topography of gamma-band coherence after the onset of the visual stimulus.

[1]F. C. Donders Centre for Cognitive Neuroimaging, Radboud University Nijmegen, 6525 EK Nijmegen, Netherlands. [2]Department of Biophysics, Radboud University Nijmegen, 6525 EZ Nijmegen, Netherlands. [3]Center for Sensory-Motor Interaction (SMI), Aalborg University, Fredrik Bajers Vej 7 D-3, 9220 Aalborg, Denmark.

*To whom correspondence should be addressed. E-mail: jan.schoffelen@fcdonders.ru.nl

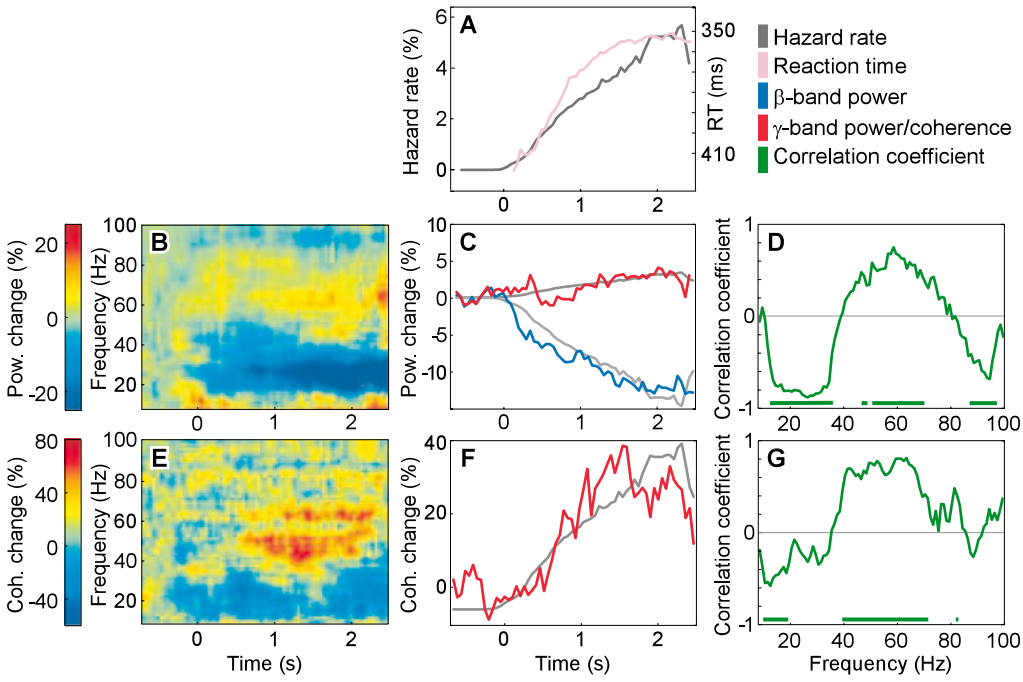

Fig. 2. Effect of increasing hazard rate on reaction times, cortical power, and corticospinal coherence ($n = 6$ subjects). (**A**) Hazard rate (gray line) with the resulting reaction times (pink line). Note the inverted reaction time axis at the right. (**B**) Time-frequency representation of MEG power over contralateral motor cortex. (**C**) Time courses of the cortical power in the gamma band (40 to 70 Hz) (red line) and the beta band (15 to 30 Hz) (blue line). For comparison of power time courses and hazard rate, two scaled copies of the latter are shown (gray lines), one upright (gamma power) and one inverted (beta power). (**D**) Pearson correlation coefficient between hazard rate and cortical power as a function of frequency of the latter. Bars indicate significant frequency bands ($P < 0.05$, nonparametric randomization test, corrected for multiple comparisons). (**E**) Time-frequency representation of corticospinal coherence. (**F**) Time course of corticospinal coherence in the gamma band (40 to 70 Hz). As in (C), the gray line is a scaled copy of the hazard rate. (**G**) Pearson correlation coefficient between hazard rate and corticospinal coherence as a function of frequency of the latter. Bars indicate significant frequency bands ($P < 0.05$, nonparametric randomization test, corrected for multiple comparisons).

ule. The sequence of schedules was counterbalanced across the six subjects studied (*20*).

The behavioral results from the recording sessions confirm earlier findings (Figs. 2A and 3A). When the hazard rate increased linearly in the UP-schedule, reaction times decreased in close correspondence (Pearson correlation coefficient $r = –0.93$, $P < 0.0001$, randomization test); the reverse was found for the DOWN-schedule ($r = –0.95$, $P < 0.0001$). Thus, subjects had implicitly learned the hazard rate for the two schedules and were effective in dynamically modulating corticospinal interaction accordingly.

Next, we investigated corticospinal coherence. Most previous studies using weak to medium force output have reported coherence primarily in the beta band, between 15 and 25 Hz (*12–15*). Coherence at frequencies in the gamma band, between 30 and 80 Hz, has so far been described during maximal voluntary contractions or during slow movements (*15*). In our paradigm, beta-band coherence was present both before and during stimulus presentation (Fig. 1A). During visual stimulation but in the absence of changes in motor output, gamma-band coherence was strongly enhanced (Fig. 1, A and B; $P < 0.05$, nonparametric permutation test, corrected for multiple comparisons). The topography of beta-band coherence before stimulus onset was very similar to that of gamma-band coherence after stimulus onset (Fig. 1, C and D), which suggests that the same neuronal group or two spatially highly overlapping neuronal groups were involved. Obviously, subjects knew that they had to be ready to respond only when the stimulus was on. Beta-band coherence was present throughout the trial and was more pronounced before the onset of the visual stimulus; this finding suggests that it has a role in maintaining a steady-state force output, in agreement with earlier studies (*12–15*). In contrast, corticospinal gamma-band coherence seemed to come into play when a movement signal was expected.

We thus compared time courses of the hazard rate and of corticospinal gamma-band coherence separately for the UP- and DOWN-schedules. Corticospinal gamma-band coherence showed rapid dynamics. In the UP-schedule, it increased over time after stimulus onset (Fig. 2, E and F) and in close correspondence with the hazard rate ($r = 0.87$, $P < 0.0001$, nonparametric randomization test). In the DOWN-schedule, gamma-band coherence first increased rapidly after stimulus onset and then fell to baseline values (Fig. 3, E and F), again in close correspondence with the hazard rate ($r = 0.86$, $P < 0.0001$). To test whether this effect is specific for the gamma band, we assessed the cross-correlation between the hazard rate and the time course of corticospinal coherence for all frequencies of the coherence spectrum. Indeed, a significant positive correlation was confined to frequencies between roughly 40 and 60 Hz for both the UP- and DOWN-schedules (Figs. 2G and 3G).

In addition to the long-range coherence of motor cortex with the spinal cord, local neuronal synchronization in motor cortex was also modulated by the task. Oscillatory motor cortical synchronization can be estimated from the power spectrum of MEG signals recorded over motor cortex. Motor cortical gamma-band power correlated positively with the hazard rate (UP: $r = 0.54$, $P < 0.0001$; DOWN: $r = 0.61$, $P < 0.0001$). In contrast, motor cortical beta-band power showed a negative correlation (UP: $r = –0.89$, $P < 0.0001$; DOWN: $r = –0.62$, $P < 0.0001$). The time course of power and the frequencywise correlation between hazard rate and power are shown in Fig. 2, B to D, for the UP-schedule, and in Fig. 3, B to D, for the DOWN-schedule.

Our results show that readiness to respond and corticospinal gamma-band coherence are tightly coupled. Dynamic modulations of the readiness to respond induce corresponding dynamic modulations of corticospinal gamma-band coherence and motor cortical gamma-band synchronization. Because readiness to respond was rising in the UP-schedule but falling in the DOWN-schedule, the parallel changes in power and coherence cannot be merely an effect of elapsing time. Furthermore, because visual stimulation and motor output (*21*) were indistinguishable between a given trial in the UP-schedule and a given trial in the DOWN-schedule, the observed effects must be ascribed to the implicitly learned hazard rates and thus constitute a purely cognitive modulation.

One concern is that the observed dynamics in corticospinal gamma-band coherence might be fully explained by the changes in local motor cortical gamma-band synchronization. Several earlier studies have found gamma-band power over different parts of the brain to predict shortened reaction times

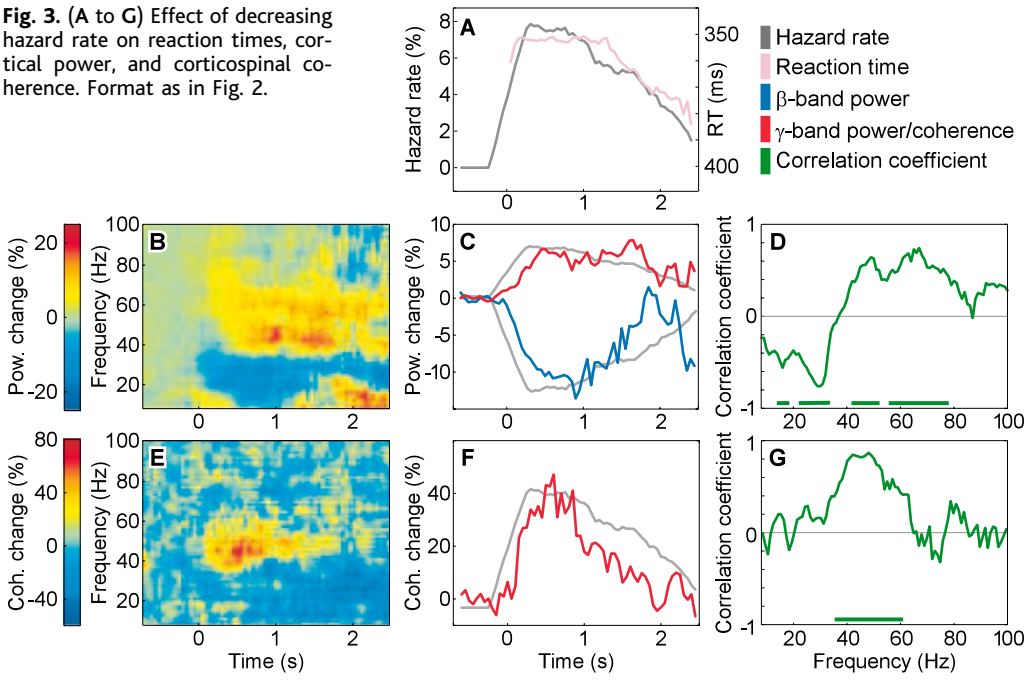

Fig. 3. (**A** to **G**) Effect of decreasing hazard rate on reaction times, cortical power, and corticospinal coherence. Format as in Fig. 2.

(*22*). The core of our hypothesis is, however, that coherence itself is a mechanism for effective corticospinal interaction, above and beyond local oscillatory neuronal synchronization. We therefore reanalyzed the dynamics of corticospinal coherence after eliminating trials until the average cortical power remained as constant as possible given the finite trial number. This left the magnitude and dynamics of gamma-band coherence essentially unaltered (*20*). Thus, the dynamics of corticospinal gamma-band coherence is not a mere consequence of the dynamics of local oscillatory synchronization, and the respective mechanisms appear at least partly independent. Previous studies have indeed revealed mechanisms that specifically modulate a neuron's tendency to phase-lock to rhythmic input (*23*) through a modulation of its ionic conductances.

Our results suggest a role for coherence in corticospinal interaction. Yet, in our paradigm, the corticospinal interaction was only one of the links in the chain from visual input to motor output. Coherence between different intervening areas might also contribute to the observed shortened reaction times during enhanced readiness to respond. Neuronal gamma-band coherence has been found in several other cases between distant neuronal groups along the visuomotor pathway (*24*–*29*) and has been implicated in visuomotor interactions.

We would like to speculate about the implications if neuronal coherence were a general mechanism of neuronal communication. Coherence likely renders neuronal interactions not only effective but also selective for the coherent groups. Input to a target group that is incoherent with the excitability fluctuations in this target group will be less effective. Often many neurons converge on a common target, but at a given moment, only part of the input is effective in influencing the target neuron's output. Selective coherence is an ideal candidate mechanism for the regulation of the efficiency of input. It would at the same time increase the impact of input that is coherent with the target and decrease the impact of input that is not coherent with the target. In addition, feedback from the target group of neurons would also be more effective at the coherent input than at the noncoherent input, even if it were anatomically directed to both. Our results suggest that neuronal coherence can serve neuronal communication and can be dynamically modulated by cognitive demands.

References and Notes

1. M. C. van Rossum, G. G. Turrigiano, S. B. Nelson, *J. Neurosci.* **22**, 1956 (2002).
2. R. Azouz, C. M. Gray, *Proc. Natl. Acad. Sci. U.S.A.* **97**, 8110 (2000).
3. E. Salinas, T. J. Sejnowski, *J. Neurosci.* **20**, 6193 (2000).
4. R. Azouz, C. M. Gray, *Neuron* **37**, 513 (2003).
5. H. Markram, M. Tsodyks, *Nature* **382**, 807 (1996).
6. P. Fries, J. H. Reynolds, A. E. Rorie, R. Desimone, *Science* **291**, 1560 (2001).
7. P. Fries, J. H. Schröder, P. R. Roelfsema, W. Singer, A. K. Engel, *J. Neurosci.* **22**, 3739 (2002).
8. E. Salinas, T. J. Sejnowski, *Nat. Rev. Neurosci.* **2**, 539 (2001).
9. P. H. Tiesinga, T. J. Sejnowski, *Neural Comput.* **16**, 251 (2004).
10. D. J. Pinto, S. R. Jones, T. J. Kaper, N. Kopell, *J. Comput. Neurosci.* **15**, 283 (2003).
11. M. Volgushev, M. Chistiakova, W. Singer, *Neuroscience* **83**, 15 (1998).
12. J. M. Kilner, S. N. Baker, S. Salenius, R. Hari, R. N. Lemon, *J. Neurosci.* **20**, 8838 (2000).
13. B. A. Conway *et al.*, *J. Physiol.* **489**, 917 (1995).
14. S. N. Baker, E. Olivier, R. N. Lemon, *J. Physiol.* **501**, 225 (1997).
15. P. Brown, *Prog. Neurobiol.* **60**, 97 (2000).
16. For conceptual clarity, we use the term corticospinal coherence instead of corticomuscular coherence. See (*20*) for evidence that this coherence originates in motor cortex.
17. The hazard rate of an event at a certain time is defined as the conditional probability of the event occurring at that time, given that it has not yet occurred. See (*20*) for more information.
18. P. Trillenberg, R. Verleger, E. Wascher, B. Wauschkuhn, K. Wessel, *Clin. Neurophysiol.* **111**, 1216 (2000).
19. A. Riehle, S. Grün, M. Diesmann, A. Aertsen, *Science* **278**, 1950 (1997).
20. See supporting data on *Science* Online.
21. To ensure that unavoidable small fluctuations in EMG activity did not confound the result, we used a stratification procedure that eliminated trials deviating from the mean EMG activity such that changes in EMG activity relative to baseline did not exceed 2% (*20*). The described results were obtained with this stratification.
22. S. L. Gonzalez Andino, C. M. Michel, G. Thut, T. Landis, R. Grave de Peralta, *Hum. Brain Mapp.* **24**, 50 (2005).
23. S. Schreiber, J. M. Fellous, P. Tiesinga, T. J. Sejnowski, *J. Neurophysiol.* **91**, 194 (2003).
24. A. K. Engel, P. König, A. K. Kreiter, W. Singer, *Science* **252**, 1177 (1991).
25. A. K. Engel, A. K. Kreiter, P. König, W. Singer, *Proc. Natl. Acad. Sci. U.S.A.* **88**, 6048 (1991).
26. A. Frien, R. Eckhorn, R. Bauer, T. Woelbern, H. Kehr, *Neuroreport* **5**, 2273 (1994).
27. M. S. Livingstone, *J. Neurophysiol.* **75**, 2467 (1996).
28. P. König, A. K. Engel, W. Singer, *Proc. Natl. Acad. Sci. U.S.A.* **92**, 290 (1995).
29. E. Rodriguez *et al.*, *Nature* **397**, 430 (1999).
30. M. R. Jarvis, P. P. Mitra, *Neural Comput.* **13**, 717 (2001).

31. We thank H. Kleijnen and E. van den Boogert for technical assistance and R. Desimone, O. Jensen, C. Gielen, E. Maris, W. Singer, and I. Toni for helpful discussions and suggestions. Supported by Netherlands Organization for Scientific Research grants 452-03-344 and 051-02-050 (P.F.), Human Frontier Science Program Organization grant RGP0070/2003 (P.F.), and Danish Technical Research Council grant 26-01-0092 (R.O.).

Supporting Online Material

www.sciencemag.org/cgi/content/full/308/5718/111/DC1
Materials and Methods
Figs. S1 to S8
References

2 November 2004; accepted 1 February 2005
10.1126/science.1107027

PDK1 Nucleates T Cell Receptor–Induced Signaling Complex for NF-κB Activation

Ki-Young Lee, Fulvio D'Acquisto, Matthew S. Hayden, Jae-Hyuck Shim, Sankar Ghosh*

Activation of the transcription factor NF-κB after engagement of the T cell receptor (TCR) is important for T cell proliferation and activation during the adaptive immune response. Recent reports have elucidated a signaling pathway that involves the protein kinase C θ (PKCθ), the scaffold protein CARD11 (also called CARMA-1), the caspase recruitment domain (CARD)–containing protein Bcl10, and the paracaspase (protease related to caspases) MALT1 as critical intermediates linking the TCR to the IκB kinase (IKK) complex. However, the events proximal to the TCR that initiate the activation of this signaling pathway remain poorly defined. We demonstrate that 3-phosphoinositide-dependent kinase 1 (PDK1) has an essential role in this pathway by regulating the activation of PKCθ and through signal-dependent recruiting of both PKCθ and CARD11 to lipid rafts. PDK1-associated PKCθ recruits the IKK complex, whereas PDK1-associated CARD11 recruits the Bcl10-MALT1 complex, thereby allowing activation of the IKK complex through Bcl10-MALT1–dependent ubiquitination of the IKK complex subunit known as NEMO (NF-κB essential modifier). Hence, PDK1 plays a critical role by nucleating the TCR-induced NF-κB activation pathway in T cells.

Stimulation of T cells by engagement of the TCR-CD3 complex along with the coreceptor CD28 initiates signal transduction cascades that lead to the activation of the IκB kinase (IKK) complex (*1*). The canonical IKK complex is composed of three subunits: IKKα, IKKβ, and NEMO (also called IKKγ). IKKα and IKKβ are catalytic kinase subunits, whereas NEMO is a structural and regulatory subunit (*2–6*). Upon TCR-mediated signaling, the IKK complex is recruited into lipid rafts, and protein kinase C θ (PKCθ) is thought to have an important role in this recruitment event (*7–9*). However, the mechanism responsible for the activation of PKCθ and its recruitment to lipid rafts remains unclear. TCR stimulation also requires recruitment of CARD11, Bcl10, and MALT1 to lipid rafts. Knockout of genes encoding these proteins causes a block in signaling to NF-κB from both T cell and B cell receptors (*10*). However, the mechanism by which these proteins initiate the NF-κB activation pathway has remained obscure. A recent report has provided some insight into this question by demonstrating that the Bcl10-MALT1 complex can ubiquitinate the NEMO subunit of the IKK complex, thereby causing the activation of IKK, and hence NF-κB, in T cells (*11*). However, it remains unclear how the IKK and Bcl10-CARD11-MALT1 complexes interact and what role,

Section of Immunobiology and Department of Molecular Biophysics and Biochemistry, Yale University School of Medicine, New Haven, CT 06520, USA.

*To whom correspondence should be addressed. E-mail: Sankar.ghosh@yale.edu

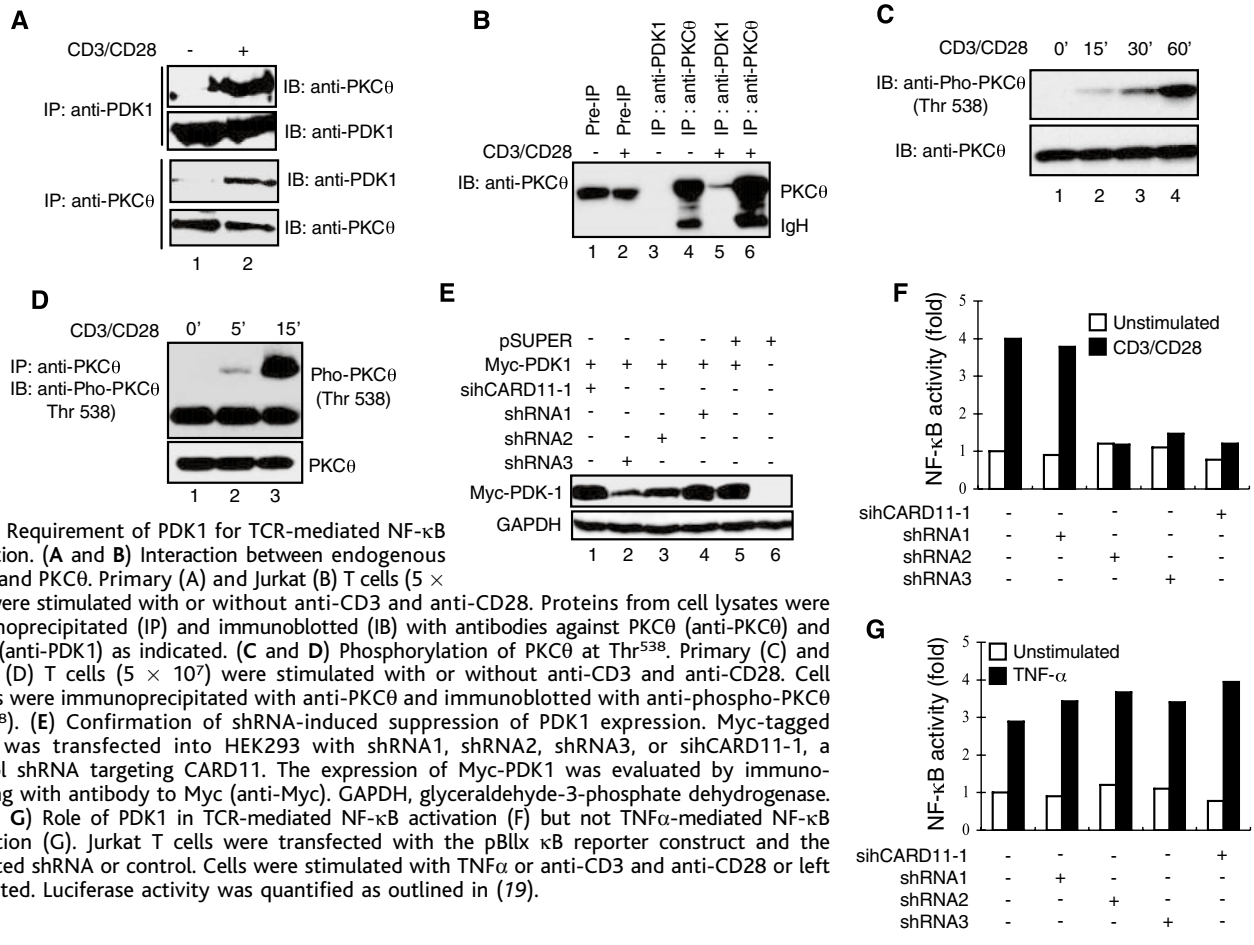

Fig. 1. Requirement of PDK1 for TCR-mediated NF-κB activation. (**A** and **B**) Interaction between endogenous PDK1 and PKCθ. Primary (A) and Jurkat (B) T cells (5×10^7) were stimulated with or without anti-CD3 and anti-CD28. Proteins from cell lysates were immunoprecipitated (IP) and immunoblotted (IB) with antibodies against PKCθ (anti-PKCθ) and PDK1 (anti-PDK1) as indicated. (**C** and **D**) Phosphorylation of PKCθ at Thr^{538}. Primary (C) and Jurkat (D) T cells (5×10^7) were stimulated with or without anti-CD3 and anti-CD28. Cell lysates were immunoprecipitated with anti-PKCθ and immunoblotted with anti-phospho-PKCθ (Thr^{538}). (**E**) Confirmation of shRNA-induced suppression of PDK1 expression. Myc-tagged PDK1 was transfected into HEK293 with shRNA1, shRNA2, shRNA3, or sihCARD11-1, a control shRNA targeting CARD11. The expression of Myc-PDK1 was evaluated by immunoblotting with antibody to Myc (anti-Myc). GAPDH, glyceraldehyde-3-phosphate dehydrogenase. (**F** and **G**) Role of PDK1 in TCR-mediated NF-κB activation (F) but not TNFα-mediated NF-κB activation (G). Jurkat T cells were transfected with the pBllx κB reporter construct and the indicated shRNA or control. Cells were stimulated with TNFα or anti-CD3 and anti-CD28 or left untreated. Luciferase activity was quantified as outlined in (*19*).

if any, PKCθ recruitment and activation has in this process.

The activity of kinases that belong to the PKC family is regulated by the activation loop, which retains the kinase in an inactive conformation. Phosphorylation of the activation loop leads to its displacement from the active site and to stabilization of the catalytically competent conformation of the enzyme (*12*). One kinase upstream of both atypical and conventional PKC isoforms is 3-phosphoinositide-dependent kinase (PDK)–1, whose activity is partly regulated by phosphoinositide 3-kinase (PI3K). PI3K-generated lipids activate PDK1, which then phosphorylates and activates several members of the conserved AGC kinase superfamily including protein kinases A (PKA), G (PKG), and C (PKC) (*12*). Activation of PDK1 by the PI3K pathway provides a possible explanation for why the lipid products of PI3K, namely phosphatidylinositol-3,4-bisphosphate (PIP_2) and phosphatidylinositol-3,4-5-trisphosphate (PIP_3) stimulate the activation of protein kinase-dependent signaling pathways (*12*–*14*). The PI3K pathway also augments signaling to NF-κB, probably through its effect on Akt (*15*). However, PDK1 knockouts exhibit early embryonic lethality, thus preventing straightforward analysis of PDK1 function in T cell activation. In addition, conditional knockout of PDK1 in the T cell lineage results in a block early in thymocyte development, and hence, PDK1-deficient T cells suitable for studying TCR signaling cannot be isolated (*16*). Therefore, the importance of PDK1 in T cell signaling remains unclear.

To assess the role of PDK1 in TCR signaling through PKCθ, we tested whether endogenous PDK1 interacted with PKCθ in primary T cells that were either unstimulated or stimulated with antibodies against CD3 and CD28 (anti-CD3 anti-CD28). Efficient interaction between endogenous PKCθ and PDK1 was observed only in stimulated cells (Fig. 1A). An inducible interaction between endogenous PDK1 and PKCθ was also observed in stimulated Jurkat T cells (Fig. 1B). PDK1 regulates the activity of PKCs by phosphorylating a specific threonine residue (Thr^{538} for PKCθ) in their activation loop (*17*). We used a phospho-specific antibody that recognizes Thr^{538}-phosphorylated PKCθ to confirm that stimulation of primary T cells (Fig. 1C) and Jurkat T cells (Fig. 1D) with anti-CD3 and anti-CD28 led to phosphorylation of Thr^{538} of PKCθ.

The lack of appropriate PDK1 knockout cells prompted us to knock down PDK1 with use of RNA interference. We designed three short hairpin RNAs (shRNAs) targeting PDK1 (fig. S1, A and B) and cloned them into the pSUPER.Retro vector (*18*, *19*). Suppression of PDK1 expression was tested in 293 cells by cotransfecting the shRNAs along with a vector expressing PDK1. ShRNA2 and shRNA3 but not shRNA1 efficiently suppressed the expression of PDK1 (Fig. 1E) in a dose-dependent manner (*20*). To test the role of PDK1 in TCR-mediated NF-κB activation, we transfected the shRNAs along with an NF-κB–dependent reporter construct into Jurkat cells. After transfection, the cells were stimulated with either anti-CD3 and anti-CD28 (Fig. 1F) or with tumor necrosis factor α (TNF-α) (Fig. 1G). Both shRNA2 and shRNA3 inhibited the activation of the immunoglobulin κ_2 ($Ig\kappa_2$)-luciferase (LUC) reporter by CD3-CD28 cross-linking, whereas the control shRNA1 had no effect. The inhibitory effect was TCR-specific, because the shRNAs had no effect on NF-κB activation by TNF-α. Similar effects were seen with the use of shCARD11-1 as a positive control (Fig. 1F) (*21*), suggesting that PDK1 is required for NF-κB activation during TCR-mediated signaling.

Stable knockdown of PDK1 ($PDK1^{kd}$) recapitulated the blockade of TCR-mediated NF-κB activation observed in transient transfection experiments (Fig. 1F). Retroviruses encoding both green fluorescent protein (GFP)

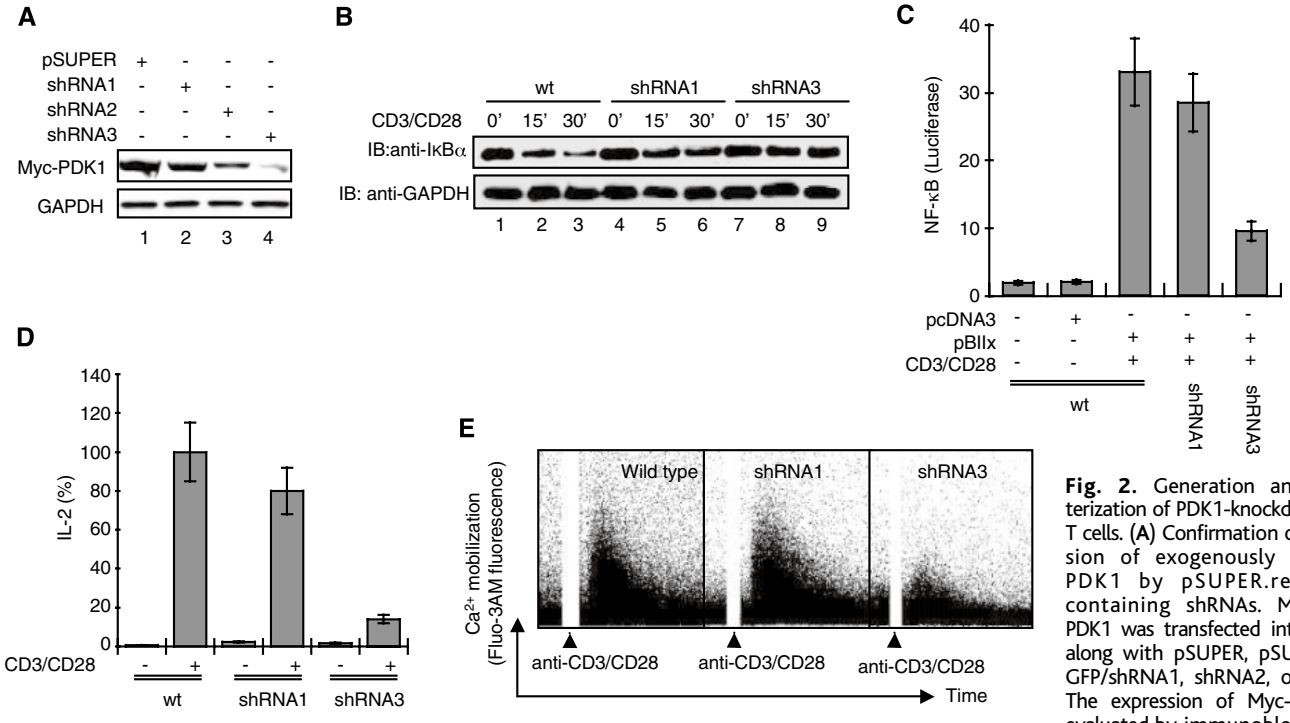

Fig. 2. Generation and characterization of PDK1-knockdown Jurkat T cells. (**A**) Confirmation of suppression of exogenously expressed PDK1 by pSUPER.retro/GFP-containing shRNAs. Myc-tagged PDK1 was transfected into HEK293 along with pSUPER, pSUPER.retro/GFP/shRNA1, shRNA2, or shRNA3. The expression of Myc-PDK1 was evaluated by immunoblotting with anti-Myc. (**B**) IκB-α degradation in PDK1-knockdown Jurkat cells. Jurkat and PDK1-knockdown Jurkat cells were stimulated with anti-CD3 and anti-CD28 for the indicated times and immunoblotted with antibody to IκBα. wt, wild type. (**C**) Effect of PDK1 knockdown on NF-κB luciferase assay. $Ig\kappa_2$-LUC (pBIIx) vector (2 μg) or equal amount of pcDNA3 was transfected into wild-type, irrelevant knockdown, or $PDK1^{kd}$ Jurkat cells. After 48 hours, cells were stimulated with anti-CD3 and anti-CD28, and luciferase assays were performed following the manufacturer's instructions. Error bars indicate standard error of the mean. (**D**) Decreased IL-2 production in PDK1-knockdown Jurkat cells after stimulation of cells with anti-CD3 and anti-CD28. Cells were stimulated or unstimulated, incubated for 5 hours with brefeldin-A, stained for intracellular IL-2, and analyzed by flow cytometry. Error bars indicate standard error of the mean. (**E**) Impaired Ca^{2+} mobilization in PDK1-knockdown Jurkat cells. Jurkat T cells were loaded with 2 μM fluo-3AM for 30 min in Hanks' balanced salt solution (HBSS) buffer containing 0.01% Pluronic F-127 (Sigma). The cells were then washed three times with HEPES buffer, resuspended in the same buffer, and analyzed after 15 min at room temperature.

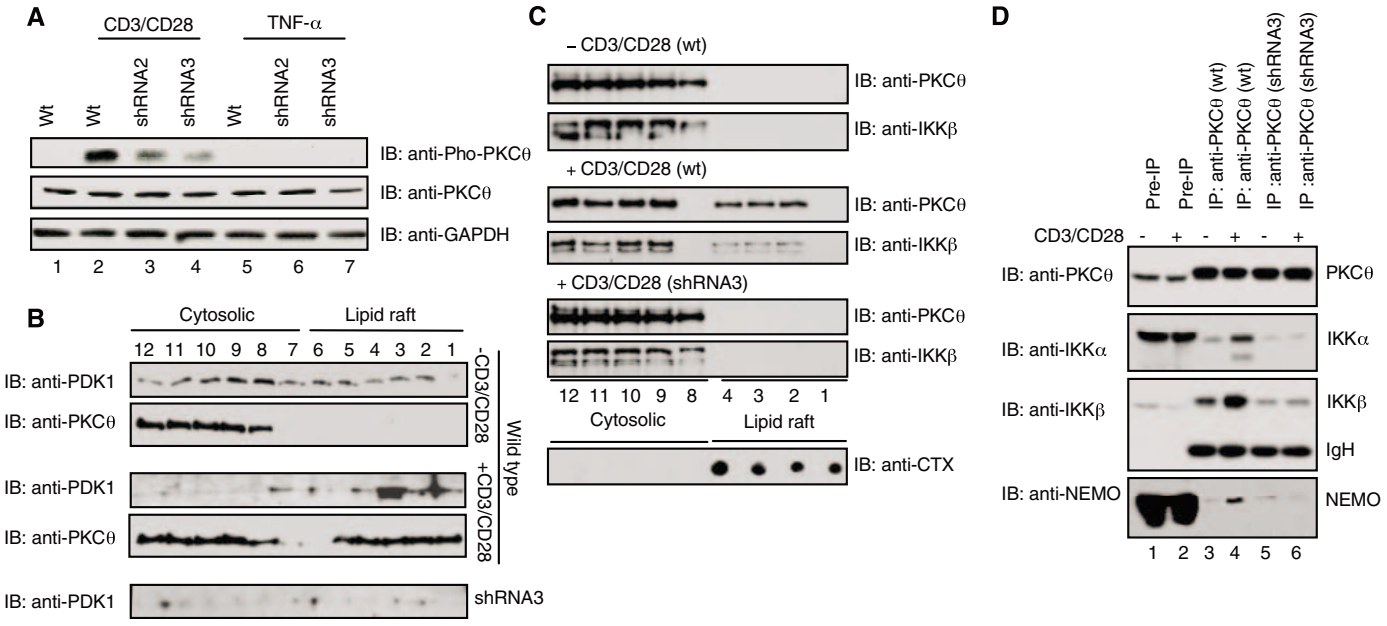

Fig. 3. Requirement of PDK1 for activation of NF-κB through the activation and recruitment of PKCθ. **(A)** Impairment of the phosphorylation of PKCθ in PDK1 knockdown Jurkat cells. Wild-type Jurkat or PDK1 knockdown cells were stimulated for 30 min with either anti-CD3 and anti-CD28 or with TNF-α. Lysates were immunoblotted with anti-phospho-PKCθ (Thr[538]) or an antibody that recognizes all forms of PKCθ. **(B)** Redistribution of PDK1 after stimulation of cells with anti-CD3 and anti-CD28. Jurkat or PDK1^{kd} cells (5×10^7) were then lysed with 1% Triton X-100 (Sigma) and subjected to sucrose density gradient centrifugation to isolate lipid rafts. The distribution of PDK1 in each fraction was determined by immunoblotting with a specific antibody. **(C)** The recruitment of PKCθ and IKKβ to lipid rafts is defective in PDK1-knockdown Jurkat cells. Jurkat or PDK1^{kd} Jurkat cells (5×10^7) were stimulated with or without anti-CD3 and anti-CD28. Proteins from equal volumes of fraction generated as in (A) were analyzed by immunoblotting with antibodies specific for PKCθ and IKKβ (anti-IKKβ). CTX, cholera toxin B subunit. **(D)** Failure of PKCθ to interact with the IKK complex in PDK1 knockdown cells. Wild-type and shRNA3-transduced Jurkat T cells were stimulated with or without anti-CD3 and anti-CD28. Cell lysates were prepared and immunoprecipiated with anti-PKCθ. Immunoblotting was performed with antibodies to PKCθ, IKKα, IKKβ, and NEMO, respectively.

and shRNA were produced (fig. S1C) and used to generate T cell lines stably expressing PDK1-specific shRNAs (fig. S1F) (*19*). PDK1^{kd} Jurkat cells showed decreased cell proliferation but normal cell cycle distribution (fig. S1, F and G) (*19*), as did a glioblastoma cell line (U87-MG) with decreased PDK1 (*22*). In PDK1^{kd} Jurkat cells generated with use of shRNA3 (and shRNA2 but not control shRNA1), both degradation of IκBα (Fig. 2E) and activation of NF-κB (Fig. 2C) were severely inhibited. Furthermore, loss of PDK1 led to impairment of functional NF-κB signaling as assessed by intracellular interleukin-2 (IL-2) quantification by flow cytometry (Fig. 2D) (*19*). In PDK1^{kd} Jurkat cells, Ca^{2+} mobilization was decreased compared with that in control cells (Fig. 2E) (*19*). PKCθ knockout T cells also have impaired Ca^{2+} mobilization after TCR stimulation (*23*). Therefore, these results suggest PDK1-mediated phosphorylation of PKCθ may be required for functional activation of PKCθ after TCR stimulation.

To determine whether PDK1 functions in the activation of PKCθ, we tested the phosphorylation of PKCθ after stimulation with anti-CD3 and anti-CD28. Phosphorylation of PKCθ was substantially decreased in the two PDK1^{kd} Jurkat cell lines (Fig. 3A). Treatment of cells with TNF-α did not lead to phosphorylation of PKCθ (Fig. 3A, lanes 5 to 7), indicating that PDK1-mediated PKCθ phosphorylation is specific to TCR signaling. Knockdown of PDK1 did not lead to a discernible alteration in the level of PKCθ protein (Fig. 3A).

To assess whether the recruitment of PKCθ to lipid rafts depends on PDK1, we prepared the detergent-insoluble membrane fractions of wild-type and PDK1^{kd} cells by centrifugation in a discontinuous sucrose gradient (*7*, *19*). In unstimulated cells, PDK1 was detected in both the cytoplasm and lipid rafts; however, after exposure of cells to anti-CD3 and anti-CD28, the fraction of PDK1 in lipid rafts increased (Fig. 3B). Almost no PKCθ was detected in lipid rafts after stimulation of PDK1^{kd} Jurkat cells with anti-CD3 and anti-CD28, whereas prominent recruitment of PKCθ was observed in wild-type Jurkat cells (Fig. 3C). Immunofluorescence analysis also showed the recruitment of PKCθ to the membrane to be decreased in PDK1^{kd} cells (fig. S2A).

The results presented above suggest that PDK1 plays an essential role in linking T cell stimulation to NF-κB activation, probably through phosphorylation of PKCθ and recruitment of PKCθ into lipid rafts. PKCθ physically interacts with IKK complexes in lipid rafts (*9*), and hence PDK1, through PKCθ, may recruit IKK complexes to the TCR-signaling complex. We observed signal-dependent recruitment of IKKβ into lipid rafts in wild-type and control shRNA1-expressing cells (Fig. 3C) (*7*). However, this recruitment was abolished in the PDK1^{kd} cells, supporting the hypothesis that PDK1, through its ability to activate and recruit PKCθ, regulates the recruitment of IKKβ. We also detected association of endogenous PKCθ with components of the IKK complex by co-immunoprecipitation from TCR-stimulated cells (Fig. 3D), and this interaction was dramatically diminished in cells lacking PDK1.

Although the results presented above indicate that PDK1 and PKCθ recruit IKK to the TCR-signaling complex, they do not address how the recruited IKK becomes activated to signal to NF-κB. Activation of IKK in response to TCR signaling depends on the regulatory ubiquitination of NEMO by the Bcl10-MALT1 complex (*11*). However, recruitment of PKCθ to the TCR is unaffected in CARD11 knockout T cells (*24*), and the association of PKCθ with IKKβ and NEMO was not affected by CARD11 deficiency (Fig. 4A), suggesting that recruitment of PKCθ-IKK to the receptor is independent of CARD11 but dependent on PDK1. Because PDK1 and CARD11 are both membrane-associated proteins, we tested the possibility that activated PDK1 might also recruit CARD11 into lipid rafts and thereby serve a critical nucleating role in the assembly of this signaling pathway. Association between endogenous PDK1 and CARD11 was observed in cells stimulated with antibodies to CD3 and CD28 (Fig. 4B). In addition, overexpressed PDK1 selectively interacted with CARD11 but

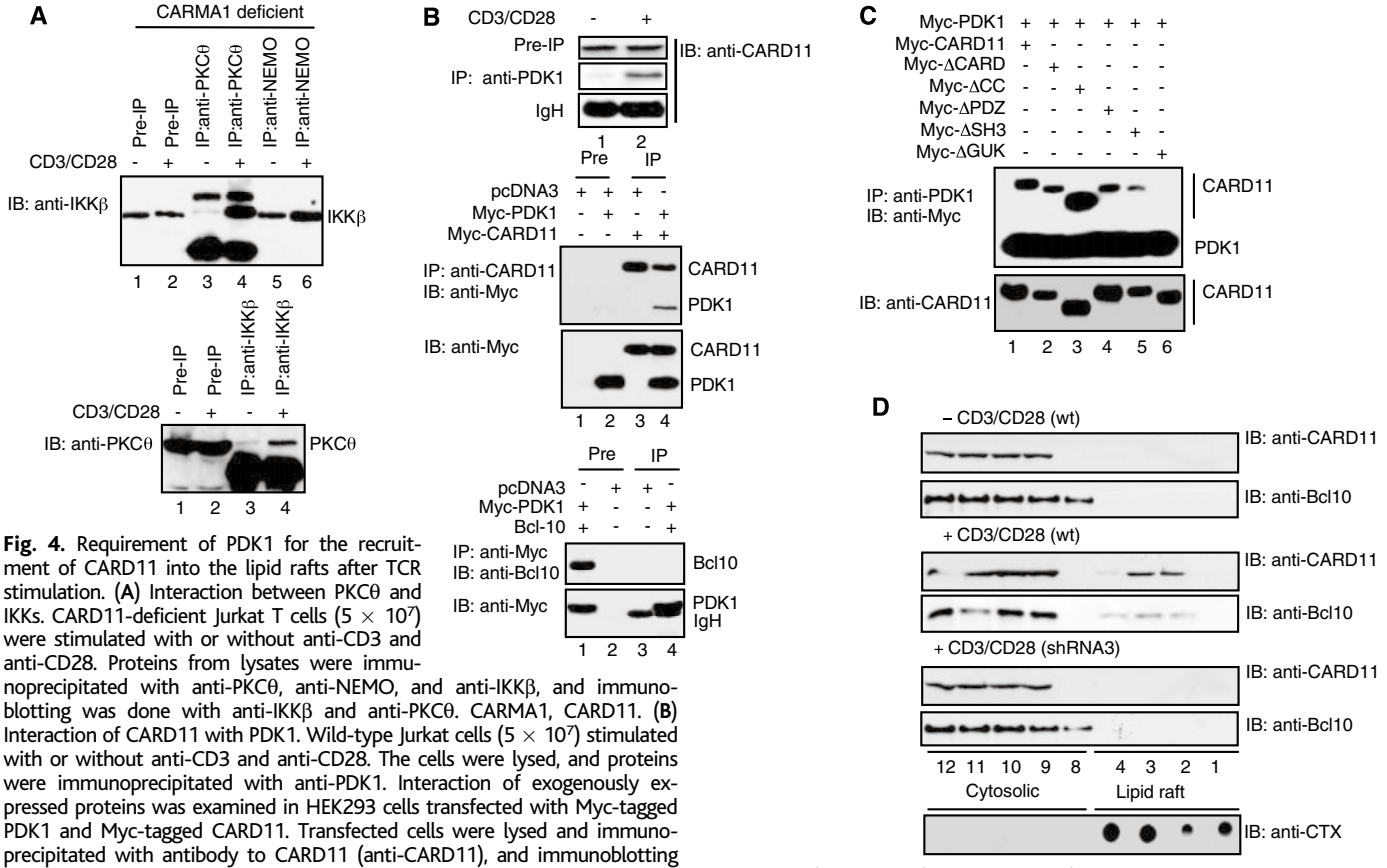

Fig. 4. Requirement of PDK1 for the recruitment of CARD11 into the lipid rafts after TCR stimulation. (**A**) Interaction between PKCθ and IKKs. CARD11-deficient Jurkat T cells (5×10^7) were stimulated with or without anti-CD3 and anti-CD28. Proteins from lysates were immunoprecipitated with anti-PKCθ, anti-NEMO, and anti-IKKβ, and immunoblotting was done with anti-IKKβ and anti-PKCθ. CARMA1, CARD11. (**B**) Interaction of CARD11 with PDK1. Wild-type Jurkat cells (5×10^7) stimulated with or without anti-CD3 and anti-CD28. The cells were lysed, and proteins were immunoprecipitated with anti-PDK1. Interaction of exogenously expressed proteins was examined in HEK293 cells transfected with Myc-tagged PDK1 and Myc-tagged CARD11. Transfected cells were lysed and immunoprecipitated with antibody to CARD11 (anti-CARD11), and immunoblotting was done with anti-Myc. For the interaction between PDK1 and Bcl10, Myc-tagged PDK1 was transfected into HEK293 cells along with Bcl10. After immunoprecipitation with anti-Myc, immunoblotting was done with anti-Bcl10 and anti-Myc. IgH, immunoglobulin heavy chain. (**C**) Requirement of GUK domain for interaction with PDK1. Myc-tagged PDK1 was transfected into HEK293 cells along with Myc-tagged CARD11, ΔCARD (caspase recruitment domain), ΔCC (coiled-coil), ΔPDZ (PSD-95, DLG, and ZO-1), ΔSH3 (src homology 3), or ΔGUK (guanylate kinase). Proteins immunoprecipitated with anti-PDK1 were immunoblotted with anti-CARD11 and anti-Myc, respectively. (**D**) Defective recruitment of CARD11 to lipid rafts in PDK1 knockdown cells. Wild-type or PDK1^{kd} Jurkat cells (5×10^7) were stimulated with or without anti-CD3 and anti-CD28. Proteins from equal volumes of fractions prepared as in Fig. 3A were separated by SDS–polyacrylamide gel electrophoresis and analyzed by immunoblotting with anti-CARD11 and anti-Bcl10.

not with Bcl10, consistent with the hypothesis that PDK1 recruits CARD11, whereas Bcl10 and MALT1 might be recruited to the membrane via CARD11 (Fig. 4B). The GUK (guanylate kinase) domain of CARD11 appeared to be responsible for this specific interaction with PDK1 (Fig. 4C). The recruitment of CARD11 and Bcl10 after TCR stimulation was completely abolished in PDK1^{kd} cells, strongly suggesting that PDK1 plays an essential role in this process (Fig. 4C). Immunofluorescence analysis also showed a reduction in membrane recruitment of CARD11 in PDK1^{kd}, but not in control, Jurkat cells (fig. S2B) (*19*).

We propose the following model to explain the sequence of events leading from the TCR to NF-κB activation (Fig. 5). Upon TCR engagement, PI3K is activated, thereby producing the lipid effectors PIP_2 and PIP_3. These lipid effectors help activate membrane-associated PDK1 and lead to its enrichment in rafts. PDK1 then recruits and activates PKCθ by phosphorylation, and the active PKCθ subsequently recruits the IKK complex into the lipid raft (Fig. 5). PDK1 simultaneously recruits the CARD11-Bcl10-MALT1 complex, and the membrane-bound Bcl10 complex then activates IKK through ubiquitination of NEMO. PDK1 therefore plays a central nucleating role by linking the TCR to two signaling cassettes, PKCθ-IKK and CARD11-MALT1-Bcl10, leading ultimately to the activation of NF-κB in response to signaling from the TCR.

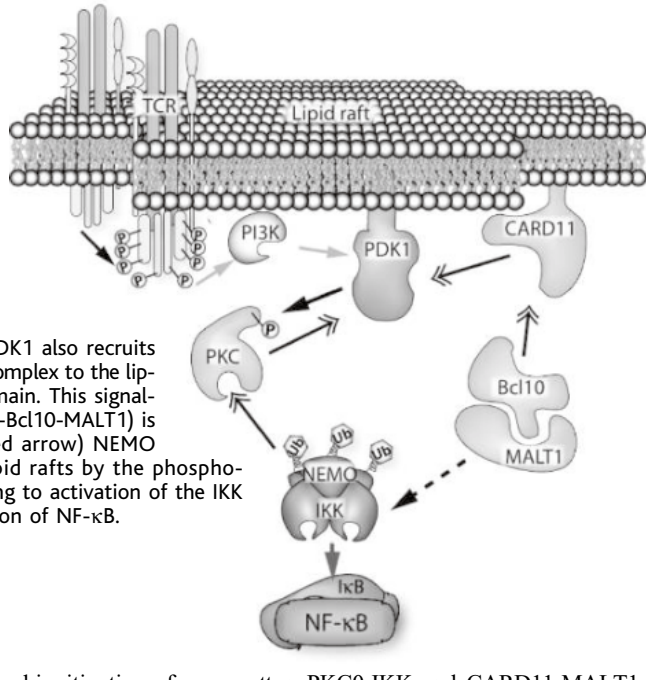

Fig. 5. A model of TCR signaling to NF-κB. Stimulation of cells through TCR complexes leads to phosphorylation of cytoplasmic immunoreceptor tyrosine-based activation motifs (ITAMs) and recruitment and activation (gray arrows) of PI3K and, subsequently, PDK1. Activated PDK1 phosphorylates (bold arrow) PKCθ, which is able to recruit (double-headed arrows) IKKs to lipid raft domains. Meanwhile, PDK1 also recruits the CARD11-Bcl10-MALT1 complex to the lipid raft through its GUK domain. This signaling complex (PDK1-CARD11-Bcl10-MALT1) is able to ubiquitinate (dashed arrow) NEMO (which was recruited to lipid rafts by the phospho-PKCθ-PDK1 complex), leading to activation of the IKK complex and, lastly, activation of NF-κB.

References and Notes

1. L. P. Kane, J. Lin, A. Weiss, *Trends Immunol.* **23**, 413 (2002).
2. M. S. Hayden, S. Ghosh, *Genes Dev.* **18**, 2195 (2004).
3. S. Ghosh, M. J. May, E. B. Kopp, *Annu. Rev. Immunol.* **16**, 225 (1998).
4. M. Karin, Y. Ben-Neriah, *Annu. Rev. Immunol.* **18**, 621 (2000).
5. S. Ghosh, M. Karin, *Cell* **109** (suppl.), S81 (2002).
6. M. J. May *et al.*, *Science* **289**, 1550 (2000).
7. D. Wang *et al.*, *Mol. Cell. Biol.* **24**, 164 (2004).
8. X. Lin, A. O'Mahony, Y. Mu, R. Geleziunas, W. C. Greene, *Mol. Cell. Biol.* **20**, 2933 (2000).
9. A. Khoshnan, D. Bae, C. A. Tindell, A. E. Nel, *J. Immunol.* **165**, 6933 (2000).
10. M. Thome, *Nat. Rev. Immunol.* **4**, 348 (2004).
11. H. Zhou *et al.*, *Nature* **427**, 167 (2004).
12. J. A. Le Good *et al.*, *Science* **281**, 2042 (1998).
13. P. S. Costello, M. Gallagher, D. A. Cantrell, *Nat. Immunol.* **3**, 1082 (2002).
14. J. Harriague, G. Bismuth, *Nat. Immunol.* **3**, 1090 (2002).
15. C. S. Mitsiades, N. Mitsiades, M. Koutsilieris, *Curr. Cancer Drug Targets* **4**, 235 (2004).
16. H. J. Hinton, D. R. Alessi, D. A. Cantrell, *Nat. Immunol.* **5**, 539 (2004).
17. B. Sparatore *et al.*, *FEBS Lett.* **554**, 35 (2003).
18. T. R. Brummelkamp, R. Bernards, R. Agami, *Science* **296**, 550 (2002); published online 21 March 2002 (10.1126/science.1068999).
19. Materials and methods are available as supporting material on *Science* Online.
20. K.-Y. Lee, S. Ghosh, unpublished results.
21. J. L. Pomerantz, E. M. Denny, D. Baltimore, *EMBO J.* **21**, 5184 (2002).
22. P. Flynn, M. Wongdagger, M. Zavar, N. M. Dean, D. Stokoe, *Curr. Biol.* **10**, 1439 (2000).
23. C. Pfeifhofer *et al.*, *J. Exp. Med.* **197**, 1525 (2003).
24. T. Egawa *et al.*, *Curr. Biol.* **13**, 1252 (2003).
25. Supported by NIH (R37-AI33443). We would like to thank J. Pober, X. H. Sun, and D. Rothstein for carefully reading the manuscript and X. Lin (University of Buffalo) for sharing the CARD11-deficient Jurkat cells. Molecular interaction data have been deposited in the Biomolecular Interaction Network Database with accession codes 209039 to 209044.

Supporting Online Material

www.sciencemag.org/cgi/content/full/308/5718/114/DC1
Materials and Methods
Figs. S1 to S3

4 November 2004; accepted 14 January 2005
10.1126/science.1107107

RNA Polymerase IV Directs Silencing of Endogenous DNA

A. J. Herr,[1] M. B. Jensen,[1] T. Dalmay,[2] D. C. Baulcombe[1]*

Plants encode subunits for a fourth RNA polymerase (Pol IV) in addition to the well-known DNA-dependent RNA polymerases I, II, and III. By mutation of the two largest subunits (NRPD1a and NRPD2), we show that Pol IV silences certain transposons and repetitive DNA in a short interfering RNA pathway involving RNA-dependent RNA polymerase 2 and Dicer-like 3. The existence of this distinct silencing polymerase may explain the paradoxical involvement of an RNA silencing pathway in maintenance of transcriptional silencing.

We previously identified an *Arabidopsis sde4* mutant that exhibited partial loss of a transgene-silencing pathway that is otherwise dependent on RNA-dependent RNA polymerase 6 (RDR6) (*1*). The *sde4* mutant plants were also defective for small interfering RNA (siRNA) production and methylation of the SINE retroelement AtSN1 (*2*) in a pathway that was subsequently associated with RDR2, Dicer-like 3 (DCL3), and other endogenous siRNAs (*3*). It is likely that this silencing pathway is related to the RNA interference (RNAi)–mediated heterochromatinization in *Schizosaccharomyces pombe* that is also dependent on siRNA, Dicer, and an RDR (*4*). Therefore, to investigate the mechanism of both transgene and retroelement silencing we investigated the molecular identity of the *SDE4* locus. We describe here how *SDE4* encodes the largest subunit of a putative RNA polymerase that is distinct from eukaryotic RNA polymerases I, II, and III (whose subunits in *Arabidopsis* are designated by the prefix *NRPA*, *NRPB*, or *NRPC*, respectively). In keeping with the convention of naming RNA polymerases, we henceforth refer to this enzyme as RNA polymerase IV (Pol IV) and the largest subunit encoded at *SDE4* as NRPD1a. The previously described *sde4* mutation is now designated *nrpd1a-1*.

[1]Sainsbury Laboratory, John Innes Centre, Norwich NR4 7UH, UK. [2]University of East Anglia, Norwich NR4 7TJ, UK.

*To whom correspondence should be addressed. E-mail: david.baulcombe@sainsbury-laboratory.ac.uk

The screen for mutants defective in transgene silencing used an *Arabidopsis* line (GxA) in which a green fluorescent protein (GFP) transgene (fig. S1A, designated G) was silenced by a potato virus X (PVX)–GFP transgene (fig. S1A, designated A) (*1*). Unlike *rdr6* mutants, which completely lose GFP silencing in the GxA background, *nrpd1a-1* displayed a delayed onset of silencing in the growing points of the plant (Fig. 1A and fig. S1F) (*1*). In young plants, the leaves initially emerged GFP-fluorescent, but, within a week, silencing appeared in localized areas and then spread throughout the leaf. This delayed onset phenotype persisted until flowering when the young inflorescences were GFP-fluorescent.

The patterns of transgene mRNA and siRNA accumulation corresponded to the amount of GFP fluorescence. Thus, the Northern analysis of wild-type and *nrpd1a-1* flowers showed that increased accumulation of GFP mRNA (4.5-fold) and PVX-GFP RNA in *nrpd1a-1* corresponded to a sixfold reduction of 21- to 24-nucleotide (nt) GFP siRNAs (Fig. 1B) relative to wild type. In fully silenced rosette leaves, where the *nrpd1a*-mediated loss of silencing was less pronounced than in flowers, GFP mRNA and siRNA amounts were comparable.

RNA-directed DNA methylation (RdDM) is associated with silencing in plants and is likely mediated by an siRNA-guided effector complex. Consistent with RdDM at the GFP locus in GxA plants, GFP DNA methylation is lost in flowers of *rdr6* and *sgs3* mutants along with GFP siRNAs (*1*) (Fig. 1C). In *nrpd1a-1* flowers, where GFP siRNAs are reduced but not absent, we detected only slight changes in the pattern of GFP DNA methylation (Fig. 1C) that contrast with a more pronounced loss of AtSN1 DNA methylation in *nrpd1a-1* plants (*2*, *5*). Thus, the NRPD1a pathway is not the only source of suitable siRNAs for RdDM.

We mapped *nrpd1a-1* to a large rearrangement on chromosome 1 that disrupted At1g63020 (fig. S1, B to G) and then used other *nrpd1a* alleles and complementation with an NRPD1a transgene to confirm that this gene encoded *NRPD1a*. The sequence of NRPD1a aligned with an *A. thaliana* NRPD1a homolog (encoded by At2g40030) and two putative proteins from rice in a plant-specific clade for the largest subunit of RNA polymerase (Fig. 2A and fig.S2, A to C). Consistent with NRPD1a being the largest subunit of a multisubunit Pol IV, the rice and *A. thaliana* genomes encode two proteins that could be the second-largest subunit (At3g18090 and At3g23780) (*6*) (Fig. 2B and fig. S2D). To test the silencing role of these putative *Arabidopsis* NRPD2 subunits, we transformed wild-type GxA plants with inverted repeat (IR) constructs that would target RNAi to *NRPD1a*, the putative *NRPD2* genes, or GUS (as a control) (fig. S3, A and B). The transformants with the IR directed against *NRPD1a* and the putative *NRPD2* genes, but not against GUS (fig. S3, C and D), exhibited a delayed onset of silencing like that of *nrpd1a-1*. Although both *NRPD2* genes would be inactivated by the IR construct (fig. S3B), two lines of evidence indicate that the active *NRPD2* locus is At3g23780 rather than At3g18090. First, gene-specific reverse transcription polymerase chain reaction (RT-PCR) analysis showed that most of the *NRPD2* transcripts come from At3g23780 (fig. S3E), and, second, an insertion mutant in At3g23780 (*nrpd2a-1*, fig. S3F) but not At3g18090 (*nrpd2b-1*, fig. S3F) eliminated endogenous siRNA (Fig. 3A).

NRPD1a and NRPD2 have sequence similarities to their NRPA, NRPB, and NRPC homologs in regions corresponding to functionally important features of yeast RNA polymerase

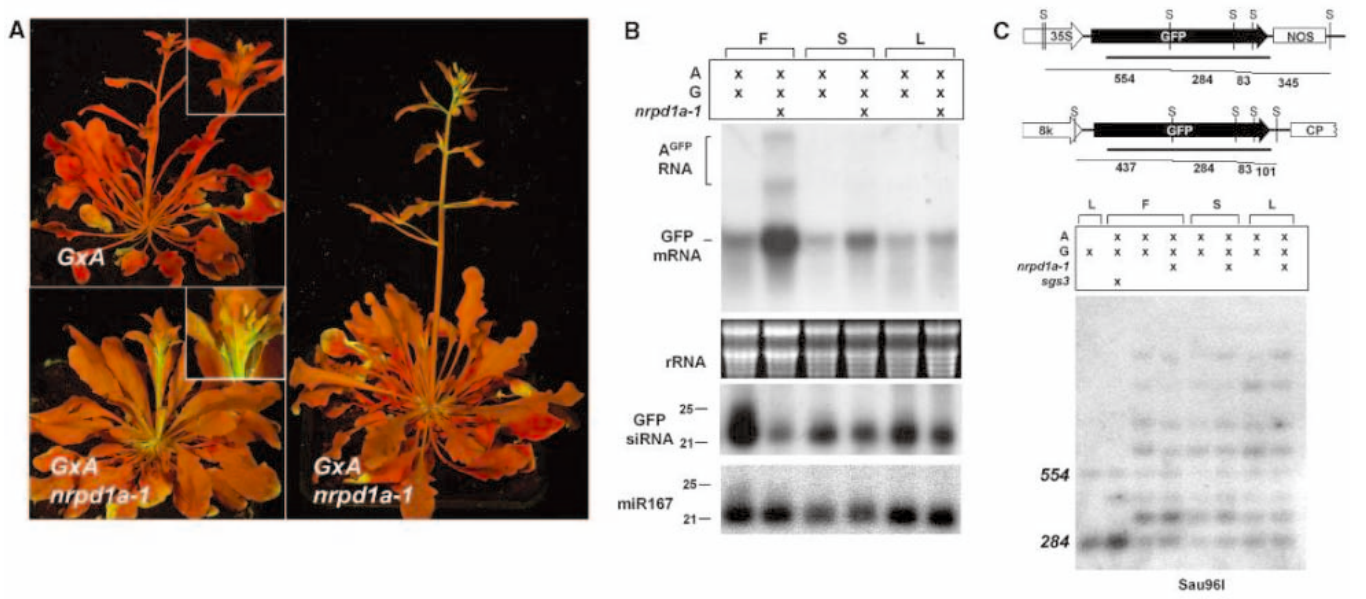

Fig. 1. GFP silencing in *nrpd1a-1*. (**A**) Ultraviolet pictures of GxA wild-type (WT) and *nrpd1a-1* flowering plants. (**B**) Northern analysis of GFP mRNA and siRNA in flowers (F), stems (S), and leaves (L) from WT and *nrpd1a-1* GxA plants. (**C**) Southern blot analysis of genomic DNA purified from the same tissues as in (B), digested with the methylation-sensitive enzyme Sau96I, and probed for GFP. Unmethylated G and GxA *sgs3* lines serve as controls. DNA fragments larger than 554 nt are caused by DNA methylation.

II (*7*). For NRPD1a, regions of identity with NRPB1 include the N-terminal clamp core (20%), the Zn metal binding sites, the active site (41%), the funnel and portions of the cleft domain (beginning, 42%, and end, 24%). The middle of the cleft domain in NRPA1, NRPB1, and NRPC1 is absent in NRPD1a (conserved region G) (fig. S2B). However, the C-terminal clamp core (fig. S2B), which defines the end of the globular domain before the C-terminal domain (CTD) of NRPB1 (*7*), is present (23% identical). NRPD2 is 34% identical to NRPB2 and has conserved regions corresponding to the binding sites of smaller core subunits (NRPB3/AC40, NRPB10, and NRPB12) (fig. S2D) that are thought to play a role in enzyme assembly (*7*). There are multiple genes for NRPB3/AC40, and some of them could be Pol IV–specific. However, for NRPB10 and NRPB12 there are only two genes each in *Arabidopsis*, and they could be shared between Pol IV and other RNA polymerases because they are in other eukaryotes (*8*).

The most striking difference between NRPB1 and NRPD1a is at the C terminus of NRPD1, where the rice and *Arabidopsis* proteins share similarity to the C-terminal half of a nuclear-encoded protein (defective chloroplasts and leaves) that regulates rRNA processing in chloroplasts (*9*) (fig. S2A). This C-terminal extension may coordinate RNA polymerase activity with downstream processing steps in a manner analogous to the CTD of Pol II (*8*). The combination of this unusual C terminus with conserved features of RNA polymerases suggests that Pol IV is an active RNA polymerase with important differences from RNA polymerases I, II, and III.

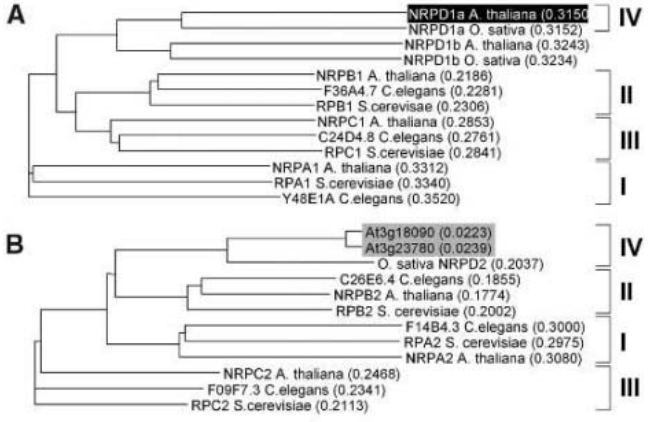

Fig. 2. Phylogenetic trees of the largest (**A**) and second largest (**B**) RNA polymerase subunit families from plants, worms, and yeast. I to IV on the right of each tree indicates RNA polymerase subfamily. Gray and black boxes indicate *Arabidopsis* Pol IV subunits.

To further investigate the mechanism of Pol IV–mediated silencing, we characterized another mutant with a delayed onset of GFP silencing (fig. S4A). It has an inversion on chromosome 4 that disrupts *RDR2* (fig. S4B, *rdr2-3*), and the GFP silencing phenotype could be complemented by transformation with wild-type *RDR2* genomic DNA (fig. S4A). In this mutant, as in *nrpd2a-1* and each of the *nrpd1a* mutants, there were lower amounts of endogenous 24-nt siRNAs (AtSN1, 1003, 02, and cluster 2) than in wild type, whereas miR167 amounts were unaffected (Fig. 3A) (*3*). These siRNAs are all in the 24-nt size class, and the *DCL3* Dicer is involved in their biogenesis (*3*). It is likely therefore that Pol IV, RDR2, and DCL3 act together in a silencing pathway. Pol IV would generate RNA species that are copied into double-stranded RNA (dsRNA) by RDR2. This dsRNA would then be processed into siRNA by DCL3.

The *RDR2* and *RDP1* mutations also affected long RNAs from the siRNA loci. However, opposite to the effect on siRNA, the long RNAs were more abundant in the silencing mutants. Thus, AtSN1 RNA was more abundant in the *nrpd1a* and *rdr2* mutants than in wild-type plants (Fig. 3C), indicating that they are not Pol IV transcripts. Presumably this RNA results from the RNA polymerase III transcription (*10*) of AtSN1 that is silenced by the Pol IV–RDR2–DCL3 pathway in wild-type plants. Our inability to detect long Pol IV transcripts from AtSN1 is presumably because they are present at only very low amounts and are masked by more abundant RNAs produced by other RNA polymerases.

The Pol IV–RDR2–DCL3 pathway associated with cluster 2 and 02 siRNAs does not require AGO4 or DNA methylation (*3*). However, the AtSN1 and 1003 loci are hypermethylated in wild-type plants relative to the *nrpd1a* mu-

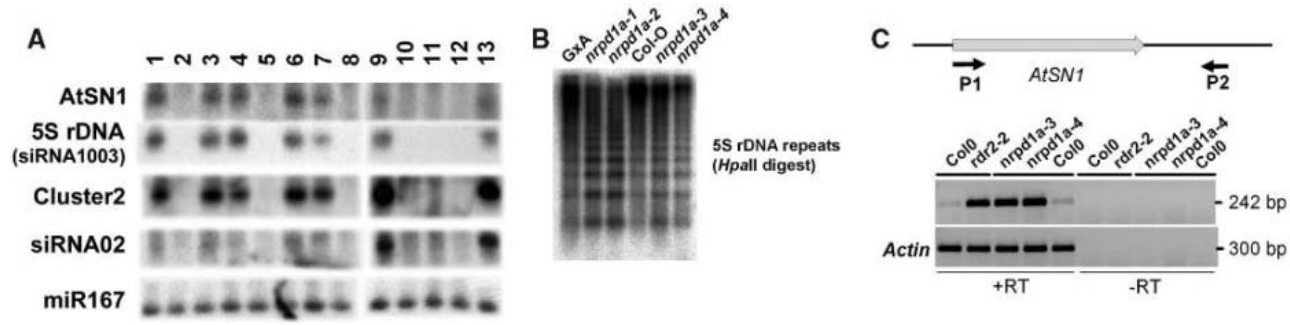

Fig. 3. Molecular indicators of silencing. (**A**) Northern analysis of endogenous small RNAs: lanes 1 to 8, GxA (C24) background; lanes 9 to 13, Col-O background. Lane 1, WT; lane 2, *rdr2-3*; lanes 3 and 4, two independent *rdr2-3 RDR2p::RDR2* T2 lines; lane 5, *nrpd1a-1*; lanes 6 and 7, two independent *nrpd1a-1 NRPD1ap::NRPD1a* T2 lines; lane 8, *nrpd1a-2*; lane 9, WT; lane 10, *nrpd1a-3*; lane 11, *nrpd1a-4*; lane 12, *nrpd2a-1*; lane 13, *nrpd2b-1*. Blots were stripped and reprobed multiple times. (**B**) Southern analysis of 5S rDNA repeats in the *NRPD1a* allelic series after digestion with the methylation-sensitive enzyme HpaII. (**C**) RT-PCR analysis of endogenous AtSN1 transcripts that are elevated in *rdr2-2* and *nrpd1a* mutants.

tants (*2*) (Fig. 3B), and accumulation of their siRNAs is dependent on the Argonaute protein AGO4, the de novo DNA methyltransferases DRM1 and DRM2 (*5*, *11*, *12*), as well as Pol IV, RDR2, and DCL3. In these examples, it seems, as has been proposed in *S. pombe* (*13*), that maintenance of silencing involves a self-reinforcing silencing pathway in which Pol IV–mediated siRNA production is dependent on the AGO4-mediated DNA methylation and vice versa.

The role of Pol IV as described here could resolve a paradox of chromatin silencing mechanisms that are dependent on RNA. If the silenced loci are transcribed by a single polymerase, such RNA-dependent mechanisms would not be stable because the suppression of transcription from these loci would also lead to loss of silencing RNA. However, a silencing-specific polymerase like Pol IV may be resistant to chromatin or DNA modifications affecting polymerases I to III and so could stably maintain the silenced state. In animals and fungi the Pol IV clade is absent, but the silencing paradox may be resolved if there are forms of the RNA polymerases I to III with silencing-specific subunits that allow transcription of heterochromatin and, consequently, maintenance of the RNA-dependent silencing.

A final general point about silencing mechanisms is illustrated by the GFP transgene silencing and endogenous 24-nt siRNA silencing pathways that are both dependent on RDR proteins (fig. S4). In rosette leaves of the plant, these two silencing pathways are independent of each other because transgene silencing is unaffected by *rdr2* (fig. S4) and because endogenous 24nt siRNA persists in *rdr6* plants (*2*). However, in flowers these pathways are interdependent, because the GFP silencing is affected by both *rdr2* and *rdr6*. This potential of silencing pathways to interact, combined with their ability to form feedback and self-reinforcing loops (*14*), illustrates the potential complexity of endogenous regulatory networks involving siRNAs.

References and Notes

1. T. Dalmay, A. Hamilton, S. Rudd, S. Angell, D. C. Baulcombe, *Cell* **101**, 543 (2000).
2. A. Hamilton, O. Voinnet, L. Chappell, D. C. Baulcombe, *EMBO J.* **21**, 4671 (2002).
3. Z. Xie *et al.*, *PLoS Biol.* **2**, e104 (2004); published online 24 February 2004.
4. T. Volpe *et al.*, *Science* **297**, 1833 (2002); published online 22 August 2002 (10.1126/science.1074973).
5. S. W. L. Chan *et al.*, *Science* **303**, 1336 (2004).
6. The Arabidopsis Genome Initiative, *Nature* **408**, 796 (2000).
7. P. Cramer, D. A. Bushnell, R. D. Kornberg, *Science* **292**, 1863 (2001); published online 19 April 2001 (10.1126/science.1059493).
8. P. Cramer, *Curr. Opin. Struct. Biol.* **12**, 89 (2002).
9. M. Bellaoui, W. Gruissem, *Planta* **219**, 819 (2004).
10. F. Myouga, S. Tsuchimoto, K. Noma, H. Ohtsubo, E. Ohtsubo, *Genes Genet. Syst.* **76**, 169 (2001).
11. D. Zilberman *et al.*, *Curr. Biol.* **14**, 1214 (2004).
12. D. Zilberman, X. Cao, S. E. Jacobsen, *Science* **299**, 716 (2003); published online 9 January 2003 (10.1126/science.1079695).
13. T. Sugiyama, H. Cam, A. Verdel, D. Moazed, S. I. S. Grewal, *Proc. Natl. Acad. Sci. U.S.A.* **102**, 152 (2005).
14. D. Baulcombe, *Nature* **431**, 356 (2004).
15. The authors acknowledge funding from the Gatsby Charitable Foundation, the Biotechnology and Biological Sciences Research Council, and the Burroughs Wellcome Fund (to A.J.H.) as well as technical assistance from L. Day.

Supporting Online Material

www.sciencemag.org/cgi/content/full/1106910/DC1
Materials and Methods
Figs. S1 to S4
Tables S1 and S2
References and Notes

29 October 2004; accepted 25 January 2005
Published online 3 February 2005;
10.1126/science.1106910
Include this information when citing this paper.

Translational Operator of mRNA on the Ribosome: How Repressor Proteins Exclude Ribosome Binding

Lasse Jenner,[1] Pascale Romby,[2] Bernard Rees,[1] Clemens Schulze-Briese,[3] Mathias Springer,[4] Chantal Ehresmann,[2] Bernard Ehresmann,[2] Dino Moras,[1] Gulnara Yusupova,[1] Marat Yusupov[1,2]*

The ribosome of *Thermus thermophilus* was cocrystallized with initiator transfer RNA (tRNA) and a structured messenger RNA (mRNA) carrying a translational operator. The path of the mRNA was defined at 5.5 angstroms resolution by comparing it with either the crystal structure of the same ribosomal complex lacking mRNA or with an unstructured mRNA. A precise ribosomal environment positions the operator stem-loop structure perpendicular to the surface of the ribosome on the platform of the 30*S* subunit. The binding of the operator and of the initiator tRNA occurs on the ribosome with an unoccupied tRNA exit site, which is expected for an initiation complex. The positioning of the regulatory domain of the operator relative to the ribosome elucidates the molecular mechanism by which the bound repressor switches off translation. Our data suggest a general way in which mRNA control elements must be placed on the ribosome to perform their regulatory task.

Initiation of translation generally determines the efficiency of protein synthesis and is the key step for the control of gene expression when fast adaptation is required. Binding of the eubacterial ribosome involves several elements of the mRNA, which affect the kinetics of the

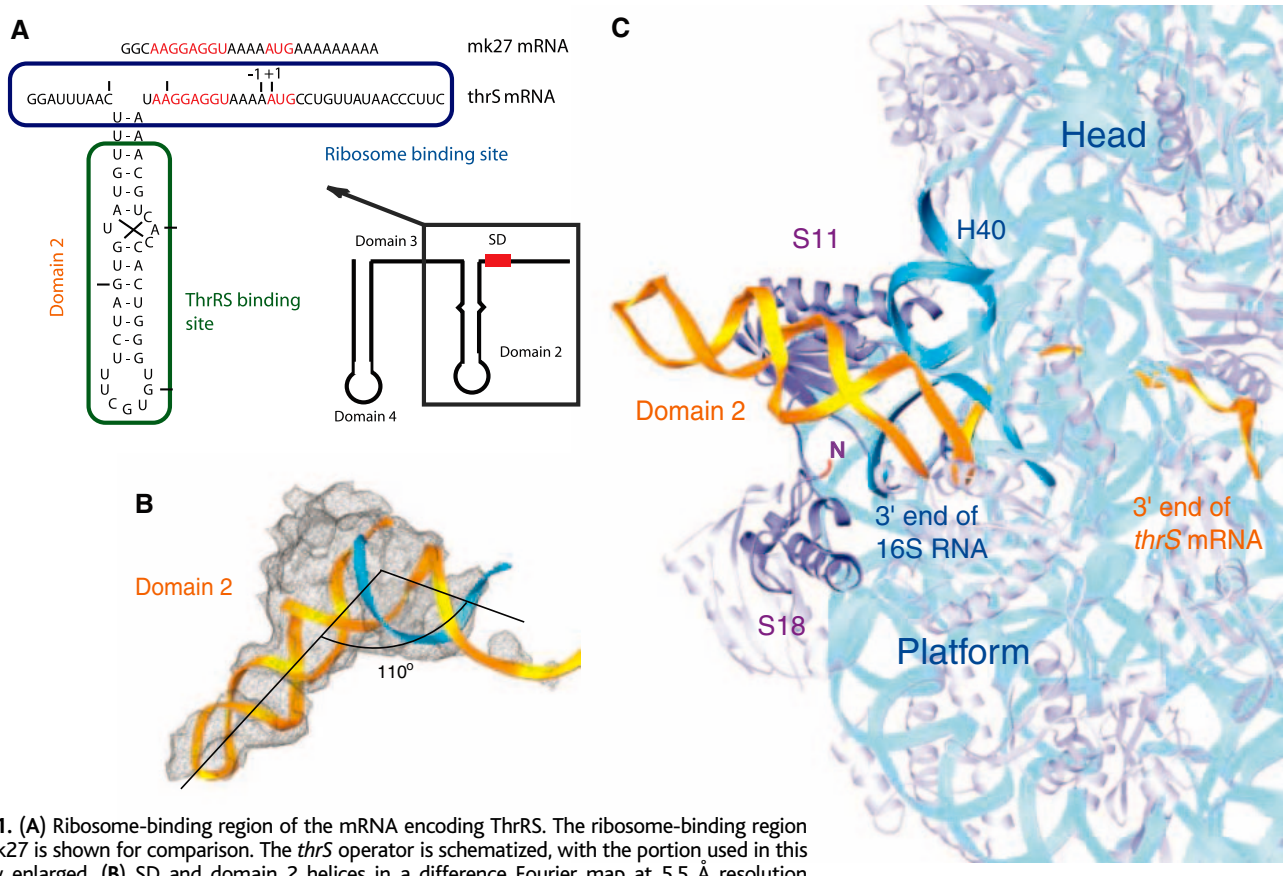

Fig. 1. (**A**) Ribosome-binding region of the mRNA encoding ThrRS. The ribosome-binding region of mk27 is shown for comparison. The *thrS* operator is schematized, with the portion used in this study enlarged. (**B**) SD and domain 2 helices in a difference Fourier map at 5.5 Å resolution contoured at 3.0 σ (signal-to-noise ratio). (**C**) Solvent side view of 30*S* subunit with domain 2 and SD helix of *thrS* mRNA in yellow. The 3′ end of 16*S* rRNA, forming base pairs with the SD helix, and helix H40 are highlighted in cyan; the proteins S11 and S18, in close contact with domain 2, are highlighted in blue.

formation of the initiation complex. These elements may include binding sites for translational regulatory proteins (*1*). *Escherichia coli* threonyl–tRNA synthetase (ThrRS) plays such a role, because it inhibits its own synthesis by binding to *thrS* (the gene that codes for ThrRS) mRNA in a region located upstream from the ribosome binding site (*2*). Although ThrRS and the ribosome compete for binding to *thrS* mRNA, their binding sites do not strictly overlap. The ribosome binds to the Shine-Dalgarno (SD) region but also to a single-stranded sequence located 50 nucleotides upstream (Fig. 1A) (*3*). The dimeric ThrRS binds specifically and symmetrically to two stem-loops (domains 2 and 4, Fig. 1A) in a way that mimics tRNA anticodon recognition (*4*, *5*). The crystal structure of domain 2, the essential component of control, complexed with ThrRS was determined previously (*5*). The complete path on the ribosome of the nonstructured mRNA of gene 32 of the bacteriophage T4 (mk27) was mapped by x-ray crystallography at 7.0 Å resolution (*6*). Here, we identify the path of *thrS* mRNA on the ribosome in the presence of the initiator $tRNA_f^{Met}$ (where f is formylated and Met is methionine) at 5.5 Å resolution by x-ray crystallography. The operator domain 2 remains structured and protrudes out of the ribosome; its position suggests how the ThrRS repressor protein interferes with the ribosome for translation initiation.

The *thrS* mRNA (–59 to +19 nucleotides) was cocrystallized with the ribosome of *Thermus thermophilus* in the presence of the initiator $tRNA_f^{Met}$. This mRNA fragment contains the essential translational operator domain 2 flanked by two single-stranded regions, which constitute the ribosomal binding site (Fig. 1A). In order to improve the binding of *thrS* mRNA with the *T. thermophilus* ribosome, the complementarity between the SD sequence and the 3′ end of the *T. thermophilus* 16*S* ribosomal RNA (rRNA) was extended to form eight base pairs. Crystals containing the functional ribosome complex with initiator $tRNA_f^{Met}$ in the absence of mRNA, or in the presence of the model mRNA mk27 (Fig. 1A), were obtained under similar experimental conditions (*6*–*9*). Data were collected to 5.5 Å resolution (table S1). Difference Fourier maps were computed using a phase set calculated from the existing model (*8*), completed and refined as described in (*10*), and the structure factor differences between the *thrS* mRNA and non-mRNA data sets were computed.

The electron density difference map clearly revealed the position of *thrS* mRNA on the ribosome and the changes associated with its binding. The *thrS* mRNA enters in the tunnel formed between the head and the shoulder, wraps around the neck, and exits through the groove between the head and the platform on the opposite side (Fig. 1C). Density was found in the 5′ mRNA region corresponding to regulatory domain 2 (Fig. 1B), which correlates with a kinked helix, as in the x-ray structure of the ThrRS domain 2 complex (*5*). However, the electron density map indicates a different conformation of the loop structure, which is similar to the anticodon loop of a free tRNA (Fig. 1B). This finding is consistent with the proposal that the domain 2 loop binds ThrRS by an induced fit mechanism (*5*). A second cylinder of density was observed in prolongation of domain 2, consistent with the formation of the SD helix involving eight base pairs (Fig. 1B). The stem of domain 2 and the SD helix form an almost continuous helix with a 110° kink. Four nucleotides (–51 to

[1]Institut de Génétique et de Biologie Moléculaire et Cellulaire, Illkirch, France. [2]Institut de Biologie Moléculaire et Cellulaire, Strasbourg, France. [3]Swiss Light Source at Paul Scherrer Institut, Zurich, Switzerland. [4]Institut de Biologie Physico-Chimique, Paris, France.

*To whom correspondence should be addressed. E-mail: marat@titus.u-strasbg.fr

–54) of the 5′ end of *thrS* mRNA are folded back into the minor groove of the SD helix, possibly resulting in a local triple helix. The junction between domain 2 and the SD helix is most likely stabilized by additional interactions with ribosomal proteins. Indeed, the ribosomal protein S11 is near enough to interact with the upper helix of domain 2 (Fig. 1C). On the opposite side, the additional electron density may be ascribed to the 15 N-terminal residues of protein S18, which were not modeled in the high-resolution 30*S* structure because of disorder (*11*), and therefore are missing in our model. The N-terminal part of S18 appears to be directed toward the major groove of both the SD helix and the upper helix of domain 2 on the 5′ side of the mRNA. This region is rich in basic and aromatic residues, which would favor RNA interactions. In addition, domain 2 may interact with the loop of helix 40 of the 16*S* rRNA (Fig. 1C). The constraints imposed by the SD helix and the ribosomal environment around the domain 2 stem place the regulatory domain on the platform of the 30*S* ribosomal subunit, protruding from the surface of the ribosome.

These data correlate with footprinting experiments showing that the ribosome protects two noncontiguous mRNA regions (nucleotides U –12 to C +16 and U –55 to C –50, Fig. 1A) and the edge of domain 2 (*3*). Domain 2 is located at a position that partially overlaps with the binding site of protein S1, which is absent from the present structure because of the ribosome purification protocol. Protein S1 interacts with ribosomal proteins S11 and S18 and with helix 40 of the 16*S* rRNA (*11*, *12*) and is involved in mRNA selection by binding to the 5′ untranslated region of the mRNA (*12*, *13*). However, it was previously shown that S1 did not enhance translational initiation of *thrS* mRNA in vivo, and it was also shown that no strong S1-specific effect could be associated with the single-stranded domain 3 (*3*), a potential S1 binding site. Thus, although protein S1 does not appear to be involved in the positioning of *thrS* mRNA, S18 may play such a role by direct interaction with the upper stem of domain 2 and the 5′ single-stranded upstream region.

Because $tRNA_f^{Met}$ was present in all ribosomal complexes, no difference was observed in the electron density for the peptidyl-tRNA binding site (P site). However, the electron density difference map shows that E-site (exit-tRNA binding site) tRNA was absent and A-site (aminoacyl-tRNA binding site) tRNA was present in the *thrS* ribosome complex, in contrast to the mk27 ribosome complex (Fig. 2). The presence of initiator tRNA in the P site and an unoccupied E site correspond to the expected signature for a bona fide initiation complex. The presence of an A-site tRNA raises questions about its origin and binding mode (cognate/noncognate or near-cognate, which represent the extent of complementarity between the mRNA codon and the tRNA anticodon in A-site tRNA). As proposed in the case of the mk27 ribosome complex, the presence of E-site tRNA was most likely due to copurification with the ribosome and is likely to be a mixture of tRNAs (*9*). This idea has been recently confirmed by analyzing the profile of the tRNA species associated with the purified ribosomes (*14*). Therefore, the tRNAs leaving the E site in the *thrS* complex most likely bind to the A site in a noncognate or near-cognate way. This result agrees with an earlier biochemical study showing that the ribosome without E-site tRNA can more easily accept noncognate tRNA in the A site (*15*). Our results further indicate that the position of the noncognate or near-cognate tRNAs in the A site is similar to the cognate A-site tRNA as previously shown (*8*, *9*). Thus, our crystal complex would imitate the conformation of the ribosome in the "post-accommodation" step, where the CCA end of the tRNA is oriented to the peptidyl transferase center (*16*).

Changes were observed in the L1 arm, which was shown to adopt different orientations in the 70*S* ribosome complex containing E-site tRNA, as compared with the free 70*S* ribosome or with the 50*S* subunit (*17*–*19*). Consistent with the absence of E-site tRNA, the 23*S* rRNA loop between helices 76 and 77 (nucleotides 2110 to 2118) in the L1 arm, which is known to interact with the E-site tRNA (*20*), becomes flexible (Fig. 2). In addition, 16*S* rRNA elements, including the neck helix (H28), helices 35 and 37, and part of helix 34, were no longer detectable in the *thrS* mRNA complex (Fig. 2). This destabilization suggests that the rRNA elements participate in E-site tRNA binding. Because *thrS* mRNA mainly differs from mk27 by the presence of domain 2 at its 5′ end (Fig. 1A), its positioning on the platform of the 30*S* subunit may cause the exit of E-site tRNA. A similar function was proposed for the initiation factor IF-3. Because the N-terminal domain of the factor neighbors the ribosomal proteins S7 and S11, it was suggested that it might exclude the tRNA from the 30*S* subunit E site during initiation (*21*). Despite these differences between the two mRNA (mk27 and *thrS*) complexes, we did not observe much movement of the head of the 30*S* subunit. Both complexes adopt a close conformation of the head (*22*) despite the differences in the occupancy of the tRNA binding sites, in agreement with the recent finding that the movement of the head is related to the formation of the 70*S* ribosome (*19*).

The precise positioning of domain 2 relative to the ribosome elucidates the molecular mechanism by which ThrRS binding switches off translation. It is impossible to dock the whole enzyme on domain 2 bound to the ribosome by using the crystallographic coordinates of the tRNA-ThrRS complex (*23*) because of a steric clash between the entire N-terminal domain and the 30*S* subunit (Fig. 3). The model supports an indirect competition mechanism, in which the whole N-terminal domain sterically hinders ribosome binding.

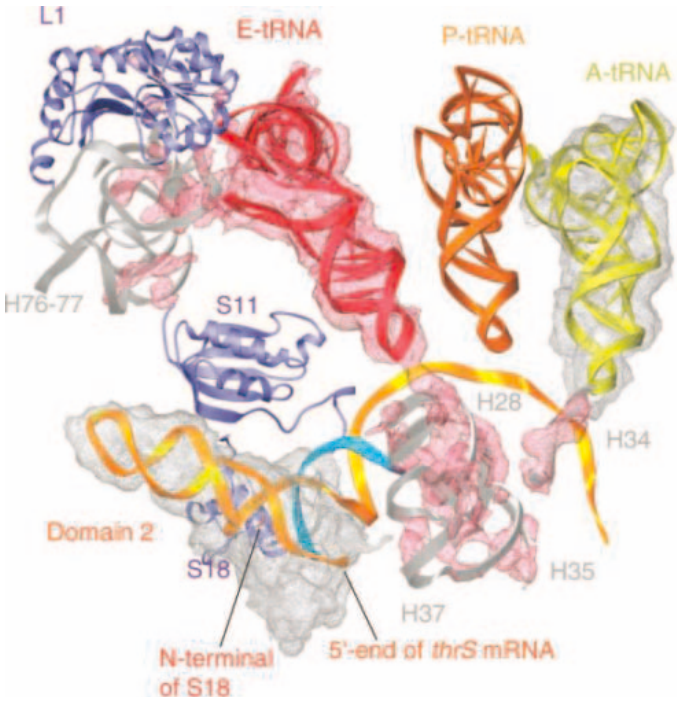

Fig. 2. Top view of the *thrS* mRNA path on the ribosome. The electron density difference between the *thrS* mRNA complex and mk27 where positive differences (density that appeared only in the *thrS* mRNA complex) are in gray and negative differences (density that appeared only in the mk27 mRNA complex) are in red, contoured at 3.0 and –3.0 σ, respectively. The map shows that although the mk27 mRNA complex contains tRNAs in the P and E sites, the *thrS* mRNA complex has tRNAs in the P and A sites. In the *thrS* mRNA complex, the 23*S* rRNA loop (nucleotides 2110 to 2118) between helices 76 and 77 becomes flexible as well as the 16*S* RNA neck helix H28 (nucleotides 919 to 933 and 1380 to 1395), the helices 35 and 37 (nucleotides 1068 to 1073 and 1082 to 1109), and part of helix 34 (nucleotides 1191 to 1199).

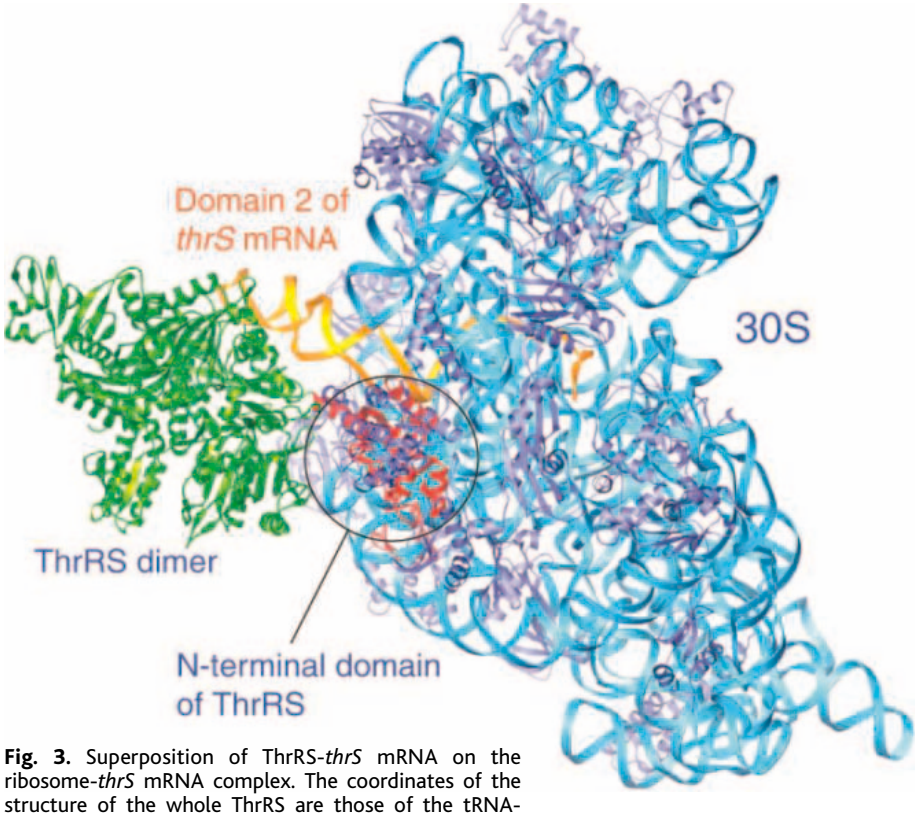

Fig. 3. Superposition of ThrRS-*thrS* mRNA on the ribosome-*thrS* mRNA complex. The coordinates of the structure of the whole ThrRS are those of the tRNA-ThrRS crystal structure (*21*). The ThrRS dimer is shown in green. The N-terminal domain of one monomer (shown in red) overlaps with the 30*S* subunit of the ribosome.

Consistent with this model, the deletion of the N-terminal domain of ThrRS was shown to abolish control in vivo, and the truncated enzyme was unable to compete with the ribosome for binding, despite its capacity to bind efficiently to the *thrS* operator (*4*). Therefore, the elongated structure of the enzyme and the positioning of the regulatory domain with respect to the 30*S* subunit contribute to the competition mechanism. Such a mechanism does not impose stringent constraints on the protein structure, because the specificity of control can be readily switched from threonyl- to methionyl-tRNA synthetase (*24*). This type of regulatory mechanism is also kinetically controlled; that is, the repressor binds the mRNA faster than the 30*S* subunit binds to mRNA, and the nontranslated mRNA is rapidly degraded, thus rendering the action of the repressor irreversible (*25*).

Our data show how the ribosome can accommodate a structured mRNA. Other structured regulatory elements found in leader regions of prokaryotic mRNAs, which are recognized by a variety of ligands ranging from metabolites to proteins (*1*, *26*), might follow the same path as that of domain 2. This could be the case for the *E. coli thiM* mRNA riboswitch, which in the absence of thiamine pyrophosphate is characterized by a structured leader region just upstream of the SD sequence (*26*).

References and Notes

1. P. J. Schlax, D. J. Worhunsky, *Mol. Microbiol.* **48**, 1157 (2003).
2. P. Romby, M. Springer, *Trends Genet.* **19**, 155 (2003).
3. C. Sacerdot *et al.*, *Mol. Microbiol.* **4**, 1077 (1998).
4. J. Caillet *et al.*, *Mol. Microbiol.* **47**, 961 (2003).
5. A. Torres-Larios *et al.*, *Nat. Struct. Biol.* **9**, 343 (2002).
6. G. Z. Yusupova, M. M. Yusupov, J. H. Cate, H. F. Noller, *Cell* **106**, 233 (2001).
7. A. Spirin, N. Belitsina, G. Yusupova, *Methods Enzymol.* **164**, 631 (1998).
8. M. Yusupov *et al.*, *Science* **292**, 883 (2001).
9. J. Cate, M. Yusupov, G. Yusupova, T. Earnest, H. Noller, *Science* **285**, 2095 (1999).
10. Materials and methods are available as supporting material on *Science* Online.
11. B. T. Wimberly *et al.*, *Nature* **407**, 340 (2000).
12. J. Sengupta, R. K. Agrawal, J. Frank, *Proc. Natl. Acad. Sci. U.S.A.* **98**, 11991 (2001).
13. A. Komarova, L. S. Tchufistova, E. V. Supina, I. Boni, *RNA* **8**, 1137 (2002).
14. G. Keith, unpublished observations.
15. G. Blaha, K. H. Nierhaus, *Cold Spring Harbor Symp. Quant. Biol.* **66**, 135 (2001).
16. K. B. Gromadski, M. V. Rodnina, *Mol. Cell* **13**, 191 (2004).
17. N. Ban, P. Nissen, J. Hansen, P. B. Moore, T. A. Steitz, *Science* **289**, 905 (2000).
18. J. Harms *et al.*, *Cell* **107**, 679 (2001).
19. A. Vila-Sanjurjo *et al.*, *Proc. Natl. Acad. Sci. U.S.A.* **100**, 8682 (2003).
20. D. Moazed, H. Noller, *Cell* **57**, 585 (1989).
21. A. Dallas, H. F. Noller, *Mol. Cell* **8**, 855 (2001).
22. J. M. Ogle, F. V. Murphy, M. J. Tarry, V. Ramakrishnan, *Cell* **111**, 721 (2002).
23. R. Sankaranarayanan *et al.*, *Cell* **97**, 371 (2001).
24. M. Graffe *et al.*, *Science* **255**, 994 (1992).
25. T. Nogueira, M. de Smit, M. Graffe, M. Springer, *Mol. Biol.* **310**, 709 (2001).
26. W. Winkler, A. Nahvi, R. R. Breaker, *Nature* **419**, 952 (2002).
27. This work was funded by CNRS (French National Center for Scientific Research). We thank H. Noller, J. Cate, and J. Doudna for critical reading of the manuscript; C. Branlant for support of this work; B. Klaholz, S. Marzi, M. Rodnina, and D. Wilson for helpful discussions; G. Keith for analysis of tRNA in ribosome samples; F. Winter for help in the mRNA preparation; D. Rose for growing *T. thermophilus* cells; M. Ruff and J.-C. Thierry for preliminary synchrotron experiments; and T. Petrova for her help in an initial stage of molecular replacement calculations. Coordinates and structure factors have been deposited in the Protein Data Bank with accession codes 1YL3 and 1YL4.

Supporting Online Material

www.sciencemag.org/cgi/content/full/308/5718/120/DC1
Materials and Methods
Table S1
References

24 September 2004; accepted 25 January 2005
10.1126/science.1105639

Protein Interaction Analysis

Biacore T100 is a new generation system for providing comprehensive information about how proteins interact with other molecules. The information generated is useful in applications such as elucidation of disease pathways, definition of therapeutic targets, selection of drug candidates, and decisions on the safety of a potential therapeutic. From a single instrument, scientists can determine affinity and rate constants, binding specificity, concentration, and thermodynamic parameters. Time-consuming applications such as antibody characterization, which could take weeks by conventional methods, can be completed in days with the Biacore T100. Biacore systems monitor protein interactions in real time, in a non-invasive and label-free process.

Biacore For information +44 (0) 20 7886 8158 www.biacore.com

Digital Imaging for Electrophoresis and Blotting

The Kodak Gel Logic 440 Imaging System features a cooled charge-coupled device (CCD) camera and integrated illumination sample cabinet to permit sensitive detection of ultraviolet/fluorescent, chromogenic, and luminescent samples in gel, membrane, or plate assay formats. The system's cooled CCD camera offers resolution of up to 69 μ/pixel and produces 16-bit image files for up to 65,000 levels of grayscale resolution for accurate quantitative analysis of image files. The Gel Logic 440's imaging cabinet includes a roll-out ultraviolet (UV) transilluminator with UV shield for visualization and excision of samples stained with ethidium bromide and other fluorescent dyes, white light trans-illumination, white light epi-illumination for visualization of samples labeled with chromogenic labels, and optional UV epi-illumination, all with an imaging area up to 24 cm by 32 cm.

Eastman Kodak For information 877-SIS-HELP www.kodak.com/go/scientific

DNA Polymerase

The new BD Taq Full DNA Polymerase efficiently and conveniently amplifies DNA from any template and can be used in any general polymerase chain reaction procedure. Taq Full DNA Polymerase can generate high yields from any DNA template, including rare ones, from bacterial and plasmid DNA, cDNA, and complex genomic DNA. Its high efficiency and sensitivity allow the user to use less enzyme and template in each reaction. It is also available with hot start antibody.

BD Biosciences

For information 877-232-8995

www.bdbiosciences.com/clontech

Automated Liquid Handling

The BioCube System is a sophisticated liquid, sample, and data handling automation platform with several new features. A Vision Positioning System (VPS) makes use of advanced machine vision technology to perform precise positioning by calibrating disposable tips on the pipettor to the actual plate well centers. The VPS makes use of two cameras, one to map positions of the tips on the pipettor and the other to map plate positioning. The robot arm is then adjusted in X, Y, and theta (rotation) to position the tips precisely in the center of the wells. This makes pipetting operations to 1536-well plates more reliable while minimizing occurrences of tip misses and plate lifting. New scheduling software features a unique steady-state optimization algorithm that produces a production schedule regardless of the number of plates used for each run. A newly redesigned plate sealer automatically adjusts for differences in plate heights, anything from 384 polymerase chain reaction or low-profile sample plates up to deep well blocks. A new high-performance, two-position centrifuge is capable of attaining more than 6000 rpm, enough force to accommodate everything from quick spin downs to column extractions. Its plate loader and stacking systems have also been updated.

Protedyne For information 860-683-1860 www.protedyne.com

High Temperature Pressure Reaction Vessel Kits

The PRV High Temperature Kit for pressure reaction vessels is designed to meet the need for observing reactions in gases and liquids under pressure at high temperatures. All coupling materials have been selected for their durability and performance in high-temperature applications. The standard polyethylene insert has been replaced by a polytetrafluoroethylene (PTFE) insert. The standard neoprene O-ring has also been replaced by a PTFE O-ring. The kits are recommended when operating temperatures are above 175°C. Applications include solubility of gases in liquids at increased pressure; chemical behavior of liquids and gases subjected to temperature and pressure changes; effect of liquids on metals; and spray and pressure characteristics.

Andrews Glass Co For information 800-845-0026 www.andrews-glass.com

Gel Documentation System

UVsolo is a compact solution for gel documentation without the need for a computer. It comes with a light-sensitive charge-coupled device (CCD) video camera with a zoom lens and ultraviolet (UV) bandpass filter. A six-button keypad, a drive for image saving, and a four-inch LCD high-resolution display are integrated in the compact darkhood at eye-level. The optimal camera parameters can be set in seconds. The instrument's smooth surfaces allow for easy cleaning. The darkhood is removable but solidly fixed on the UV transilluminator with 20 cm × 20 cm filter size. A safety-interlocking door protects the user from UV exposure. A high-resolution video thermal printer completes the system and provides gel images in photo quality on high gloss paper. The system is suitable for working groups who want to save and print gel images.

Biometra For information 0049-551-50 68 6-0 www.biometra.com

Newly offered instrumentation, apparatus, and laboratory materials of interest to researchers in all disciplines in academic, industrial, and government organizations are featured in this space. Emphasis is given to purpose, chief characteristics, and availability of products and materials. Endorsement by *Science* or AAAS of any products or materials mentioned is not implied. Additional information may be obtained from the manufacturer or supplier by visiting www.science.labvelocity.com on the Web, where you can request that the information be sent to you by e-mail, fax, mail, or telephone.

ScienceCareers.org

Classified Advertising

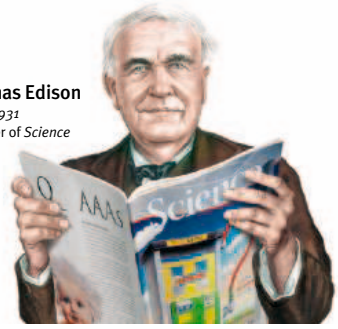

Thomas Edison
1847–1931
Founder of *Science*

For full advertising details, go to **www.sciencecareers.org** and click on **How to Advertise,** or call one of our representatives.

United States & Canada

E-mail: advertise@sciencecareers.org
Fax: 202-289-6742

JILL DOWNING
(CT, DE, DC, FL, GA, MD, ME, MA, NH, NJ, NY, NC, PA, RI, SC, VT, VA)
Phone: 631-580-2445

KRISTINE VON ZEDLITZ
(AK, AZ, CA, CO, HI, ID, IA, KS, MT, NE, NV, NM, ND, OR, SD, TX, UT, WA, WY)
Phone: 415-956-2531

KATHLEEN CLARK
(AR, IL, LA, MN, MO, OK, WI, Canada, Caribbean, Central and South America, Meetings & Announcements, and Graduate Programs)
Phone: 510-271-8349

EMNET TESFAYE
(Display Ads: AL, IN, KY, MI, MS, OH, TN, WV; Line Ads)
Phone: 202-326-6740

BETH DWYER
(Internet Sales Manager)
Phone: 202-326-6534

Europe & International

E-mail: ads@science-int.co.uk
Fax: +44 (0) 1223-326-532

TRACY HOLMES
Phone: +44 (0) 1223-326-525

GARETH STAPP
Phone: +44 (0) 1223-326-527

HELEN MORONEY
Phone: +44 (0) 1223-326-528

CHRISTINA HARRISON
Phone: +44 (0) 1223-326-510

JASON HANNAFORD
Phone: +81 (0) 52-777-9777

To subscribe to *Science*:
In U.S./Canada call 202-326-6417 or 1-800-731-4939
In the rest of the world call +44 (0) 1223-326-515

Science makes every effort to screen its ads for offensive and/or discriminatory language in accordance with U.S. and non-U.S. law. Since we are an international journal, you may see ads from non-U.S. countries that request applications from specific demographic groups. Since U.S. law does not apply to other countries we try to accommodate recruiting practices of other countries. However, we encourage our readers to alert us to any ads that they feel are discriminatory or offensive.

ScienceCareers.org
We know science AAAS

POSITIONS OPEN

The CBR Institute for Biomedical Research

The CBR Institute for Biomedical Research, Inc.
A Harvard Medical School Affiliate

The CBR Institute for Biomedical Research, Inc. (CBRI), located in the Harvard Longwood Medical Campus, invites applications for the newly created position of **CHIEF SCIENTIFIC ADMINISTRATIVE OFFICER** reporting to the Scientific Director.

The mandate of this unique opportunity is to serve as the principal aide/sounding board for the Scientific Director by directly handling matters on behalf of the Scientific Director. The incumbent of this position will have an exceptional ability to understand, appreciate, and discern outstanding science. The incumbent will also have eight plus years' research administrative experience; a flexible, creative leadership style with exceptional management and communications skills, and demonstrated experience in faculty recruitment. The incumbent, as deemed appropriate by the Scientific Director, must be able to identify scientific opportunities, solve problems in scientific matters that affect the Institute, and foster a cooperative, collegial, and productive environment among the CBRI community. The incumbent will work closely with the Scientific Director to manage the implementation of the Institute's strategic plan and possess the ability to "telescope" from long-range strategy to short-term details. The incumbent will serve the faculty by critiquing grant proposals, advising on funding strategies, and assisting in the implementation of new research-critical capabilities.

Prior experience in organizations that have undergone leadership change is strongly preferred. Experience in evaluating scientific accomplishments of candidates and departments as well as training of research staff, development, and supervision of academic research initiatives a must. A Ph.D. with evidence of outstanding investigation and a record of collaborative interaction are essential.

To apply, submit curriculum vitae, statement of interest/plans, and names of three references to: **Doreen Donovan, Human Resources Director, CBR Institute for Biomedical Research, 800 Huntington Avenue, Boston, MA 02115.**
Affirmative Action/Equal Opportunity Employer.

RESEARCH ASSISTANT PROFESSOR/SENIOR POSTDOCTORAL POSITION

Several positions available to study the mechanism of action of regulatory T cells in autoimmunity (*J. Immunol.* **170:**2195, 2003; **170:**5511, 2003; **173:**2866, 2004) and the role of human IG20 gene splice variants in apoptosis and cancer. (*J. Biol. Chem.* **276:**47202, 2001; *Cancer Res.* **63:**8768, 2003; *Oncogene* **23:**1076, 2004; *Oncogene* **23:**6083, 2004). Both projects require expertise in molecular biology and protein chemistry, and working knowledge of transgenic/knockout technology. Ph.D. or M.D. required. Send curriculum vitae by May 1, 2005, to: **Bellur S. Prabhakar, Ph.D., Professor and Head, Department of Microbiology and Immunology, University of Illinois College of Medicine, 835 S. Wolcott, M/C 790, Chicago, IL 60612-7344** or **e-mail: bprabhak@uic.edu.** *University of Illinois at Chicago is an Affirmative Action/Equal Opportunity Employer. Women and minorities are encouraged to apply.*

ASSISTANT PROFESSOR. Two tenure-track positions, starting September 2005, in the Department of Anatomy. Minimum requirements: Ph.D. degree and an active research program. No restrictions on research focus, except that up-to-date experimental methodology must be employed. Teaching responsibilities in either gross anatomy or neuroscience. Send curriculum vitae, three letters of recommendation, and cover letter to: **John Young, Department of Anatomy, Howard University College of Medicine, 520 W Street, N.W., Washington, DC 20059.** *An Equal Opportunity Employer.*

POSITIONS OPEN

The Department of Pathology and Anatomical Sciences at the University of Missouri School of Medicine is seeking an **ANATOMIST** for a tenure-track position. The position includes a commitment to education, including medical students, nursing and health care professions students, and undergraduate students. The collegial environment provides substantial opportunities for intellectual creativity and research. Applicants should be committed to excellence in teaching, scholarship, and research. The position requires an M.D. or Ph.D., or equivalent professional training and experience. Preference will be given to candidates who have experience sufficient to satisfy criteria for appointment as **ASSISTANT PROFESSOR** on the tenure track, with interest/experience in basic, clinical, or translational research. Applications will be accepted until the position is filled.

Interested individuals should submit a letter of interest, current curriculum vitae, and a list of three references by May 1, 2005, via mail or e-mail (preferred) to:

Douglas C. Anthony, M.D., Ph.D.
Professor and Chair
Department of Pathology and Anatomical Sciences
M263 Medical Sciences Building
University of Missouri
School of Medicine
One Hospital Drive
Columbia, MO 65212
E-mail: nicholsrkn@health.missouri.edu

For ADA accommodations, please contact our ADA coordinator at **telephone: 573-884-7278** (V/TTY).

The University of Missouri is an Equal Opportunity Employer/Affirmative Action and welcomes applications from members of underrepresented physician groups.

FACULTY POSITION IN PROTEOMICS

The Department of Medicinal Chemistry and Pharmacognosy, University of Illinois at Chicago, invites applications for a full-time, tenured, or tenure-track faculty position at the **ASSISTANT, ASSOCIATE,** or **FULL PROFESSOR** level. A Doctorate is required; postdoctoral experience and a background in pharmacy are desirable. Outstanding facilities for proteomics include matrix-assisted laser desorption/ionization–time of flight mass spectrometry, a new two-dimensional liquid chromatography linear ion trap mass spectrometry, two dimensional gel electrophoresis with spot picking, and a new Fourier transform ion cyclotron resonance mass spectrometer. The successful candidate must develop a strong, extramurally funded, independent research program in proteomics that complements existing programs in the Department and fosters collaborative interactions with others. Teaching in the professional and graduate programs of the College of Pharmacy is required. Candidates should send curriculum vitae, a one- to two-page research plan, and three letters of reference to: **Dr. Steven M. Swanson, Chair, Proteomics Search Committee, Department of Medicinal Chemistry and Pharmacognosy (M/C 781), University of Illinois at Chicago, 833 S. Wood Street, Chicago, IL 60612-7231. E-mail: mcp@uic.edu.**

Further information can be found at **website: http://www.uic.edu/pharmacy/depts/pmch/.**

For fullest consideration, submit all application materials by June 1, 2005.

The University of Illinois is an Equal Opportunity/Affirmative Action Employer.

POSTDOCTORAL/SENIOR SCIENTIST POSITION. Research positions are available in a laboratory studying the cell cycle and tumor suppressor genes using cell culture and mouse models. Applicants with strong background in molecular biology and mouse models are invited to apply. Please send applications to: **Pradip Raychaudhuri, Department of Biochemistry and Molecular Genetics, University of Illinois at Chicago, 900 S. Ashland Avenue, Chicago, IL 60607.**

Positions @ NIH
THE NATIONAL INSTITUTES OF HEALTH

Position Available
Electron Microscopist

The Biophysics Section in the Laboratory of Cell Biology, Center for Cancer Research, NCI, NIH invites applications from a dynamic individual with a strong background in electron microscopy to join our research team. The technological infrastructure of the laboratory includes electron microscopes capable of operation at 120 kV and 300 kV, extensive facilities for high speed and parallel computing, complete infrastructure for biochemistry and cell biological experiments, state-of-the-art equipment for specimen preparation for cryo elecctron microscopy including a high pressure freezer, cryo ultramicrotome and Vitrobot for preparation of frozen-hydrated specimens. The laboratory is located in a highly interdisciplinary research environment in Building 50 on the NIH campus in Bethesda, which houses groups whose interests range from computational biology, bioinformatics, X-ray and electron crystallography to cell biology, genetics and genome research.

Applicants should have an outstanding record of performance in transmission electron microscopy, and should be thoroughly familiar with fundamental principles of electron optics. An intimate knowledge of computers and experience with programmming will be a strong plus. Prior experience with cryo electron microscopy or with operation of a field emission gun microscope is desirable, but not essential. Salary and appointment mechanism will be commensurate with qualifications of the candidate.

Interested applicants should send a CV, a brief statement of research interests, and the names of three references by electronic or regular mail to: **Sriram Subramaniam , Chief, Biophysics Section, Laboratory of Cell Biology, Rm. 4306, Building 50, National Cancer Institute, Bethesda, MD 20892, e-mail: ss1@nih.gov**

POSTDOCTORAL FELLOW
Systems Neuroscientist-Animal fMRI Neuroimaging

The National Institute on Drug Abuse (NIDA), Intramural Research Program (IRP), a major research component of the National Institutes of Health (NIH), Department of Health and Human Services (DHHS), is recruiting a neurobiologist interested in joining an interdisciplinary group of neurobiologists and MR physicists dedicated to understanding brain mechanisms of drug abuse primarily using rodent models and functional MRI. Also under investigation are the physiological and biophysical mechanisms underlying fMRI signals and their application to the neuropharmacology of abused drugs. Imaging experiments are performed either on a 9.4T small bore MRI scanner, or a 3T human scanner (equipped with animal imaging coils). Both machines are research-dedicated instruments housed in the Neuroimaging Research Branch. Additional multimodal, non-imaging bench experiments are also ongoing using electrophysiological and laser Doppler techniques. The successful candidate must possess a Ph.D. in Neuroscience, Physiology, Pharmacology (or a related field). Small animal systems neuroscience and/or fMRI/Neuroimaging research experience is desirable.

Interested applicants must submit a CV, a statement of research interests and goals, three letters of recommendation from noncollaborators, and a copy of the doctoral degree (if in a foreign language, include a certified English translation). Send applications to: **Dr. Elliot Stein or Dr. Yihong Yang, Neuroimaging Research Branch, NIH/NIDA/IRP, 5500 Nathan Shock Drive, Baltimore, MD 21224 (410-550-1440 (voice); 410-550-1441 (fax); estein@intra.nida.nih.gov or yihongyang@intra.nida.nih.gov).**

National Human Genome Research Institute
Post-doctoral Position

The Developmental Genomics Section of the National Human Genome Research Institute is seeking a post-doctoral fellow with interest in vertebrate genetics and genome analysis. The lab studies large-scale reverse genetics and gene trapping screen in zebrafish. This is a funded position to participate in a large-scale international effort to create a "library" of zebrafish gene knockouts using retroviral mapping technologies developed in the lab (Wu et al. *Science*, 300: 1749-51). This will be in combination with zebrafish mutagenesis (Golling et al *Nat. Gen,* 31: 135-40) and an *in vivo*, tissue specific enhancer trap screen, using recently developed retroviral vectors. Experience in retroviral production, zebrafish genetics, or database development a plus, but not essential.

The National Human Genome Research Institute at the National Institutes of Health in Bethesda provides an exciting scientific environment in one of the largest biomedical research facilities in the world.

Candidates should possess an MD and/or PhD and have less than five years of postdoctoral experience. Please send a letter, CV, and three letters of reference to: **Dr. Shawn Burgess c/o Ms. Dana Jordan, NHGRI/NIH, 50 South Dr., Bldg. 50, Rm. 5334, Bethesda, MD 20892-8004; E-mail: dgsapply@mail.nih.gov.**

National Human Genome Research Institute
Division of Intramural Research
Training Program Coordinator

The Intramural Training Office (ITO) of the National Human Genome Research Institute is seeking an individual to develop and coordinate training programs within the Division of Intramural Research, with an emphasis on the training of underrepresented minorities.

The ITO serves as the focal point for training in the NHGRI Intramural Program, offering a variety of information and resources related to mentoring, career development, and funding opportunities. It also assists in matching trainees to individual research laboratories. The ITO focuses on a wide range of important training-related areas, including trainee orientations, mentorship programs, educational programs, conflict resolution and problem solving, and recruitment.

Working with the ITO Director, the Training Program Coordinator will aim to increase the involvement of underrepresented trainees in genomic research on the NIH campus through recruitment, as well as the development and implementation of new, innovative programs. The Training Program Coordinator will also be involved in other activities and programs overseen by the ITO.

The ideal candidate will have a doctoral degree in the biological sciences. Demonstrated effectiveness in working with underrepresented populations is highly desirable. This position requires strong oral and written communication skills. Applicants must have leadership abilities and be capable of working independently.

Interested applicants should send a *curriculum vitae*, a detailed letter of interest, and the names of three potential references through our online application system, at *http://research.nhgri.nih.gov/apply*. Applications will be reviewed beginning April 1, 2005 and continue until the position is filled. **For more information on the ITO and the NHGRI Intramural Program, please visit** *http://genome.gov*.

WWW.NIH.GOV

SCIENTIFIC DIRECTOR
NATIONAL INSTITUTE OF ARTHRITIS AND
MUSCULOSKELETAL AND SKIN DISEASES

THE POSITION: The National Institute of Arthritis and Musculoskeletal and Skin Diseases (NIAMS), a major research component of the National Institutes of Health (NIH) within the Department of Health and Human Services, is recruiting for a Scientific Director of the Intramural Research Program. The NIAMS Intramural Research Program conducts clinical and laboratory research related to arthritis and musculoskeletal and skin diseases. It also conducts basic research in biochemistry, immunology, pathology, histochemistry, chemistry, molecular biology, structural biology, and pharmacology. The Scientific Director serves as the principal advisor to the Director of the NIAMS concerning all ongoing and projected intramural research programs of the NIAMS and is responsible for the development of broad decisions concerning program planning, budget and policy formulation, and research allocation of the intramural program. The Scientific Director represents the NIAMS in discussions of NIH-wide intramural policies and programs, and serves as a vital member of the senior staff of the Institute. In addition to the managerial/administrative responsibilities outlined above, the Scientific Director will carry out her/his own research program. Resources commensurate with the proposed research program will be provided.

THE CHALLENGE: To provide strong and effective leadership in the overall scientific management of an innovative basic and clinical research program in the field of arthritis and musculoskeletal and skin disease with a budget of $50 million and a staff of 250. The NIAMS is currently pursuing cutting-edge research on a broad spectrum of investigations, from fundamental analyses of protein structure and function by physical, genetic, and biochemical means to research on the etiology, pathogenesis, and treatment of selected rheumatologic, musculoskeletal, and skin diseases.

THE IDEAL CANDIDATE: Will have demonstrated scientific leadership and research experience in both a basic and clinical research program of national and international standing in an area relevant to arthritis and other rheumatic diseases, musculoskeletal diseases, and/or skin diseases. Applicants must have an M.D. and/or Ph.D. degree or equivalent degree, in a biomedical or related field.

SALARY: Commensurate with qualifications and research experience and includes a full Federal benefits package (which includes retirement; health, life, and long-term care insurance; Thrift Savings Plan, etc.).

HOW TO APPLY: An application accompanied by a current curriculum vitae and bibliography should be submitted to: **Robert Balaban, Ph.D., Chair, Search Committee, c/o The National Institute of Arthritis and Musculoskeletal and Skin Diseases, Attn: Ms. Lynn Pupkar, 6706 Democracy Boulevard, Suite 400, Bethesda, MD 20892-3062.** For further information, please call **Dr. Robert Balaban, 301-496-3658 (E-mail: balabanr@mail.nih.gov)** or visit the Web site at **www.nih.gov/niams.**

Selection for this position will be based solely on merit, with no discrimination for nonmerit reasons such as race, color, religion, gender, national origin, political affiliation, marital status, disability, age, sexual orientation, or membership/nonmembership in an employee organization.

QUALIFIED APPLICATIONS SHOULD BE RECEIVED BY April 29, 2005 TO BE CONSIDERED FOR THIS POSITION.
Applications received after this date may be considered if the position has not been filled.

Directors of Research

The Italian Institute of Technology ("IIT"; **www.iit.it**) is a Foundation created to promote scientific research and technological innovation at the highest levels in Italy. Established by the Ministry of Economy and Finance and the Ministry of Education, University and Research with a consistent funding, IIT aims at becoming an international centre of excellence for scientific research and training in high technology, with active participation of private organizations. During its start-up phase IIT intends to set up state-of-the-art research programs in Nano-biotechnologies, Neuroscience and Robotics. The IIT scientific plan and the background material, approved by the Steering and Regulatory Committee, provide more detailed information and are available for download on IIT website.

In order to start scientific research activity, IIT invites applications for the following positions:

Directors of Research in Nano-biotechnologies

Directors of Research in Neuroscience

Directors of Research in Robotics

Successful candidates will start IIT research activities in the respective fields, developing a detailed research program, organizing and leading a research team and building laboratories in IIT definitive site in Genoa (I). Adequate laboratory space, start-up budget and equipment will be provided. Directors of Research will also develop close collaboration with industry and other research institutions.

Applicants should have an established record of significant scientific accomplishments, as well as scientific leadership and administrative skills. To ensure full consideration, **candidates will have to submit applications (electronic format preferred), with detailed cv, by the end of May** to:

Simone Collobiano
applications@iit.it
Fondazione IIT
Via Sicilia, 194
00187 – Rome, Italy
ph: +39 06 4201 0848

Short-listed candidates will be invited for a talk, which will take place in Genoa (I) during the first 2 weeks of July. On this occasion candidates will have the opportunity to present their current research activities and scientific goals.

Italian Institute of Technology is an Equal Opportunity Employer

---

Institute of Materials Research and Engineering
A*STAR

Established in 1996, IMRE's mission is to create materials knowledge, develop human capital and to transform technology through innovative research. IMRE is a member of the A*STAR research family and undertakes research in selected fields of materials science and engineering, including optoelectronics, nanomaterials, chemicals and polymers. Our innovations and discoveries help create and refine advance materials processes and applications. For more information, you may log on to our website at **www.imre.a-star.edu.sg**

Here in Singapore, you will also find a dynamic city rich in contrast and colour, together with a harmonious blend of culture, cuisine, arts and architecture, offering a unique experience of a slice of life within Southeast Asia.

PRINCIPAL INVESTIGATORS / RESEARCH SCIENTISTS

(Ref: IMRE/SC/RS)

As part of our growing vision, we are seeking individuals with outstanding credentials in the field of materials science to join us. Individuals with keen interest as well as an excellent publication record in any field of materials science and engineering, and particularly in the broad areas of optoelectronics, nanomaterials, chemicals, polymers and characterisation, are welcome to submit their resumes to us.

In addition, specific positions are available for the following projects:

RESEARCH ASSOCIATES

Molecular & Performance Materials Cluster

Responsibilities:
- Synthesise, characterise, and purify materials for potential application in organic and polymer electronics including OLEDs, solar cells and thin film transistors
- Process and characterise devices based on the newly developed materials

Requirements:

Position A1: (Ref: IMRE/SC/A1)
- Familiarity with materials characterisation techniques
- Experience in air-sensitive chemical syntheses, schlenk techniques, materials purification techniques and glove box

Position A2: (Ref: IMRE/SC/A2)
- Familiarity with materials characterisation techniques – FT-IR, UV-vis, AFM/STM, SEM, IV/CV characterisation is a must
- Experience in fabrication and characterisation of organic, polymeric, or molecular electronic devices such as thin film transistors, light emitting devices and photovoltaic devices

Materials Science and Characterisation Cluster

Responsibilities:
- Perform materials characterisation within a multi-disciplinary environment

Requirements:

Position B1: (Ref: IMRE/SC/B1)
- Experience in technique development and applications of surface analysis, particularly photoemission (XPS/UPS) and/or SIMS
- Experience in UHV techniques and sample preparation

Position B2: (Ref: IMRE/SC/B2)
- Experience in technique development and applications of transmission electron microscopy and microstructural analysis
- Knowledge of EELS or HR-XRD will be beneficial

Position B3: (Ref: IMRE/SC/B3)
- Experience in technique development and applications of chemical analysis
- Knowledge of NMR, TGA and FTIR
- Experience in polymer and organic sample preparations

All successful applicants must have PhD qualifications, and are able to work well in a team within a cross-disciplinary environment and possess excellent communication skills. The level of appointment and remuneration will be commensurate with qualifications and experience.

Interested candidates should write to us, enclosing a full resume (stating current and expected salaries), copies of academic transcripts, a list of publications and a list of references to **hr@imre.a-star.edu.sg** (Please indicate the position of interest and job reference code within the subject header.)

Others call it research.

We call it changing the medical textbooks.

For over 28 years, Genentech has been at the forefront of the biotechnology industry, using human genetic information to discover, develop, commercialize and manufacture biotherapeutics that address significant unmet medical needs. A considerable number of the currently approved biotechnology products originate from or are based on our science, and Genentech manufactures and markets multiple products in the United States, providing innovative treatments for cancer, heart disease, respiratory disease, growth disorders and other serious illnesses.

Genentech's research organization features world-renowned scientists who are some of the most prolific in their fields and in the industry. Genentech researchers have consistently published at a rate of 150+ papers per year and have secured more than 4,600 patents worldwide (with 5,000 more pending). Genentech's research organization combines the best of the academic and corporate worlds, allowing researchers not only to pursue important scientific questions but also to watch an idea move from the laboratory into development and out into the clinic.

Postdoctoral Opportunities

Molecular Biology

(Ph.D./M.D. with experience in cancer biology, developmental biology or signal transduction. Experience with in vivo models is preferred.)

- A postdoctoral position is available in the department of Molecular Biology at Genentech to study the Hedgehog signaling pathway in development and cancer. Areas of interest include (1) the etiology of cancers caused by aberrant Hh signaling using animal models and (2) the identification and validation of new targets in the pathway from unpublished leads. **Req # 1000006443**

Antibody Engineering

(Ph.D. in Immunology, Chemistry, Biochemistry or related discipline)

- Develop novel antibody variants and affinity maturation strategies in support of Genentech's effort to create therapeutic antibodies for a wide range of indications. Experience in molecular biology, protein chemistry and biophysical characterization techniques is required. **Req # 1000003531**

Pathology and Translational Oncology

(Ph.D. in Molecular Biology, Cell Signaling and/or Biochemistry or related discipline or M.D.)

- Develop novel molecular diagnostic strategies in breast cancer. The project is a collaborative effort between Pathology (mentor, Howard Stern) and Translational Oncology (co-mentor, Mark Sliwkowski). The successful applicant will utilize genomic and biochemical techniques to study therapeutic responsiveness to drugs that disrupt the ErbB/HER pathway. **Req # 1000005820**

Molecular Oncology

(Ph.D. in Biology or related field with a strong publication record.)

- Genentech's Molecular Oncology Department is seeking an independent researcher to study the role of ubiquitin in cellular signaling. **Req # 1000005306**

Protein Chemistry

(Ph.D. in Biochemistry, Chemistry or Immunology.)

- A postdoctoral position is available in the Department of Protein Chemistry to study the interaction between the immuno-inhibitory receptor B and T lymphocyte attenuator (BTLA) a CD28 family member, and its ligand Herpesvirus Entry Mediator (HVEM) a TNFR family member. The study will focus on further delineating the mechanism by which HVEM activates BTLA and the signaling consequences of this activation in B and T cells. **Req # 1000006664**

Drug Discovery

(Ph.D. in Molecular Biology, Cell Biology, Cancer Biology, Developmental Biology, Neurobiology or related discipline.)

- Perform basic laboratory research related to the developmental functions and mechanisms of action of members of the Robo/Slit, Neuropilin/VEGF/Semaphorin, UNC5/netrin, Hedgehog/Smoothened and Wnt/frizzled signaling pathways. Present hypotheses and independently design and conduct laboratory experiments to address parallels and differences in their roles in angiogenesis, cancer biology and nerve growth. Oral and written communication of results, including publication in peer-reviewed journals, is essential. **Req # 1000004870**

Genentech offers one of the most comprehensive benefits packages in the industry. Our culture emphasizes working hard, collaborating and sharing rewards. Our employees enjoy an environment that supports a work-life balance through benefits and programs that include sabbaticals, near-site child-care and concierge services. Join a company that attracts, retains and rewards the best and brightest employees. For immediate consideration, please visit **www.gene.com/careers** and reference the Req #. Please use "Ad-Science Magazine" when a "source" is requested. Genentech is an equal opportunity employer.

Genentech

IN BUSINESS FOR LIFE

www.gene.com

DEAN

Penn Veterinary Medicine

The University of Pennsylvania invites nominations and applications for the position of the Dean of the School of Veterinary Medicine. The University seeks a new Dean who is a dynamic, visionary scholar and strong leader and who can position the School for continued eminence by capitalizing on the School's many academic, clinical and research strengths.

The School of Veterinary Medicine is one of twelve schools that make up the University. The School comprises four departments, two basic science and two clinical, and includes two internationally renowned hospitals – the Matthew J. Ryan Veterinary Hospital in Philadelphia and the George D. Widener Hospital for Large Animals at New Bolton Center. The School's facilities, both urban and rural, provide teaching, research and clinical opportunities to 131 full-time faculty; 440 students; and 130 postdoctoral fellows, graduate students, residents and interns.

The School ranks first among all veterinary schools in the country in basic science research and research training. The case load at both the Ryan and Widener Hospitals is unrivaled. The School provides outstanding patient care, particularly in equine medicine and surgery, orthopedics, companion animal medicine, emergency medicine and critical care, food animal health and productivity, and epidemiology.

The Dean reports to the Provost and interacts directly with the President of the University. The Dean is the chief academic and administrative officer of the school and its faculty and is expected to lead and articulate a vision for the future direction of the educational, research and clinical programs. The Dean has overall responsibility for defining the school's priorities, developed in collaboration with department chairs and faculty; maintaining a faculty of international excellence and educational programs of the highest quality; attracting superb students; facilitating links between the clinical and basic biomedical sciences; forging academic links with various schools and departments within the University; and maintaining productive relationships with alumni and representatives of business and industry as well as local, state, and federal policy makers.

The ideal candidate will possess the following: a doctorate in veterinary medicine or the equivalent; a record of distinguished professional and scholarly achievement that merits appointment with tenure to the rank of full professor; the intellectual leadership and vision to guide the School in maintaining and strengthening its reputation for excellence in professional education; an understanding of the nature and operations of veterinary medicine and its role in society; demonstrated administrative experience, including fiscal management; and the ability to relate effectively to donors and attract their financial support.

Dr. Richard O. Davies, Professor of Physiology/Animal Biology and Chair of the Search Committee, requests that all inquiries, nominations and applications be directed to the University's consultants:

Paula Carabelli and Jennifer Bol
Spencer Stuart
10900 Wilshire Boulevard, Suite 800
Los Angeles, CA 90024
(310) 209-0610
pennvetmed@spencerstuart.com

Applications should include a curriculum vitae and a short letter of interest describing the candidate's qualifications. Nominations and applications will be reviewed on an ongoing basis beginning in April 2005 and will be accepted until the position is filled. The Search Committee anticipates conducting preliminary interviews in June 2005. All inquiries, nominations, and applications will be treated in the strictest of confidence.

The University of Pennsylvania is an equal opportunity, affirmative action employer. Women and minority candidates are strongly encouraged to apply.

www.vet.upenn.edu

UNIVERSITY OF PENNSYLVANIA

The Basic Urology Research Laboratory in the Division of Urology at the University of Pennsylvania has openings for highly motivated cell/molecular biologists, biochemists or physiologists. Appointments are available as postdoctoral fellows (Ph.D., D.V.M.-Ph.D., M.D.-Ph.D., or D.V.M.) and Research Associates. Our training program is different from conventional postdoctoral training, since there is an emphasis on translational research and a mechanistic approach to understanding pathophysiology. The fellows will have exposure and opportunities to translate basic science information into new diagnostic, preventive and therapeutic strategies. The rapid and effective translation of basic scientific discoveries is greatly facilitated by mentoring from basic and clinical scientists. This is an NIH-sponsored postdoctoral fellowship, which requires U.S. citizenship or immigrant status.

The current research interests in the Division of Urology at the University of Pennsylvania Medical Center* include (1) investigating the regulatory role of caldesmon in smooth muscle structure and function by disrupting the caldesmon gene expression using site-directed mutagenesis, siRNA interference and gene knock out technologies, (2) alterations of intracellular kinases, phosphatases, and anchoring proteins in smooth muscle in urological diseases, (3) smooth muscle signaling mechanisms and regulation in diabetes and smooth muscle remodeling, (4) bladder and prostate cancer, (5) gene therapy, (6) channel proteins and (7) extracellular matrix.

Interested candidates should forward their CV and the names of two references to: **Dr. Samuel K. Chacko, Director of Basic Urological Research, 3010 Ravdin-Courtyard, HUP, University of Pennsylvania, 3400 Spruce Street, Philadelphia, PA 19104. Fax: (215) 349-5026; E-mail: chackosk@mail.med.upenn.edu**. Start date is open.

**An Affirmative Action/Equal Opportunity Employer.*

VIB, the Flanders Interuniversity Institute for Biotechnology, is an entrepreneurial research institute. 900 scientists and technicians in 60 research groups conduct strategic spearhead research in a wide range of life science domains: molecular biology, cell biology, developmental biology, structural biology, systems biology, genetics, biochemistry, microbiology and proteomics. VIB's main objective is to understand the mechanisms that are responsible for normal development (e.g. angiogenesis, apoptosis, plant growth and development,...) and diseases such as cancer, inflammation, neurodegeneration, haemophilia,... VIB holds a long-term perspective in research, stability, technology transfer of new findings by means of patents and licenses and creation of new start-up companies. More than one third of all post-doctoral fellows and group leaders have their roots outside Belgium, making VIB an international and intercultural community. Due to the continuing growth of our research activities we currently have open positions in several departments :

Post-doctoral researchers (m/f)

I. Department of Transgene Technology and Gene Therapy, K.U.Leuven

Lab Functional Genomics of Cardiovascular Biology and Disease

This lab recently developed a novel frog model to identify large numbers of novel (lymph) angiogenic candidates and to study their function. A fully operational Xenopus facility, equipped for oocyte/embryo injection and embryo phenotyping, is available. The applicant will be integrated according to his/her expertise and professional experience into the exisiting Xenopus research team, taking responsibility for particular technological aspects and major scientific objectives. The position involves a two-year post-doctoral period with possibility for extension.

Successful candidates should be highly motivated post-doctoral fellows with experience in Xenopus transgenesis and gene knockdown technology to be applied to research on blood and lymph vessel formation. Applicants should think creatively and work independently as well as collaborate within the center's research team in a synergistic and productive manner.

*Contact **prof. Peter Carmeliet** at peter.carmeliet@med.kuleuven.ac.be*

II. Department of Molecular Microbiology, K.U.Leuven

Coordinator of a Marie-Curie Research Training Network CANTRAIN

This lab coordinates an RTN on *candida albicans* and *candida dubliniensis* – Host-pathogen interactions. This CANTRAIN network has 3 post-doctoral positions available for a duration of 3 years and 2 post-doctoral positions of one year. The 3-year postdoc positions are in the lab of Dr. Rosalia Diez-Orejas, Madrid, Spain *(rosaliad@farm.ucm.es; www.ucm.es/info/mfar)*; the lab of Dr. Per Ljungdahl, Stockholm, Sweden *(plju@licr.ki.se; www.licr.ki.se)* and at the faculty of Life Sciences at the university of Manchester, UK, Dr. Lubomira Stateva *(l.stateva@manchester.ac.uk; www.manchester.ac.uk/lifesciences/lstatevaresearch)*.

The one-year positions are available in the lab of Dr. Steffen Rupp, Stuttgart, Germany *(rupp@igb.fhg.de, www.igb.fhg.de)* and the lab of Dr. Patrick Van Dijck, Leuven, Belgium, the coordinator of this project *(patrick.vandijck@bio.kuleuven.ac.be)*.

All candidates should have at least 4 but not more than 10 years of research experience since gaining university degree. All fellowships are funded by the European Commission and it is required that the applicants are from another nationality than the host institute. Within the CANTRAIN network, ample possibilities for further training will be offered.

*More information on all positions and the network itself can be found with **Dr. Patrick Van Dijck** at cantrain@bio.kuleuven.ac.be and www.cantrain.be.*

We also have post-doctoral positions in our department for Molecular Biomedical Research (UGent), department of Plant Systems Biology (UGent) and at the center of Human Genetics (K.U.Leuven). For details about the above mentioned positions, please visit the job section of our website www.vib.be.

Ph.D. students (m/f)

Department for Molecular Biomedical Research

Both positions are within the framework of a Marie-Curie 'excellent grant' project.

The first position is directed at generating a specialized protein expression system for eukaryotic membrane proteins. The successful candidate is a junior scientist knowledgeable in the production, purification and characterization/crystallization of (membrane) proteins. You preferably have experience in yeast molecular biology.

The goal of the second project is to establish a technology platform to enable the unbiased identification of genes involved in microbial glycoconjugate biosynthesis, with a multitude of biomedical applications. You are a junior scientist knowledgeable in bacterial molecular biology and/or biochemistry to work on a cutting-edge project in functional glycomics. You preferably have experience in genetic screens based on the interaction with cell-surface molecules and have an interest in diseases of the developing world.

For both vacancies it is required you have a non-Belgian nationality (EU project). Female candidates are strongly encouraged to apply.
*Contact **Dr. Nico Callewaert** at nico.callewaert@dmbr.ugent.be.*

In addition to the required background in terms of specific experience and skills for each function, VIB is focused on people who are communicative and collaborative. An excellent command of English, enjoying teamwork, creativity, and being eager to work in a multidisciplinary and international environment are important assets.

*VIB offers a strong, stimulating and collaborative research environment with ample opportunities and with access to several core facilities. In order to gain a better understanding of what VIB stands for and for obtaining more detailed information about each job opening, please visit our website **www.vib.be** or contact mrs. Marijke Lein, HR-manager at marijke.lein@vib.be*

Interested?

Please send a full CV, a list of publications and the names and coordinates of at least 2 references to the contact person of the job(s) you are interested in.

MOUNT SINAI SCHOOL OF MEDICINE

The Fishberg Department of Neuroscience at Mount Sinai School of Medicine is seeking an outstanding faculty member of any academic rank, from assistant to full professor, in coordination with a translational neuroscience initiative and a new Center for Stem Cell Research.

Neuroscience Faculty

The Department of Neuroscience and associated Neurobiology of Aging Laboratories focus on linking structural and molecular mechanisms to behavior, and seek to strengthen this collaborative approach.

Candidates with active research programs in the biology of stem cells, neural plasticity, neural development, or aging, are encouraged to apply. Multidisciplinary approaches are favored.

Applicants should send their letter of application, CV and the names of three potential references to: **Department of Neuroscience Search Committee, Mount Sinai School of Medicine, One Gustave L. Levy Place, New York, NY 10029. Or e-mail to: Connie.Guzman@mssm.edu.** We are an equal opportunity employer.

Mouse Genetics Core Facility Director

The Wistar Institute, a non-profit biomedical research facility and NCI-designated Cancer Center located on the campus of the University of Pennsylvania, is seeking a Ph.D.-level scientist for the position of Mouse Genetics Core Facility Director. Exceptional candidates with a master's degree will also be considered. The primary mission of the core is to facilitate the generation of mouse models of human disease for Wistar faculty. The successful candidate will have extensive knowledge and proven ability in the generation of transgenic and sequence-targeted mice. Responsibilities will include, but may not be limited to, transgenic production, ES cell manipulations and blastocyst injection, production of chimeric mice, rederivation of mouse lines and cryopreservation. The successful candidate will also have the technical expertise to devise and construct transgenic and targeting vectors.

Interested candidates should submit a curriculum vitae, summary statement outlining qualifications and expertise, and names of three references to: **Dr. Anthony Capobianco, Chair, Search Committee, The Wistar Institute, 3601 Spruce Street, Philadelphia, PA 19104.** Wistar offers a competitive salary and comprehensive benefits package, including health/dental insurance and tuition assistance. EOE/AA/M/F/D/V.

www.wistar.org

THE WISTAR INSTITUTE

The **Institute for Cancer and Stem Cell Biology and Medicine** at **Stanford University** is holding an open search for **tenure-line faculty** in the area of cancer gene discovery. The faculty slots can be at the assistant, associate or full professor level.

Successful candidates will have an outstanding record of research in cancer gene discovery and a strong interest to help translate these discoveries to preclinical research and potential therapies. A strong focus of the Institute group is the discovery of cancer and leukemia stem cells, and new faculty would be expected to interact with the established Cancer/Stem Cell group to help elucidate steps in the progression from normal cells to frankly malignant cells. Stanford has established a Comprehensive Cancer Center, and cancer gene discovery will be a focus for the Cancer Center.

The most successful candidates will have defined high through-put methods to discover activated proto-oncogenes resulting from genetic or epigenetic regulation as well as inactivated tumor suppressor genes. Relevant examples would be outstanding mouse geneticists with an exceptional record of research who use, and are developing, novel technologies and genetics approaches that will lead to the better understanding and treatment of cancer and other human genetic diseases.

All appointments to the Institute and the Cancer Center will be in departments at Stanford University, so interested candidates should indicate which departments at Stanford would be among their first choices for department affiliation.

The appointees will be in laboratories in the Institute, and will participate in Institute research and teaching activities. While teaching is an important endeavor at Stanford University, these appointments (Institute for Cancer and Stem Cell Biology and Medicine appointments) will be primarily based on research accomplishments and the promise of future research advances.

Salary will be commensurate with the level of employment, relevant experience and accomplishments. Please send letters of application, including full curriculum vitae and the name and addresses of three references to: **Randy Mont-Reynaud for I. L. Weissman, Director of the Institute for Cancer and Stem Cell Biology and Medicine, Room L322, Stanford University School of Medicine, Stanford, CA 94305-5324**.

Stanford University is an Equal Opportunity, Affirmative Action Employer.

TENURED PROFESSOR WITHIN THE COLLEGE OF ARTS AND SCIENCES

University of New Mexico
Albuquerque, New Mexico

The University of New Mexico seeks an outstanding senior research professor in environmental science or a related area to assume a leadership role on campus and in the wider scientific community. This individual is expected to have an established, internationally conspicuous research program, proven ability to develop and manage large, multi-investigator, interdisciplinary research projects, and demonstrated experience working with diverse constituencies including scientists in other disciplines, political and business leaders, and philanthropists. We seek a candidate with vision, passion and energy, who can move UNM into greater prominence in ongoing and forthcoming funding opportunities at national and international levels. The successful candidate will hold a position as a tenured full Professor in UNM's College of Arts and Sciences.

Interested individuals are asked to visit our website: **http://www.unm.edu/~fco/enter.htm** for a complete job description. Applicants must send a signed letter of intent, a detailed curriculum vitae, and a 1-2 page description of teaching and research objectives. For best consideration, nominations and applications should be submitted by **May 17, 2005**; nominations and applications will be accepted until the position is filled.

Chair, Tenured Professor in A&S Search
Attn: Juliette Lagassé-Martínez
Office of the VP for Research & Econ. Dev.
Scholes Hall 222, MSC05 3400
University of New Mexico
Albuquerque, NM 87131-1001

The University of New Mexico is a Carnegie Doctoral/Research University-Extensive and an Equal Opportunity/Affirmative Action Employer and Educator.

EXECUTIVE ASSOCIATE DEAN FOR RESEARCH

Emory University School of Medicine invites nominations and applications for the full-time position of Executive Associate Dean (EAD) for Research. This leadership position offers outstanding resources and institutional commitment in the setting of a major academic health center. The EAD for Research reports directly to the Dean of the School of Medicine and partners to chart a visionary course for achieving and sustaining preeminence in research.

Duties include developing and creatively implementing strategic research plans; fostering research and program development; promoting internal and external collaborations; advising the Dean on space allocation; planning and justifying new research buildings with others; ensuring research compliance and training; overseeing the research infrastructure; developing strong relationships with federal agencies; and expanding the School's strong research program with Georgia Institute of Technology through the joint Biomedical Engineering Department. Direct reports include the Clinical Trials Office, core laboratories, DAR, IRB and IACUC Office, and General Clinical Research Center. The EAD for Research is advised by the Research Advisory Committee.

The successful candidate for Executive Associate Dean for Research must have a doctoral-level degree and academic credentials sufficient for appointment to the faculty as Professor with tenure; a distinguished record of scholarship and funded research; experience in effective senior academic research leadership in a medical school or related setting; outstanding leadership in developing and managing major research programs; superb skills in communication, organization, and administration; and extensive knowledge of federal and university policies that govern research-related areas. Personal traits must include a commitment to quality and integrity, a collaborative management style, and engaging and collegial interpersonal and communication skills.

Applications and nominations should include a letter of interest summarizing qualifications and expertise; a current curriculum vitae; and names and addresses of three references. Please submit materials by email to ljtowns@emory.edu. Applications by mail should be addressed to Ms. Linda Townsend, Office of the Dean, Emory University School of Medicine, 1440 Clifton Road, N.E., Ste. 321, Atlanta, Georgia 30322. The Search Committee will review applications until the position is filled.

EMORY UNIVERSITY SCHOOL OF MEDICINE

Emory University is an Equal Opportunity/Affirmative Action Employer

2005 Request for Applications – Science Fellows Program

California Bay-Delta Authority Science Program
California Sea Grant College Program

The California Bay-Delta Authority Science Program, in cooperation with California Sea Grant, is seeking applications from highly qualified predoctoral students and postdoctoral researchers who are interested in a career in multidisciplinary, multi-institutional, field-based research in riverine and estuarine systems. For 2005, the Science Program is interested in research that addresses the three priority topics as outlined in the recent CBDA Science Program 2004 Proposal Solicitation Package (PSP): Water Operations and Biological Resources; Ecological Processes and Their Relationship to Water Management and Key Species; and Performance Assessment to Improve Tools and Implications of Future Changes.

ELIGIBILITY – Prospective Predoctoral Science Fellows, at the time of application, must be in or recently been admitted to a PhD degree program in natural resources, environmental sciences, coastal, aquatic or related studies at any accredited US institution of higher education. Prospective Postdoctoral Science Fellows must hold a PhD or complete a PhD before the starting date of the fellowship in a doctoral degree program in environmental sciences or in a related field from any accredited US institution of higher education. US citizenship or residency is required.

AWARD – The fellowship will provide support for up to three years for both predoctoral and postdoctoral fellows in the form of a grant/award that includes funds for a stipend ($45,000/yr-postdoctoral; $25,000/yr-predoctoral) and for research-related expenses (up to $25,000/yr-postdoctoral; $14,500/yr-predoctoral).

SELECTION – Selection will be made competitively from applications submitted to the California Sea Grant College Program by May 18, 2005. In 2005, approximately five postdoctoral and two predoctoral fellowships will be awarded to begin approximately by September 1, 2005.

APPLICATION/CONTACT – For complete details and application instructions, please refer to the CBDA Science Fellows Program - 2005 Request for Applications, on the Sea Grant web site: www-csgc.ucsd.edu (follow the Education link to Science Fellows). If you have specific questions or require additional information contact: CALFEDfellow@seamail.ucsd.edu or phone (858) 534-4440.

CALIFORNIA BAY-DELTA AUTHORITY

Sea Grant California

Program Director
Environmental Genomics and Health
Duke University

DUKE INSTITUTE FOR GENOME SCIENCES & POLICY

We are seeking a visionary in the field of Environmental Genomics and Health to lead a series of broad-based, interdisciplinary initiatives that will focus on environmental exposures and human health. The Program Director position will have appointments in the Duke Institute of Genome Sciences and Policy (IGSP) (**http://www.genome.duke.edu**), the Department of Medicine and the Nicholas School of Environment and Earth Sciences (**http://www.nicholas.duke.edu**). The Director will lead all aspects of basic, clinical and translational research in the areas of gene -environment interactions relevant to understanding complex disease and environmental genomics.

The Director will assume leadership of ongoing programs in Environmental Genomics and Health research that are currently focused on the comparative biology of vulnerable populations and the role of genetic susceptibility in pathogenic responses to specific types of environmental stress. These are funded programs, and the Director will have the opportunity to develop new programs as he or she sees fit. This position is predicated on the use of genomic technologies, comparative biology, and human studies and is expected to have a significant impact on society and human health.

Electronic applications (PDF files), including a curriculum vitae, should be sent to **kathy.hay@duke.edu**.

Duke University is an Equal Opportunity/Affirmative Action Employer. Female and minority candidates are especially encouraged to apply.

POSTDOCTORAL FELLOWS
Scripps Florida
A Division of The Scripps Research Institute

Scripps Florida is a new cross-disciplinary institute in West Palm Beach, Florida. The Institute seeks to advance the understanding and treatment of a wide range of human conditions through basic biomedical research, advanced technology development, and drug discovery. Applications are now being sought for postdoctoral fellows for multiple positions within the Institute. Applicants must have a Ph.D. or M.D. with expertise in molecular biology and an interest in utilizing high-throughput technologies.

Areas of study include:

- **Circadian Biology, Dr. John Hogenesch** – Work involves the study of the transcriptional regulation of cycling genes within a well-developed research program. Both whole organism and in vitro studies are utilized with an emphasis on the exploitation of emerging technologies.
- **Functional Neuroanatomy, Dr. Teresa Reyes** – Research to focus on defining the central nervous system molecules and pathways that underlie appetite regulation and metabolism, in normal and challenged animal models.
- **Behavioral Genetics, Dr. Mathew Pletcher** – Directed towards the identification of genes involved fear conditioning, learning and memory, anxiety, and social behavior using both classical and novel mouse and human genetic techniques.
- **Genome Technologies, Drs. Josephine Harada and Trey Sato** – The group utilizes high throughput instrumentation and genome-scale cDNA and siRNA collections to identify novel gene activities in cell-based assays. Fellows will interact with biologists, engineers and bio-informaticians to utilize high throughput robotics and develop cellular screens for the identification of genes involved in signal transduction, cancer biology, protein trafficking and virology.
- **Nuclear Hormone Receptors and Structural Biology, Dr. Kendall Nettles** – A position is available to study the links between small molecule, receptor structure, and endocrine physiology. The laboratory is equipped with robots for high throughput cloning, protein purification, solution mixing and crystallization, and automated crystal visualization.

Interested parties should send a letter of interest, curriculum vitae, and contact information for three references to: **Scripps Florida, Attention: (name of principal investigator), 5353 Parkside Dr., Jupiter, FL 33458**.

TWO SCIENTIFIC INVESTIGATOR POSITIONS

The Van Andel Research Institute (VARI) invites applications for two Investigator positions at the Assistant/Associate Professor level. Located in a rapidly growing medical community in Grand Rapids, Michigan, VARI currently houses 16 laboratories devoted to basic cancer research, technology development and translational research. The facility also includes access to an exceptional group of special program core support facilities. Investigators will have the opportunity to participate in the training and teaching of graduate and undergraduate students. Applicants are required to have a Ph.D., M.D. or equivalent degree with a background in molecular biology, genetics and/or biochemistry. Areas of interest include, but are not limited to, human clinical studies, animal models, pathology, toxicology or medicinal chemistry with an emphasis on cancer biology. Candidates will be expected to have a demonstrated record of productivity. Consideration for either Scientific Investigator (Assistant Professor) or Senior Scientific Investigator (Associate Professor) positions will be commensurate with experience and previous success in obtaining funding. Institutional support and a generous start-up package are available to exceptional candidates. All investigators will be encouraged to apply for external financial support.

Qualified applicants should submit by email attachment a single PDF file containing their curriculum vitae, a statement of research interests and goals, along with the names of three references by July 1, 2005 via email to VARI-employment@vai.org and letter to: **Search Committee Chair, c/o Pam Murray; Van Andel Research Institute; 333 Bostwick NE; Grand Rapids, MI 49503** or visit www.vai.org. Van Andel Research Institute is an Equal Opportunity Employer.

The VanAndel Institute

THE J. DAVID GLADSTONE INSTITUTES

POSTDOCTORAL FELLOWSHIP OPPORTUNITIES

Postdoctoral Fellowships in the laboratory of Dr. Bob Pitas to study mechanisms that contribute to the development of cardiovascular disease. This will involve a multidisciplinary approach using in vitro and in vivo transgenic models to study the disease process, with emphasis on the importance of oxidized lipids and lipoproteins in the development of disease. Job #C04-12S

Postdoctoral Fellowship in the laboratory of Dr. Bob Pitas to study mechanisms contributing to the development of Alzheimer's disease and other neurodegenerative disorders. This will involve a multidisciplinary approach using in vitro and in vivo transgenic models to study molecular processes leading to these important neurological disorders. Job #N05-04S.

Postdoctoral Fellowship in the laboratory of Dr. Israel F. Charo to study chemokines and chemokine receptors. Research focuses on the role of chemokines in obesity/insulin resistance, hematopoiesis, the immune response, and atherosclerosis. Projects will make extensive use of novel knock-out and knock-in mice. Experience in obesity/diabetes or immunology is desirable. P05-01S.

We offer an exceptional trianing program for postdoctoral fellows, including rigorous scientific training, personalized attention and mentoring, and a rich research environment to allow our fellows to develop to the fullest of their abilities.

Candidates should possess a Ph.D., M.D., or both. Please send cover letter, curriculum vitae, and three references to:

The J. David Gladstone Institutes
Postdoctoral Opportunities
1650 Owens Street
San Francisco, California 94158

AA/EOC M/F/D/V

For more about Gladstone's Postdoctoral Training Program or to view current opportunities visit http://www.gladstone.ucsf.edu

HELMHOLTZ GEMEINSCHAFT

The Helmholtz Association of National Research Centres in Germany is seeking excellent young scientists and engineers as leaders for

20 Helmholtz Young Investigators Groups in six Research Fields: Energy, Earth and Environment, Health, Key Technologies, Structure of Matter, Transport and Space

The Helmholtz Association is Germany's largest organisation for scientific research and development. The 15 Research Centres united in the Association have a staff of 24,000 and an annual budget of about two billion euros. They perform top-rate research in strategic programmes and thus contribute to solving grand challenges which face society, science and industry. The Association's potential for realising these ambitious objectives lies in the excellence of its personnel, its world-class large-scale facilities and excellent scientific infrastructure and its experience in researching systems of great complexity.
The Young Investigators Groups will promote and further strengthen collaborations between the Helmholtz Centres and universities.

Eligibility: Individuals who have earned a doctoral degree within the last six years and have achieved a superior record of accomplishment during their doctoral and postdoctoral research.

Award:
- Group leader position (salary BAT Ia/Ib),
- Adequate laboratory space,
- Funds for laboratory set-up and operation,
- Positions for post-docs, graduate students and technical staff.

Duration: 5 years with a peer evaluation.

Perspective: Permanent employment, if evaluation attests excellence of group leaders.

Application: **Step 1** Candidates contact the Helmholtz Centre of their choice with a CV, publication list and two letters of recommendation.
Step 2 The formal applications have to be handed in by the chairman of the executive board of the Centre.

For further details and application information: **www.helmholtz.de/yig**

Deadline: **30 June, 2005**

The Helmholtz Association is an equal opportunity employer and is committed to increasing the percentage of women in group leader positions.

Contact: baerbel.koester@helmholtz.de

Tenure-Track Faculty Position at Michigan State University

The Center for Integrative Toxicology (CIT) at Michigan State University is accepting applications for a tenure-track academic year faculty position at the Assistant Professor level. We are seeking candidates with an interest and expertise in immunotoxicology and/or inflammation as it relates to adverse consequences of drugs or other chemicals in living systems. Candidates should have a Ph.D. degree in Toxicology or related discipline, postdoctoral research experience and demonstrated success in obtaining extramural funding.

The candidate will be jointly appointed in the CIT and in a basic science department (e.g., Pharmacology and Toxicology, Biochemistry and Molecular Biology) consistent with his/her expertise and interests. In addition to contributing to the CIT, the candidate will have the opportunity to participate in one or more other interdisciplinary research and training programs including the National Food Safety and Toxicology Center, the Cell and Molecular Biology Program, the Center for Biological Modeling, the Genetics Program and the Neuroscience Program. The successful candidate will be expected to establish an independent and extramurally funded research program and to contribute to the teaching and service missions of the department and the CIT.

Interested individuals should send their curriculum vitae, statement of research interests and future research plans, and 3 letters of recommendation to:

Chair, Faculty Search Committee
Center for Integrative Toxicology
C-231 Holden Hall
Michigan State University
East Lansing, MI 48824

Review of applications will begin on **April 1, 2005** and will continue until the position is filled.

MSU is an Affirmative Action/Equal Opportunity Institution.

Chair of the Department of Microbiology and Immunology

The Sophie Davis School of Biomedical Education at The City University of New York invites applications and nominations for the position of Chair, Department of Microbiology and Immunology. The goal of this combined BS/MD program, for more than 30 years, has been to provide a comprehensive education in the basic sciences of medicine to students who transfer after 5 years to a cooperating medical school for the final two years of clinical training. The mission of The Sophie Davis School of Biomedical Education is to increase the numbers of practicing minority physicians and to train physicians who will practice primary care medicine in physician shortage areas of New York State.

Duties: Provide leadership to the Department of Microbiology and Immunology, teach courses, maintain an active research program supported in part by external funding, and serve on department, school and college-wide committees.

Qualifications: Preference will be given to candidates who have earned an M.D. or Ph.D. in the field of Microbiology, Immunology, Infectious Disease or related disciplines. Applicants are expected to have an active research program with a national reputation. The Chair will work cooperatively with all departments in the school in the implementation of a new interdisciplinary curriculum. The Chair should de devoted to delivering a quality education to highly committed students in a multicultural environment.

Salary: Commensurate with qualifications and experience.

Closing Date: Open until filled with application review to begin immediately.

To Apply: Interested applicants should send a copy of their curriculum vitae, a personal statement of interest, and the names and contact information for three professional references to: **Dani L. McBeth, Ph.D., Chair of the Search Committee, Office of Student Affairs, H-113, The Sophie Davis School of Biomedical Education, 160 Convent Avenue, New York, N.Y. 10031.**

CUNY The City University of New York

Additional information available at www.ccny.cuny.edu.

The City College/CUNY is an EEO/AA/IRCA/ADA Employer.

Albany Medical College

Faculty Position
Center for Neuropharmacology and Neuroscience

The Center for Neuropharmacology and Neuroscience (CNN) of Albany Medical College invites applications for a tenure-track faculty position at the assistant or associate professor level. We seek a highly motivated individual with a strong record of research productivity and a desire to participate in graduate and medical education. The applicant's research should complement and/or enhance existing programs in the CNN as well as in collaborating clinical departments (e.g., neurology and psychiatry). We are particularly interested in building a program focused on Alzheimer's disease and other neurodegenerative disorders but will also consider candidates having expertise in stroke research, substance abuse research, research on neuropsychiatric disorders, or neural stem cell biology. A Ph.D. or M.D./Ph.D. degree and three years of postdoctoral experience are minimal requirements for appointment at the assistant professor level. Applicants for associate professor should have appropriate experience and a nationally recognized and funded research program. The Albany area offers diverse cultural and recreational attractions with easy access to Boston, New York City, and the Adirondack, Catskill and Berkshire Mountains. For further information about the CNN, please visit our website at **http://www.amc.edu/academic/research/cnn.htm**.

Applicants should send a curriculum vitae, description of research interests, and three letters of recommendation by **May 15, 2005** to:

Stanley D. Glick, Ph.D., M.D.
Director, Center for Neuropharmacology and Neuroscience
Albany Medical College, MC-136
47 New Scotland Avenue
Albany, NY 12208

An Equal Opportunity/Affirmative Action Employer.
Women and Minorities are encouraged to apply.

Science AAAS

Editor in Earth and Space Sciences

Join the editorial team at *Science*. We are seeking a new Associate Editor in the physical sciences. Applicants should have a broad range of interests and research experience in geochemistry, geophysics, planetary science, and astrophysics. Applicants should have post-doctoral experience, multiple publications, and a breadth of knowledge of cutting-edge research in these and related fields. Responsibilities include managing the review, selection, and editing of manuscripts, working with authors on revisions, solicitation of Reviews and special issues, and fostering contacts and communication with the scientific community. The position is for either our Washington, DC, or Cambridge, UK, offices. EOE. Non-smoking work environment.

For consideration, send a resume and cover letter along with salary requirements to:

AAAS
Human Resources Department, Suite #101
1200 New York Avenue
Washington, DC 20005

Applications can also be sent by e-mail to hrtemp@aaas.org or Fax to 202-682-1630. Visit us at http://www.aaas.org.

Science Career Forum

Bring your career concerns to the table. Dialogue online with professional career counselors and your peers.

- How can you write a resume that stands out in a crowd?
- What do you need to transition from academia to industry?
- Should you do a postdoc in academia or in industry?
- How do you negotiate a salary increase?

Let a trusted resource like *Science* Careers help you answer these questions.

Science Careers has partnered with a professional moderator and three well-respected advisers, who along with your peers will field career-related questions.

Visit ScienceCareers.org and start an online dialogue.

Moderator: Dave Jensen, *HR Consultant*
Mr. Jensen has over 20 years of experience in human resource consulting and staffing for the biotechnology and pharmaceuticals industry.

Advisers:
Bill Lindstaedt, *Director UCSF Career Center*

Naledi Saul, *Assistant Director, UCSF Career Center*

Mr. Lindstaedt and Ms. Saul bring a combined 17 years of career counseling experience with a particular emphasis on working with graduate-level trainees in the life sciences.

Jim Austin, *Editor,* Science*'s Next Wave*

Dr. Austin has a Ph.D. in physics and worked in academia before coming on board to write about traditional and nontraditional career paths for scientists.

ScienceCareers.org
We know science AAAS

POSITIONS OPEN

PHYSICIAN-SCIENTIST AND NEPHROLOGIST
Department of Medicine
University of California San Francisco

The Department of Medicine, Division of Nephrology at the University of California, San Francisco seeks an outstanding Physician-Scientist and Nephrologist at the rank of **ASSISTANT, ASSOCIATE,** or **FULL PROFESSOR** in the In Residence series to establish a high quality, independent research program in basic cell biology, physiology, or genetics. The successful candidate must have an M.D. or M.D./Ph.D. degree and evidence of a strong capability in basic science research as demonstrated by publications, presentations at national meetings, and grant support. Board certification in internal medicine and board certification or eligibility in nephrology is required. Opportunities for clinical service in nephrology are available and encouraged. Salary and academic rank will be determined by previous experience. Generous startup funds are available for the competitive candidate. The candidate will also become a member of the graduate program in biomedical sciences.

Please send curriculum vitae, brief statement of research interest, and the names and addresses (including e-mail addresses) of three references to: **Stephen L. Gluck, M.D., Chief of Nephrology, University of California, San Francisco, 513 Parnassus Avenue, HSE 672, Box 0532, San Francisco, CA 94143-0532;** or **e-mail: glucksl@medicine.ucsf.edu.** Deadline for applications: two months post ad publication date.

UCSF is an Affirmative Action/Equal Opportunity Employer. The University undertakes Affirmative Action to assure Equal Employment Opportunity for underutilized minorities and women, for persons with disabilities, and for Vietnam-era veterans and special disabled veterans.

FACULTY CLUSTER HIRE
Marine Environmental Science
University of Southern California

As part of the College's Senior Hiring Initiative, the University of Southern California (USC) is seeking outstanding scholars in any area of the marine environmental sciences. We wish to hire an integrated group, a mix of **FULL, ASSOCIATE,** and **ASSISTANT PROFESSORS,** who are innovative, entrepreneurial, interdisciplinary leaders with a clear vision for the most exciting future research in their fields. This group will be resident either at our University Park Campus, at the Wrigley Marine Science Center on Catalina Island, or both. They will be encouraged to create a significant science program that makes use of the unique capabilities of the facilities on Catalina Island. This will be a cluster hire and we ask that faculty propose their own group and their own plans for innovative teaching and research. Undergraduate teaching responsibilities will be met by participation in an expanded USC Catalina Semester or through an appropriate department. For more information contact: **Dr. Anthony F. Michaels, Director, University of Southern California Wrigley Institute, 3616 Trousdale Parkway, Los Angeles, CA 90089-0371. E-mail: tony@usc.edu.** *USC is an Affirmative Action/Equal Opportunity Institution. We particularly encourage women and minority candidates.*

POSTDOCTORAL POSITION
Biochemical Toxicology

A position is available to study in vitro P450-related metabolism of emerging chemical warfare threats. A strong interest in the application of instrumental techniques to the study of xenobiotic metabolism and a background in toxicology/biochemistry are preferred. *U.S. citizenship is required.* Send curriculum vitae with contact information for three references to: **Dr. Alan A. Brimfield, Biochemical Pharmacology Branch, U.S. Army Medical Research Institute of Chemical Defense, 3100 Ricketts Point Road, Aberdeen Proving Ground, MD 21010-5400. E-mail: alan.a.brimfield@us.army.mil.**

USDA ARS Agricultural Research Service
www.ars.usda.gov

RESEARCH PLANT GENETICIST
GS-11/12/13
Salary Range $50,541 to $93,643 per annum

The U.S. Department of Agriculture, Agricultural Research Service, Plant Science and Entomology Research Unit, Manhattan, Kansas, is seeking a permanent full-time Research Plant Geneticist (GS-11/12/13) (Salary Range $50,541 to $93,643 per annum) to lead an innovative applied and basic research program on hard winter wheat germplasm enhancement. For details and application directions, see **website: http://www.afm.ars.usda.gov/divisions/hrd/vacancy/resjobs/X5W-0203.HTM.**

To have a printed copy mailed, **telephone: 785-776-2737.** *U.S. citizenship is required.* Announcement closes May 23, 2005. *USDA/ARS is an Equal Opportunity Employer and Provider.*

Achillion Pharmaceuticals

We are seeking a qualified **SCIENTIST/RESEARCH ASSOCIATE** candidate to join our Pre-Clinical Candidate Selection team. This individual will support in-house anti-infective programs in the characterization of small molecule drug physicochemical, absorption, distribution, metabolism, excretion, and toxicity (ADMET), and pharmacokinetic (PK) properties. Responsibilities will include: conducting in vitro assays to characterize ADMET properties of drug candidates and expanding the Department's capabilities through the development and execution of new ADMET techniques and assays. Qualified candidates will possess a Ph.D. in pharmaceutics/biology, analytical chemistry/biochemistry, or related discipline. Exceptional candidates with B.S./M.S. degrees in a comparable discipline will be considered. A minimum of one to three years of related experience is required. Knowledge and experience with ADME and PK in drug discovery and assay development required. Analytical or bioanalytical experience a plus. Candidates must have excellent written and oral communication skills. The ability to prioritize and multitask is required. For prompt consideration for this position, please send your curriculum vitae indicating the position of interest and the names of three references to: **Human Resources, Achillion Pharmaceuticals, 300 George Street, New Haven, CT 06511. E-mail: jobs@achillion.com.** Please reference Job Code: PCS. No telephone inquiries please.

The Department of Neurobiology and Developmental Sciences in the College of Medicine at the University of Arkansas for Medical Sciences (UAMS) has tenure-track openings for the **DIRECTOR** of the Division of Cellular and Molecular Neurosciences and **FACULTY** working in the area of developmental and/or reproductive sciences, who can develop programmatic funding. Our Department is distinguished by rapid growth in funding and resources during the past five years, which has led to the formation of two Centers with significant space and resources. (**Website: http://www.uams.edu/neuroscience_cellbiology/**). This is an exceptional opportunity for well-funded researchers with the vision and desire to lead a division and/or help build a strong magnet area in the developmental sciences. A statement of research interest and curriculum vitae should be sent to: **Gwen V. Childs, Ph.D., Chair, Department of Neurobiology and Developmental Sciences, The College of Medicine, University of Arkansas for Medical Sciences, 4301 W. Markham Street, #510 Little Rock, AR 72205. Telephone: 501-686-7020; fax: 501-686-6382; e-mail: childsgwenv@uams.edu.** *UAMS is an Equal Opportunity Employer, promoting workplace diversity, and does not discriminate on the basis of race, color, religion, national origin, sex, age, or developmental disability.*

CHIEF, LABORATORY BRANCH
Division of Viral Hepatitis
Centers for Disease Control and Prevention
Atlanta, Georgia

The Centers for Disease Control and Prevention (CDC), Division of Viral Hepatitis, a World Health Organization (WHO) Collaborating Center, is seeking senior-level candidates with hepatitis, or other infectious disease experience, to serve as Chief of the Laboratory Branch. The Branch Chief provides leadership, direction, and oversight to approximately 22 full-time equivalent positions, and 40 additional visiting scientists, guest researchers, and laboratory staff. The Branch Chief directly supervises five laboratory team leaders (virology, pathology, molecular epidemiology, developmental diagnostics, and reference diagnostics). Applicants must be qualified to oversee a comprehensive research agenda that includes studies of all viruses causing hepatitis, A-E, as well as new and potentially pathogenic viruses. The Laboratory Branch, which is moving into a new, state-of-the-art laboratory and office building, works closely with the Epidemiology and Prevention Branches to accomplish its overall mission. The applicant must possess a broad range of scientific knowledge with particular emphasis on the molecular biology, pathogenesis, virology, diagnostics, and immunology of viral hepatitis or other infectious disease. A comprehensive knowledge of literature pertaining to hepatitis as well as scientific approaches taken by professional peers in government, industry, and academia is also important. Candidates for the position must meet qualifications for the GS-15 level for the federal civil service and have a doctoral-level degree in medicine, microbiology, biology, or other appropriate field. Salary is commensurate with experience with the possible addition of a recruitment bonus of up to 25 percent of the base salary; a physician's comparability allowance also may be available.

For more information contact: **Stephen Morse, Ph.D., Search Committee Chair,** at **telephone: 404-639-3559** or **e-mail: smorse@cdc.gov,** or **Jeff Efird** at **e-mail: jefird@cdc.gov.** To apply for the position, please submit curriculum vitae and bibliography postmarked no later than May 22, 2005, to: **Tom Brooks, Centers for Disease Control and Prevention, Atlanta Human Resources Center, 4770 Buford Highway, MS K-15, Atlanta, GA 30341-3724. E-mail: tbrooks@cdc.gov.** *CDC is an Equal Opportunity Employer.*

POSTDOCTORAL FELLOW

A Postdoctoral Fellow position is immediately available to study the molecular mechanisms associated with mood disorders and suicide. The candidate should be a Ph.D. with experience demonstrated in molecular biology and/or immunohistochemistry, analysis such as reverse transcription polymerase chain reaction, cloning, immunolabeling, Western blot, enzyme-linked immunosorbent assay, and in-situ hybridization. Preference will be given to those who have prior experience with human subjects and/or rodents. Send your curriculum vitae along with three references to: **Ghanshyam N. Pandey, Ph.D., Department of Psychiatry, University of Illinois at Chicago, 1601 W. Taylor, Room 315 W, M/C 912, Chicago, IL 60612** or **fax: 312-413-4547** or **e-mail: gpandey@psych.ui.cedu.** *University of Illinois at Chicago is an Affirmative Action/Equal Opportunity Employer.*

POSTDOCTORAL POSITIONS at The Rockefeller University, New York, are available to study a new line of multidisciplinary research on the mechanisms of reprogramming of differentiated adult human and mouse cells to stem cell-like cells using neurotrophic bacteria/bacterial components. Applicants should be highly motivated individuals with thorough background in molecular biology and cell biology or neurobiology. Experience in stem cell biology and transgenic mice are a plus. Send curriculum vitae and three letters of references to: **Dr. Anura Rambukkana; e-mail: rambuka@imap.rockefeller.edu.**

Biochemistry Careers

A *Science* Advertising Supplement

Need to attract great scientists?

Talk to someone who knows science.

Marie Curie
1867–1934

Science's qualified circulation of 129,590[1] plus our pass-along readers brings total global weekly readership to over 710,000.[2]

25% discount for multiple insertions of the same ad. Call your sales rep for more information.

1 *Science* June 2004 BPA Publisher's Statement.
2 *Science* June 2004 circulation as applied to 14 January 2000 Harvey Readership Survey and 2002 Harvey Cumulative Report, publisher's own data.

Issue date 20 May **Reserve ad space by** 3 May

For more information contact:
U.S. Daryl Anderson
phone: 202-326-6543
e-mail: danderso@aaas.org

Europe and International
Tracy Holmes
phone: +44 (0) 1223 326 500
e-mail: ads@science-int.co.uk

Japan Jason Hannaford
phone: +81 (0) 52 789-1860
e-mail: jhannaford@sciencemag.jp

ScienceCareers.org
We know science AAAS

POSITIONS OPEN

PROTEOMICS RESEARCH CENTER
University of Washington

The Department of Genome Sciences at the University of Washington School of Medicine in Seattle is seeking two new faculty to establish an interdepartmental Proteomics Research Center. The Center's mission is to develop and to apply state-of-the-art technologies to further our understanding of protein composition and function, dynamics, localization, and/or interactions. Center members will collaborate with laboratories throughout the University, playing a leadership role in the University's wider proteomics program.

Initially the Center will occupy almost 7,000 square feet of recently completed space on the School's new Lake Union Campus. The Center has obtained committed and substantial long-term financial support of its mission, allowing for equipment acquisition and renewal, development of computing resources, and recruitment of key personnel. Following this initial phase, additional space and resource commitments may be available.

The Department invites applications for two mid-level tenured or tenure-track faculty at the rank of **ASSOCIATE** or **FULL PROFESSOR.** Exceptional candidates at the rank of **ASSISTANT PROFESSOR** may be considered. Both positions involve teaching duties as well as an active research effort. Applicants should hold a Ph.D. or M.D. degree.

Applications received by April 30, 2005, will receive consideration. Thereafter, applications will be reviewed upon receipt until both positions are filled.

Contact:

The Department of Genome Sciences
Proteomic Center Search
Department of Genome Sciences
University of Washington
Box 357730, HSB–K353A
Seattle, WA 98195
E-mail: proteomics@gs.washington.edu

Candidates should e-mail their curriculum vitae, statement of research and teaching interests, and arrange to have three signed letters of reference sent by mail to the address above.

For additional information that may be helpful in preparing an application, see the Department's **website: http://www.gs.washington.edu.**

The University of Washington is building a culturally diverse faculty and strongly encourages applications from women and minority candidates. The University of Washington is an Affirmative Action/Equal Opportunity Employer.

VISITING ASSISTANT PROFESSOR POSITIONS, BIOLOGY
Claremont Mckenna, Pitzer, and Scripps Colleges

The Joint Science Department of Claremont McKenna, Pitzer, and Scripps, three liberal arts colleges in the Claremont Colleges Consortium in Southern California, seeks to hire two Visiting Assistant Professors for the 2005-2006 academic year, beginning August 2005. Teaching responsibilities for position one include developmental biology with laboratory and introductory biology with laboratory and for position two include molecular biology with laboratory, genetics, and a nonmajors biology course with laboratory. Participation in research, particularly directing undergraduate research projects is encouraged. A Ph.D. in biology or related subject, and prior teaching experience are required.

Please submit curriculum vitae and a statement of interest, specifying which position is of interest to you, and arrange to have three letters of reference sent to: **Temporary Biology Positions, W.M. Keck Science Center, 925 N. Mills Avenue, Claremont, CA 91711-5916. Telephone: 909-621-8298.** Inquiries to: **Dr. David Sadava** at **e-mail: dsadava@jsd.claremont.edu.** Review of applications begins April 15, 2005, and the positions will remain open until filled.

In a continuing effort to enrich its academic environment and provide Equal Educational Employment Opportunities, The Claremont Colleges actively encourage applications from women and members of historically underrepresented groups in higher education.

NATURAL HISTORY MUSEUM

INSECT CYBERTAXONOMIST APPOINTMENT AT JUNIOR TO SENIOR LEVEL
Department of Entomology
Salary will commensurate with experience up to £29,350 p.a.
South Kensington

Building a leading programme in the creation and use of digital taxonomic tools and methods, you will develop and implement innovative approaches to insect taxonomy utilizing cyber-technologies, participate in diverse taxon-focused team projects, provide general information technology (IT) guidance and leadership to the Department, and join MOA team implementing new collection management software.

You will have a Ph.D. in insect taxonomy or a related field and demonstrate competencies in IT. Postdoctoral experience is preferred.

For further information, please contact: **Dr. Quentin D. Wheeler, Keeper and Head, Department of Entomology** at **e-mail: q.wheeler@nhm.ac.uk.**

For further information and details of how to apply, please send an A5 self-addressed envelope (first class) to: **The Natural History Museum, c/o Tribal Resourcing, The Atrium, Wollaton Street, Nottingham NG1 5FW, London, England** or **e-mail: nhm@tribalresourcing.com.**

Please quote reference: NHM/IC.

Closing date: 28 April 2005 or until suitable candidate is identified.

To confirm receipt of your application call the Museum response line at **telephone: 0870-241-9031** from 11 a.m. to 2 p.m., Monday to Friday only. No telephone requests for details will be accepted.

At the Natural History Museum we value the diversity of our employees and the unique perspectives they bring to our business.

FACULTY POSITION
University of Minnesota

The Hematology, Oncology, and Transplantation (HOT) Division and the Department of Medicine at the University of Minnesota Medical School are seeking M.D.-Ph.D. or M.D. applicants for a tenure-track position at the **ASSISTANT PROFESSOR** level. Applicants should have a research focus on proteomics applications in hemostasis, thrombosis, and/or vascular biology to complement our existing vascular biology strengths in endothelial biology, stem cell biology, angiogenesis, inflammation, and hemostasis/thrombosis. Successful candidates will have evidence of successful external funding and research productivity. The selected applicant will be expected to establish an outstanding, externally funded, independent research program, and to participate collaboratively with the local scientific community. The applicant should be board certified or board eligible in hematology and/or oncology, and be willing to perform limited attending duties on the in-patient hematology/oncology service. The Medical School provides a resource-rich and intellectually stimulating atmosphere for research development. Interested candidates should submit curriculum vitae, a statement of research interest and future goals, and the names of three references with address, e-mail, and phone contact information. Review of applications will begin on May 15, 2005. Please submit applications to:

Nigel S. Key, M.D.
Department of Medicine, HOT Division
University of Minnesota Medical School
Mayo Mail Code 480
420 Delaware Street, S.E.
Minneapolis, MN 55455

Applications are particularly encouraged from minority and female candidates.

ASSISTANT PROFESSOR ANATOMY/PHYSIOLOGY
College Misericordia

College Misericordia invites qualified candidates to apply for a full-time (ten-month) position of Assistant Professor commencing August 2005. The position is a nontenure-track appointment. The successful candidate may apply for a tenure-track position opening that will be available in the fall of 2006. The successful candidate must hold a Ph.D. at the time of appointment, and will be expected to teach courses in anatomy, physiology, and general biology.

College Misericordia is committed to excellence and actively supports cultural diversity. To promote this endeavor, we invite individuals who contribute to such diversity to apply. Our 80-year-old institution offering baccalaureate and Master's degree programs is located adjacent to the Pocono Mountains region of Northeastern Pennsylvania, approximately two to three hours from New York City, Philadelphia, and Baltimore. The College's approach of combining a quality liberal arts education with professional preparation and service leadership has resulted in its wide regional acclaim.

For confidential consideration please enclose in your application package a letter of application which includes your telephone number and e-mail address, curriculum vitae, statement of teaching philosophy, and three letters of reference to: **College Misericordia, Attention: Human Resources Department, 301 Lake Street, Dallas, PA 18612** or **e-mail: hr@misericordia.edu.** Inquiries only, should be directed to: **Dr. Frank DiPino, Department Chair of Biology, e-mail: fdipino@misericordia.edu.**

Review of applications will begin immediately and will continue until position is filled. For additional information about College Misericordia, visit our **website: http://www.misericordia.edu.**

FACULTY POSITIONS
STEM CELL BIOLOGY
School of Natural Sciences
University of California, Merced

University of California (UC), Merced is the 10th UC campus and the first new U.S. research university of the 21st century. The campus is located at the base of the Sierra Nevada foothills, near Yosemite and the San Francisco Bay Area. The School of Natural Sciences at UC Merced invites faculty applications at the **ASSISTANT PROFESSOR** (tenure track), **ASSOCIATE PROFESSOR** (tenured), and **FULL PROFESSOR** (tenured) levels in the area of stem cell biology. Candidates must have a Ph.D. or equivalent, a record of research, publication, and teaching commensurate with a faculty appointment at the UC, and a strong interest in creating a curriculum characterized by cross-disciplinary links. Applicants are sought in all areas of stem cell biology, including stem cell signaling and cell fate decisions, self renewal and differentiation, hematology, cancer cell biology, developmental biology, and interactions between stem cells and their microenvironment. To apply or for further information, please visit our **website: http://jobs.ucmerced.edu/view_academic_position.faces?positionId=88.** Application deadline: May 15, 2005. *Affirmative Action/Equal Opportunity Employer.*

POSTDOCTORAL/RESEARCH ASSOCIATE position is available at the University of Colorado Health Sciences Center (Denver, Colorado) to study mechanisms of mitochondrial oxidative stress in neuronal disorders including epilepsy and Parkinson's disease. The focus of the laboratory is to study mechanisms of free radical damage using neuronal cell lines, primary neuronal cultures, and genetically modified mice in combination with state-of-the-art approaches to assess oxidant stress. A Ph.D. with a background in biochemistry, pharmacology, or molecular biology and experience with animal models and cellular/molecular techniques is highly desirable. Qualified applicants should send curriculum vitae, statement of research interests, and names of three references to **e-mail: manisha.patel@uchsc.edu.**

Postdoctoral Positions in Mammalian Molecular and Developmental Genetics

McLaughlin Research Institute is a small non-profit research organization near the east slopes of the Rocky Mountains and provides an outstanding environment to train for a career in mammalian genetics. Applicants for these positions should provide evidence, including publication in internationally recognized journals, for their potential for an independent research career. Refer to www.montana.edu/wwwmri for additional information about the following research programs.

- **Genetic Regulation of Myelination (J. Bermingham)**
- **Genetics of Susceptibility to Neurodegenerative Disease. (G. Carlson)**
- **Molecular Motors & Chemical Genetics (J. Mercer)**
- **Development of the Auditory and Renal Systems (P. Xu)**

To apply, state clearly the program to which you wish to apply, send your curriculum vitae, a statement of research interests, and the names of three individuals whom we may contact for references to:

Training Office
McLaughlin Research Institute
1520 23rd Street South
Great Falls, MT 59405
tg@po.mri.montana.edu

Columbia University
Department of Microbiology
Postdoctoral Position

Postdoctoral position to study CD4 silencing. Seeking recent Ph.D. recipients with experience in biochemistry. Our lab is interested in mechanisms controlling heterochromatin packaging during T-cell development. We are using mouse models to characterize genes involved in epigenetic CD4 silencing.

Submit curriculum vitae and three references to:

Yong-Rui Zou, Ph.D.
Department of Microbiology
Columbia University
701 West 168th Street, HHSC 1406
New York, NY 10032
Telephone: 212-305-0202
Fax: 212-305-1468
E-mail: yz2001@columbia.edu

Columbia University is an affirmative action/equal opportunity employer.

Where people who think differently think together™

CREATIVE SCIENTISTS AND ENGINEERS

Kimberly-Clark is a recognized global health and hygiene leader in the manufacture of tissue, personal care and health care products with sales over 15 billion dollars.

We are part of a corporate research and development unit that is creating new science and technology in support of an ambitious new business growth plan. Our group is seeking creative, versatile and dynamic scientists to join us as part of the R&D infrastructure expansion program. Many new positions are available to qualified applicants:

- **Molecular biologist** with a proven record of accomplishment. A background in the expression and biophysical characterization of recombinant proteins is required. An innovative scientist who can link experiment with simulation methodology is especially desired (several openings).
- **Cell biologist** with a focus in various aspects of women's health and physiology. A background in alternative therapeutics is desirable. A working knowledge of cervical and vaginal cell culture models is required (several openings).
- **Biomedical engineer** with a background in device design and device/drug systems including the evaluation of delivery mechanisms. Strong high level computer programming skills are required. A knowledge of, or work experience in, laboratory automation systems, SolidWorks modeling and microfluidics is highly desirable (several openings).
- **Polymer or materials chemist** with strong physical polymer analysis skills. A creative scientist who is also highly familiar with polymer gels and their synthesis. A proven track record of accomplishment is required. Previous industrial experience is highly desirable, but not required.
- **Quality Systems expert** must be familiar with implementing and running a quality system, including design control and other project files. Responsibilities include creating/editing QS documents, document control, and interfacing with other Kimberly Clark Quality and Regulatory personnel.

Candidates at all educational levels (BS, MS, PhD) will be considered for these positions. The successful candidate must have strong initiative, quick learning ability, an entrepreneurial spirit, and the ability to perform novel and independent research.

These unique opportunities are located at our R&D campus in Roswell, Georgia, an attractive and growing suburb north of Atlanta. We offer a competitive salary and benefit package commensurate with education and a demonstrated track record.

Principals Only-
To apply go to **www.kc-careers.com**. Click North America, Submit Resume. To ensure consideration be sure to include code **380BR** in the submission form where indicated.

Kimberly-Clark

Looking for a JOB?

- Job Postings
- Job Alerts
- Resume/CV Database
- Career Advice
- Career Forum

NEW

ScienceCareers.org
We know science AAAS

MEETINGS

west
WOMEN ENTREPRENEURS IN SCIENCE & TECHNOLOGY

Showcase 2005:
The Realm of Opportunities

An Exploration of
Entrepreneurship
Intrapreneurship & Careers

A unique opportunity for women to learn from and connect with other accomplished entrepreneurs and corporate leaders.

For event details:
www.westorg.org

West's mission is to advance women in science and technology to achieve success and recognition as contributors and leaders through entrepreneurial thinking.

POSITIONS OPEN

PHYSICIAN-IMMUNOLOGIST AND TRANSPLANT NEPHROLOGIST

The Department of Medicine, Division of Nephrology at the University of California, San Francisco (UCSF) seeks an outstanding Physician-Transplant Immunologist and Nephrologist at the rank of **ASSISTANT, ASSOCIATE,** or **FULL PROFESSOR** in the In Residence series to establish a high quality, independent research program in basic immunology. The successful candidate must have an M.D. or M.D./Ph.D. degree and evidence of a strong capability in immunology as demonstrated by publications, presentations at national meetings, and grant support. Board certification in internal medicine and board certification or eligibility in nephrology is required. Opportunities for clinical service in transplant nephrology are available and encouraged. Salary and academic rank will be determined by previous experience. Generous startup funds are available for the competitive candidate. The candidate will also become a member of the graduate program in biomedical sciences.

Please send curriculum vitae, brief statement of research interest, and the names and addresses (including e-mail addresses) of three references to: **Stephen L. Gluck, M.D., Chief of Nephrology, University of California, San Francisco, 513 Parnassus Avenue, HSE 672, Box 0532, San Francisco, CA 94143-0532;** or **e-mail: glucksl@medicine.ucsf.edu.** Deadline for applications: two months post ad publication date.

UCSF is an Affirmative Action/Equal Opportunity Employer. The University undertakes Affirmative Action to assure Equal Employment Opportunity for underutilized minorities and women, for persons with disabilities, and for Vietnam-era veterans and special disabled veterans.

VISION SCIENTIST

The Department of Ophthalmology of the University of Oklahoma College of Medicine/Dean A. McGee Eye Institute is seeking applicants for two positions in vision research at or above the **ASSOCIATE PROFESSOR** level. The successful candidate will have an active research program on molecular mechanisms of eye disease, an outstanding record of grant support and publications, and current R01 funding. There are currently 20 independent vision scientists on campus. Core facilities are supported by a National Eye Institute core grant and National Center for Research Resources Center of Biomedical Research Excellence grant. The Department of Ophthalmology ranks sixth in the country in NIH funding. Adjunct appointments are available.

Interested candidates should submit curriculum vitae, statement of research interest, and names and contact information of three references to: **David W. Parke II, M.D., Edward L. Gaylord Professor and Chair, Department of Ophthalmology, Dean A. McGee Eye Institute, 608 Stanton L. Young Boulevard, Oklahoma City, OK 73104.** *The University of Oklahoma is an Affirmative Action/Equal Opportunity Employer.*

TENURE-TRACK POSITIONS
Cellular and Molecular Biology
University of Montreal

The Research Center of the Maisonneuve-Rosemont Hospital (affiliated with the Université de Montréal) is seeking to fill two tenure-track positions at the level of **ASSISTANT PROFESSOR.** Areas of emphasis include cellular responses to DNA damage, immunology/oncology, signal transduction, nephrology, and visual sciences. Outstanding candidates will be considered for a Canada Research Chair. Montreal is a thriving multicultural urban center offering a highly affordable standard of living.

Please forward a detailed curriculum vitae including statement of research interests and three letters of recommendation to:

Dr. Alain Bonnardeaux
Director, Centre de Recherche
Hôpital Maisonneuve-Rosemont
5415 boulevard de l'Assomption
Montréal, Québec, Canada H1T 2M4
E-mail: alain.bonnardeaux@umontreal.ca

POSITIONS OPEN

POSTDOCTORAL AND CLINICAL FELLOWSHIPS
at the
National Institutes of Health
U.S. Department of Health and Human Services

Website: http://www.training.nih.gov

NIH is dedicated to building a diverse community in its training and employment programs.

VISITING POSITION
Vertebrate Ecology and Conservation Biology
Biology Department
St. Lawrence University

The Biology Department at St. Lawrence University (SLU) seeks to fill a one-year sabbatical replacement position for the 2005-2006 academic year. Candidates should have a Ph.D. [all but dissertation candidates will be considered] and be able to offer undergraduate-level field courses in vertebrate ecology (e.g., mammalogy, ornithology, herpetology, vertebrate natural history) and conservation biology. The candidate may have the opportunity to teach in our introductory biology sequence and will be able to offer an upper-level course of the candidate's interest. We seek candidates who understand the liberal arts and science education environment and who can bring multicultural perspectives to their teaching. St. Lawrence University is located in the St. Lawrence River Valley very close to the six-million acre Adirondack State Park. The Biology Department is well equipped for teaching courses with solid field components. Interested candidates should send an application letter, a resume, a statement on teaching philosophy and interest, and three letters of reference to: **Dr. Erika Barthelmess, Biology Department, St. Lawrence University, Romoda Drive, Canton, NY 13617.**

Review of applications is in process.

For more information please visit SLU's homepage at **website: http://www.stlawu.edu.** *St. Lawrence University is an Affirmative Action/Equal Employment Opportunity Employer. We welcome applications from candidates who bring diverse cultural, ethnic, and national perspectives to their work and participation in campus life and encourage women, minorities, veterans, and persons with disabilities to apply.*

TIME FOR A CAREER CHANGE?

CPE Communications, a leader in pharmaceutical healthcare communications, is looking for enthusiastic, self-motivated **MEDICAL WRITERS.** If you enjoy writing and learning about the pharmacologic management of disease, have excellent communication and presentation skills, can adhere to deadlines, and manage multiple projects, this job may be for you! Send inquiries, curriculum vitae, and salary requirements to **e-mail: hr@dpmadvert.com** referring to code #MW-1104. Advanced degree required (Ph.D., Pharm.D., or M.D.). Immunology, oncology, or pharmacology expertise preferred. Willing to train. Experience a plus.

POSTDOCTORAL POSITION available immediately to study mechanisms of leukocyte activation through G protein-coupled receptors. Knowledge and experience in cell transfection, RNA interference, biochemical characterization of proteins, and in vivo inflammation assays are desired. For fullest consideration, send curriculum vitae, statement of research interests, and names of three references to: **Richard D. Ye, Professor, Pharmacology, M/C 868, University of Illinois at Chicago, 835 S. Wolcott Avenue, Chicago, IL 60612. E-mail: yer@uic.edu.** *University of Illinois at Chicago is an Affirmative Action/Equal Opportunity Employer.*

POSITIONS OPEN

ACADEMIC CARDIOLOGIST. The University of California, San Diego (UCSD) School of Medicine is actively recruiting for an Academic Cardiologist for a tenure-track/tenured position in the Division of Cardiology (**website: http://medicine.ucsd.edu/med**). Will consider both M.D. and M.D./Ph.D. candidates. The position will be primarily dedicated to performing basic research within the broad area of cardiovascular diseases and will also involve teaching of medical students, residents, and postdoctoral fellows. Effort as attending physician on the clinical services of the cardiology division will be expected. Candidates should have demonstrated productivity in basic research and acquisition of research support. Candidates must be board certified/eligible in cardiovascular medicine and be eligible for a California Medical License. Appointment level will be commensurate with experience and qualifications, and compensations based upon established UCSD salary scales. Interested individuals should send curriculum vitae and contact information for three references by April 28, 2005, to: **Kirk Knowlton, M.D., Chief, Division of Cardiovascular Medicine, University of California San Diego Medical Center, 200 West Arbor Drive, San Diego, CA 92103-8411,** or **e-mail: clgroves@ucsd.edu.** *Affirmative Action/Equal Opportunity Employer.*

Dystonia Medical Research Foundation Request for Applications (RFA): Innovative Therapeutics 2005

A major part of the Dystonia Medical Research Foundation's (DMRF) mission is to support research leading to a cure for all forms of dystonia. The goal of this RFA is to focus on identification and pre-clinical testing of promising new treatments for dystonia in order to accelerate the translation of basic research findings to treatments in the clinic and provide new therapy options for the over 300,000 persons who suffer from dystonia in the United States.

The scope of this RFA includes only activities directly focused on dystonia therapy development necessary to begin clinical testing. Projects will typically include either an assay that has demonstrated relevance to dystonia or candidate therapeutics that have a significant effect on dystonia. Mechanistic or basic studies will not be supported.

Award amount: Proposals may request up to $100,000 for the first year of support, and up to an additional $100,000 for a second year of support.

Deadline: The application deadline is September 15, 2005.

For additional information and an application please visit **website: http://www.dystonia-foundation.org.**

STAFF ASSOCIATE (Manh). Perform laboratory procedures related to molecular cloning including cDNA library screening, denaturing high-performance liquid chromatography mutation detection, microsatellite mapping, fluorescence polarization–template-directed dye terminator-incorporation/pyrosequencing for single nucleotide polymorphism genotyping. Master's degree in biology or related fields with minimum three years experience required. Send curriculum vitae to: **Ana Ignat, Columbia University, 1150 St. Nicholas Avenue, Room 620, New York, NY 10032.**

COURSE

Short Course: BioCD-2005
Circular Dichroism Spectroscopy of Proteins and Nucleic Acids
Hands-on conventional and synchrotron CD experiments
Web based data analysis
Brookhaven National Laboratory
Upton, New York, U.S.A.
June 20 to 24, 2005
Website:
http://www.nsls.bnl.gov/newsroom/events/workshops/biocd/Default.htm.

Great scientists don't just fall from the sky.

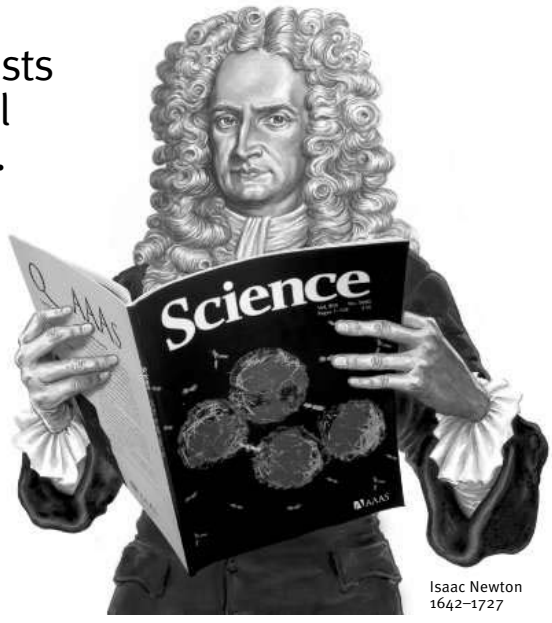

Isaac Newton
1642–1727

Post your jobs on ScienceCareers.org with **Post and Go.**

- Jobs are posted within one business day and stay up for 8 weeks.
- Applicable jobs are also searchable on the following websites:
  - Biocompare
  - National Postdoctoral Association (NPA)
  - Stanford University School of Medicine
  - *Science*'s Signal Transduction Knowledge Environment (STKE)
  - *Science*'s Aging Knowledge Environment (SAGE)
  - *Science*'s Next Wave
- ScienceCareers.org averages over 1 million page views and over 75,000 unique visitors each month.[1]
- All jobs are included in our Job Alerts e-mail system.

All this exposure means you can find the right scientist for your vacancy quickly and inexpensively.

For more information,
contact Beth Dwyer
Phone: 202-326-6534
E-mail: bdwyer@aaas.org

ScienceCareers.org
We know science AAAS

1 *Science* Webtrends Reports.

The power of small.

It's a small world.
The NanoDrop® Spectrophotometer has the power to analyze it.

1 µl samples · No dilutions · No cuvettes · Full spectrum

- **Nucleic Acid** concentration and purity measurements (from a 2ng/µl detection limit up to 3700ng/µl for dsDNA)
- **Microarray** nucleic acid and dye concentrations to determine labeling efficiency (Cy3, Cy5, Alexa Fluor dyes . . .)
- **Protein**, labeled and unlabeled, concentration and purity measurements (A280, protein arrays, Bradford, BCA, Lowry, antibody conjugates, metallo-proteins . . .)
- **General UV/Vis Spectrophotometry**

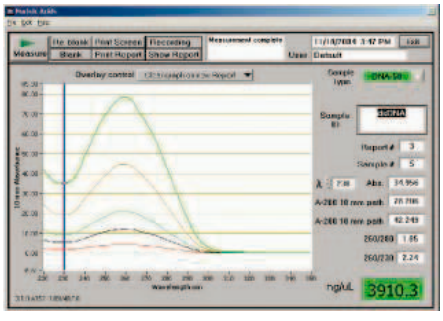

Measurement is as easy as pipette and read. The sample is read using two different path lengths (1mm and 0.2mm) to achieve an extensive dynamic range that virtually eliminates the need for dilutions. Then just a quick wipe clean and you're ready for your next sample. What could be easier—or more powerful?

Ready to experience the power of small? Contact us today and find out what our satisfied users worldwide have to say about the NanoDrop® ND-1000 Spectrophotometer.

FREE one week evaluation

Call for details.

(302) 479-7707 www.nanodrop.com

NanoDrop
when every drop counts.

Instead of an inkpad, DNA will leave its mark on future generations as an infallible means of personal identification. It also holds the clues to the greatest molecular mysteries of our time—provided we are able to unlock them.

accelerate > fingerprints

Invitrogen ChargeSwitch® Technology (CST) is the first significant breakthrough in DNA extraction techniques in more than 20 years. This revolutionary new approach to nucleic acid purification is flexible and sensitive enough to purify extremely small amounts of DNA—even the sort of heavily contaminated samples found at crime scenes or under other, uncontrolled circumstances.

Cigarette butts, hair follicles, a discarded piece of chewing gum—if ChargeSwitch® can extract high quality DNA from samples like these, imagine the reliability and performance you can expect from small or poor quality samples in basic, clinical or diagnostic research.

Unlike other purification kits, CST accelerates your research by eliminating ethanol precipitation and centrifugation. It also completely eliminates common enzyme inhibitors, which can negatively impact downstream applications.

The more DNA you can extract from a given sample, the more reliable your results are likely to be. ChargeSwitch® gives you more—and it gives it to you in a cleaner, purer form. So whether you're recovering evidence from a crime scene, or conducting disease research in the lab, ChargeSwitch® is the most effective and efficient route to extract the answers you're searching for.

Take advantage of our introductory promotion, please visit www.invitrogen.com/naprep1

invitrogen™

These products may be covered by one or more Limited Use Label Licenses (See the Invitrogen catalog or our web site, www. invitrogen.com).